ULTRAFAST PHOTOREDUCTION OF NITRIC OXIDE SYNTHASE BY ELECTRON TUNNELING WIRES

Thesis by

Wendy Belliston Bittner

In Partial Fulfillment of the Requirements for the

degree of

DOCTOR OF PHILOSOPHY

CALIFORNIA INSTITUTE OF TECHNOLOGY

Pasadena, California

2005

(Defended May 13th, 2005)

Dedication

This thesis is dedicated to Dr. Sharon Burgmayer, without whom my scientific career would have ended before it had begun.

ACKNOWLEDGEMENTS

In a situation such as this, where does one begin? There are so many people to thank, so many that have aided and abetted, pushed and prodded, and supported me down the road to completion of this Ph.D., that I am certain to forget more than one. So will I just dive in and see where my somewhat befuddled and exhausted brain takes me.

First, and foremost, I must thank my incredibly patient husband, Garrett, who has taken the time to fetch dinner and make the bed without complaint over the past six weeks while I have been mired in the writing of this tome. Over the past three years, he has supported me in everything I have chosen to attempt, and he is a continual reminder of how amazingly fortunate I am. He is a wonderful man, and I would be lost without him.

Next, I want to recognize the unfailing friendship and assistance of Libby Mayo who has read chapters, listened to me whine and cry, and donated her house, her desk, her time, and numerous bottles of wine to the completion of this thesis. The example she set last year in her own graduation epic was nothing short of brilliance under pressure, and I have more than once relied on that example to prevent panic. Our friendship began somewhat improbably over a hand grenade in the French Quarter, and it has grown into one of the most important in my life.

Thinking of Libby leads me to Jeremiah Miller, a great friend almost from my first day in the Gray group. While he was here, he was my partner in crime and commiseration on the party committee of two (no small job in the Gray group), and our coffee breaks (during the day) and alcohol breaks (at all other times) kept me going.

Jeremiah has definitely been one of those who propped me up along the way, even after he escaped Los Angeles. I still miss him dreadfully, and I look forward to the day when he, Libby, and I are running our successful winery/catering/fire-tent business.

Alex Dunn was the catalyst to whatever success I've had with the wire project. I will never forget the chance passing on the fourth floor of the BI during which Harry paired the two of us, nor will I forget Alex's formula for success: "If it can't be done in three tries, it's not worth doing!" Alex is not only one of the most brilliant thinkers with whom I've ever come into contact, but he is one of the kindest, funniest, and most generous people I know.

Yen Nguyen joined the project soon after Alex departed, and her excitement about synthesis has been a great complement to my own lack of enthusiasm in that department. I have no doubt that she will take NOS wires to a whole new level in the years to come.

Yen, along with Libby Mayo, Cora MacBeth, and, later, Steve Baldwin was also an integral part of "the Committee." While we managed together to do great things with FRESH over the past eighteen months, at times it has been our mutual moral support over drinks at the Croc that has been our most important function!

The wires subgroup was put together as a forum in which our SURFs could interact with students and postdocs working on other aspects of the project, but the bi-weekly meetings with Yen, Andrew Udit, Steve Contakes, and, occasionally, Phoebe Glazer have become a helpful and indispensable portion of my time at Caltech. Not only have the free-flowing ideas been helpful, but it has been great to get to know Steve, Phoebe, and Andrew better.

Jay Winkler has been an incredible resource over the past year. Without his help, the picosecond TA experiments would not have come to fruition, and his willingness to read and comment on the experimental details in this thesis—even in the midst of grant writing and conference preparation—was truly spectacular.

In the early days of my time in the Gray group, Will Wehbi was always available for a cup of coffee and some chocolate (and I will never forget the lunch of a lifetime at Le Bec Fin during the Philly ACS meeting—thank you again!), and Malin Abrahamsson and Oliver Wenger always brightened the atmosphere in the lab. Kristine Kilså Jensen was not only a great help with everything mathematical, but she and Hans were also a pleasure to know. Thanks to Judy Kim for having been a patient office mate who was, fortunately, not offended by my taste in music. Xenia Amashukeli and Adrian Ponce continue to be good friends (it's been a pleasure to have inherited your office, AP!), and Kate Pletneva has been a wonderful lunch partner during the past year. Thanks also to everyone else in the Gray group over the past few years. Despite the ups and downs of graduate school, I wouldn't trade my experiences for anything.

Away from the office, Garrett and I have had the good fortune to share two houses with Dave Michalak, Juliane Fry, Christine Ueda, and our honorary housemate, Robert Dirks, over the past three years. Even though we continue to miss Palm Street (black carpet and all!), our time at Los Robles has been good to us. We've shared everything from Christmas-ornament making and drunken, pool-splashing, Fourth-of-July fests to Easter Brunch and some of the best Thanksgiving food I've ever had, and it's been a pleasure to live with all of you! I will miss our house.

Now to those who have not been a part of Caltech, but who have yet been integral to my success. I met Milly Welsh the summer before my senior year of high school, and she has become a surrogate mother to me. Her willingness to take a chance on a rough-edged teenager from Montana started me down this winding path to a Ph.D. She is a continual inspiration to me, and I am honored to have her for a friend.

My parents, all four of them, have been supportive of every decision I have chosen to make since I left home ten years ago, and that trust has been very empowering to me. They've stood by me through years in England and Germany and supported me even when I thought I might give it all up to do who knows what. My dad and Ceci's unflagging pride has kept me going when all I could see in myself was failure. While we see each other too infrequently, they have been an important part of my life. My stepdad, Ed, has been my hero since the week I first met him, and he will continue to fill that role in my life. He is successful, intelligent, hard-working, and kind—everything that I would wish to be. Finally, my mother is responsible for the strong, independent thinker that I've become. The strength and self-sufficiency she taught me have been indispensable to me. I love you all.

Finally, I must thank the man that has made all of this possible. Harry Gray has been the perfect advisor for me during the past three years. Not only is he a brilliant scientist, but he is also a thoughtful, caring mentor who genuinely has the best interests of his students at heart. This is a combination that is all too infrequent in the cutthroat world of 21st century academic science, and I will forever feel grateful to have been a part of his group. Harry, you're the best!

ABSTRACT

The Gray group has a long-standing interest in the study of electron transfer and the development of methods for rapid delivery of electrons to enzyme active sites. This thesis describes picosecond to nanosecond reduction of the heme active site of the inducible nitric oxide synthase oxygenase domain (iNOSoxy) bound to a series of rhenium- and ruthenium-diimine electron-tunneling wires. The Re wires have the form $[LRe^{I}(CO)_3L']^{+}$ where L is 4,7-dimethylphenanthroline and L' is a perfluorinated biphenyl bridge connecting a rhenium-ligated imidazole or aminopropylimidazole to a distal imidazole (F_8bp-im (**1**) and C_3-F_8bp-im (**2**)) or F (F_9bp (**3**) and C_3-F_9bp (**4**)). All four bind tightly (K_d = μM to nM) in the active site channel of iNOSoxy. The two fluorine-terminated wires displace water from the active site, and the two imidazole-terminated wires ligate the heme iron. Upon excitation with 355 nm light, the bound rhenium of **1**, **2**, or **4** is quenched in fewer than 200 ps, possibly by electron donation from a nearby tryptophan residue. When a through-bond pathway from the rhenium to the heme iron exists, the active site Fe(III) is then reduced to Fe(II) within 300 ps, approximately ten orders of magnitude faster than the naturally occurring reduction. Calculations based on the yield of Fe(II) give a rate constant for electron transfer of $k_{ET} \sim 6 \times 10^8$ s^{-1}, demonstrating one of the fastest ET reactions ever observed in a protein environment over a distance of ≥ 18 Å. The Ru-diimine wire, $[(4, 4', 5, 5'\text{-tetramethylbipyridine})_2Ru(bpyF_9bp)]^{2+}$ (tmRu-F_9bp (**5**)), also binds tightly to iNOSoxy. The binding of **5** is independent of tetrahydrobiopterin, arginine, imidazole, and **1**, indicating that tmRu-F_9bp resides on the surface of the enzyme. Förster energy transfer

calculations support this conclusion and suggest that this wire binds in a hydrophobic surface patch that has been postulated to be the docking site for the reductase module of the enzyme. Reductive flash-quench studies have shown that the bound wire is capable of reducing the imidazole- (inhibitor) bound active-site heme in approximately 50 ns (k_{ET} = 2.4(4) × 10^7 s^{-1}), fully seven orders of magnitude faster than the comparable *in vivo* process. Preliminary work indicates that this flash/quench system is also capable of nanosecond reduction of the arginine- (substrate) bound active site. This work represents the first demonstration of electron-tunneling wires that specifically target and rapidly reduce an enzyme without blocking the active site channel.

TABLE OF CONTENTS

LIST OF FIGURES AND TABLES

Page

CHAPTER 1:

INTRODUCTION

Chapter 1

INTRODUCTION

Nitric Oxide Synthase

Background

Nitric oxide (•NO), *Science*'s 1992 molecule of the year, is an important signaling agent in nearly all biological systems.[1] Its small size allows it to be membrane permeable at roughly diffusion-limited rates, while its short lifetime prevents it from doing appreciable amounts of damage to surrounding structures and tissues. The major source for nitric oxide in the human body is the heme enzyme, nitric oxide synthase (NOS).[2] Mammalian NOS has three different isoforms—endothelial (eNOS), neuronal (nNOS), and inducible (iNOS). The constitutive forms (eNOS and nNOS) are responsible for basal •NO levels, while iNOS is expressed intermittently in response to immunostimulation.[3] Together, these three isozymes, because of their •NO production, are ultimately responsible for a wide array of physiological functions including relaxation of smooth muscle tissue, formation of new capillaries and cell migration in a wound, collagen synthesis and fibril alignment, bone growth, anti-viral, anti-bacterial, and anti-inflammatory activity, signal transduction—both peripheral sensation and memory signaling—and mediation of the analgesic effects of morphine.[4-12] Because of this sweeping functional importance, NOS malfunction is implicated in a long list of diseases from immune-type diabetes, in which all three NOS isoforms malfunction in a continuing

downward spiral, to hypertension, arteriosclerosis, and even Alzheimer's and Parkinson's diseases.[9, 13-19] Not surprisingly, these functions have made NOS and its mechanism and inhibition targets of intense study in a variety of scientific fields.

Structure and Cofactors

All three isoforms of NOS are large, complex homodimers that bind a variety of cofactors (Figure **1**).[20] Each monomeric unit comprises approximately 1100-1400 amino acids that fold into an N-terminal oxygenase domain (NOSoxy), a C-terminal reductase module (NOSred), and an intervening calmodulin-binding domain.[20] The oxygenase domain of each monomer contains a heme-thiolate active site as well as tetrahydrobiopterin (H_4B). In the absence of substrate, the sixth coordination site of the heme is generally occupied by a water molecule. When substrate binds, the water is displaced, generating a high-spin, five-coordinate heme that is poised for catalysis (Figure **2**). Each reductase module binds flavin mononucleotide (FMN), flavin adenine dinucleotide (FAD), and nicotinamide adenine dinucleotide phosphate (NADPH).[21-23] The two constitutive isoforms require Ca^{2+} in order to bind calmodulin and adopt their active structures. Inducible NOS, however, binds calmodulin tightly in the presence or absence of calcium, rendering it generally more active than eNOS or nNOS.[20, 24-27]

While no structures of a NOS holoenzyme have been determined, both the oxygenase domains[2, 28, 29] and reductase modules[30] of different isoforms have been crystallized as dimers by various groups. The constitutive forms of NOSoxy have tight dimeric structures; only inducible NOS exhibits any appreciable monomer/dimer equilibrium *in vivo*.[9, 31-33] As expressed in the absence of H_4B, iNOSoxy is partially

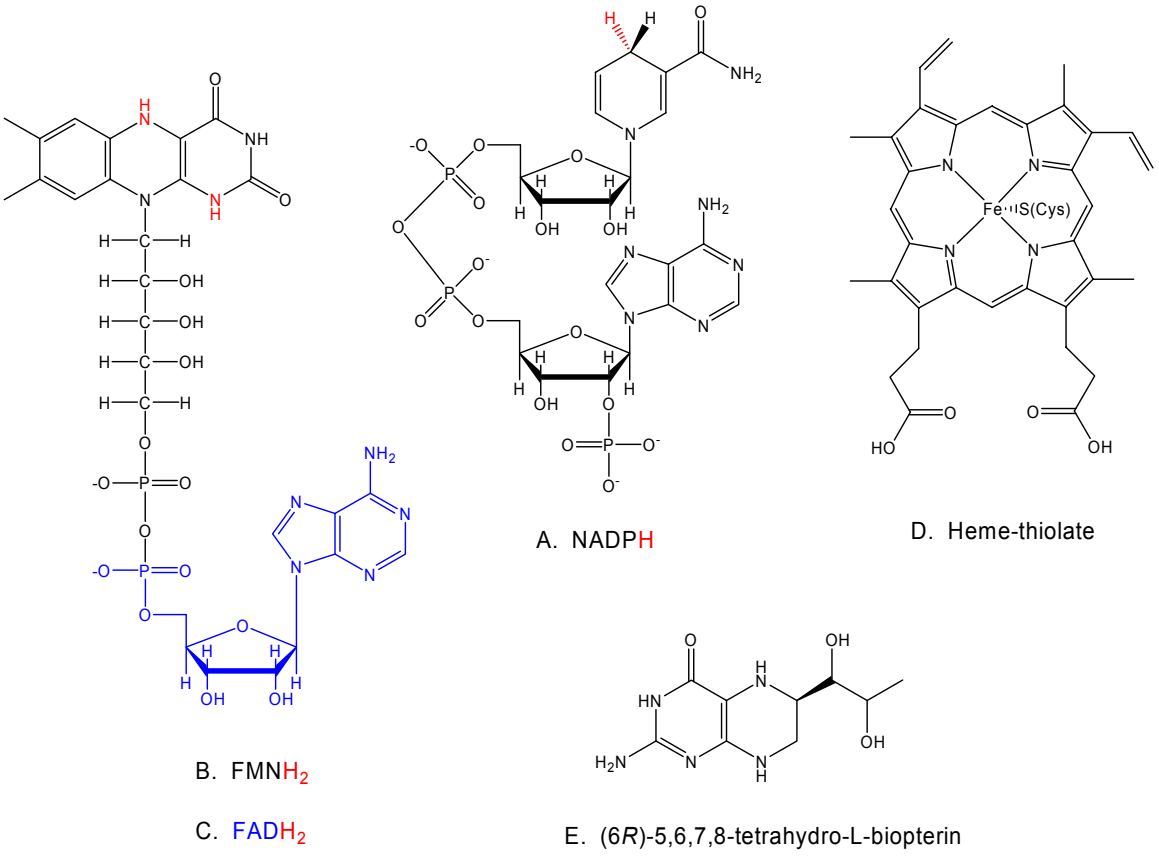

Figure 1. Cofactors of nitric oxide synthase. a) NADPH binds in the reductase domain and is the ultimate electron source for the enzyme. b) FMN (black) and c) FAD (black and blue) are intermediate electron acceptors. d) Iron protoporphyrin IX binds at the active site of the oxidase domain through a cysteine thiolate. e) Tetrahydrobiopterin binds near the heme at the dimerization interface of the oxidase domain and participates in at least one electron transfer process during enzyme turnover.

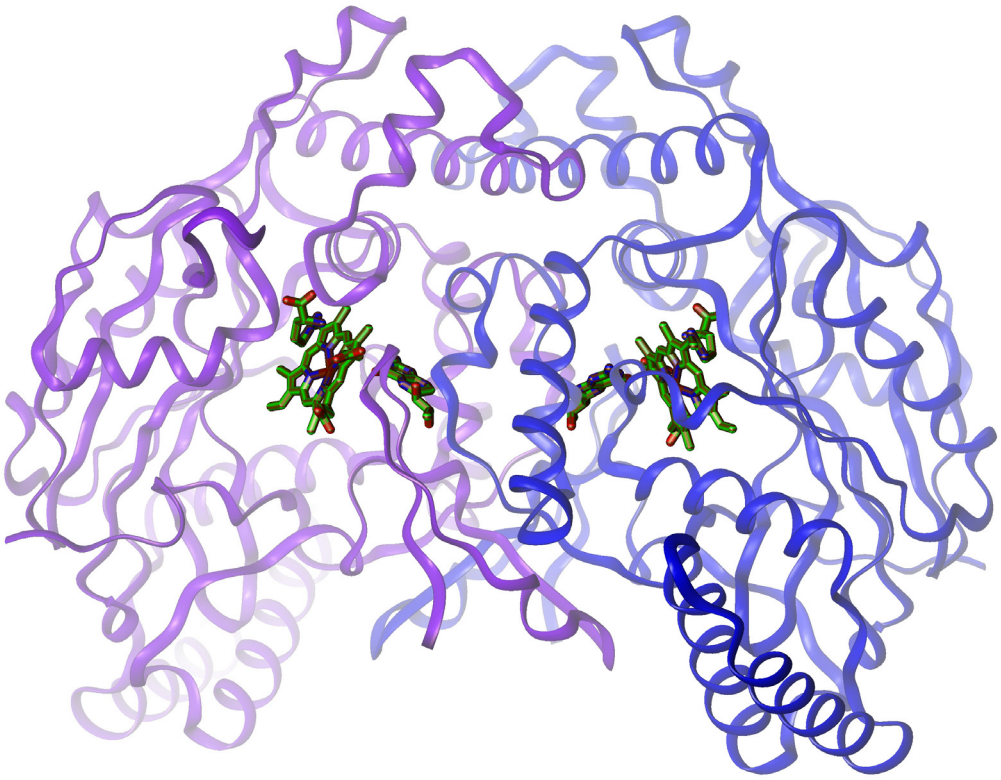

Figure 2. Crystal structure of dimeric Δ65 iNOSoxy with pterin and arginine bound (PDB code 1nod).[34]

monomeric and partially in the form of a "loose dimer."[9, 35] In both the monomer and the loose dimer, the active site channel is expected to be more open than in the tight dimeric form, leaving the heme more solvent-accessible (Figure **3**a).[36] Binding of H_4B induces formation of a strong dimer with a narrow channel and restricted access to the heme-thiolate active site (Figure **3**b).[9, 34] In all NOS isoforms, the dimeric oxygenase domain is catalytically competent in the presence of reducing equivalents and tetrahydrobiopterin even in the absence of the reductase module.[29, 37-39]

The work described in this thesis focuses exclusively on the iNOS oxidase domain, and three versions of iNOSoxy have been employed: Δ114, Δ65, and as-purified "full-length" iNOSoxy. Δ114 and Δ65 contain N-terminal truncations at residues 114 and 65, respectively, and were supplied by the Stuehr lab at the Cleveland Clinic. Full-length iNOSoxy was expressed and purified in-house following the procedure of Hurshman *et al.*, which ultimately produces a mixture of N-terminal truncations from Δ1 to Δ54.[40] The dimerization domain and pterin binding site of iNOSoxy lie between residues 65 and 114.[35] As such, it has been shown that N-terminal truncations of up to 65 residues can be made without interfering with dimerization capability or oxidase domain function.[35, 40] Therefore, Δ65 and "full-length" iNOSoxy are used interchangeably unless otherwise specified. Because it is lacking the dimerization domain, however, Δ114 iNOSoxy is fully monomeric and catalytically inactive.[34, 36]

The reductase module of NOS contains multiple domains that bind FMN, FAD, and NADPH as the ultimate electron source for the NOS catalytic reaction.[20, 30, 41] Because of the lack of holoenzyme structural information, the positioning of the reductase module with respect to the oxidase domain is unclear. It is known, however,

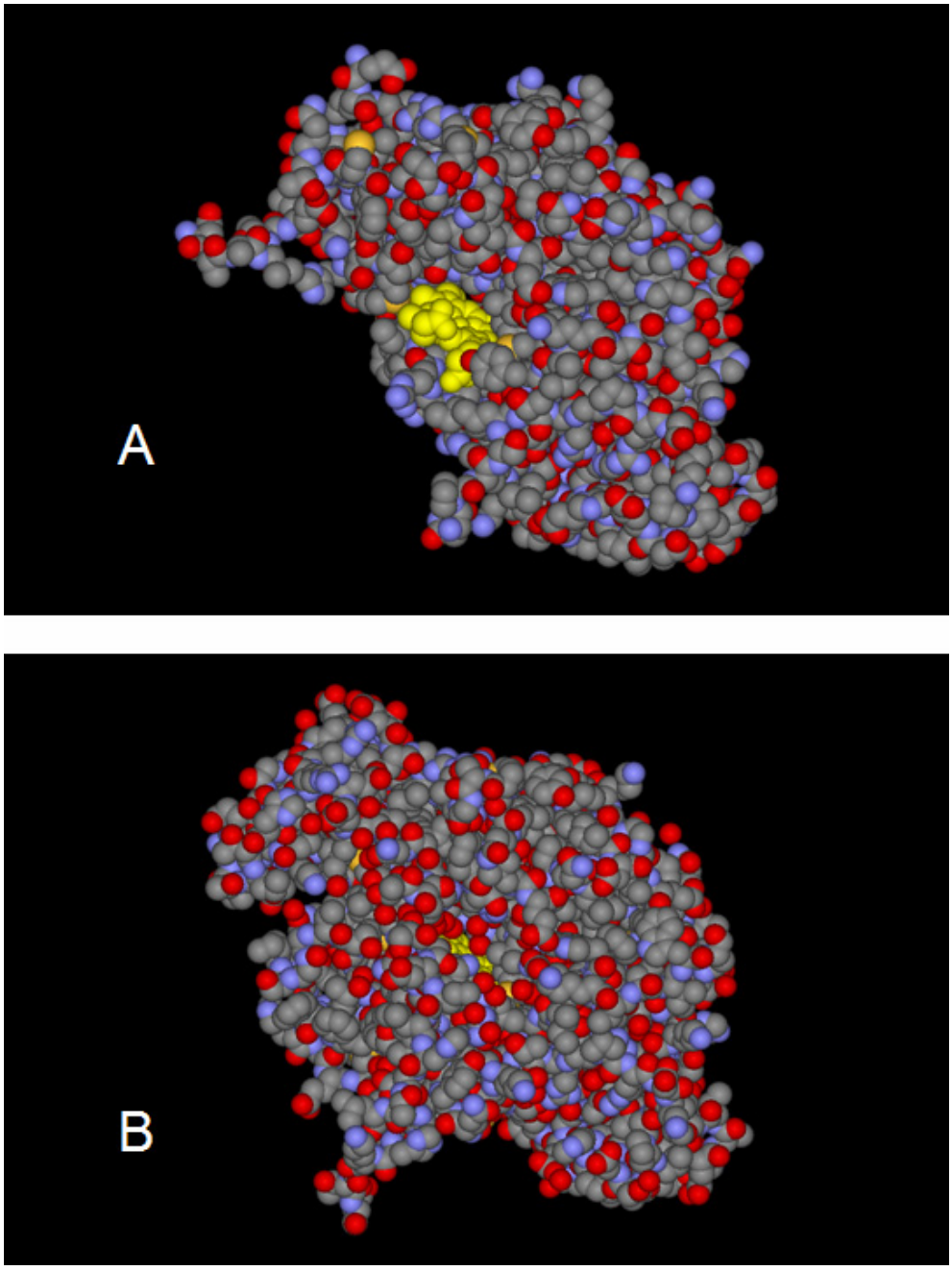

Figure 3. Comparison of the heme accessibility in monomeric (a) and dimeric (b) iNOSoxy. a) Crystal structure of the fully monomeric Δ114 iNOSoxy (PDB code 1nos).[36] b) Crystal structure of dimeric Δ65 iNOSoxy (only one monomer shown) (PDB code 2nod).[34] In each case, the heme is shown in yellow. Because Δ114 is missing some

of the channel-forming residues, its heme is very exposed. The heme of monomeric/loosely dimeric Δ65 or full-length iNOSoxy is expected to have intermediate solvent accessibility.

that the FMN domain of one monomer supplies electrons to the oxidase domain of the other.[28, 30] Relatively facile (although rate-limiting) electron transfer from FMN to the heme (~1 s^{-1})[42, 43] suggests that the flavin is likely to approach within 10-20 Å of the heme during turnover. The flexibility of the FMN-binding domain of the reductase module as well as the presence of a concave, partially hydrophobic patch on the back face of the oxidase domain[30, 36] have led to the hypothesis that the entire FMN-domain undergoes a large-scale shift after accepting an electron from FAD and docks with the oxidase in order to reduce the heme.[30] Chapters 2 and 4 of this work discuss Ru-diimine electron tunneling wires that bind to iNOSoxy at the proposed FMN-domain docking site. Chapter 5 discusses electrochemical experiments with iNOSoxy which show that a well coupled electron transfer (ET) pathway from the surface of the enzyme to the heme exists, supporting the idea that approach of FMN to the heme, and not ET itself, is rate-limiting in NOS.

Catalytic Mechanism

NOS catalyzes the transformation of L-arginine and two equivalents of molecular oxygen to L-citrulline and nitric oxide. The full transformation requires two cycles of the enzyme, the first taking arginine to N^{ω}-hydroxy-L-arginine (NHA), and the second completing the transformation to citrulline and •NO (Figure **4**). A proposed mechanism for •NO production is shown in Figure **5**.[4, 20, 42, 44, 45]

The first turnover is thought to proceed through a P450-like mechanism.[46, 47] The resting enzyme binds substrate, shifting the ferric heme to high spin and adjusting its potential from –300 mV to –260 mV.[48] This potential shift induces one-electron heme

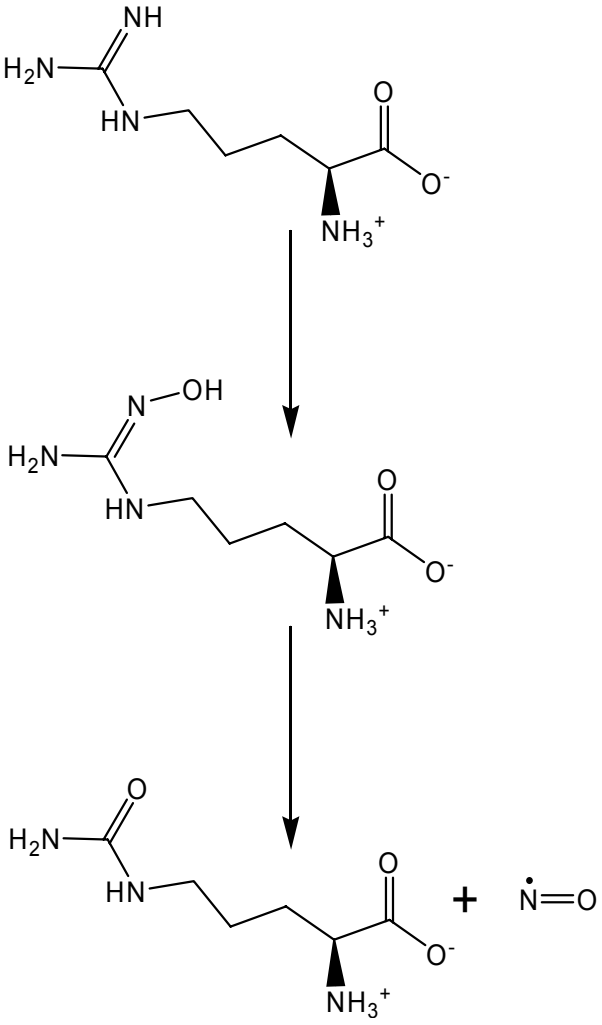

Figure 4. Overall reaction catalyzed by nitric oxide synthase. The enzyme utilizes NADPH and molecular oxygen to effect the conversion of L-arginine (top) to L-citrulline and •NO (bottom). The reaction occurs in two turnovers with N^{ω}-hydroxy-L-arginine (center) as an intermediate product.

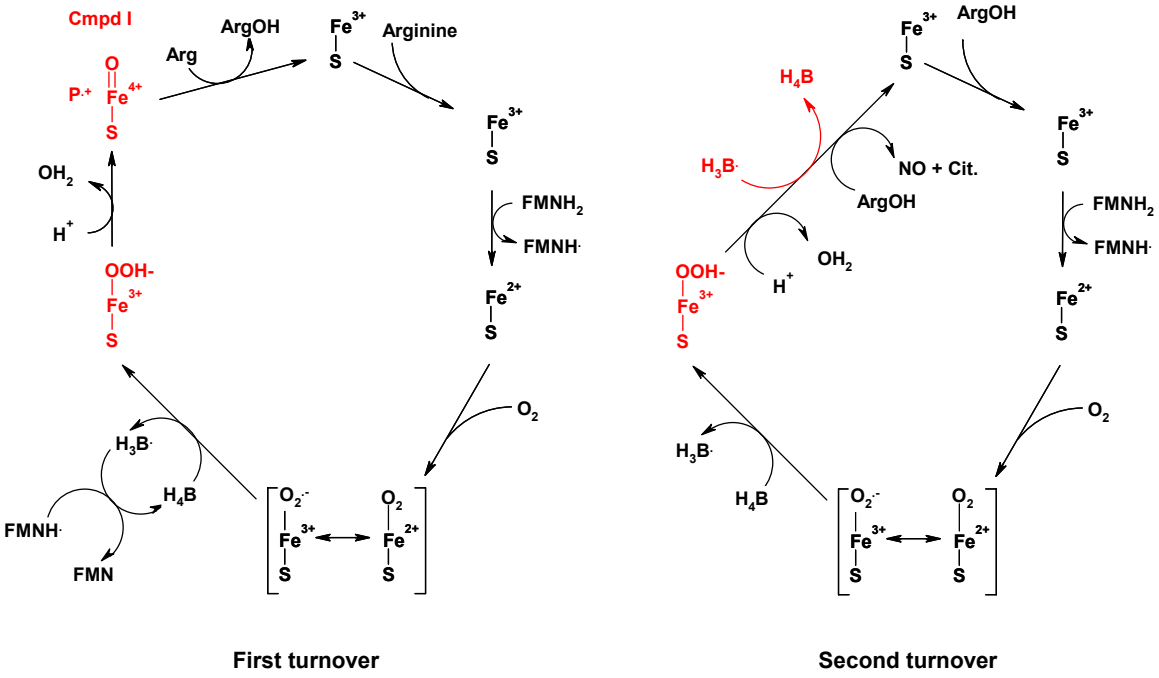

Figure 5. Proposed mechanisms for the first and second turnovers of NOS.[4, 20, 42, 45] The high-valent intermediates and controversial species of particular interest to this work are shown in red.

reduction by FMN at a rate of ~ 1 s^{-1}, the overall rate-limiting step in the turnover reaction.[42, 43] Dioxygen binds to the 5-coordinate, ferrous heme to create a ferric-superoxo species, the last observable intermediate in the turnover.[49] A second, slow reduction step then occurs at a rate of ~12 s^{-1} with H_4B as the apparent reductant.[42, 50-54] The remainder of the mechanism of the first turnover is a mystery. If it continues on a P450-type pathway (as shown in Figure **5**), the ferric-peroxo species would be protonated to give the ferric-hydroperoxo, followed by a second protonation and splitting of the O-O bond to generate compound I (ferryl-porphyrin$^{+\bullet}$) and water.[46, 47, 55-57] Compound I would then act as the oxygen-donating species to generate the intermediate product, NHA.

The second turnover is even less well understood than the first. Initially, the enzyme proceeds as in the first cycle, with the ferric-superoxo species as the last observable intermediate. It is now generally accepted that the pterin again provides the second reducing equivalent,[42, 52] but the mechanism of the actual O-atom transfer is highly speculative. While the second reaction may proceed through compound I as the first is expected to do,[42, 52] there has been some evidence to suggest that NHA may be oxidized directly by a ferric-peroxo species.[45, 58, 59]

It is owing to their extreme instability that the high-valent heme intermediates in this mechanism (red species in Figure **5**) have remained elusive. In 1998, Bec *et al.* reported a low-temperature optical spectrum of a compound they thought to be compound I,[57] but while this paper has been heavily cited since, to our knowledge, no further spectra of compound I in NOS have been reported. Additionally, Davydov *et al.* have published EPR spectra of ferric-peroxo species generated at cryogenic temperatures in eNOS.[45] While these are very promising first steps, the NOS community still awaits spectroscopic

characterization and confirmation of the existence of these intermediates at room temperature. The ultimate goal of the work detailed in the following chapters is to speed up the reduction steps in NOS in order to generate observable amounts of the uncharacterized, high-valent heme intermediates in solution. Chapters 3 and 4 describe Re- and Ru-diimine wires that are capable of electron injection into the heme of iNOSoxy at speeds approaching 10^9 s^{-1}, creating observable Fe(II) signals within as few as 300 ps of excitation.

Wires

Background

Initial experiments performed in the Gray group for the rapid generation of high-valent heme intermediates used photogenerated high-valent Ru-diimines in solution to oxidize the enzymatic metal center. This approach was successful for horseradish peroxidase[60] and microperoxidase 8.[61] Likely due to relatively poor electronic coupling between the deeply-buried heme and the surface of the enzyme, however, this technique did not work for P450cam.[62]

In 1999, Wilker *et al.*[62] showed that rapid electron/hole transfer to the buried heme of cytochrome P450cam was possible. This was achieved by tethering the ruthenium-based photosensitizer through a hydrocarbon linker to either a substrate or an inhibitor with high binding affinity for the active site pocket (Figure **6**). They then employed flash/quench methodology to excite and then reduce or oxidize the Ru-sensitizer. The photogenerated Ru(I) or Ru(III) species, in turn, rapidly reduced/oxidized

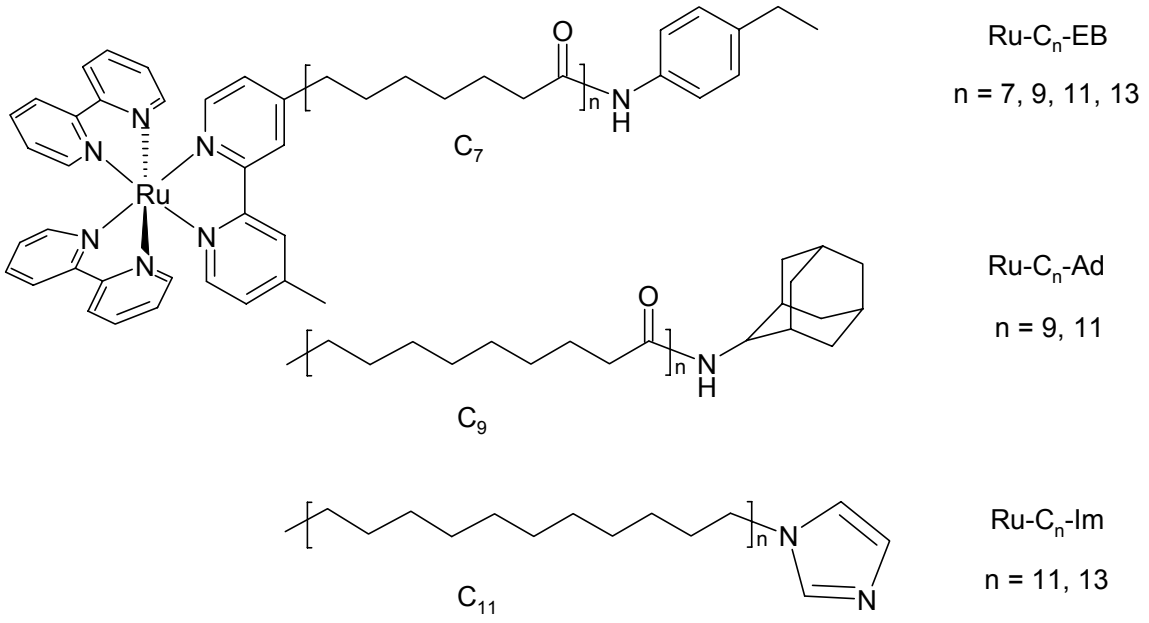

Figure 6. First generation Ru-diimine wires for P450cam.[63, 64]

the heme of P450cam. The basic scheme is outlined in Figure **7**. By this method, heme reduction on a millisecond timescale was observed.

In the second generation of wires for P450, Alex Dunn and Ivan Dmochowski turned to a conjugated, electron-withdrawing perfluorobiphenyl bridge with the aim of further increasing the ET rate (Figure **8**). This modification increased the donor/acceptor coupling to the point that an external quencher was no longer necessary in order to observe very rapid heme reduction.[65] Not only was the ET rate significantly increased ($k_{ET} = 2.8 \times 10^7$ s^{-1} for tmRu-F_8bp-Im:P450cam), but the perfluorobiphenyl unit provided numerous other benefits, including synthetic malleability and the ability to interact favorably with aromatic amino acid residues.[66] Indeed, the use of perfluorobiphenyl-based wires has been central to the studies of NOS described in this thesis. While none of the original methylene-based wires shown in Figure **6** bind to NOS, all of the perfluorobiphenyl wires that have been produced in our laboratory to date, including Ru-F_8bp-Ad and Re-Im-F_9bp (which bear little resemblance to any previously known NOS-binding molecules), bind to iNOSoxy with μM to nM dissociation constants.[67, 68] The NOS-binding interactions of six perfluorobiphenyl wires are discussed in Chapters 2 and 3.

Design and Evolution

While luck has certainly played a part with respect to enzyme affinity and specificity, design of a successful wire for a photoinduced ET study encompasses several key features. First, the metal sensitizer should have a high luminescence quantum yield in order to maximize the number of excited state molecules that are available for

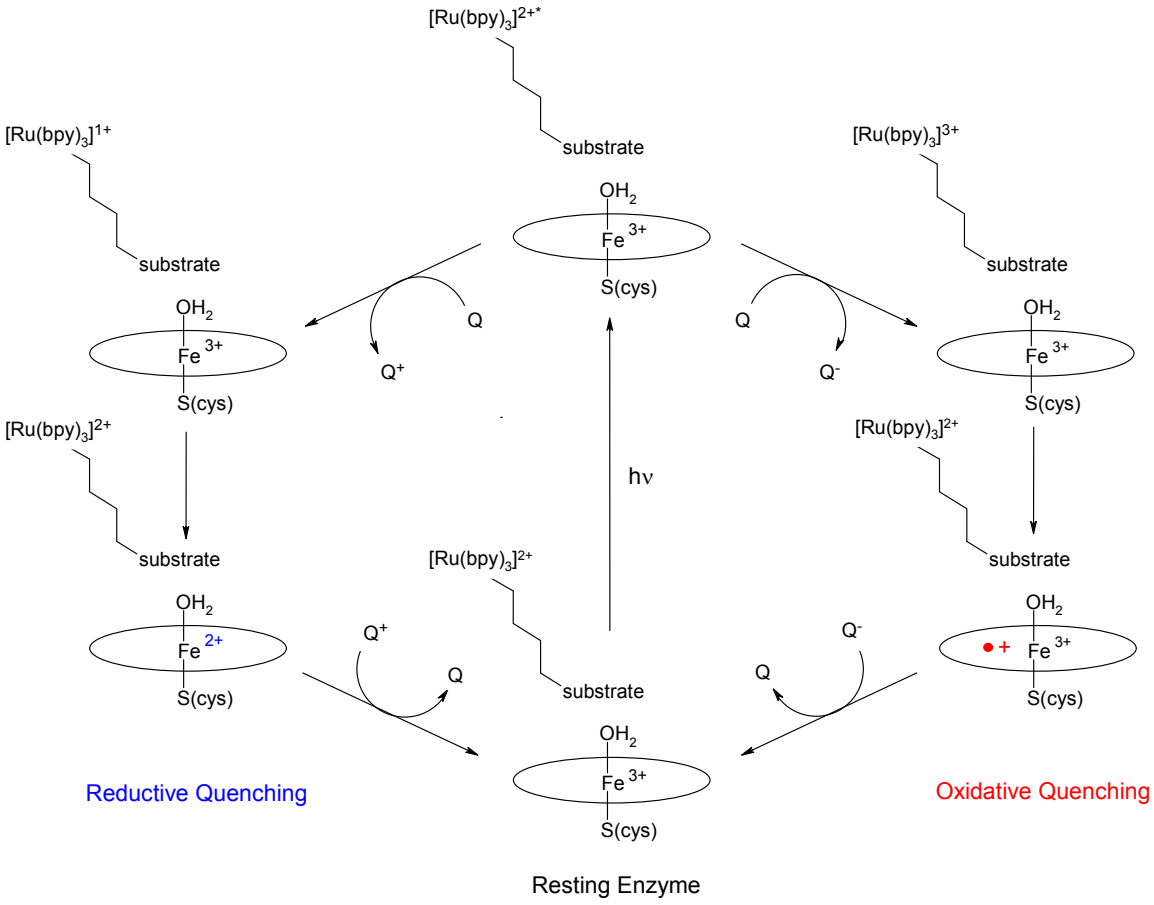

Figure 7. Basic scheme for the reductive/oxidative flash quench experiment with a wire bound to P450cam.

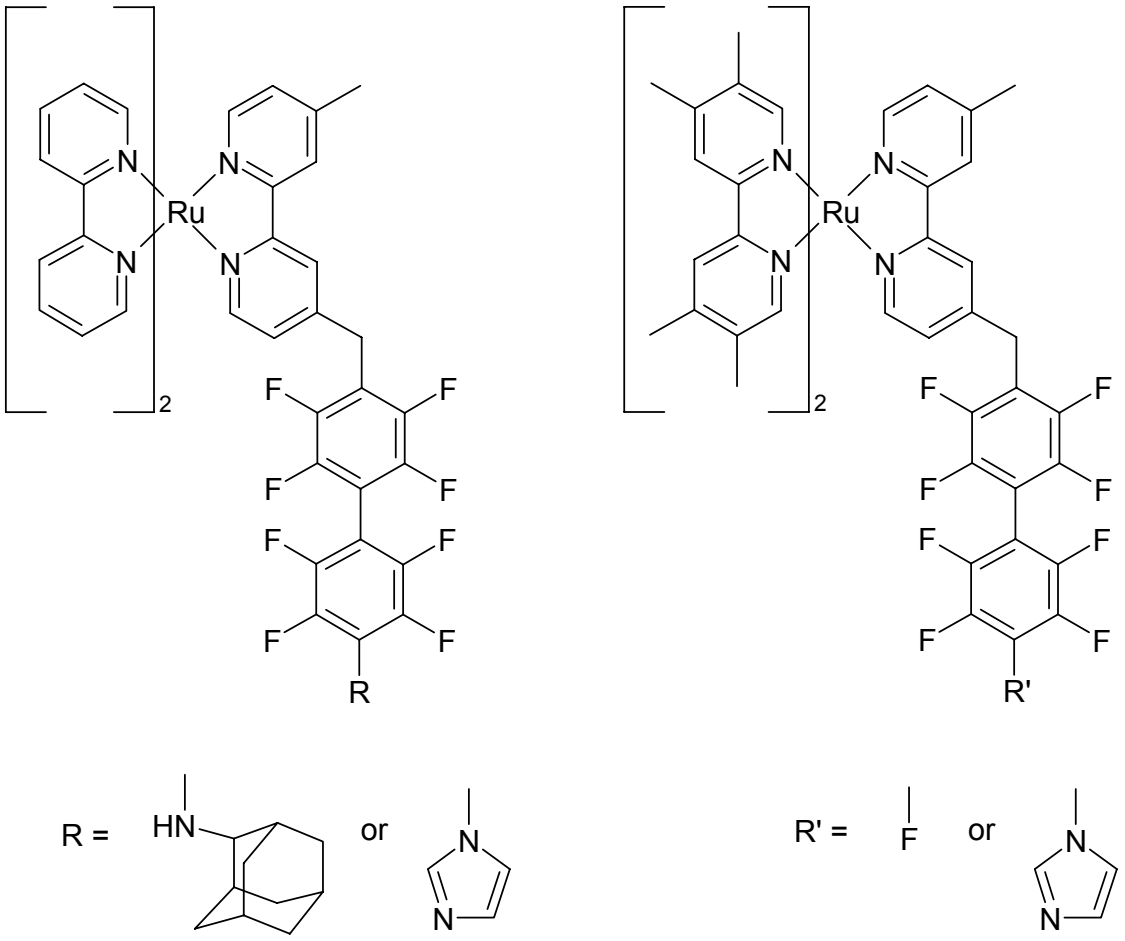

Figure 8. Second generation Ru-diimine wires for P450cam.[65, 69]

quenching with each excitation pulse. Secondly, the photoexcited and/or quenched sensitizer should have a high redox potential in order to maximize the driving force for the electron/hole transfer.[§70-74] Thirdly, the wire bridge between the sensitizer and protein active site should be capable of supporting rapid electron transfer. Finally, the probe should bind 1:1 to the target enzyme, preferably in an easily identifiable manner. While it was originally assumed that a tight-binding substrate/inhibitor would be necessary for targeting the wire to the enzyme, in practice it has been found that the linker is likely to have a significant effect on binding affinity, sometimes even eliminating the need for a substrate/inhibitor mimic at the wire tip.[66, 67]

Although channel-binding wires were originally developed for the rapid delivery of electrons and holes to the heme of P450cam, wires have since evolved into versatile tools for communicating many kinds of information to and from the active sites of numerous different enzymes. A thiol-terminated wire has been built for linking copper amine oxidase from *Arthrobacter globoformis* (AGAO) to a gold electrode in order to obtain the first direct redox potential measurements of the AGAO active site.[75] Ru-diimine wires were used in x-ray crystallographic studies to develop models for the structural flexibility and substrate promiscuity of P450cam.[66, 69, 76, 77] Numerous fluorescent probes for P450cam, in which the redox-active Ru-sensitizers were replaced with highly fluorescent dansyl molecules, were employed in structural studies and competitive binding assays.[78, 79] In ongoing work in our laboratory, a series of variable length, Ru-based wires have demonstrated that AGAO can bind short, very bulky

molecules, indicating that the enzyme is more conformationally flexible than was previously believed,[80] and substrate-based wires have been designed to bind in the narrow, kinked channel of the highly-oxidizing enzyme, myeloperoxidase.[81]

Development of wires that do not block the active site channel has also begun. A peptide-based wire that binds to cytochrome c peroxidase in an artificially created channel to the heme was reported by Hays *et al.* in 2003.[82] Additionally, Immoos *et al.* have described ET chemistry in *apo*-myoglobin reconstituted with a heme tethered through a methylene linker to $Ru(bpy)_3^{2+}$ at the surface.[83] In order to study cyclic voltammetry of P450BM3 at a graphite electrode, Udit *et al.* covalently attached a pyrene-linked wire to a cysteine residue at the surface of the enzyme.[84] Finally, the first surface-binding wires that do not require chemical modification of the protein target are described in Chapters 2 and 4 of this work.[67]

Electron Transfer

Electron transfer plays a central role in a wide variety of biological processes, including the turnover of NOS described above. In systems such as the photosynthetic reaction center,[85, 86] DNA photolyase,[87, 88] and ribonucleotide reductase[89] electrons are shuttled specifically and rapidly (sometimes in $<< 1$ μs) over distances ≥ 30 Å. These findings have led to intense study over the past half century to unravel the mechanism(s) by which such long-range and rapid ET can occur.

[§] While extremes in driving force can push the system into the inverted region (see Chapter 1, Electron Transfer), thereby slowing ET, evidence has shown that photoexcited and/or one-electron oxidized/reduced Ru- and Re-diimines with redox potentials in the 0.7-2.0 V range allow for nearly activationless ET in many heme- and Cu-protein systems.

Biological electron transfer occurs between donors (**D**) and acceptors (**A**) that are weakly coupled. Under these circumstances, electron transfer rates can be modeled by semiclassical ET (SCET) theory as described by Marcus and Sutin in 1985 (Equation 1).[90]

$$k_{\mathrm{ET}} = \sqrt{\frac{4\pi^3}{h^2 \lambda k_B T}} H_{AB}^2 \exp[\frac{-(\Delta G^0 + \lambda)^2}{4\lambda k_B T}] \qquad (1)$$

where H_{AB} is the electronic coupling matrix element between the donor and acceptor at the transition state, $-\Delta G^0$ is the driving force for the reaction (which can be approximated by the redox potential difference between **D** and **A**), and λ is the nuclear reorganization energy for the system. λ is comprised of λ_{in}, the energy required to reorganize the nuclei of **D** and **A**, and λ_{out}, the energy required to reorient the nuclei of the solvent or surrounding medium.

One counterintuitive result of the SCET model is that increasing the driving force does not always increase the ET rate! Rather, the maximum rate of electron transfer is observed when the driving force for the reaction is exactly equal to the reorganization energy (Figure **9**).[91] This type of electron transfer reaction is called "activationless." Once the driving force exceeds the reorganization energy, the reaction enters what is known as the Marcus inverted region, and k_{ET} begins to decrease again. Nature uses this fact to her distinct advantage by encapsulating redox centers in relatively inflexible protein environments and thereby minimizing the reorganization energy for an ET event.[72, 92, 93] This maximizes the rates of electron transfer between relatively low-potential

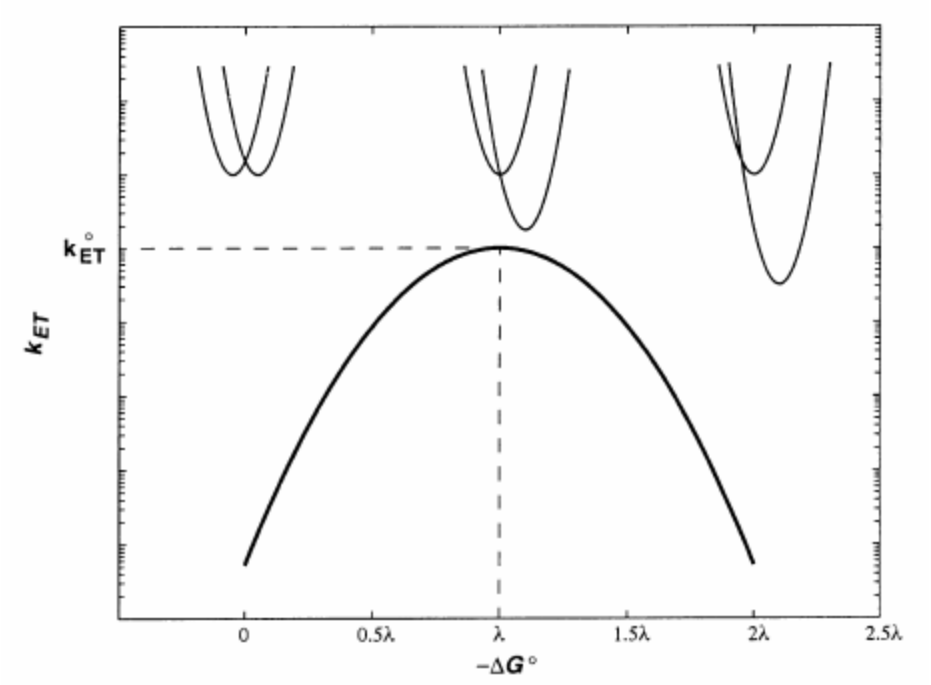

Figure 9. Graphical representation of electron transfer rates (k_{ET}) predicted by semi-classical ET theory (Eq. 1) as a function of driving force ($-\Delta G^0$) and reorganization energy (λ). At low driving force ($-\Delta G^0 < \lambda$), k_{ET} increases with driving force (normal ET). k_{ET} is maximized when $-\Delta G^0 = \lambda$ (activationless ET). As driving force continues to increase, the reaction barrier once again increases and electron transfer slows (the inverted region).

centers while minimizing the chance for damage from high-potential sites or misdirected ET.

While ET rates in the inverted region have been observed both in synthetic donor-acceptor models[94-99] and in biological systems,[70, 71, 100] there are a number of escape routes through which a system can avoid the inverted effect. One such mechanism is the formation of excited state products such that the overall driving force for the reaction is reduced by the energy of the excited state.[71, 91, 101] A second method is through "hopping" (discussed below). Additionally, in Equation 1, nuclear motions (λ) are treated classically. Especially in the inverted region, however, quantum mechanical refinements are often required in order to adequately describe observed ET rates.[91, 94, 102]

Aside from the driving force:reorganization energy ratio, the ET rate is also governed by the strength of the electronic coupling between donor and acceptor (H_{AB}). Over long distances (> van der Waals radii) such as those that generally exist between biological **D**/**A** pairs, the coupling between donor and acceptor is weak (ET is nonadiabatic) and H_{AB} is governed by the intervening medium. If this medium is treated as a simple square barrier, H_{AB} follows Equation 2:

$$H_{AB} = H_{AB}^{0} \exp\left[\frac{\beta}{2} \times R\right] \qquad (2)$$

where H_{AB}^{0} is the direct overlap of the electronic states of the donor and acceptor, R is the **D**-**A** distance and β is the decay constant associated with the intervening medium. Tunneling through a vacuum is highly disfavored with β = 2.9-4.0 Å^{-1}, while tunneling rates through water drop off with β = 1.55-1.65 Å^{-1} (Figure **10**).[103] When the intervening

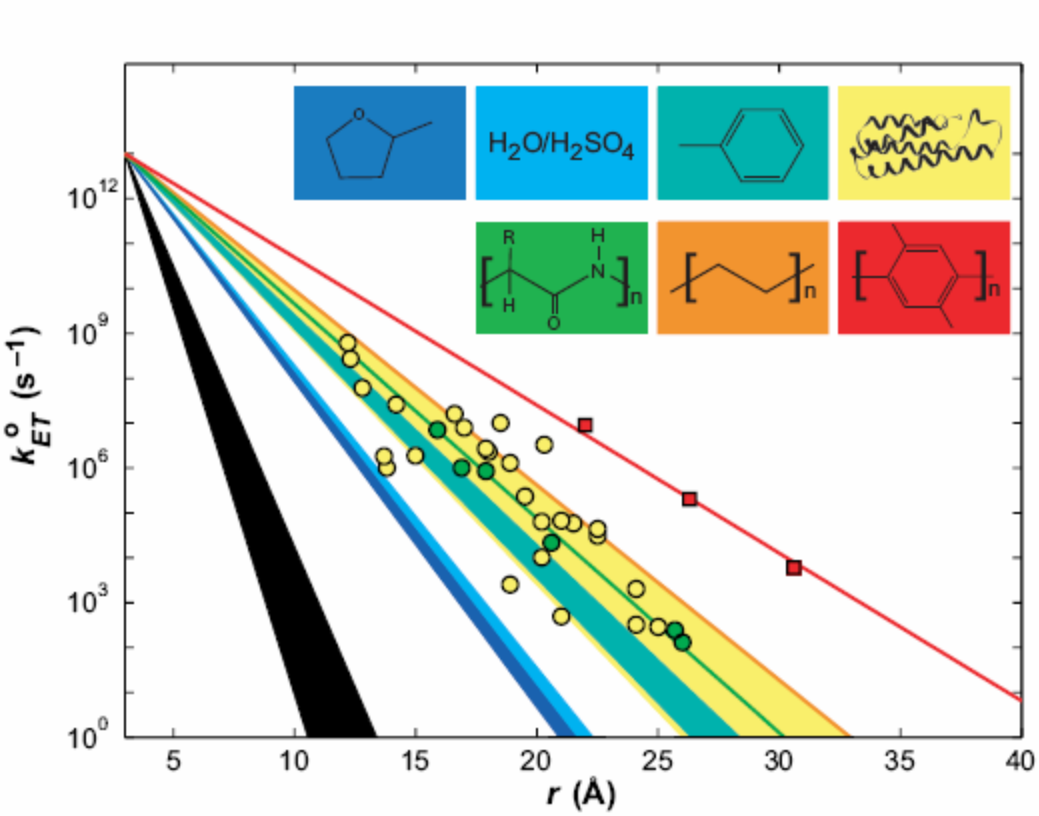

Figure 10. Timetable for activationless tunneling through various media: Vacuum (black, β = 2.9-4.0 $Å^{-1}$), methyl-THF glass (dark blue, β = 1.57-1.67 $Å^{-1}$), aqueous glass (light blue, β = 1.55-1.65 $Å^{-1}$), toluene glass (teal, β = 1.18-1.28 $Å^{-1}$), aqueous glass (light blue, β = 1.55-1.65 $Å^{-1}$). Tunneling through various bridging species have also been studied: Proteins (green, yellow wedge β ≈ 1.1 $Å^{-1}$), methylene bridges (orange, β = 1.0 $Å^{-1}$) and oligoxylyl bridges (red, β = 0.76 $Å^{-1}$). This figure was kindly provided by Jay Winkler and Brian Leigh.[104]

medium has electronically accessible states, such as when **D** and **A** are covalently linked by a bridge (**D**-**B**-**A**), the square barrier model becomes inadequate for describing H_{AB}. By treating the bridge as a set of *n* identical repeat units, one can instead apply the McConnell superexchange model (Equation 3):[103, 105]

$$H_{AB} = \frac{h_{Ab}}{\Delta\varepsilon}\left(\frac{h_{bb}}{\Delta\varepsilon}\right)^{n-1} h_{bB} \qquad (3)$$

where $\Delta\varepsilon$ is the energy gap between the donor and empty orbitals on the bridge and h_{Ab}, h_{bb}, and h_{bB} represent the donor-bridge, bridge-bridge, and bridge-acceptor couplings, respectively. Assuming that the size of each bridging unit is δ, and using Equations 1 and 3, the distance decay constant can be redefined as (Equation 4):[103, 104]

$$\beta = \left(\frac{2}{\delta}\right)\ln\left(\frac{\Delta\varepsilon}{h_{bb}}\right) \qquad (4)$$

A great deal of experimental work on synthetic **D**-**B**-**A** systems and Ru-modified proteins[72-74, 91, 106-113] has led to a well-developed "tunneling timetable" (Figure **10**) that describes distance decay rates (β) for a variety of synthetic and biological bridging units.[103]

Even the development of this large body of work, however, has not served to explain some of the fast rates observed for truly long-range (≥ 20 Å) biological ET. How, for instance, does an electron manage to cover more than 28 Å in the photosynthetic reaction center in ~ 100 ps?[72, 85] A popular mechanism for this kind of rapid, long-distance ET is known as "hopping." In simplified terms, hopping can be described as a multistep ET process in which the bridge between the donor and acceptor

becomes directly involved in the reaction. In the superexchange model, the bridge itself is neither oxidized nor reduced but rather contributes to the overlap of the overall wavefunction for the system. In the hopping model, however, the bridge becomes an intermediate donor/acceptor, in effect creating two (or more) shorter tunneling steps instead of a single long one. Because ET rates vary exponentially with distance, hopping can decrease k_{ET} by orders of magnitude.[89, 103] Chapter 3 of this thesis describes Re-diimine wires that bind to NOS and induce electron transfer to the heme within ~300 ps of photoexcitation despite a predicted Re-Fe distance of ≥ 18 Å, suggesting that hopping may occur.

CHAPTER 2:

INVESTIGATING THE BINDING INTERACTIONS OF RU- AND RE-DIIMINE WIRES WITH INDUCIBLE NITRIC OXIDE SYNTHASE[†]

Acknowledgement:

This work was done in close collaboration with Alex Dunn who also synthesized the Ru wires. Thanks also to Dennis Stuehr at the Cleveland Clinic Foundation for supplying Δ65 and Δ114 iNOS samples.

Chapter 2

INVESTIGATING THE BINDING INTERACTIONS OF RU- AND RE-DIIMINE WIRES WITH INDUCIBLE NITRIC OXIDE SYNTHASE

Abstract

Ru(II)- and Re(I)-diimine wires bind to the oxygenase domain of inducible nitric oxide synthase (iNOSoxy). In the ruthenium wires, $[Ru(L)_2L']^{2+}$, L' is a perfluorinated biphenyl bridge connecting 4,4'-dimethylbipyridine to a bulky hydrophobic group (adamantane, **1**), a heme ligand (imidazole, **2**), or F (**3**). **2** binds in the active site of the murine iNOSoxy truncation mutants Δ65 and Δ114, as demonstrated by a shift in the heme Soret from 422 to 426 nm. **1** and **3** also bind Δ65 and Δ114, as evidenced by biphasic luminescence decay kinetics. However, the heme absorption spectrum is not altered in the presence of **1** or **3,** and Ru-wire binding is not affected by the presence of tetrahydrobiopterin or arginine. These data suggest that **1** and **3** may instead bind to the distal side of the enzyme at the hydrophobic surface patch thought to interact with the NOS reductase module. Complexes with properties similar to the Ru-diimine wires may provide an effective means of NOS inhibition by preventing electron transfer from the reductase module to the oxygenase domain. Rhenium-diimine wires $[Re^{I}(CO)_3L_1L_1']^{+}$, where L_1 is 4,7-dimethylphenanthroline and L_1' is a perfluorinated biphenyl bridge connecting a rhenium-ligated imidazole to a distal imidazole (F_8bp-im) (**4**) or F (F_9bp) (**5**) also form complexes with Δ114. Binding of **4** shifts the Δ114 heme Soret to 426 nm, demonstrating that the terminal imidazole ligates the heme iron. Steady-state

luminescence measurements establish that the **4**:Δ114 dissociation constant is 100 ± 80 nM. Re-wire **5** binds Δ114 with a K_d of 5 ± 2 μM, causing partial displacement of water from the heme iron. Our finding that both **4** and **5** bind in the NOS active site suggests novel designs for NOS inhibitors. Importantly, we have demonstrated the power of time-resolved FET measurements in the characterization of small molecule:protein interactions that otherwise would be difficult to observe.

Introduction

The enzyme nitric oxide synthase (NOS) is the major biological source of nitric oxide (•NO), a secondary messenger acting in a myriad of circumstances that include neuronal development, regulation of blood pressure, apoptosis, neurotransmission, and immunological response.[11, 19, 114-118] Because of the central importance of •NO, NOS has been implicated in septic shock, inflammation, a variety of neurodegenerative disorders, and heart disease.[119-121]

Full-length NOS consists of oxygenase, reductase, and calmodulin binding domains. The NOS oxygenase domain (NOSoxy), which contains cysteine-ligated heme and tetrahydrobiopterin (H_4B) cofactors, catalyzes the conversion of arginine and molecular oxygen to •NO and citrulline.[122] The electrons necessary for this reaction are provided by the reductase module, which is attached to NOSoxy by a calmodulin-binding linker.[25, 123] NOS functions as a homodimer; the reductase module from one half of the dimer reduces the oxygenase domain of the other.[28, 124, 125] Calmodulin binding is known to modulate electron transfer, and hence catalysis.[126-128] Several crystal structures of the

NOS oxygenase domain have been determined,[2, 29, 34, 36, 129] but the structure of the full-length enzyme remains elusive.

We have a long-standing interest in the high-valent intermediates thought to play key roles in heme-mediated oxidations.[60-63, 65, 66, 77-79] In order to observe these intermediates, we have designed Ru-diimine photosensitizers (Ru-wires) that bind to the mechanistically related enzyme cytochrome P450, and inject an electron into the active site upon excitation with 470-nm light.[65] Energy transfer between the excited state of the Ru-wire and the heme also serves as a sensitive structural probe.[63, 79] Like NOSoxy, cytochrome P450 enzymes possess a cysteine-ligated heme in the active site, and catalyze the oxidation of substrates using molecular oxygen and two electrons supplied by a reductase (in the case of P450 a separate protein).[130]

Given the postulated mechanistic similarities between NOS and cytochrome P450, we have endeavored to develop similar photosensitizer-wires for NOS. Our initial investigation showed that complexes **1-3** (Figure **11**) bind the oxygenase domain of murine inducible NOS (iNOSoxy) with micromolar dissociation constants. Intriguingly, a combination of fluorescence energy transfer (FET) measurements and structural modeling suggests that **1** and **3** bind to the surface patch thought to interact with the reductase module. Second generation compounds **4** and **5**, which are structurally analogous to **2** and **3**, bind in the iNOSoxy active site with micro- and nanomolar dissociation constants.

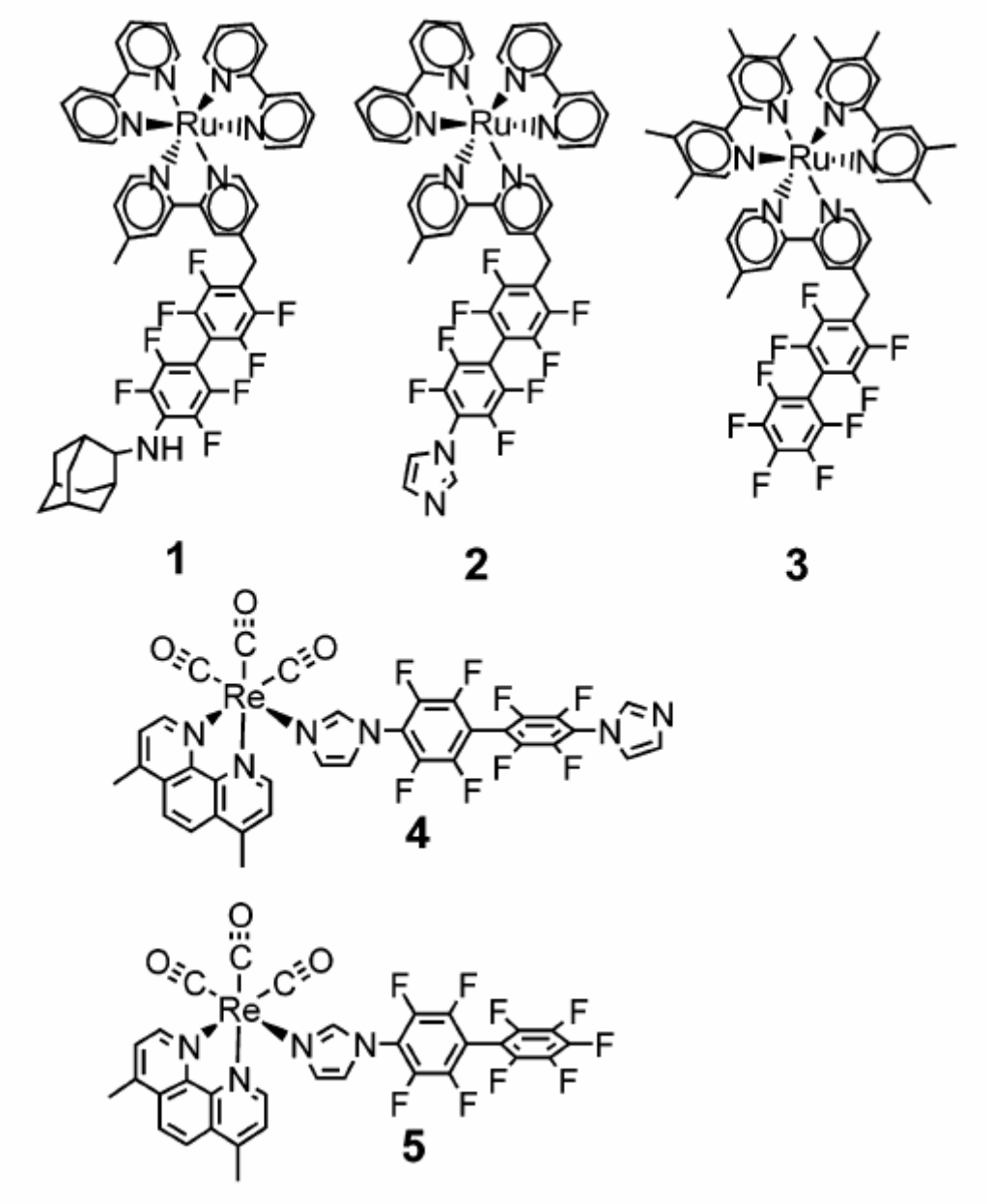

Figure 11. Ru-wires (**1**-**3)** and Re-wires (**4**, **5)** bind iNOSoxy; they also bind cytochrome P450cam (Appendix B).[65]

Experimental

Murine inducible NOS oxygenase domain constructs with N-terminal truncations at residues 65 (Δ65) and 114 (Δ114) were prepared as previously described.[35] Small aliquots of the protein solutions were exchanged into phosphate buffer (50 mM potassium phosphate, 100 mM potassium chloride pH 7.2) using a desalting column immediately before use. The measurement of the heme Soret peak at 422 nm verified successful removal of the dithiothreitol (DTT) present in the storage buffer.

High-spin, dimeric Δ65 iNOS was generated by incubating Δ65 with 1 mM tetrahydrobiopterin (H_4B) and 1 mM arginine (Arg) for 2 h at 4 °C before diluting the sample to final concentrations of 0.1 mM H_4B and 1 mM Arg. Satisfactory Arg and H_4B binding was signaled by a shift of the Soret to 396 nm. NOS extinction coefficients were determined using the hemochromogen assay: 1 mL of NOS solution was diluted with 0.125 mL 0.5 M NaOH and 0.125 mL pyridine, then reduced with several grains of sodium dithionite. The resulting ferrohemochromogen concentration was calculated using an extinction coefficient of 31 mM^{-1} cm^{-1} at 556 nm. The assays were calibrated using cytochrome P450cam (ε_{416} = 115 mM^{-1} cm^{-1}).[131] The NOS extinction coefficients calculated using this method are substrate-free Δ65 (-H4B, -Arg) ε_{422} = 75 mM^{-1} cm^{-1}, Δ65 (+H4B, +Arg) ε_{396} = 75 mM^{-1} cm^{-1}, and substrate-free Δ114 ε_{422} = 85 mM^{-1} cm^{-1}.

Ru-wires (**1**-**3**) were prepared by the literature procedure.[69] The fluorinated biphenyl bridging moieties for Re-wires **4** and **5** were synthesized by reacting imidazole and perfluorobiphenyl in dimethylsulfoxide. The resulting mono- and disubstituted perfluorobiphenyl-imidazole ligands were separated by flash silica chromatography.

Re(dimethylphenanthroline)$(CO)_3Cl$ was treated with silver triflate, and then reacted with either the mono- or disubstituted perfluorobiphenyl-imidazole ligand to form **4** and **5** as triflate salts (Chapter 3).[68]

Both time-resolved and steady-state spectroscopic measurements were performed as previously described.[65] Luminescence decay profiles were fit to a biexponential function (Equation 1):

$$I(t) = c_1 e^{-k_1 t} + c_2 e^{-k_2 t} \qquad (5)$$

using a nonlinear least squares algorithm. The ratio of enzyme-bound to free ruthenium complex is c_1/c_2, where k_1 and k_2 are the luminescence decay rate constants for the enzyme-bound and free ruthenium complexes. Dissociation constants were derived from c_1/c_2 as previously described.[65]

Characteristic FET distances (R_0) for the Ru- and Re-diimine wires with iNOSoxy were calculated from the probe emission and NOS absorption spectra (Figure **12**).[65] These distances are: 24.3 Å, **1** and **2** with Δ114; 19.6 Å, **3** with Δ114; 32 Å, **4** and **5** with Δ114; 24.3 Å, **1** and **2** with substrate-free Δ65; 19.5 Å, **3** with substrate-free Δ65; 23.9 Å, **1** and **2** with Arg- and H_4B-bound Δ65; 19.3 Å, **3** with Arg- and H_4B-bound Δ65.

Results and Discussion

Ru-Wires

Two murine iNOSoxy truncation mutants Δ114 and Δ65 were investigated. Importantly, Δ114 is predominantly monomeric, while Δ65 exists in a monomer-dimer equilibrium, forming a strong dimer in the presence of H_4B.[35] For clarity, both Δ65 without bound H_4B and Δ114 are referred to below as "monomeric." Monomeric

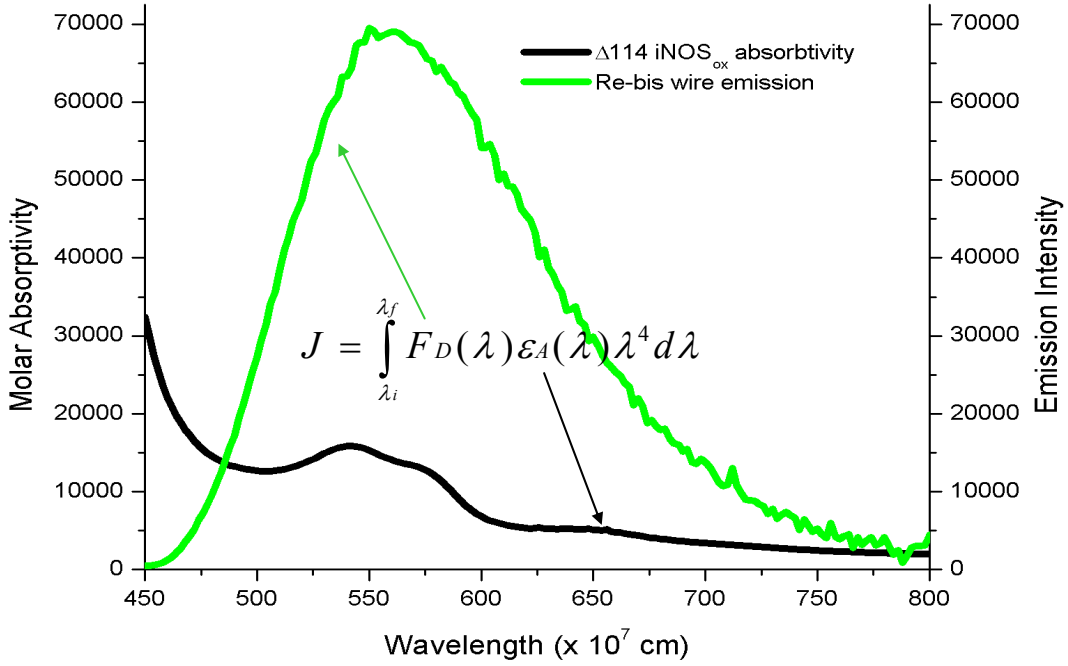

Figure 12. Overlap of the low-spin Δ114 iNOSoxy Q-band absorbance (reported as molar absorptivity, black) and the normalized emission spectrum of Re-Im-F_8bp-Im (green). The integral (J) under the overlapping sections of the donor emission and acceptor absorbance is used to calculate the characteristic Förster energy transfer distance (R_0) for the wire:NOS conjugate.

iNOSoxy has an exposed active site (see below), while dimeric iNOSoxy has a much more constricted substrate access channel.

No change in the iNOSoxy heme absorption spectrum was observed upon stoichiometric addition of **1** or **3** to either Δ114 or Δ65. In contrast, the addition of excess **2** to Δ114 or monomeric Δ65 (-H_4B, -Arg) resulted in a heme Soret shift from 420 or 422 to 426 nm, consistent with imidazole ligation of the heme (Figure **13**). The absorption spectrum of dimeric Δ65 (+H_4B, +Arg) was not altered in the presence of **1**-**3**, indicating that none of the Ru-wires displace Arg from the dimeric iNOSoxy active site.

In all cases, biexponential Ru-wire luminescence decays were observed in the presence of stoichiometric Δ114 or Δ65, indicating that the Ru-wires bind to the enzyme (Figures **14** and **15**). Quenching of the Ru-wire excited state could in principle occur by either energy or electron transfer to the iNOSoxy heme. Since no electron transfer products were observed by transient UV-visible absorption spectroscopy, and because the rate of luminescence quenching is consistent with FET, energy transfer is the probable mechanism of Ru-wire luminescence quenching. The weightings of the fast and slow luminescence decay phases were used to calculate dissociation constants, while the rates of energy transfer were used to calculate Ru to heme-Fe distances. Ru-Fe distances so obtained for Ru-wire:P450cam conjugates matched those observed in the corresponding crystal structures to within 0.4 Å.[63]

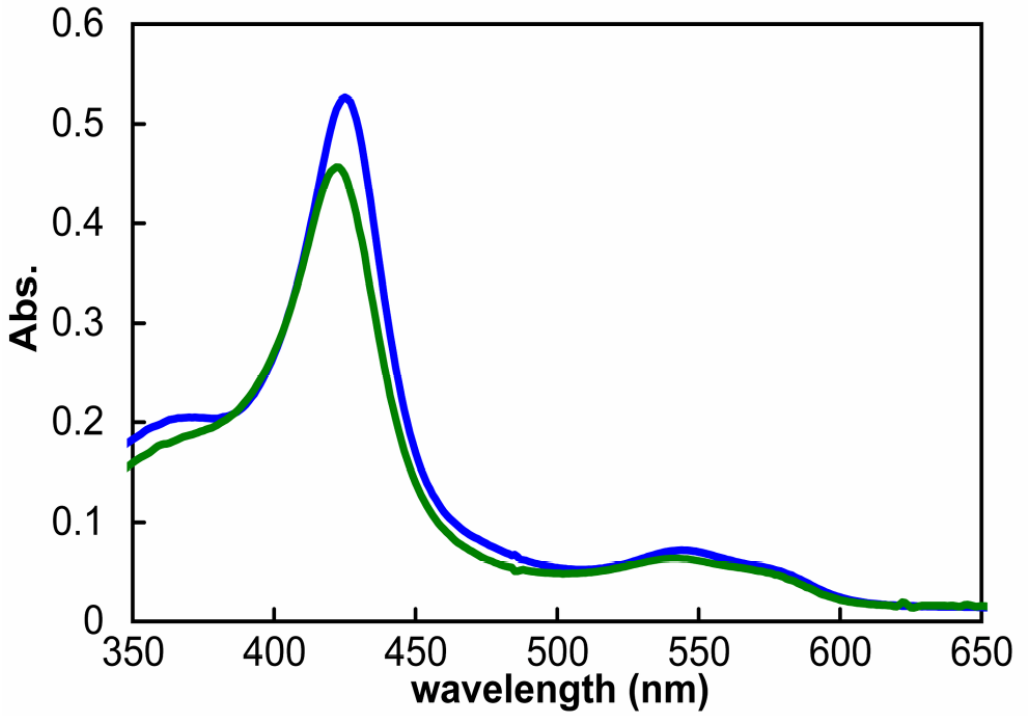

Figure 13. UV-visible absorption spectrum of Δ114 alone (5.7 μM; green) and bound to **2**, corrected for the absorption attributable to the Ru-wire (+ 20.5 μM **2**; blue).

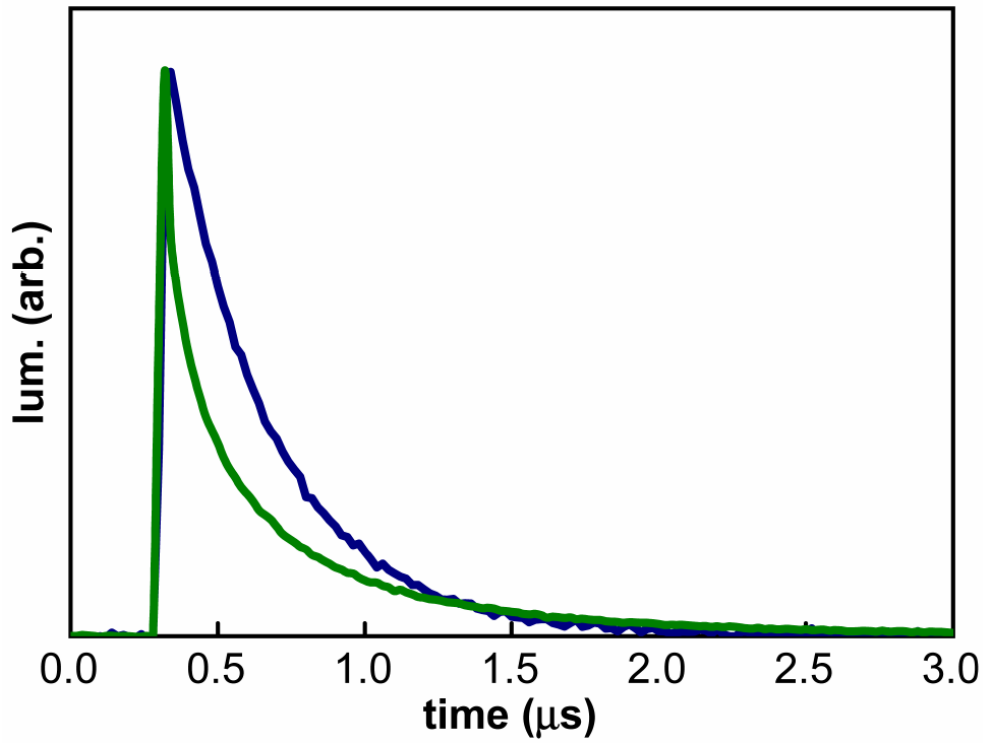

Figure 14. Sample transient luminescence decay data for **1** (blue) and a 1:1 mixture of **1** and Δ65 (1.8 μM; green). The fast component of the luminescence decay corresponds to **1** bound to Δ65.

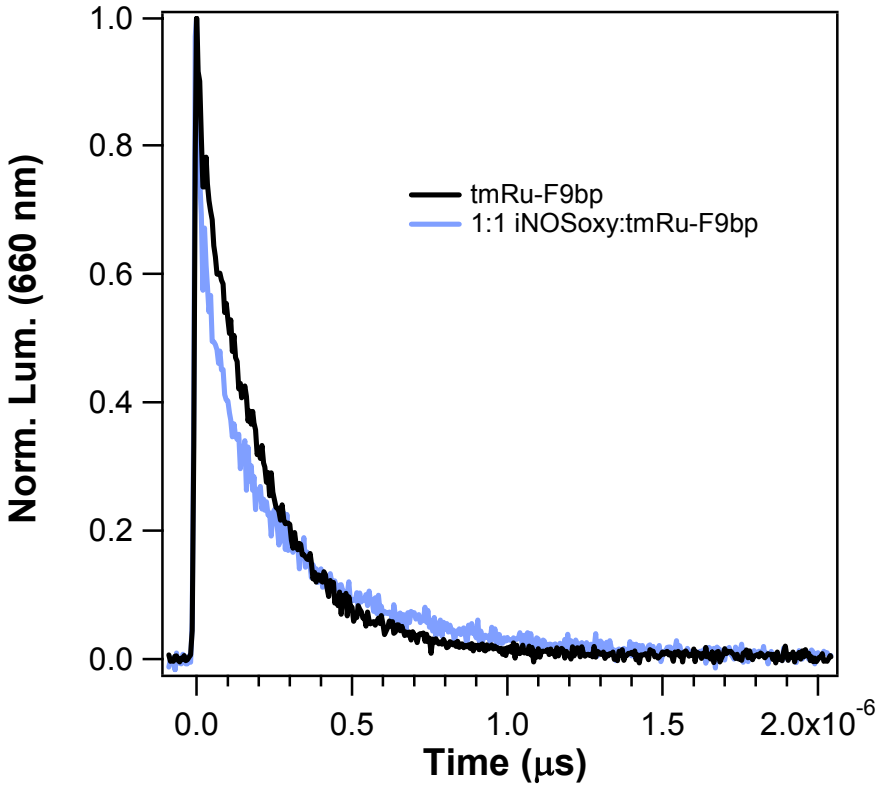

Figure 15. Transient luminescence of **3** (10 μM) in the presence (light blue) and absence (black) of one equivalent of Δ65 iNOSoxy. The light blue trace shows a biexponential decay indicative of wire bound to the enzyme and wire free in solution. λ_{ex} = 480 nm.

The Ru-wires bind with micromolar dissociation constants and with Ru-Fe distances of 18-21 Å (Table **1**). Interestingly, **1** and **3** bind Δ114, Δ65, and dimeric Δ65 (+ H_4B, + Arg) with dissociation constants that are virtually identical. The Ru-Fe distances calculated for **1** and **3** are similar for Δ114 and Δ65, and are unaffected by the presence of H_4B and Arg (Table **1**).

The spectroscopic evidence suggests that **1** and **3** do not bind in the active site: the heme absorption spectrum is not altered in the presence of **1** or **3**, and the K_d's and Ru-Fe distances determined for these Ru-wires are not altered by the addition of H_4B and Arg. Addition of stoichiometric **4**, which binds in the iNOS active site (see below), does not alter the binding of **3** to monomeric Δ65, again demonstrating that **3** does not bind in the active site (Figure **16**).

Consistent with these data, modeling suggests that **1** and **3** cannot fit into the substrate access channel of dimeric Δ65 (+H_4B, +Arg), owing to the bulk of the ruthenium tris-bipyridyl moiety. Instead, the calculated Ru-Fe distances indicate that **1** and **3** may bind on the distal side of the enzyme, at the proposed binding site of the reductase module (Figure **17**b).[28] The proposed binding site is concave and hydrophobic. The Ru-wires present few opportunities for specific interactions with the protein surface. Instead, extensive wire:protein hydrophobic contacts likely mediate binding. Of interest in this regard is that other Ru(II)-diimines bind cytochrome *c* oxidase at the physiologically relevant cytochrome *c* binding site.[132, 133]

Table 1. Ru-wire dissociation constants and Ru-Fe distances from FET kinetics. Uncertainties are the root-mean-square deviations calculated from independent measurements (3 for Δ114, 2 for Δ65, 3 for Δ65 + Arg, + H_4B).

	Δ114		Δ65		Δ65 + Arg +H_4B	
Cmpd	K_d (μM)	Ru-Fe (Å)	K_d (μM)	Ru-Fe (Å)	K_d (μM)	Ru-Fe (Å)
1	0.88 ± 0.15	18.9 ± 0.1	0.54 ± 0.04	19.6 ± 0.2	1.7 ± 0.4	19.6 ± 0.4
2	7.1 ± 0.4	17.8 ± 0.5	6.5 ± 2.4	19.3 ± 0.6	7.2 ± 3.4	20.9 ± 0.8
3	0.71 ± 0.09	20.1 ± 0.1	0.58 ± 0.16	20.2 ± 0.4	0.89 ± 0.15	21.0 ± 0.3

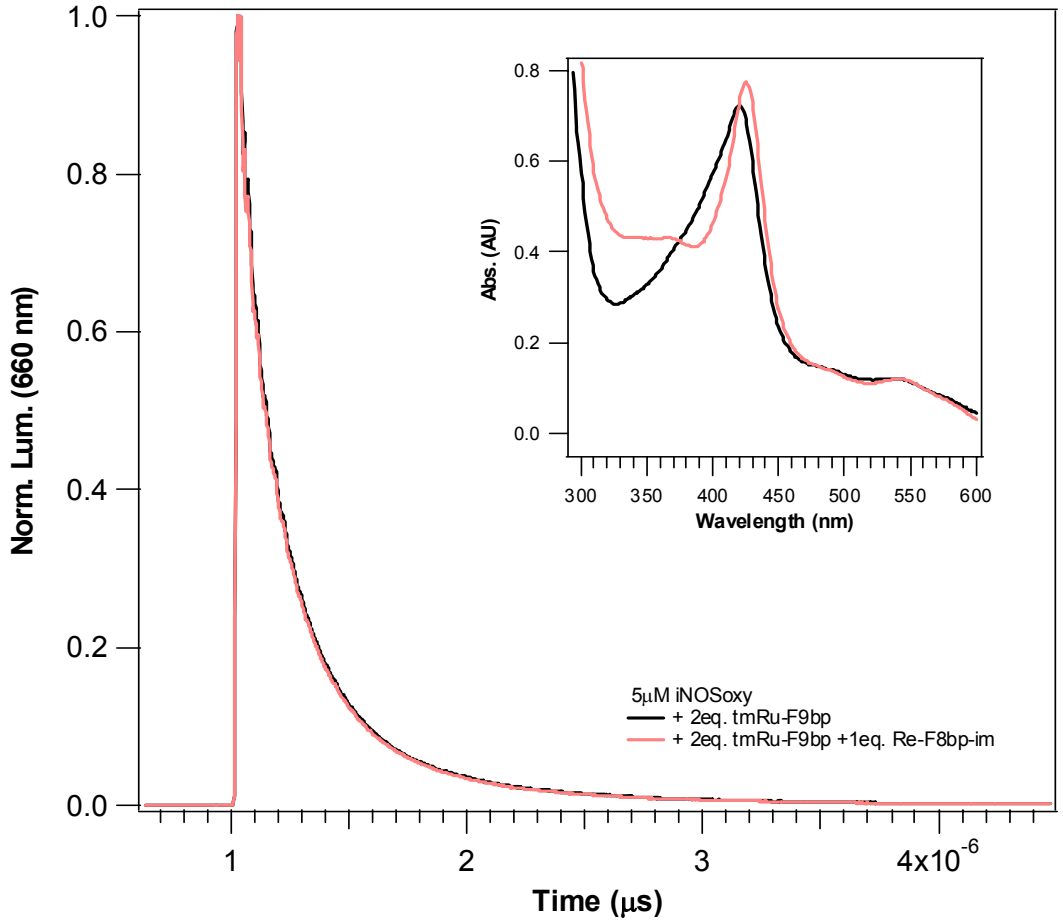

Figure 16. Luminescence decay (λ_{ex} = 480 nm) of excess tmRu-F_9bp bound to iNOSoxy (5 μM) in the absence (black) and presence (red) of one equivalent of Re-Im-F_8bp-Im showing that the presence of the channel-binding wire does not affect the binding of tmRu-F_9bp. Inset: UV/visible absorption spectrum of iNOSoxy:tmRu-F_9bp in the absence (black) and presence (red) of one equivalent of Re-Im-F_8bp-Im, corrected for absorption due to tmRu-F_9bp. This spectrum confirms that Re-Im-F_8bp-Im is binding in the channel.

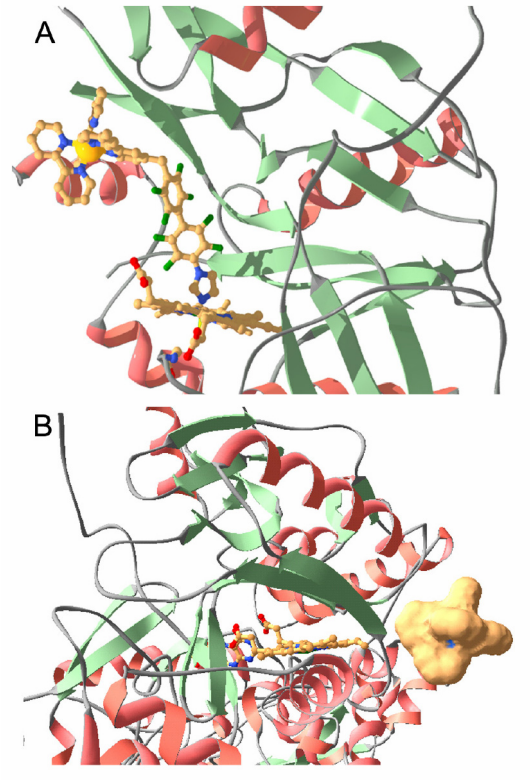

Figure 17. A) Model of **2** bound to the exposed heme of monomeric Δ114. The Ru-Fe distance in this model is 16.9 Å. B) The NOS dimer, shown with $Ru(bpy)_3$ (van der Waals surface) docked at the proposed reductase binding site. The Ru-Fe distance is ~19 Å, consistent with the Ru-Fe distances measured for the Δ65:**1** and Δ65:**3** conjugates.

In contrast, the shifts in the absorption spectra of monomeric Δ65 and Δ114 in the presence of excess **2** clearly indicate that the imidazole of **2** ligates the heme (Figures **13**, **17**a).[36] Structural modeling suggests that the less bulky **2**, which lacks the adamantyl group of **1** and the tetramethylbipyridine ligands of **3**, can bind in the more exposed active site of monomeric iNOSoxy (Figure **17**a). However, **2** may also bind iNOSoxy at the site occupied by **1** and **3**: 1.5 equivalents of **2** bind to monomeric Δ65 (-H_4B, -Arg) when the Ru-wire is present in 6-fold excess, and **2** binds to dimeric Δ65 (+H_4B, +Arg), in which the active site is occupied. In contrast to **1** and **3**, the Ru-Fe distances determined for the **2**:Δ114 and **2**:Δ65 +H_4B +Arg conjugates increase markedly from 17.8 to 20.9 Å, suggesting a different mode of binding to monomeric (Δ114) and dimeric (Δ65 +H_4B +Arg) iNOSoxy. These data together suggest that **2** binds to both the active site of monomeric iNOSoxy and another portion of the protein with similar K_d's.

Re-Wires

Luminescent rhenium diimines, $[Re(CO)_3L_2L_2']+$, where L_2 is a 2,2'-bipyridyl or phenanthryl derivative and L_2' is a nitrogen donor such as imidazole or pyridine, typically have microsecond excited state lifetimes. Like $Ru(bpy)_3^{2+}$, the excited states are both good oxidants (~1.2 V vs. NHE) and reductants (-0.7 V vs. NHE).[134] In addition, photochemically generated $[Re(CO)_3(L_2)(L')]^{2+}$ complexes are extremely strong oxidants (~1.8 V vs. SCE).[135]

In order to take advantage of rhenium photochemistry, we synthesized Re-wires **4** and **5** (Figure **11**). The complexes are structurally similar to **1** and **3**, but the Re-photosensitizer is smaller. The surface areas of the core lumophores $[Ru(bpy)_3]^{2+}$ and

$[Re(CO)_3(dimethylphenanthroline)(imidazole)]^+$ are 650 and 550 Å^2.[136] Additionally, the *fac*-carbonyls of **4** and **5** result in a more compact profile on one side of the complex, allowing a closer approach to the protein. The virtually identical absorption spectra of **4** (Figure **18**) and **5** are typical of Re-diimines. Both complexes are luminescent, with emission spectra centered at 560 nm (quantum yields are 0.055 in phosphate buffer).

Upon addition of **4** to Δ114 murine iNOSoxy, the Soret shifts from 422 to 426 nm, signaling imidazole ligation to the heme iron (Figure **19**b). Time-resolved luminescence measurements indicate that **4** is almost completely bound to NOS in 1:1 micromolar solutions (Figure **20**). Indeed, a K_d could not be determined from the luminescence decay data due to the rapidity of the decay[§] and the almost complete absence of a slow decay rate corresponding to free **4** in solution. Instead, a dissociation constant of 100 ± 80 nM was calculated from a comparison of the steady-state luminescence spectra of **4** alone and bound to Δ114 iNOSoxy (Figure **21**).

Re-wire **5** causes a blue-shift in the Δ114 Soret, indicating partial conversion to a high-spin, 5-coordinate heme (Figure **19**a). In addition to a small shift in peak wavelength, a noticeable shoulder appears in the Soret, consistent with partial displacement of the iron-ligating water from the active site. The time-resolved luminescence decay spectra (Figure **22**) suggest that **5** binds with a dissociation constant of 5 ± 2 μM and a Re-heme distance of ~18 Å. Both the change in the Soret

[§] Initial data suggest that the luminescence quenching is attributable to rapid electron transfer (see Chapter 3).

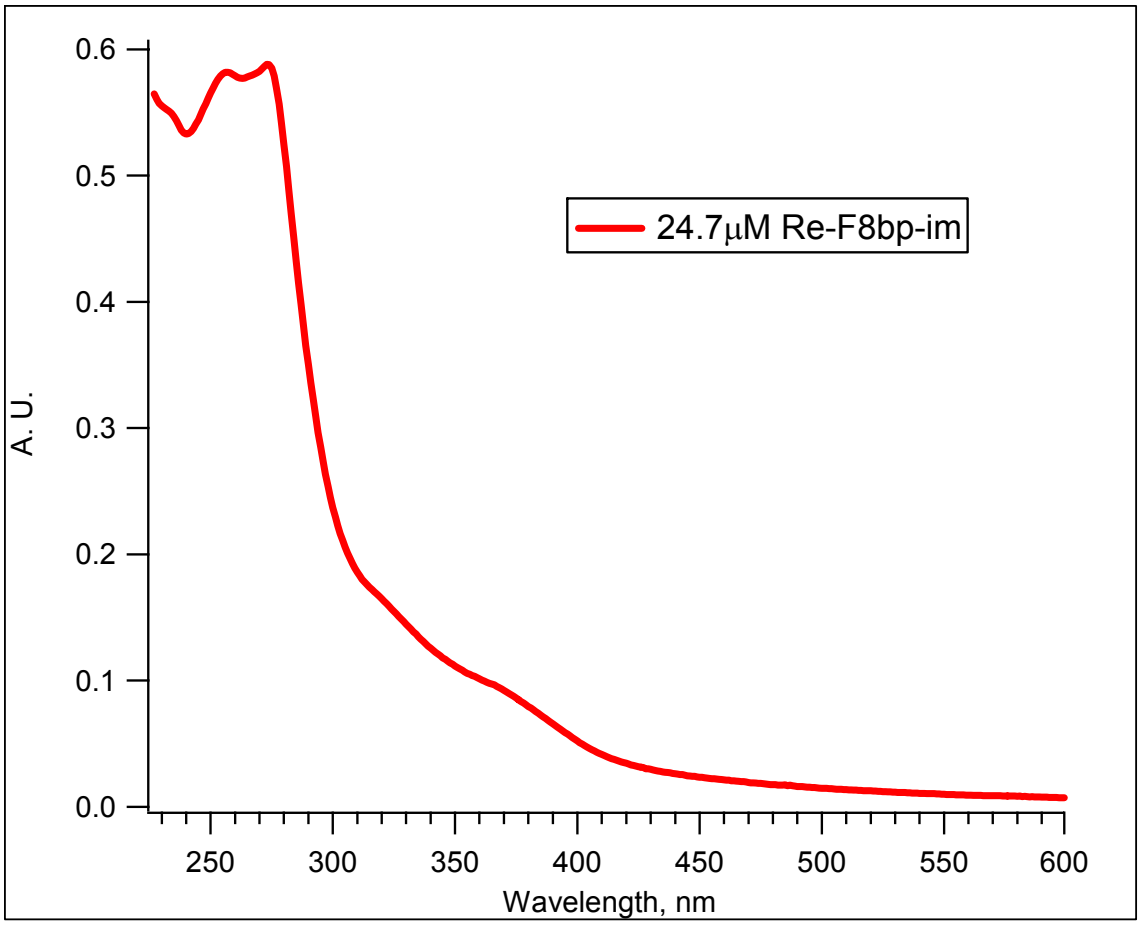

Figure 18. UV/visible absorption spectrum of Re-Im-F_8bp-Im (25 μM in buffer). The absorption spectrum of Re-Im-F_9bp shows slightly less intense π-π* bands from 250-280 nm, but nearly identical MLCT bands between 310 and 400 nm.

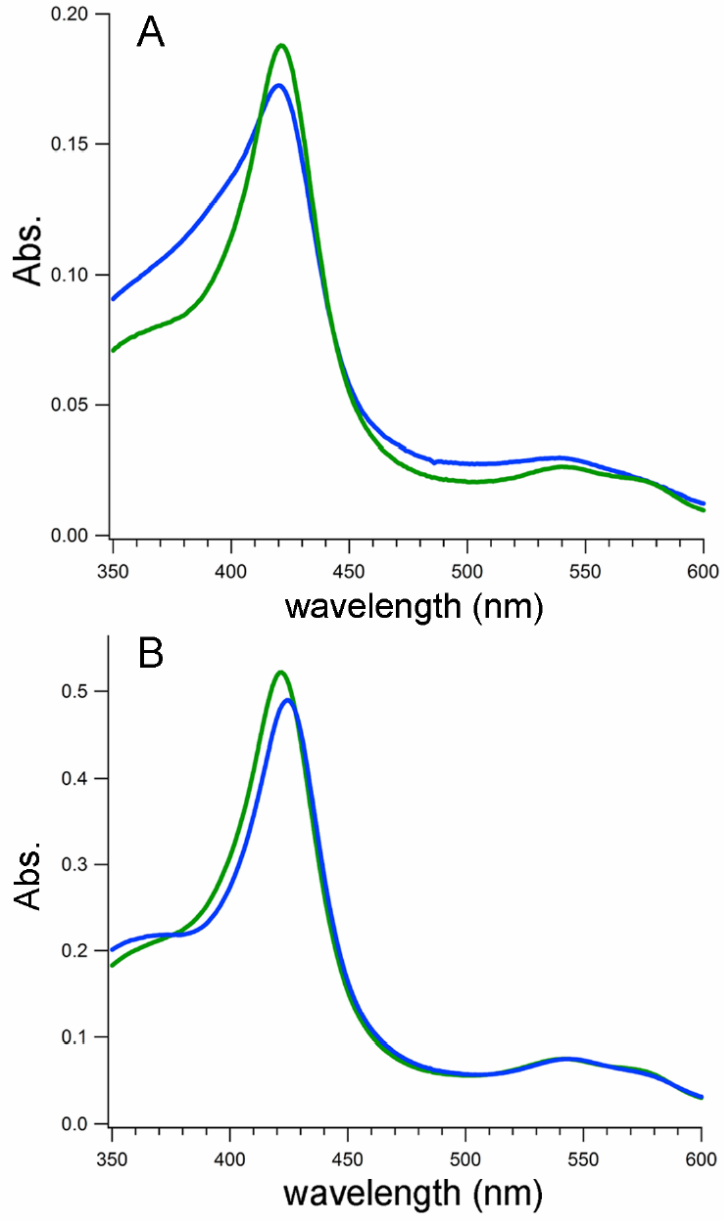

Figure 19. A) 2.2 μM Δ114 alone (green) and with stoichiometric **5** (blue). Both the slight shift in peak wavelength and development of a pronounced shoulder indicate partial conversion to high-spin, five-coordinate heme. B) 6.0 μM Δ114 alone (green) and with stoichiometric **4** (blue). The red-shift in peak wavelength is consistent with imidazole ligation of the heme.

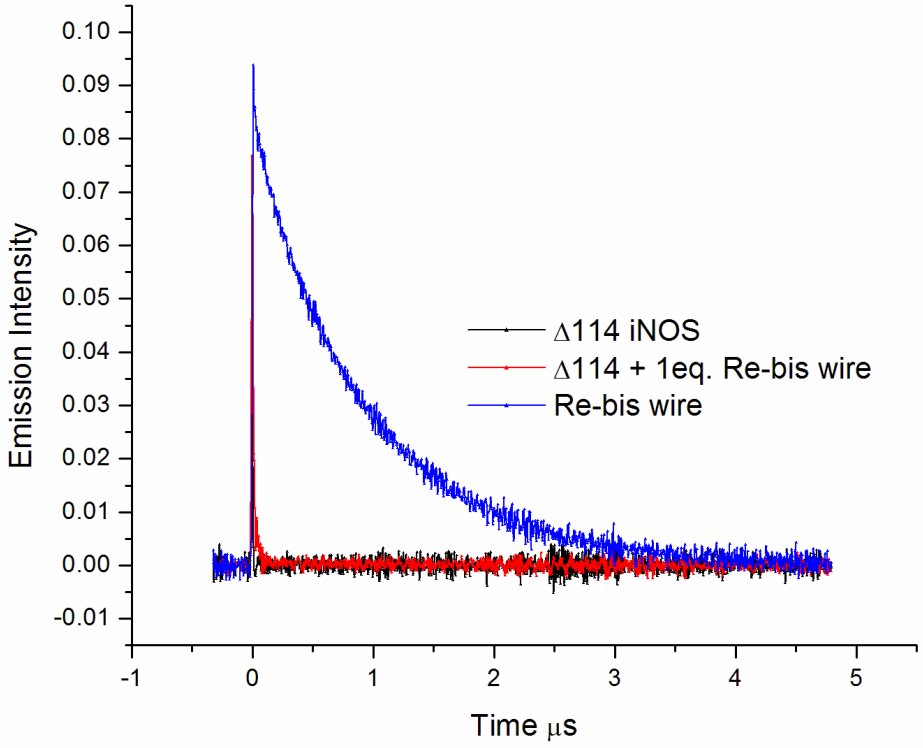

Figure 20. Transient luminescence of Re-Im-F_8bp-Im alone (10 μM, blue), and in the presence of one equivalent of Δ114 iNOSoxy (red) at 575 nm (λ_{ex} = 355 nm). These data indicate that, at this concentration, Re-Im-F_8bp-Im is almost completely bound to Δ114 iNOSoxy.

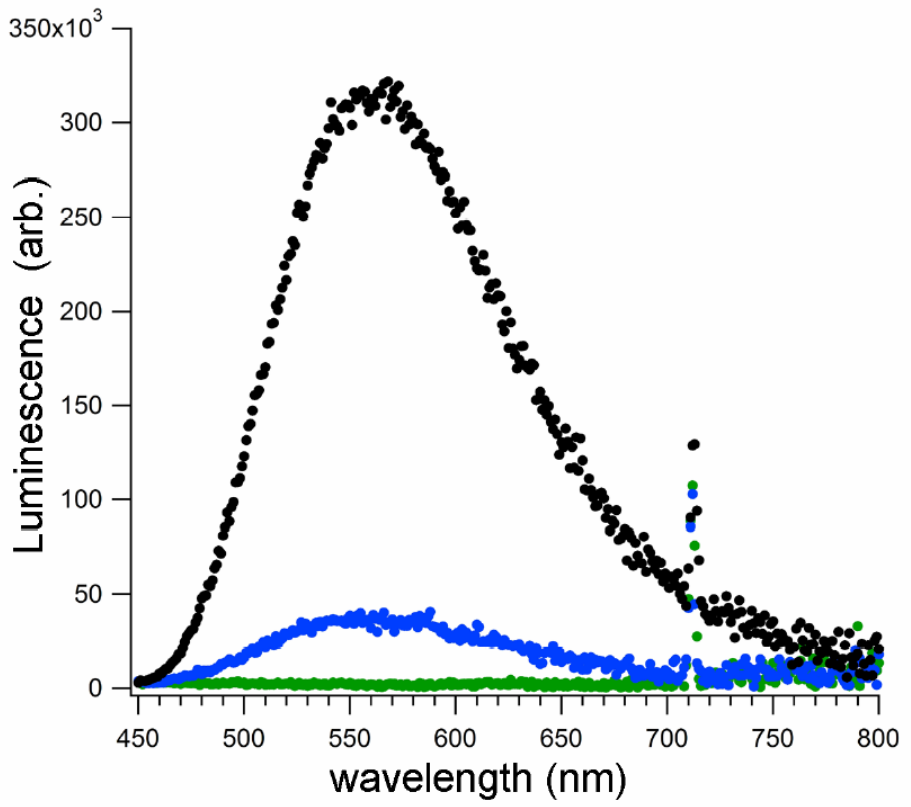

Figure 21. Steady-state luminescence spectra of 2.6 μM samples of Δ114 (green), **4** (black), and a 1:1 mixture of Δ114 and **4** (blue). The luminescence of **4** is strongly quenched in the presence of Δ114, making it a sensitive indicator of the presence of the enzyme. The sharp spike at 710 nm is an artifact arising from scattered 355-nm excitation light.

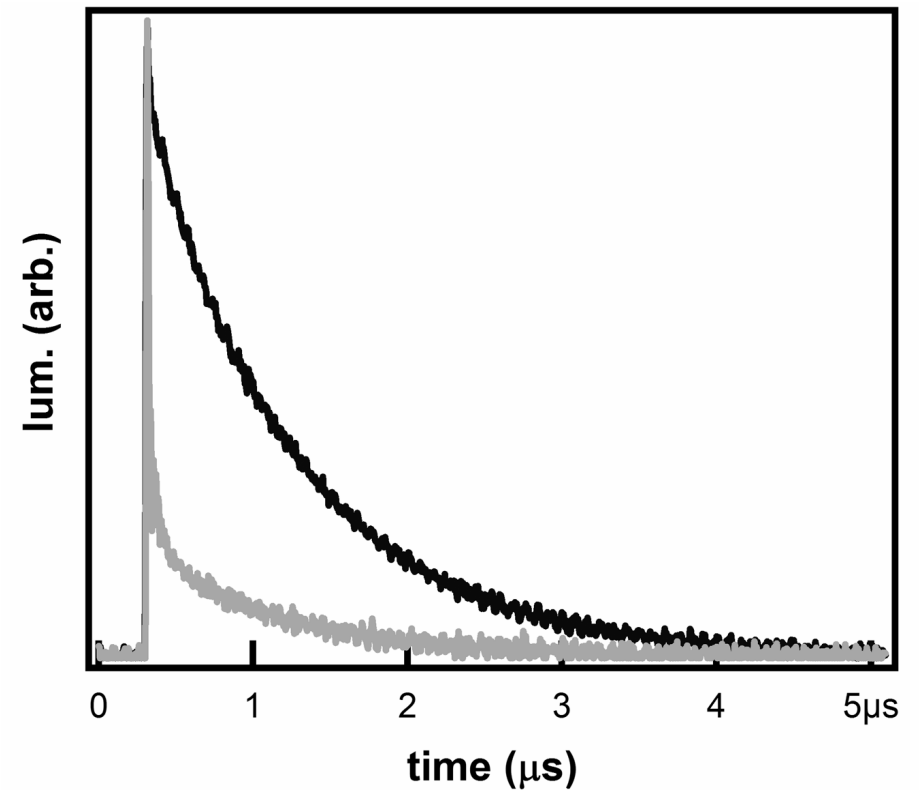

Figure 22. Transient luminescence decay at 575 nm for **5** (black) and a 1:1 mixture of **5** and Δ114 (9 μM, gray). The fast component of the luminescence decay corresponds to **5** bound to Δ114. λ_{ex} = 355 nm.

absorption band and the calculated Re-Fe distance are consistent with **5** binding in the active site. Structural modeling indicates that **5** can fit in the active site of monomeric iNOSoxy, unlike the sterically bulkier **3**. The structural dissimilarities of **5** and Arg make it surprising that **5** binds at all. However, the relatively exposed active site of the monomeric Δ114 iNOSoxy provides good surface complementarity with the fluorinated biphenyl moiety.

Concluding Remarks

Small molecules that interfere with NOS function are being investigated as potential treatments for several diseases.[137, 138] All currently known inhibitors in this class bind in the active site of the enzyme. In contrast, Ru-wires or similar compounds may provide an effective means of NOS inhibition by preventing electron transfer between the reductase module and oxygenase domain. Inhibitors that disrupt protein:protein interactions could be of great value, owing to the biological ubiquity of transient protein complexes.

The interactions of **2** and **4** with Δ114 are in many ways analogous to those observed with small molecules that prevent NOS holoenzyme dimerization.[32] Because only iNOS exhibits an appreciable monomer-dimer equilibrium *in vivo*, these inhibitors are highly isoform selective.[32] The low dissociation constant of **4** makes it a useful lead compound for further development. The ~70-fold difference in dissociation constants between **2** and **4** illustrates the steric influence of the $Ru(bpy)_3$ moiety.

The ability of **5** to bind in or near the iNOSoxy active site is remarkable given its dissimilarity to Arg or known inhibitors. As with the Ru-wires, it seems likely that

binding is driven principally by hydrophobic interactions. Although **3** binds more tightly than **5** to NOS, it does not produce a similar shift in the absorption spectrum, again demonstrating the importance of steric bulk in modulating wire-NOS interactions.

Most notably, we have shown the usefulness of FET kinetics in characterizing small-molecule:protein interactions. Conventional UV-visible absorption measurements or competition binding assays would have overlooked the ability of **1** and **3** to bind iNOSoxy. What is more, FET measurements yield distance constraints, which provide additional information about the interaction between the wire and target enzyme. As demonstrated by these results, FET data greatly facilitate the formulation of structural models for wire:enzyme conjugates.

CHAPTER 3:

PICOSECOND PHOTOINDUCED REDUCTION OF INDUCIBLE NITRIC OXIDE SYNTHASE BY RE-DIIMINE WIRES[†]

 Belliston-Bittner, W., Dunn, A. R., Nguyen, Y. H. L., Stuehr, D. J., Winkler, J. R., and Gray, H. B., *J. Am. Chem. Soc.*, **submitted**.

Acknowledgement:

Yen Nguyen synthesized the two longer wires (Re-C_3-F_9bp and Re-C_3-F_8bp-Im) that are discussed in this paper.

Chapter 3

PICOSECOND PHOTOINDUCED REDUCTION OF INDUCIBLE NITRIC OXIDE SYNTHASE BY RE-DIIMINE WIRES

Abstract

In a continuing effort to unravel mechanistic questions associated with metalloenzymes, we are developing methods for rapid delivery of electrons to deeply buried active sites. Herein, we report picosecond reduction of the heme active site of inducible nitric oxide synthase bound to a series of rhenium-diimine electron-tunneling wires, $[Re(CO)_3LL']^+$, where L is 4,7-dimethylphenanthroline and L' is a perfluorinated biphenyl bridge connecting a rhenium-ligated imidazole or aminopropylimidazole to a distal imidazole (F_8bp-im (**1**) and C_3-F_8bp-im (**2**)) or F (F_9bp (**3**) and C_3-F_9bp (**4**)). All four wires bind tightly (K_d ~ μM to nM) to the tetrahydrobiopterin-free oxidase domain of inducible nitric oxide synthase (iNOSoxy). The two fluorine-terminated wires displace water from the active site, and the two imidazole-terminated wires ligate the heme iron. Upon excitation with 355 nm light, the fluorescence of bound **1**, **2**, and **4** is quenched in less than 200 ps. When a through-bond pathway from the rhenium to the heme iron exists, the active site Fe(III) is then reduced to Fe(II) within 300 ps, almost ten orders of magnitude faster than the naturally occurring reduction.

Introduction

Nitric oxide synthase (NOS) is a P450-type iron-heme enzyme that catalyzes the synthesis of nitric oxide (•NO) and L-citrulline from L-arginine and O_2.[122] There are at least three types of NOS expressed by mammals. Two, neuronal NOS (nNOS) and endothelial NOS (eNOS), are constitutive. The third, inducible NOS (iNOS), is expressed transiently in a variety of cells as a response to immunostimulation.[139] Owing mainly to the role •NO plays as a signaling molecule in an astonishing number of bodily processes, NOS malfunction is implicated in a wide array of diseases.[19, 117, 118, 140, 141] Specifically, •NO overproduction by iNOS is involved directly in the pathology of inflammation in diseases such as rheumatoid arthritis, septic shock, atherosclerosis, and diabetes.[139, 141] These findings have brought NOS and its catalytic mechanism into the spotlight as targets of great pharmacological interest.

All three mammalian NOS enzymes exist *in vivo* as homodimers, with each monomer consisting of a C-terminal reductase module, an intervening calmodulin-binding domain, and an N-terminal oxidase domain.[20, 44] The reductase module of one subunit provides reducing equivalents to the catalytically active, heme-containing oxidase domain of the other subunit.[28] NOS turns over twice en route to •NO production. The mechanism of the first turnover (from L-arginine to *N*-hydroxy-L-arginine) is expected to be similar to that of P450, while the second turnover is believed to proceed differently (Figure **23**).[20, 42, 44, 45, 51] The first steps of each oxygenation are well-characterized, and include reduction of the heme followed by O_2 binding and a second reduction.[42, 50, 142] Because of the sluggishness of the second electron transfer (~12 s^{-1}),[42, 50, 142] and the speed of subsequent reaction(s), the ultimate active species remain elusive.[45, 57]

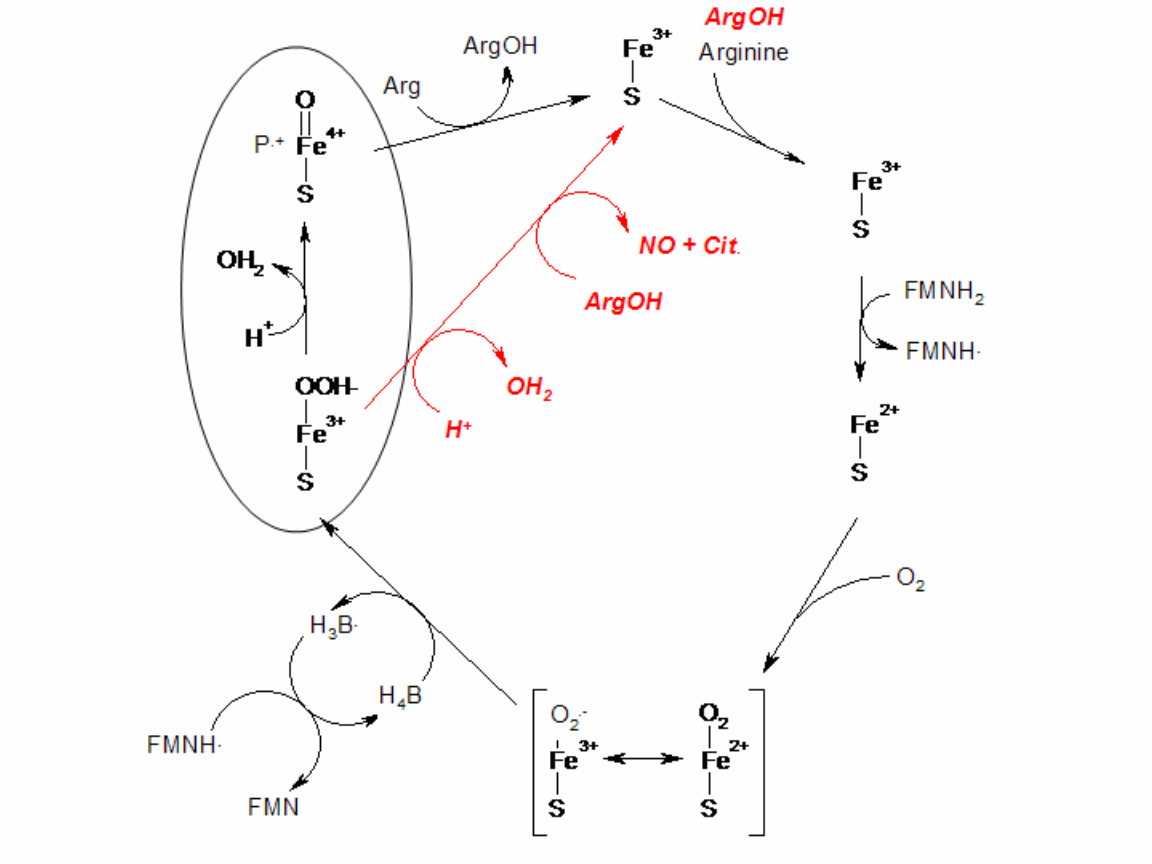

Figure 23. Proposed mechanisms for the first and second turnovers of NOS.[4, 20, 42, 45] Potential differences between the first and second turnovers are noted in red. The high-valent intermediates of particular interest to this work are in the upper left ellipse.

The long-term goal for our work with NOS is to use photoactive wires to trigger the second electron transfer in an attempt to observe these elusive, high-valent intermediates directly. In recent work, we took the first step toward this goal by building ruthenium- and rhenium-wires (Re wires **1** and **3**, Figure **24**) that bind tightly to the monomeric oxidase domain of iNOS (iNOSoxy).[143] These wires were based on complexes that had been shown previously to bind to and rapidly reduce P450cam upon photoexcitation.[62, 63, 65] The second step toward our goal is to accomplish fast, laser-triggered electron transfer to the heme. Herein, we report the synthesis of two new wires (**2** and **4**, Figure **24**) as well as picosecond photoinduced reduction of iNOSoxy (~3×10^9 s^{-1}), nearly ten orders of magnitude faster than the natural reduction.[43]

Results

Synthesis and Characterization of Wires

Nucleophilic substitution of decafluorobiphenyl proceeds readily (Figure **25**). Addition of 2 equivalents of nucleophile to decafluorobiphenyl will produce the doubly-substituted product (such as **7** in Figure **25**) in approximately 100 percent yield. In our hands, addition of fewer than two equivalents of nucleophile always produces a mixture of singly- and doubly-substituted products. These mixtures were easily separable by flash chromatography or sublimation.

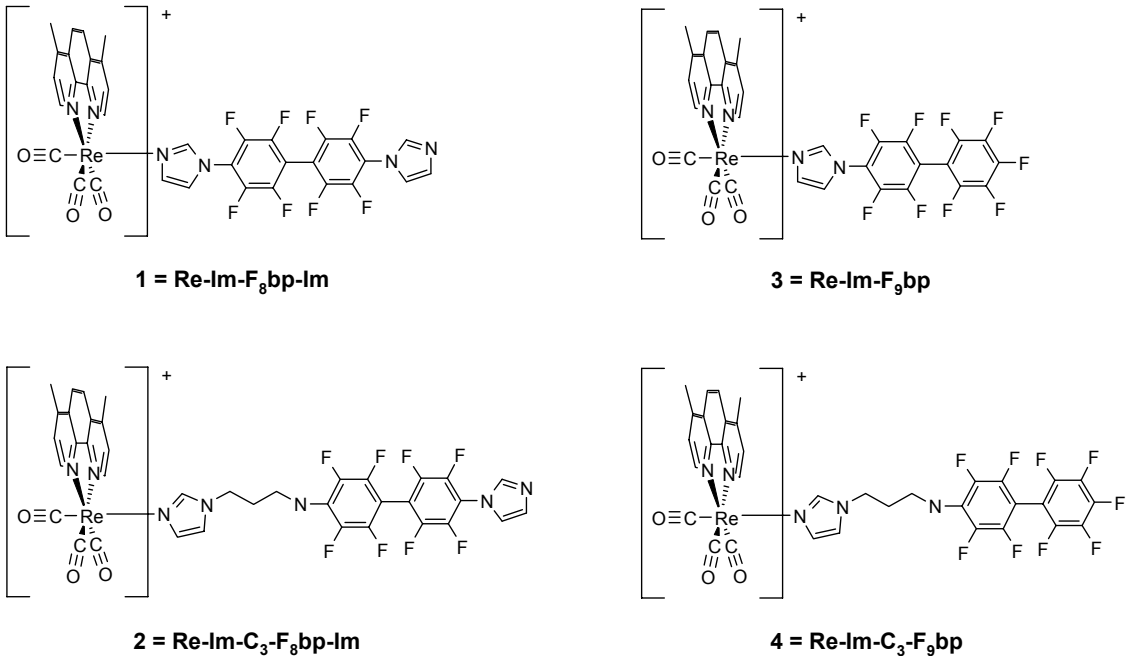

Figure 24. Re-wires that bind iNOSoxy. The luminescence of **3** is quenched by Förster energy transfer upon binding to the enzyme. The luminescence of bound **1**, **2**, and **4** is quenched too rapidly to be explained by energy transfer. Excitation of bound **1** and **2** triggers reduction of the enzyme within 300 ps.

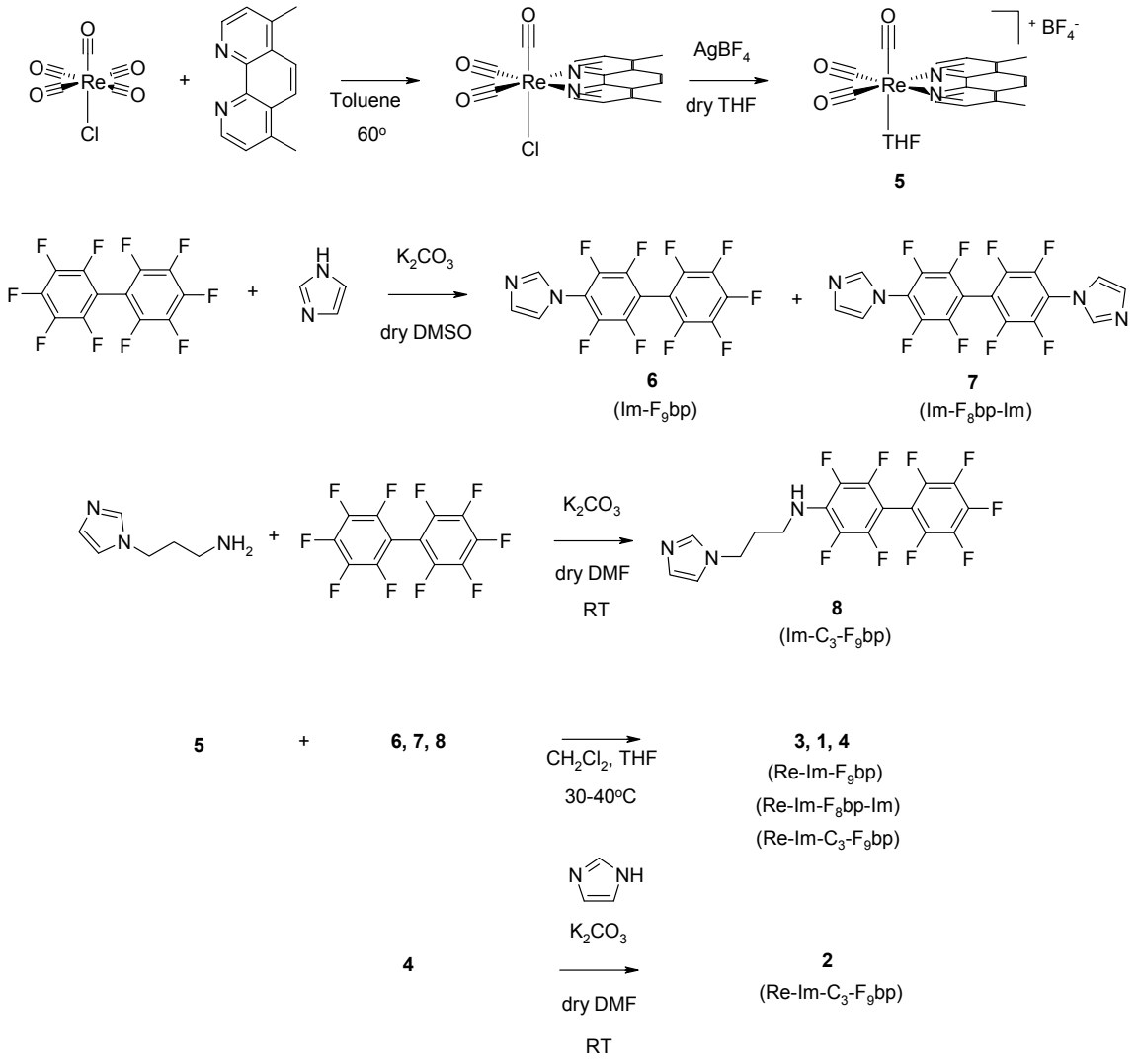

Figure 25. Synthesis of Re-diimine wires.

Ligation of imidazole-based complexes **6**, **7**, and **8** to rhenium is a slow and inefficient reaction. Attempts to speed up the reaction by heating above 40°C generally caused a decrease in yield. In some samples, the BF_4^- counterion was exchanged for trifluoromethanesulfonate (triflate, OTf^-) due to empirical observations that the triflate salts were easier to purify. Notably, there were no measureable differences in the solubility, protein binding, or photophysical properties of the triflate and BF_4^- salts. Graphical representations of the ^1H and ^{19}F NMRs of **1** and **3** and crystallographic data for the **3**BF_4^- complex can be found in Appendix A.

Typical of Re-diimines, all four complexes have very similar spectroscopic behavior with MLCT absorption bands centered at ~320 and 360 nm, emission maxima at 560 nm, and microsecond luminescence lifetimes (Table **2**). All four wires have 4-5 percent luminescence quantum yields in water and **1** and **3** have Förster distances (R_0) of 32±8 Å in the presence of Δ65 iNOSoxy. The 25 percent error in the FET calculations occurs due to the assumptions that κ^2 (see Experimental section, Equation 10) is equal to 2/3 and that n is 1.34 (the refractive index of water). The danger in setting $\kappa^2 = 2/3$ is that the rhenium and heme species are not likely to be freely rotating with respect to one another in this bound system. This restricted motion is less of a problem for calculating similar values for $Ru(bpy)_3$-based wires due to the existence of three perpendicular transition dipoles for the pseudo-octahedral $Ru(bpy)_3^{2+}$ species. The rhenium species being studied here, however, has a unidirectional transition dipole in the plane of the phenanthroline ligand. This suggests that assuming $\kappa^2 = 2/3$ could cause a large error in

Table 2. Re-wire characterization and dissociation constants in conjugates with Δ65 iNOSoxy. Except where noted, numbers in parentheses are standard deviations based on at least three separate measurements.

Wire	ε_{360} *(mM^{-1} cm^{-1})*	τ_L *(μs)*	ϕ	R_0 *(Å)*	K_d *with Δ65 (μM)*
1	4.1(4)	0.97(3)	0.055(2)	32(8)	0.13(7)
2[a]	5.0(4)	0.78(1)	0.04(1)[b]		< 10
3	4.1(6)	0.95(4)	0.054(1)	32(8)	1.4(5)
4[a]	4.3(4)	0.79(1)	0.042(6)[b]		< 10

a. Measured in 50 percent glycerol. *b*. Average of two measurements.

the calculated R_0 value. The largest error would occur if the rhenium transition dipole was oriented exactly perpendicular to that of the heme. In this case, κ^2 would be 0, and no FET would occur. Because quenching has been observed, this extreme case is unlikely. Otherwise, because the sixth root is taken to determine R_0, κ^2 values ranging from 1 to 4 produce ≤ 25 percent error in the calculation. Crystal structures of the wire-NOS complexes and anisotropy measurements could help to sort out this problem in the future, but given the current limited understanding of the orientation of the rhenium with respect to the heme in this system, the maximal 25 percent error was assumed. Some error could also come from assuming water as the solvent for this system. While the system was studied in buffer solution, the environment of the donor and acceptor is the protein channel. Because of the difficulty of determining the specific refractive index inside a protein and because the error due to the κ^2 factor is likely to be much greater, the error in n was not considered to be as important.

Wire Binding to Δ65 iNOS

All four complexes described above bind in the active site channel of Δ65 iNOSoxy. Imidazole-terminated wires **1** and **2** ligate the heme iron, causing a characteristic red shift in the Soret band. Fluorophenyl-terminated complexes **3** and **4** displace water from the active site, causing a partial (blue) shift toward high-spin Fe(III) (Figure **26**).

The **3**:Δ65 conjugate has a dissociation constant of 1.4 ± 0.5 μM, as determined by transient luminescence decay kinetics (Figure **27**b). These data are similar to those

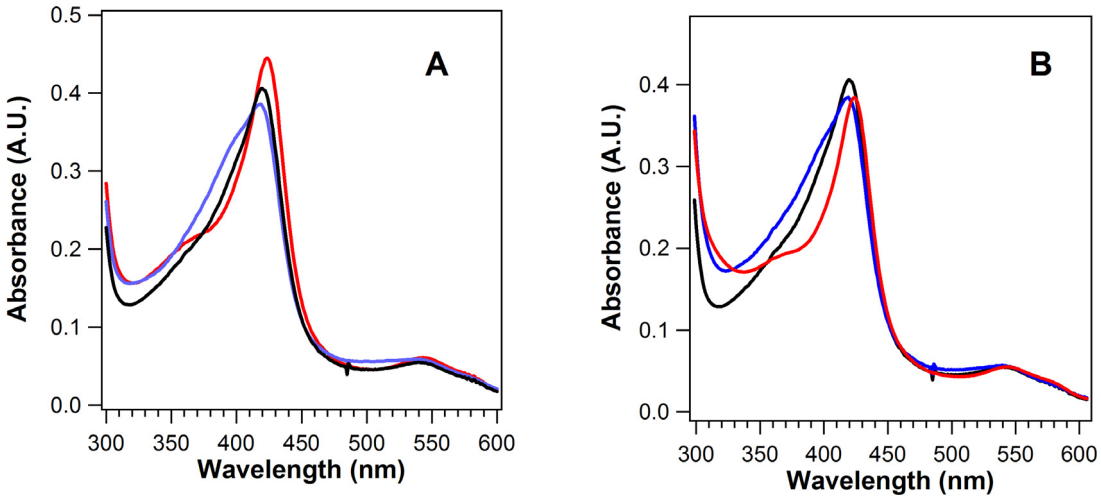

Figure 26. UV-visible absorption spectra of Δ65:wire complexes. A) Δ65 alone (5 μM; black) and bound to one equivalent each of **1** (Re-Im-F_8bp-Im; red) and **3** (Re-Im-F_9bp; blue). B) Δ65 alone (5 μM; black) and bound to approximately one equivalent each of **2** (Re-Im-C_3-F_8bp-Im; red) and **4** (Re-Im-C_3-F_9bp; blue).

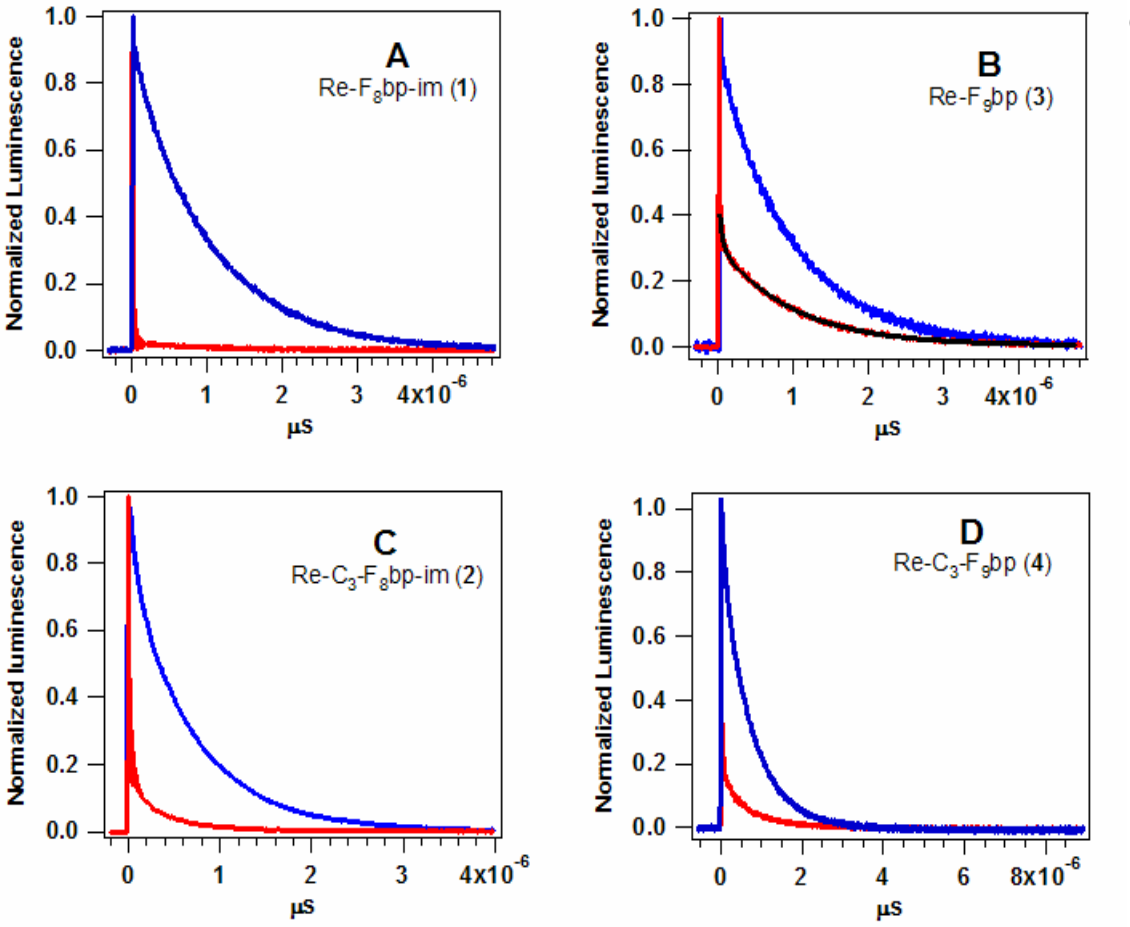

Figure 27. Transient luminescence decays of wires in solution and bound to Δ65 iNOSoxy. a) **1** (blue) and a 1:1 mixture of **1** and Δ65 (11 μM; red). The lack of an apparent slow decay indicates that almost all of the wire is bound to the enzyme. b) **3** (blue) and a 1:1 mixture of **3** and Δ65 (7 μM; red) and biexponential fit (k_L = 8(1) × 10^6 s^{-1}, k_0 = 1.0(3) × 10^6 s^{-1}, black). The fast component of the luminescence decay (k_L) corresponds to 3 bound to Δ65. c) **2** (blue) and a 1:1 mixture of **2** and Δ65 (5 μM; red). d) **4** (blue) and a 1:1 mixture of **4** and Δ65 (2 μM; red). In both C and D, the fastest component of the luminescence decay, corresponding to **2** or **4** bound to Δ65, is unresolvable on this timescale. The slower, visible, biexponential decay matches the

biexponential decay of the wire alone in water solution (blue trace) and likely corresponds to a mixture of free and aggregated wire (fits are shown in Figure **28**).

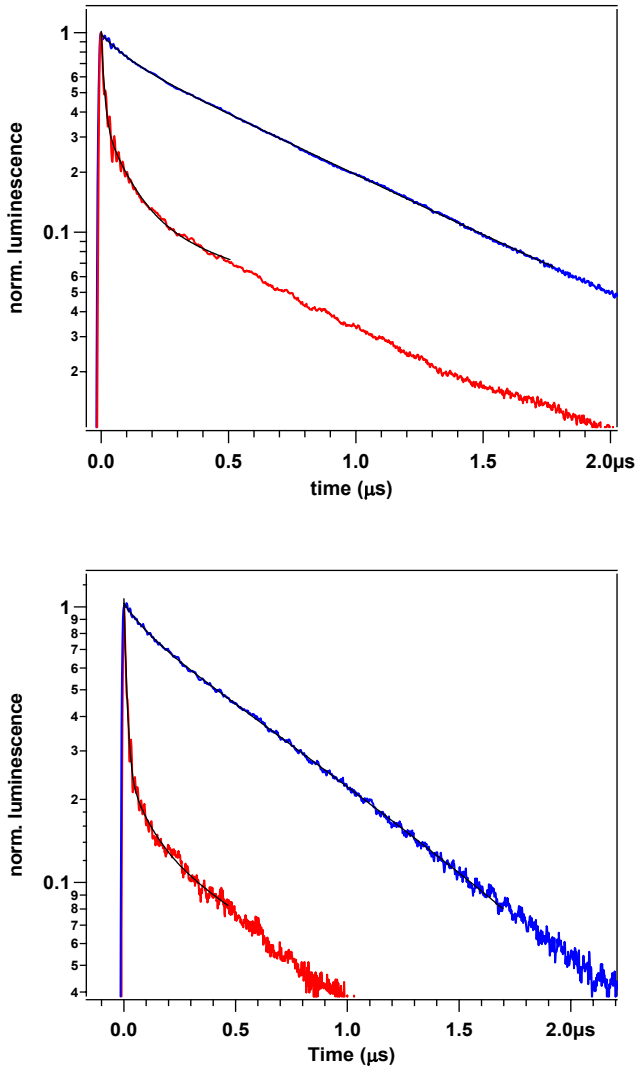

Figure 28. Semilog plot of luminescence at 560 nm vs. time for a) **2** (blue) and a 1:1 mixture of **2** and Δ65 (red) and b) **4** (blue) and a 1:1 mixture of **4** and Δ65 (red). The wire-only traces were fit to a biexponential decay with k_{em1} = 1.0(1) × 10^7 s^{-1} and k_{em2} = 1.35(5) × 10^6 s^{-1}. The protein plus wire traces were fit to three exponentials with k_{em1} and k_{em2} held constant at the values found for the wire-only traces. In the fits shown in black above, k_{em3} = 9.1(6) × 10^7 s^{-1}, a number that is indistinguishable from the instrument response.

previously described for the **3**:Δ114 iNOSoxy complex, suggesting Förster energy transfer quenching of the Re excited state and a Re-heme distance of ~18Å.[143]

Transient luminescence decay measurements on a 1:1 mixture of Δ65 and imidazole-terminated wire **1** (Figure **27**a) show that the bound wire is quenched too rapidly to be measured on this timescale.‡ The binding of **1** to iNOSoxy is reversible as indicated by competition experiments with arginine (Figure **29**). Steady-state luminescence shows that the inhibitor, imidazole, is also capable of at least partially displacing **1** from the active site (Figure **30**). The lack of complete recovery of the luminescence of Re-Im-F_8bp-Im even at 13000-fold imidazole concentrations could indicate either concomitant binding of imidazole and wire at the active site or, potentially, a second binding site for the wire.†,[36] Another finding is that, at equimolar concentrations of wire and protein, there is no apparent free wire in solution (as evidenced by the lack of a long-lived species, Figure **27**a). A dissociation constant for the complex could not, therefore, be calculated from the transient luminescence data. Instead, a dissociation constant of 130 ± 70 nM was calculated from steady-state luminescence measurements of **1** alone and in the **1**:Δ65 complex (Figure **31**).[67]

---

‡ An attempt was made to measure the luminescence lifetime of the bound wire using the faster instrument on which the ps transient absorbance measurements were taken. Unfortunately, however, an intrinsic fluorescence from the protein sample itself with a lifetime of ~200 ps overwhelmed the luminescence of the bound wire, leading to a lifetime estimation of ≤ 200 ps for the bound wire.

† Δ114 iNOSoxy has been crystallized with two imidazole molecules bound at the active site, suggesting that concomitant binding of wire and imidazole may be possible.

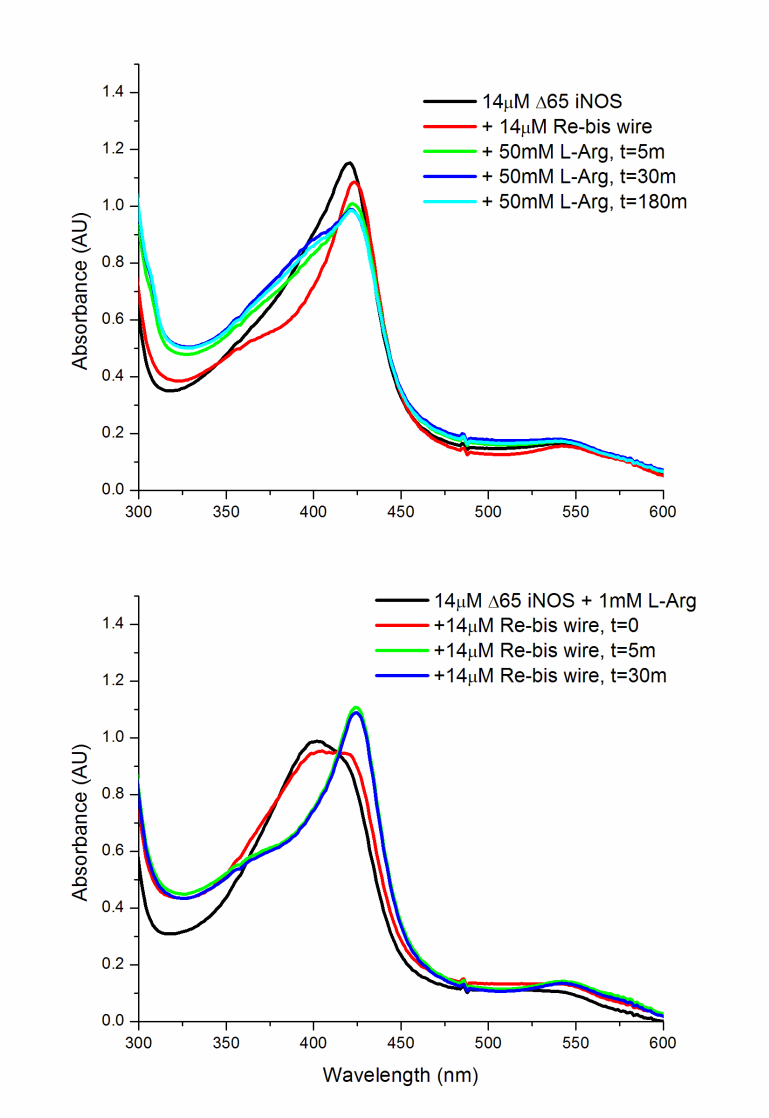

Figure 29. UV/visible absorption spectra of Δ65 iNOSoxy in the presence of various concentrations of Re-Im-F_8bp-Im and arginine, confirming the reversibility of the binding of Re-Im-F_8bp-Im.

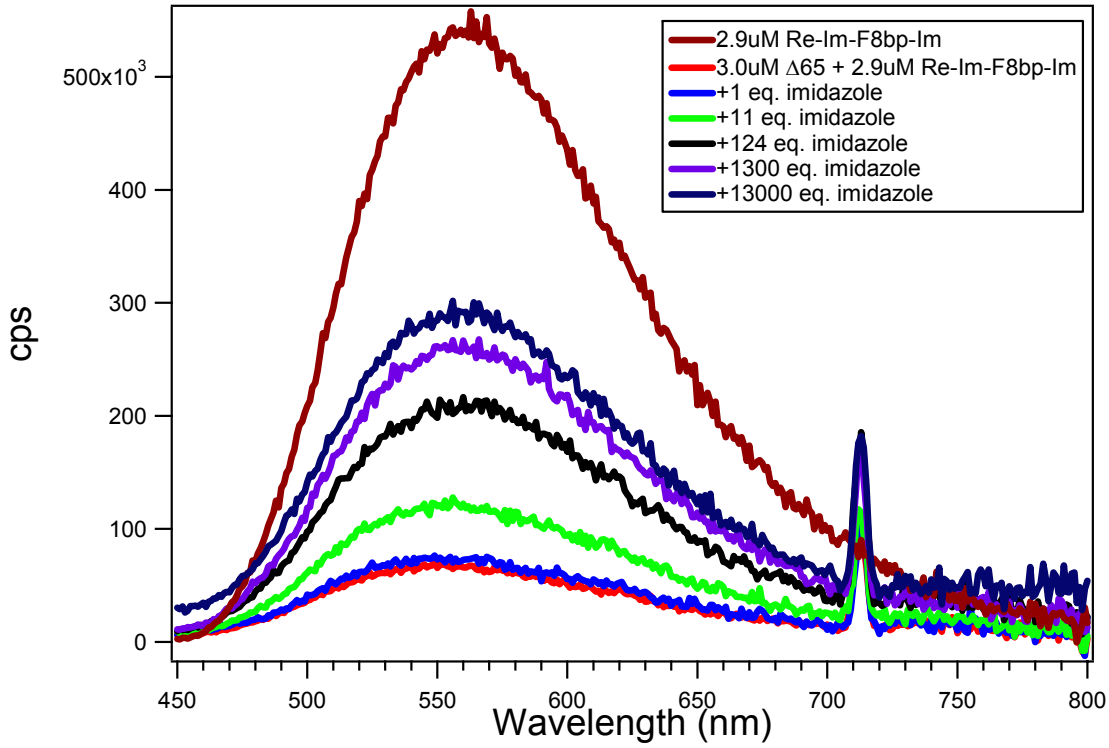

Figure 30. Steady-state emission spectra of Re-Im-F_8bp-Im alone (3 μM, brown), and bound to one equivalent of Δ65 iNOSoxy (red) in the presence of multiple concentrations of imidazole showing the partial displacement of the wire by imidazole.

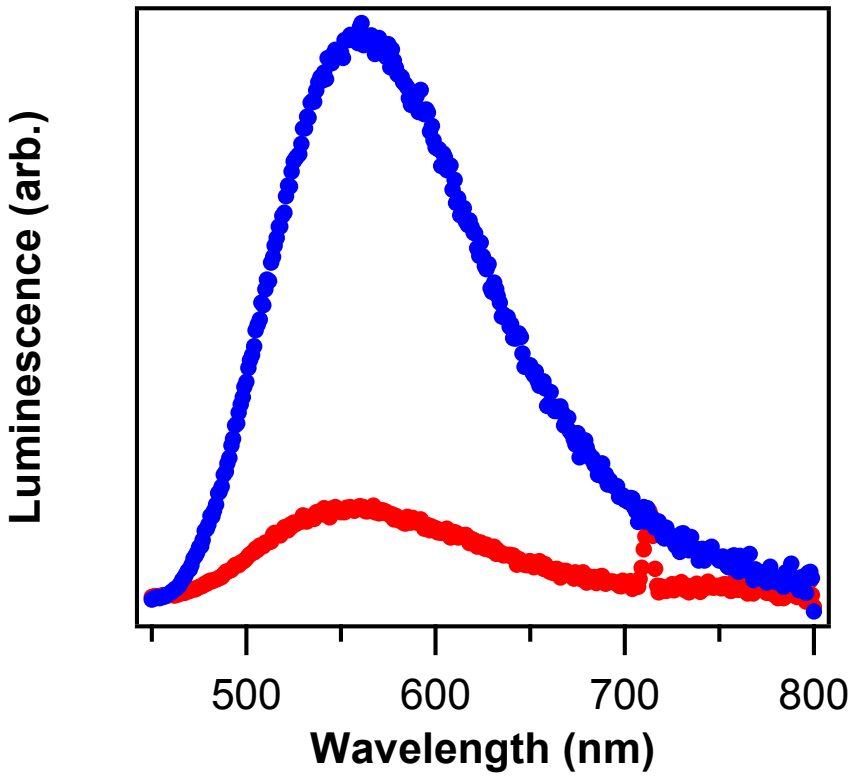

Figure 31. Steady-state fluorescence spectra of **1** (blue) and a 1:1 mixture of **1** and Δ65 (2 μM; red) with λ_{ex} = 355 nm. The small spike at 710 nm is an artifact arising from scattered excitation light.

Owing to low solubility and a tendency to aggregate in water, the concentrations of wires **2** and **4** in buffer could not be measured precisely, so the micromolar dissociation constants for both wires conjugated with Δ65 were estimated from UV/visible (Figure **26**b) and transient luminescence spectra (Figure **27**c and d). Addition of approximately one equivalent of each wire to micromolar solutions of Δ65 produced Soret band shifts similar to those observed with the shorter, more soluble wires **1** and **3**. Transient luminescence spectra also indicated an appreciable proportion of bound, quenched wire in each case (Figure **28**). In the protein:wire mixtures, the wires show an extremely fast phase (below the instrument response time), indicating bound wire and the same biexponential decay that is observed with free wire in buffer solution (presumably indicating free and aggregated wire). The visible signal attributable to unbound wire was similar to that observed for the protein:**3** mixture, suggesting that these wires likely bind as tightly as **3**.

Electron Transfer

Transient absorbance measurements show that, upon 355 nm excitation, imidazole-terminated wires **1** and **2** reduce iNOS (Figures **32** and **33**). Reduction is indicated by a bleach centered near 420 nm (the disappearance of 6-coordinate Fe(III)) and an OD increase centered around 445 nm (the appearance of 6-coordinate Fe(II)). Difference spectra were constructed from single-wavelength transient absorbance traces 80 ns after excitation of the **2**:Δ65 complex (Figure **34**, blue) and 3 μs after excitation of the **1**:Δ65 complex (Figure **34**, red). These spectra bear a striking resemblance to that

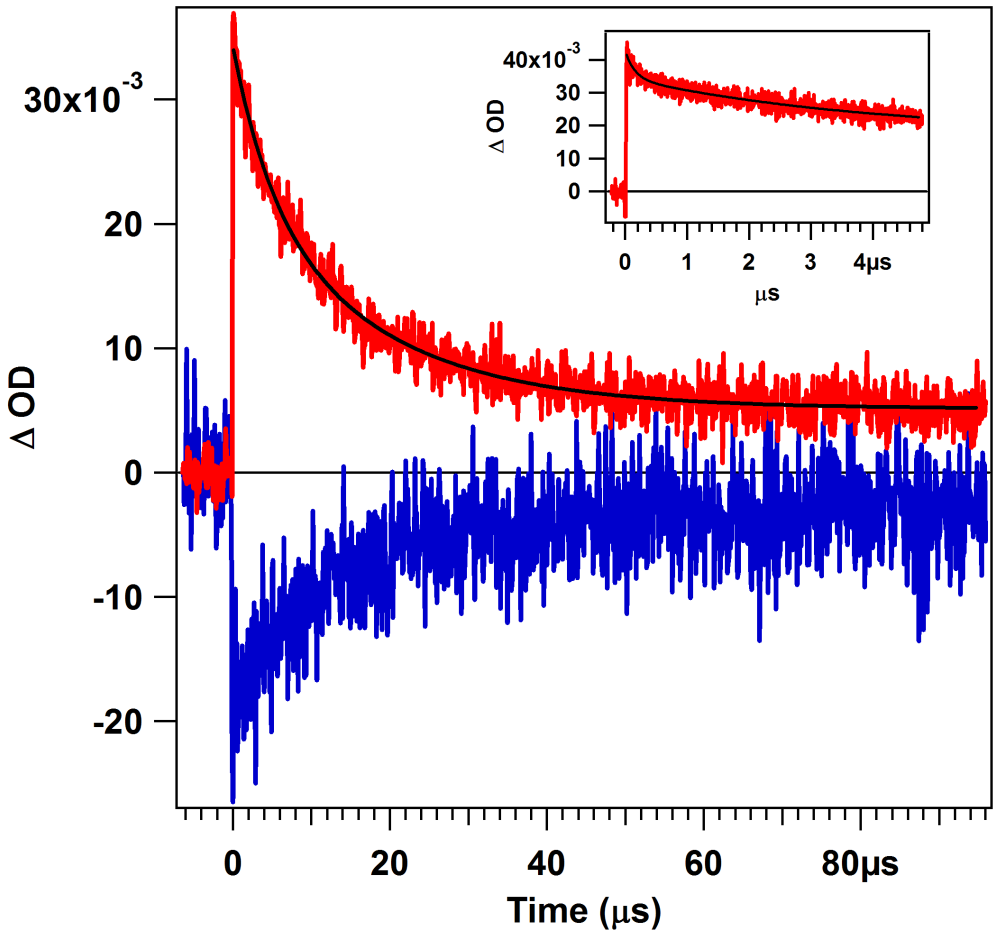

Figure 32. Transient absorbance of a 1:1 mixture of **1** and Δ65 (11 μM) showing the prompt formation and initial decay of 6-coordinate, ferrous heme. λ_{ex} = 355 nm, λ_{obs} = 445 nm (red), λ_{obs} = 420 nm (blue), biexponential fit (k_{b2} = 2.1(1) × 10^5 s^{-1}, k_{b3} = 6(1) × 10^4 s^{-1}, black). Inset shows the data at 445 nm taken on a shorter timescale (red) fit to two exponentials (k_{b1} = 6(1) × 10^6 s^{-1}, k_{b2} = 2.5(4) × 10^5 s^{-1}, black). Taken together, these traces show that the Fe(II) signal has a complicated decay pathway that requires at least three exponentials in order to be fit adequately.

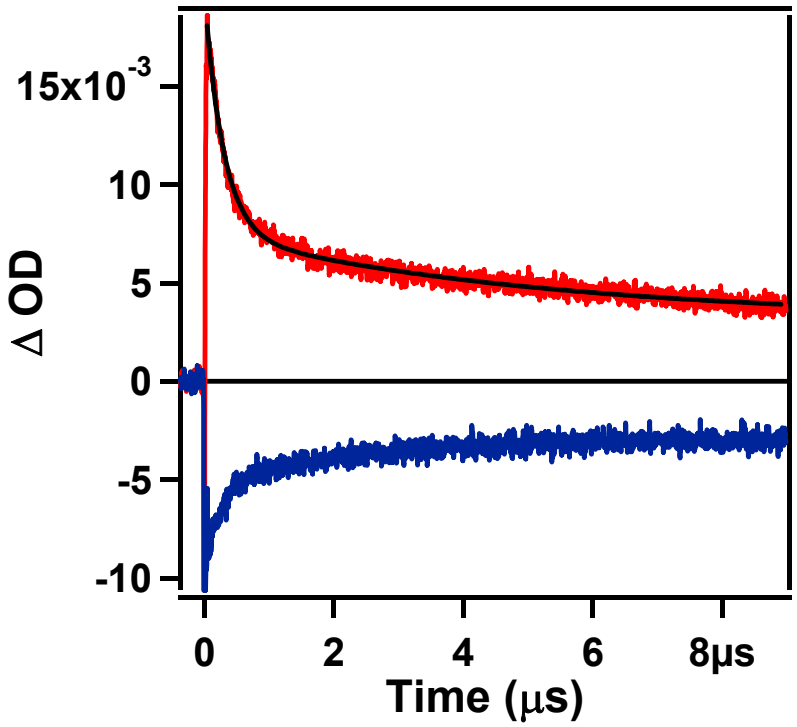

Figure 33. Transient absorbance of an approximate 1:1 mixture of **2** and Δ65 (5 μM) showing the prompt formation and initial decay of Fe(II). λ_{ex} = 355 nm, λ_{obs} = 445 nm (red), λ_{obs} = 422 nm (blue), biexponential fit (k_{b1} = 4(1) × 10^6 s^{-1}, k_{b2} = 2.1(1) × 10^5 s^{-1}, black).

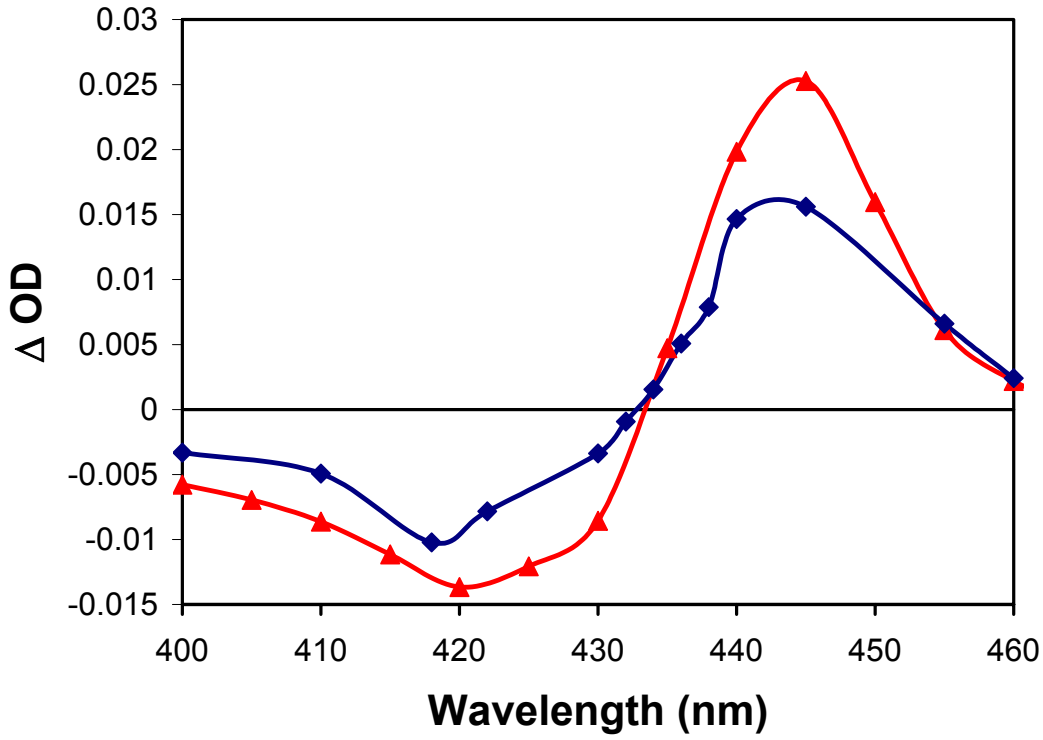

Figure 34. Difference spectra of a 1:1 mixture of **2** and Δ65 (5 μM, 80 ns after 355 nm excitation, blue squares) and a 1:1 mixture of **1** and Δ65 (11 μM, 3 μs after 355 nm excitation, red triangles) showing a bleach of a 6-coordinate Fe(III) Soret (420 nm) and the appearance of a 6-coordinate Fe(II) Soret (445 nm). Individual points were taken from single-wavelength transient absorbance traces.

previously reported for photoreduction of N-phenylimidazole-ligated P450cam, another heme-thiolate enzyme.[65]

With both wire complexes, the photoproduced Fe(II) signal shows complicated, multi-exponential decay kinetics that consist of three dominant phases, k_{b1}=6(1) × 10^6 s^{-1}, k_{b2}=2.5(4) × 10^5 s^{-1}, and k_{b3}=6(1) × 10^4 s^{-1} (Figures **32** and **33**). Using $\Delta\varepsilon_{445}$ = 59.6 mM^{-1} cm^{-1} (see the Experimental Section), the calculated average yield of ferrous heme for both wires is 8 ± 2 percent. The finding that the Fe(II) absorbance maximum does not shift from 445 nm over times up to 250 μs confirms that the wire does not dissociate from the heme upon excitation.

Picosecond transient absorption measurements demonstrated rapid formation of Fe(II) in the presence of wires **1** and **2**. By pumping with 70 ps, 355 nm pulses and probing with the 442 nm line from a continuous wave He:Cd laser, we were able to obtain transient absorbance traces that show the formation of the ferrous heme at very short times (Figures **35** and **36**). The traces were then fit to one exponential (Equation 6) to give k_f = 7(3) × 10^9 s^{-1} for formation of Fe(II). The lack of a signal in the protein:**4** trace confirms that the observed absorbance is attributable to Fe(II) and not to Re(I)* (Figure **36**).

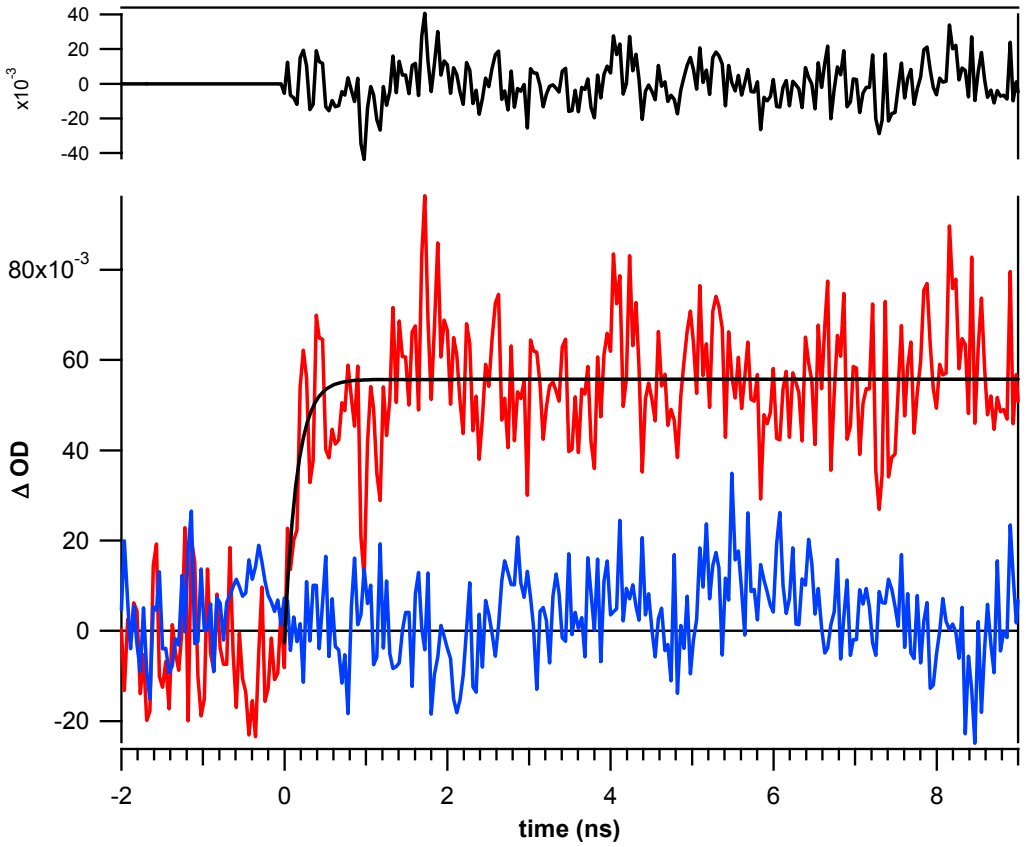

Figure 35. Transient absorbance at 442 nm of Δ65 iNOSoxy alone (8 μM, blue) and in the presence of excess **1** (red) with λ_{ex} = 355 nm. The red trace shows the rapid formation of ferrous heme fit to one exponential (k_f = 7(3) × 10^9 s^{-1}, black) with the residual shown above.

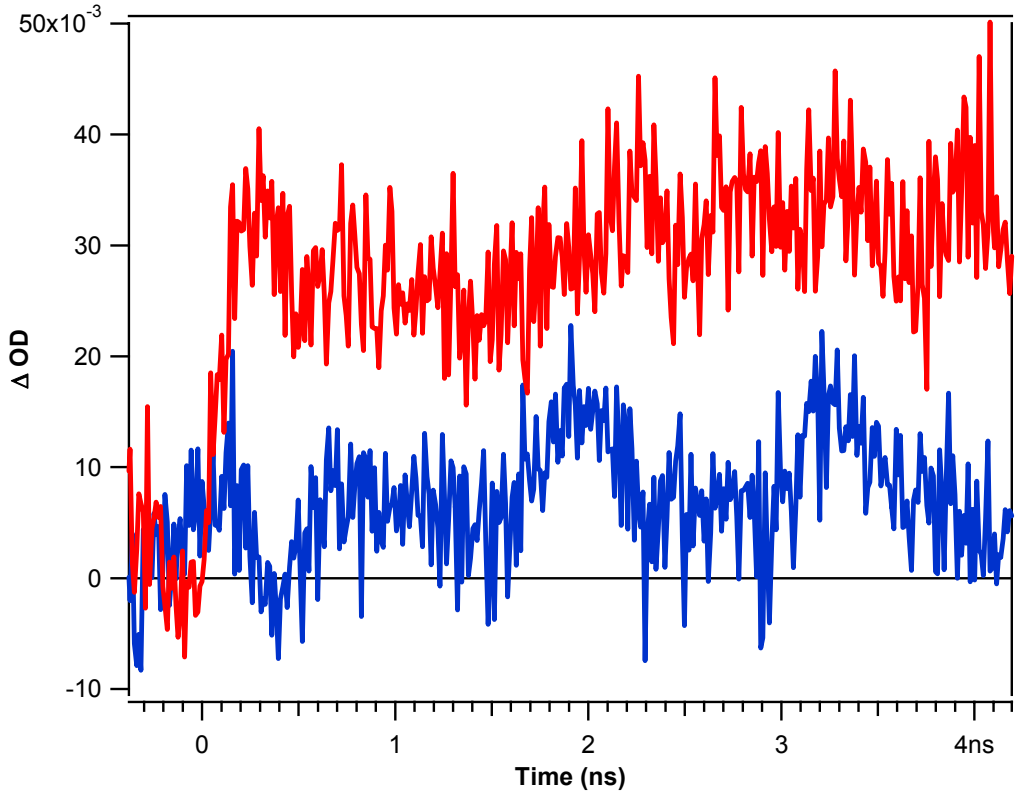

Figure 36. Transient absorbance at 442 nm of Δ65 (16 μM) bound to approximately 1.5 eq. **2** (red) or **4** (blue). The red trace shows the rapid formation (≤ 300 ps) of heme-Fe(II) while the blue trace shows no indication of Fe(II) formation. λ_{ex} = 355 nm.

Discussion

Synthesis

Wires **1** and **3** were synthesized concomitantly. Their design was based on those of Ru-bpy-based wires that bind tightly to P450cam.[62, 63, 65] In our prior work, substituted perfluorobiphenyls were not only shown to be synthetically versatile but also to be very efficient bridges for electron transfer. Further investigation also has suggested that their hydrophobicity and potential ability to pi-stack facilitate binding to target proteins, even when a bulky sensitizer prevents them from binding in an active site channel.[65, 143]

The purpose of switching to a rhenium-based species was two-fold: To take advantage of the smaller *fac*-tricarbonyl-Re(I) phenanthryl sensitizer in comparison with the bulkier $Ru(bpy)_3$ complex,[143] and to increase the luminescence lifetime (1 μs vs. 200 ns) of the sensitizer in order to have a better chance to quench reductively.

Luminescence Quenching and Electron Transfer

In the case of **3**, quenching of the bound wire is consistent with Förster energy transfer from electronically excited rhenium to the heme roughly 18 Å away. These data support a model in which the wire is wedged far enough down the active site channel for its terminal fluorine to displace water from the sixth coordination site on the iron (see Figure **37**). This conclusion is further supported by UV-visible absorption data that show the heme shifting toward a 5-coordinate, high-spin structure (Figure **26**a).

In the case of the other three wires, luminescence quenching is too rapid (≤ 200 ps)[‡] to be explained by Förster energy transfer. Because of the rigidity of the perfluorobiphenyl moiety, no sensible binding model can be created in which the

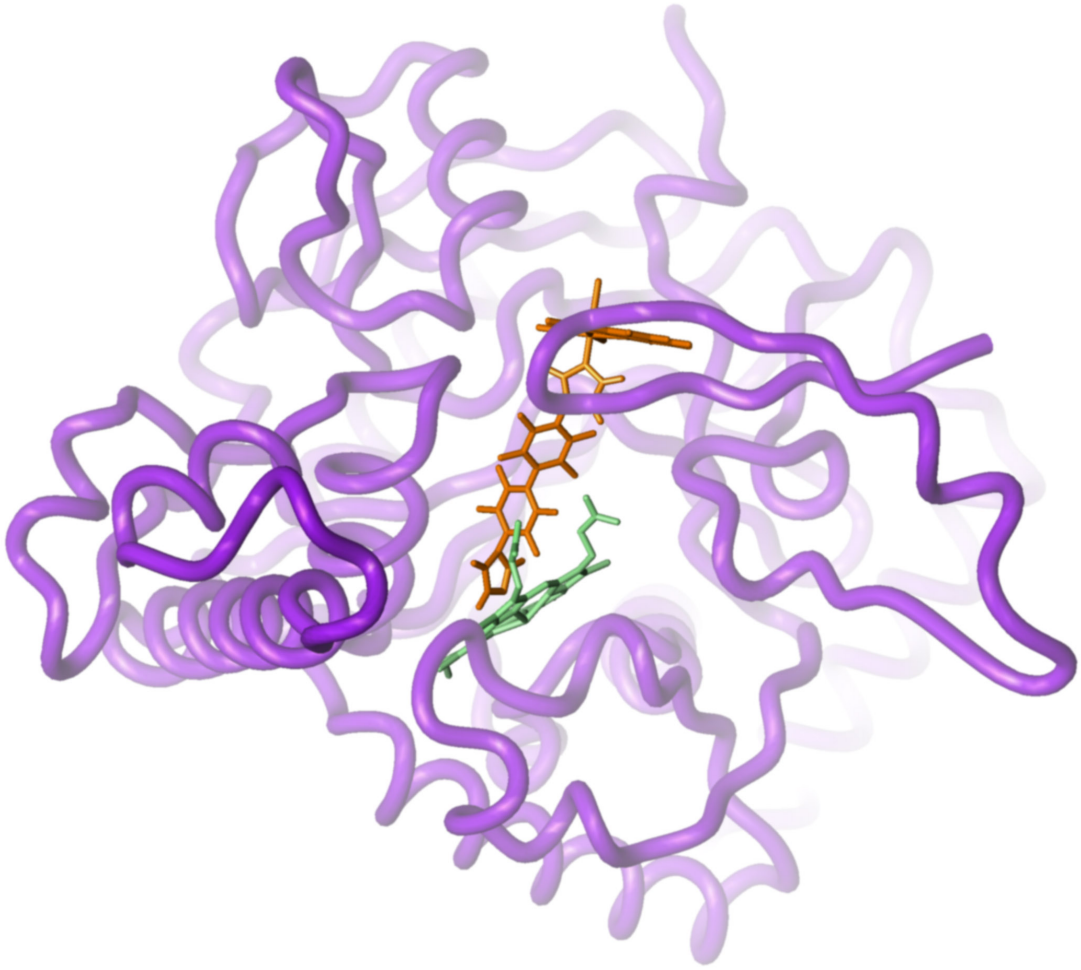

Figure 37. Model of wire **1** bound to Δ65 iNOSoxy. The wire is shown in orange, the protein backbone in purple, and the heme cofactor in green. The modeled Re-Fe distance is 18 Å. The model was created using Insight II from a crystal structure of pterin-bound, fully dimeric NOS [34] that likely has a more closed channel than is present in pterin-free iNOSoxy. The rigidity of the wire and our finding that the distal imidazole ligates the heme suggest, however, that the rhenium-heme distance should be fairly independent of the channel conformation. The other three wires are expected to bind in similar fashion.

terminal imidazole or fluorine can come near the heme while allowing the rhenium sensitizer to approach closely enough to be quenched by energy transfer in less than 200 ps. Some other mechanism surely must be operative. The production of Fe(II) confirms that electron transfer must be involved in the luminescence quenching of **1** and **2**.

In follow-up experiments, the rate of formation of Fe(II) after excitation of the samples was measured. Interference by stray fluorescence from the protein was eliminated by placing the sample far from the detector and using a laser rather than a flash lamp to probe the absorbance before and after excitation. The resulting traces (Figures **35** and **36**) demonstrate ferrous heme formation with a time constant less than 300 ps with wires **1** and **2** bound and additionally confirm the absence of an Fe(II) signal with wire **4** bound. This remarkably rapid photoreduction occurs almost ten orders of magnitude faster than the initial reduction of NOS by its reductase module.[42]

Mechanistic Considerations

The observed picosecond reduction of the NOS heme by **1** and **2** is well outside the time/distance range established for single-step electron tunneling through protein.[103] How can an electron make its way from a photoexcited rhenium to a heme approximately 20 Å distant with such incredible speed?

Ruling out direct photoreduction

In 2003, we reported direct photoreduction of cytochrome P450cam by Ru-analogs of **1** and **2** on a timescale of tens of nanoseconds.[65] Based on this work, our original thought was that the rapid luminescence quenching was due to direct electron transfer from photoexcited rhenium to the heme. The initial nanosecond transient

absorbance experiments with fully-conjugated wire **1**, showing a prompt Fe(II) signal (Figure **32**), appeared to support this interpretation.

Wires **2** and **4** were, therefore, designed to test this model. The addition of a three-carbon linker between the sensitizer and the heme should have slowed photoinduced ET, both by increasing the Re-Fe distance and by disrupting the conjugation in the bridging unit. Additionally, the extended Re-Fe distance should have increased the luminescence lifetime of the Re sensitizer in **4**, the longer analog of wire **3**. Both new wires, however, showed the same, dramatically fast luminescence quenching that had been observed with wire **1**. With wire **4**, this was true even though there was no Fe(II) signal observed. Additionally, measurement of the rate of formation of Fe(II) showed that heme reduction by wire **2** was equally as rapid as that observed with wire **1** (Figures **35** and **36**). Finally, Fe(II) formation itself is simply too fast to be explained by this simple model. The $Re^{II/I*}$ couple has approximately the same reduction potential as the $Ru^{III/II*}$ couple in $Ru(tmbpy)_3$, the 6-coordinate heme $Fe^{III/II}$ potentials for iNOSoxy and P450cam are not very different (Table **3**), and the bridging units between sensitizer and heme for **1** and the Ru-wires we reported[65] are virtually identical, leaving few possibilities to account for the > 100-fold faster heme reduction by the Re-wires. Even if activationless tunneling through a bridge as strongly coupled as poly-xylyl is invoked, the observed ET reaction is still orders of magnitude faster than expected (Chapter 1, Figure **10**).[103]

Table 3. Reduction potentials

Redox Couple	*Potential (V vs NHE)*
$[Re(CO)_3(phen)(im)]^{II/I*}$	-0.7[a]
$[Re(CO)_3(phen)(im)]^{I*/0}$	~1.5[a]
$TrpH^{\bullet+}/TrpH$	1.15[b]
$[Ru(tmbpy)_3]^{III/II*}$	-0.75[c]
low-spin iNOSoxy ($Fe^{III/II}$)	-0.35[d]
low-spin P450cam ($Fe^{III/II}$)	~-0.3[e]

a. Reference [134]. b. Reference[144] c. Reference[145].
d. Reference[48]. e. Reference[131, 146].

A proposal

Electronically excited $[Re(CO)_3(phen)(im)]^+$ is a powerful oxidant; indeed Re(I)* can in principle oxidize tryptophan (Table **3**).[147] In the model of wire **1** bound to Δ65 iNOSoxy (Figure **37**), two tryptophan residues, Trp_{490} and Trp_{73}, lie near the mouth of the active site channel and in close proximity to the modeled wire. We propose that one of these nearby tryptophan residues reductively quenches (4,7-dmp)Re(I)* to generate $TrpH^{\bullet+}$ and "Re(0)". Because Trp_{73} is missing in Δ114 iNOSoxy, in which the same rapid quenching of the wire **1** had earlier been observed,[143] the most likely culprit for reduction of Re(I)* is Trp_{490} (highlighted in blue in Figure **38**).

Based on the structural model shown in Figure **38**, we propose the quenching and electron transfer mechanisms shown in Figure **39**. In the case of each wire bound to the protein, excitation at 355 nm produces Re(I)*. Owing to its short length or other binding constraints, excited wire 3 is quenched by Förster energy transfer in approximately 30 ns. The other three bound, photoexcited wires are quenched in less than 200 ps by electron transfer that generates "Re(0)" and a tryptophan radical cation. Recombination in this charge-separated state is likely to occur rapidly. In the case of wire 4, in which no through-bond pathway to the heme exists, it can be assumed that thermal recombination is the dominant pathway back to the resting state. In the cases of imidazole-terminated wires 1 and 2, however, a direct bond to the heme allows for rapid electron transfer in competition with recombination, thereby producing Fe(II) within a few hundred

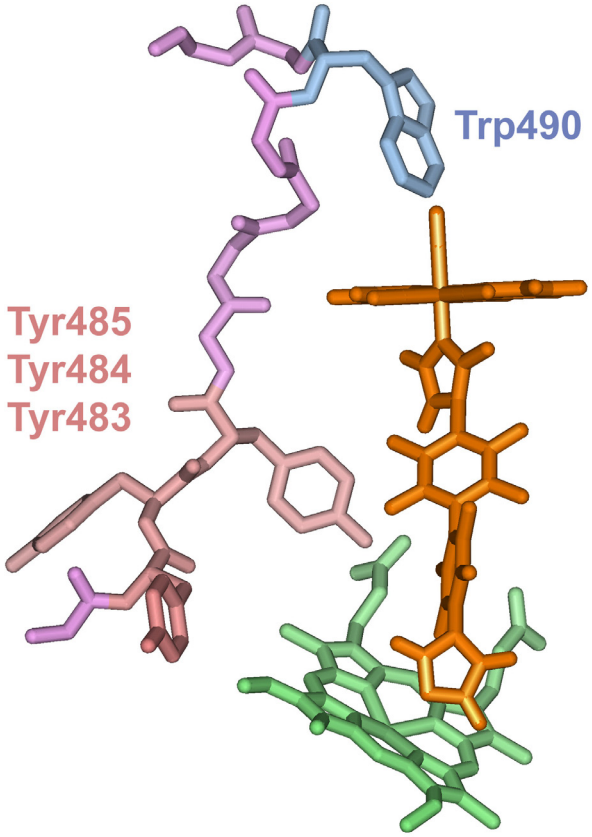

Figure 38. A cutaway view of the model in Figure **37** highlighting the putative tryptophan quencher and three tyrosine residues that could be involved at some stage of the redox chemistry.

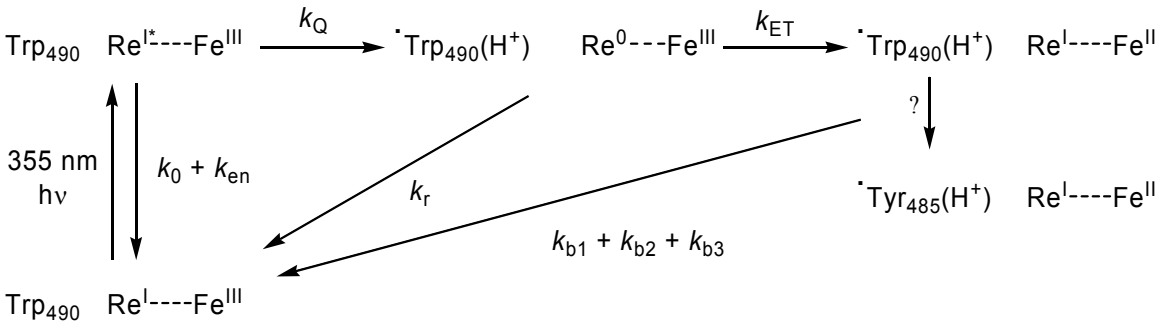

Figure 39. Proposed quenching and ET processes in photoexcited Re-diimine:iNOSoxy conjugates. Re(I)* either oxidizes a nearby Trp residue (k_Q) or decays back to the ground state through a combination of Förster transfer (k_{en}) or intrinsic decay (k_0). The transient "Re(0)" species either reduces the heme (k_{ET}) or reacts with the Trp radical (k_r). The charge-separated species produced by this route then decays back to the ground state through multiple pathways (k_{b1}, k_{b2}, k_{b3}).

picoseconds after excitation. The reduced heme then reacts with oxidized amino acids by multiple pathways over a period of a few hundred microseconds.*

Measurement of the rate of formation and yield of Fe(II) in the reaction allows us to estimate $k_{ET} \sim 6 \times 10^8$ s^{-1} (see the Experimental Section, Equation 8). Even for activationless ET in a fully-conjugated donor-bridge-acceptor system, this rate is too high to be accounted for by single-step tunneling over a distance ≥ 18 Å.[103] This suggests the intriguing possibility that the electron is "hopping" through the perfluorobiphenyl bridge. Simulations based on the kinetic model in Figure **39** with estimated driving forces and reorganization energies for the system show that a hopping mechanism is viable (Figure **40**). This possibility will soon be put to rigorous experimental testing in our laboratory.

Concluding Remarks

We have designed and constructed four Re(I)-diimine wires that bind to the oxidase domain of inducible NOS. Strikingly, two of these wires are capable of reducing the enzyme almost ten orders of magnitude faster than naturally occurring electron transfer from the reductase module. We propose a mechanism in which a tryptophan residue near the opening of the active site channel reduces photoexcited Re(I), leading to production of Fe(II) when a through-bond pathway between reductively generated "Re(0)" and Fe(III) exists. While this model is very tentative, it provides a springboard from which to launch

* The multiple lifetimes for the back electron transfer may be explained by the fact that the oxidized tryptophan could, in turn, oxidize one or more nearby tyrosine residues (three of which are shown in red in Figure **38**). Once formed, any of these amino acid radicals could also deprotonate, creating a host of different redox partners with which the ferrous heme could recombine at different rates.

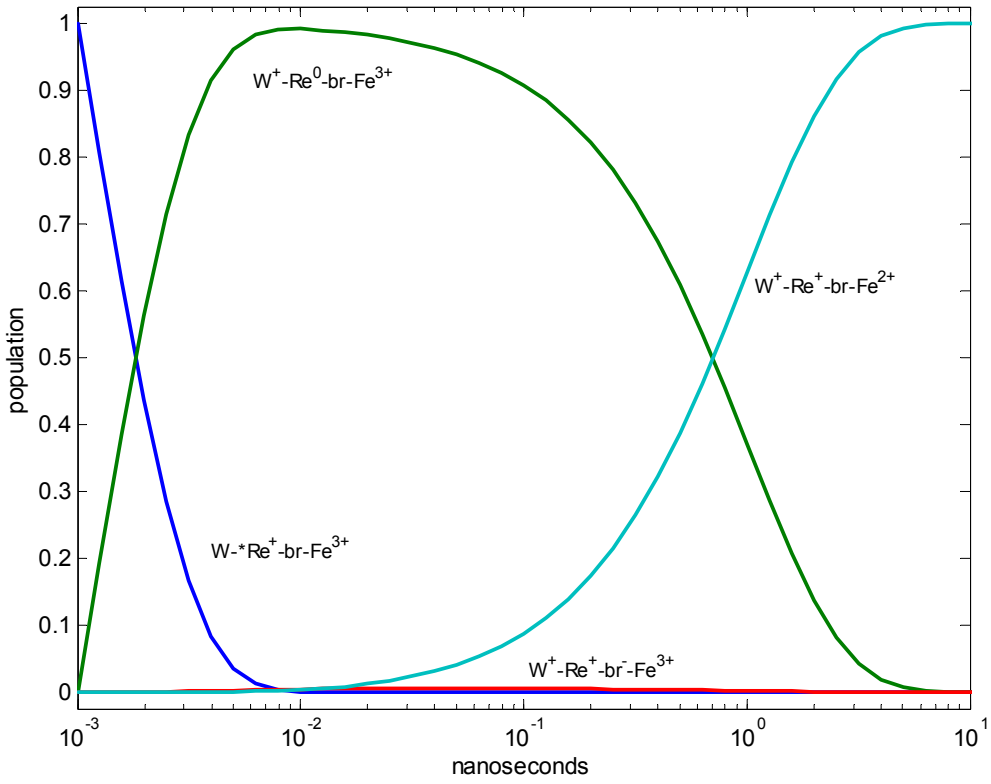

Figure 40. Simulation of the kinetics of formation and decay of the various redox states in the proposed hopping mechanism for ultrafast formation of Fe(II) (light blue trace). Figure courtesy of Jay Winkler.

further experiments including crystallographic characterization of the protein-bound wires and testing of various Trp and Tyr mutants.

The key point is that demonstration of photoinduced, sub-nanosecond production of Fe(II) represents an important step toward the unraveling of the catalytic mechanism of NOS through wire-based technology. Being able to trigger rapid heme reduction in the absence of exogenous quenchers could lead to x-ray structural characterization of high-valent, catalytic intermediates in crystals of enzyme:wire conjugates.

Experimental

Syntheses

Dimethylsulfoxide (DMSO) was purchased from EM Science and dried over calcium hydride. Anhydrous, inhibitor-free tetrahydrofuran (THF) was purchased from Aldrich and used without further purification. All other solvents were either "OmniSolv" grade reagents from EM Science or Burdick and Jackson High Purity solvents and were used as received. Rhenium (I) pentacarbonyl chloride, silver tetrafluoroborate, and silver trifluoromethanesulfonate were purchased from Strem Chemicals. All other reagents were purchased from either Aldrich or EM Sciences. All reagents were used as received. Preparative chromatography on the wire complexes was performed using silica gel (40 μm, 60 Å pore diameter) from JT Baker.

Electrospray ionization mass spectrometry (ESI/MS) was performed on a Finnigan LCQ ion trap mass spectrometer. ^{1}H and ^{19}F NMR spectra were recorded on a Varian Mercury 300 MHz spectrometer. The chemical shifts are reported relative to TMS for ^{1}H NMR. ^{19}F NMR spectra were taken without a standard and were used solely

for verification of number of fluorine-containing species. Their quoted chemical shifts are, therefore, qualitative.

(4,7-dmp)Re(CO)$_3$Cl

$Re(CO)_5Cl$ (1.0g, 2.8mmol) and 4,7-dimethyl-1,10-phenanthroline (4,7-dmp) (0.63g, 3.0mmol) were suspended in 50mL of toluene and stirred at 60^{o}C overnight. The suspension was removed from heat, filtered and washed with toluene to obtain a bright yellow solid (1.436g, 2.8mmol, 100 percent yield) which was used without further purification.

[(4,7-dmp)Re(CO)$_3$(THF)][BF$_4$] (5)

(4,7-dmp)$Re(CO)_3Cl$ (0.500g, 0.98mmol) was weighed into a sealed, 50mL, 3-neck round bottom flask and purged with argon for 30 minutes. 30mL anhydrous THF was added, and the yellow suspension was stirred for 15 minutes. 0.9 equivalents of silver tetrafluoroborate (171mg, 0.88mmol) were transferred into the flask under argon flow. The reaction was sealed and left to stir for 24 hours. The suspension was then filtered over Celite and rinsed with dry THF to remove silver chloride and obtain a bright yellow solution. The solution was rotary evaporated to dryness to obtain a yellow solid (theoretical yield: 0.88mmol) that was used without further purification.

Im-F9bp (6) and Im-F8bp-Im (7)

Potassium carbonate (1.24g, 9mmol) was added to a vacuum-dried 100mL Schlenk flask under argon flow and dried under heat and vacuum for one hour. The heat was removed and imidazole (0.61g, 9mmol) was added to the flask under argon flow. The flask was then returned to vacuum for 30 minutes. ~50mL dry DMSO was vacuum-

distilled into the flask. Decafluorobiphenyl (2.0g, 6mmol) was added to the suspension under argon flow. The reaction was then sealed under argon and stirred for 12 hours at 30°C. The reaction was removed from heat and stirring, and 100mL water was added. The resulting mixture was extracted with dichloromethane (3 × 100mL). The combined organic layer was washed with a further 100mL of water to remove traces of DMSO. The organic layer was then dried over magnesium sulfate, filtered, and rotary evaporated to a light yellowish oil. The oil was re-dissolved in minimal dichloromethane and flash chromatographed over silica gel (2:1 ethyl acetate:hexanes). Three organic fractions were collected and rotary evaporated to dryness. The first fraction contained unreacted decafluorobiphenyl. The second contained product **6** as a white solid (0.461g, 1.2mmol, 20 percent yield). ^{1}H NMR, CD_2Cl_2 (ppm): 7.30 (s, 1H); 7.35 (s, 1H); 7.84 (s, 1H). ^{19}F NMR, CD_2Cl_2 (ppm): -161.2 (2F); -150.5 (1F); -148.2 (2F); -138.0 (2F); -137.3 (2F). The third fraction contained product **7** as a white solid (1.243g, 2.9mmol, 48 percent yield). ESI/MS $(m/z)^+$: 431.3 (calc: 431.3). ^{1}H NMR, CD_2Cl_2 (ppm): 7.30 (s, 2H); 7.35 (s, 2H); 7.90 (s, 2H). ^{19}F NMR, CD_2Cl_2 (ppm): -148.0 (4F); -136.9 (4F).

[(4,7-dmp)Re(CO)$_3$(Im-F$_9$bp)][BF$_4$] (3)

Product **5** was dissolved in a mixture of 12mL dichloromethane and 5mL THF and added to **6** (0.342g, 0.88mmol). The reaction was stirred at 30°C. Aliquots were tested by ESI/MS at various time points, and the reaction was removed from heating when the product peak stopped growing (48-120 hours). The reaction was then rotary evaporated to an orange oil. The oil was re-dissolved in minimal dichloromethane and flash chromatographed over silica gel under the following conditions: 3 percent

methanol in dichloromethane until the first two bands (one fluorescent orange band containing various rhenium species and one colorless band containing free **6**) were collected. The methanol was then gradually increased to 40 percent. The fluorescent yellow-green product was collected and rotary evaporated to dryness to yield a yellow solid (0.122g, 0.128mmol, 14.5 percent yield). ESI/MS $(m/z)^+$: 860.8 (calc: 861). ^1H NMR, CD_2Cl_2 (ppm): 3.0 (s, 6H); 6.8 (s, 1H); 7.1 (s, 1H); 7.9 (s, d, 3H); 8.3 (s, 2H); 9.35 (d, 2H). ^{19}F NMR, CD_2Cl_2 (ppm): -161.1 (2F); -150.2 (1F); -148.0 (2F); -137.6 (2F); -136.4 (2F).

[(4,7-dmp)Re(CO)$_3$(Im-F$_8$bp-Im)] (1)

7 (0.379g, 0.88mmol) was added to a 100mL, 3-neck round bottom flask fitted with a stir bar and condenser. **5** (0.44mmol by theoretical yield, 0.5 subcess to prevent bis-Re-substituted wire formation) was dissolved in a mixture of dichloromethane and THF added to the flask. The reaction was stirred at 30^{o}C until ESI/MS showed that the product peak had stopped growing (2-5 days). The reaction was removed from heat and stirring, and the product was then extracted into dichloromethane and washed with water. The organic solution was dried over magnesium sulfate and rotary evaporated to dryness. The product was re-dissolved in dichloromethane and flash chromatographed under the same conditions as **3**. The clean product was rotary evaporated to dryness to obtain a yellow solid (0.0807g, 0.076mmol, 17.3 percent yield based on Re concentration). ESI/MS $(m/z)^+$: 908.7 (calc: 909). ^1H NMR, CD_2Cl_2 (ppm): 3.0 (s, 6H); 6.8 (s, 1H); 7.1 (s, 1H); 7.25 (s, 1H); 7.35 (s, 1H); 7.8 (s, 1H); 7.9 (d, 2H); 7.95 (s, 1H); 8.3 (s, 2H); 9.4 (d, 2H). ^{19}F NMR, CD_2Cl_2 (ppm): -147.9 (4F); -136.3 (4F).

Im-C_3-F_9bp (8)

Decafluorobiphenyl (3g, 9.22mmol) and K_2CO_3 (2.3g, 16.76mmol) was stirred in anhydrous DMF (15mL) under argon. Aminopropylimidazole (1mL, 8.38mmol) was added via syringe, and the mixture was stirred overnight at room temperature. Precipitated HF was removed by vacuum filtration through celite. Water was added to the filtrate, and the product was extracted with dichloromethane (3 x 10mL). Organic layers were combined, dried over magnesium sulfate, and concentrated. The product was purified by column chromatography on silica gel (CH_2Cl_2:MeOH = 50:1) to obtain a light brown oil (2.2g, 5.01mmol, 59.7 percent yield). ^{1}H NMR, $CDCl_3$ (ppm): 2.2 (m, 2H), 3.5 (t, 2H), 4.3 (t, 2H), 4.7 (s, 1H), 7.0 (s, 1H), 7.2 (s, 1H), 8.65 (s, 1H). ^{19}F NMR, $CDCl_3$ (ppm): -161.8 (2F); -160.2 (2F); -152.4 (1F); -141.0 (2F); -138.2 (2F).

[(4,7-dmp)Re(CO)$_3$(Im-C_3-F_9bp)][BF_4] (4)

5 (1g, 1.71mmol) and **8** (0.75g, 1.71mmol) were stirred in a 2:1 mixture of CH_2Cl_2:THF (5mL) at 40^{o}C for 5 days. The reaction mixture was cooled to room temperature, filtered through celite, and washed with CH_2Cl_2. The filtrate was concentrated and flash chromatographed over silica gel (CH_2Cl_2:MeOH = 50:3). The product fraction was rotary evaporated to dryness to obtain a bright yellow solid (900mg, 0.89mmol, 52.2 percent yield). ESI/MS $(m/z)^+$: 917.9 (calc: 918.1). ^{1}H NMR, CD_2Cl_2 (ppm): 1.95 (m, 2H), 3.0 (s, 6H), 3.3 (t, 2H), 3.9 (t, 2H), 4.6 (s, 1H), 6.5 (s, 1H), 6.8 (s, 1H), 7.25 (s, 1H), 7.9 (d, 2H), 8.3 (s, 2H), 9.3 (d, 2H). ^{19}F NMR, DMSO (ppm): -161.8 (2F); -160.8 (2F); -152.2 (1F); -148.6 (4F) (BF_4); -142.4 (2F); -139.4 (2F).

[(4,7-dmp)Re(CO)$_3$(Im-C$_3$-F$_9$bp-Im)][BF$_4$] (2)

Imidazole (74.3mg, 1.09mmol) and K_2CO_3 (150mg, 1.09mmol) were stirred in anhydrous DMF (5mL). **4** (1g, 0.99mmol) was added, and the reaction was stirred under argon overnight at room temperature. The reaction mixture was then filtered through celite and washed with CH_2Cl_2. The filtrate was concentrated and flash chromatographed over silica gel (CH_2Cl_2:MeOH = 50:3). The product fraction was rotary evaporated to dryness to obtain a bright yellow solid (700mg, 0.66mmol, 67 percent yield). ESI/MS $(m/z)^+$: 965.1 (calc: 966.1). ^{1}H NMR, CD_2Cl_2 (ppm): 1.95 (m, 2H), 3.0 (s, 6H), 3.3 (t, 2H), 3.9 (t, 2H), 4.6 (s, 1H), 6.5 (s, 1H), 6.8 (s, 1H), 7.25 (s, 1H), 7.3 (s, 1H), 7.35 (s, 1H), 7.8 (s, 1H), 7.9 (d, 2H), 8.3 (s, 2H), 9.3 (d, 2H). ^{19}F NMR, CD_2Cl_2 (ppm): -161.2 (2F); -152.2 (4F) (BF_4); -149.4 (2F); -142.2 (2F); -137.8 (2F).

Sample Preparation

Δ65 iNOSoxy samples were prepared as described previously.[35] Small aliquots of the protein solutions were exchanged into phosphate buffer (50 mM potassium phosphate, 50 mM potassium chloride, pH 7.4 ("buffer") using a desalting column immediately before use. The measurement of the heme Soret maximum at 422 nm confirmed the presence of low-spin, water-bound heme. Monomeric, heme-containing protein concentration was determined using the extinction coefficient ε_{422} = 75 mM^{-1} cm^{-1}.[67]

Due to their low solubilities in water (~20 μM for **1** and **3** and ≤ 1 μM for **2** and **4**), concentrated (0.5-1.5 mM) wire solutions were prepared in absolute ethanol. Small aliquots were then added to buffer/protein samples such that the overall ethanol

concentration never exceeded 2 percent.[#] Repeated experiments indicated a large degree of error in measured concentration by this method. As the measured concentration was consistently lower than expected, the error is likely due to the affinity of the hydrophobic wires for either glass syringes or plastic pipette tips. As such, protein:wire samples for rigorous quantitation were prepared by adding wire solutions to buffer, measuring the concentration by UV-visible absorption, and then adding a known quantity of protein.

Samples of **2** and **4** for rigorous quantitative characterization were prepared in 50 percent glycerol in buffer. Attempts were made to conduct protein:wire studies in this type of mixture, but both glycerol and ethylene glycol blue-shifted the heme Soret, indicating that they were binding to the enzyme. These mixtures also interfered with wire binding, supporting the hypothesis that hydrophobic burial of the perfluorobiphenyl unit provides a good deal of binding energy to the wire:protein conjugates.

UV-visible absorption spectra were taken on an Agilent 8453 UV spectrometer. Steady-state emission measurements were made in buffer using a Fluorolog Model FL3-11 fluorometer equipped with a Hamamatsu R928 PMT. Emission quantum yields (ϕ) were determined in deoxygenated solutions relative to tris-(2,2'-bipyridine) ruthenium(II) ($\phi = 0.042$ in water).[148] All steady-state emission and transient spectroscopic measurements were made in sealed quartz cuvettes with deoxygenated samples (at least 30 cycles of partial evacuation followed by backfilling with argon) unless otherwise stated.

[#] Testing with Δ65 showed that micromolar protein solutions could tolerate ≤ 5 percent ethanol with no evidence of heme loss or precipitation.

Transient Spectroscopy

Nanosecond luminescence lifetime and transient absorption measurements were taken using a tripled Nd:YAG laser (λ=355 nm) as the excitation source in an apparatus that has been described elsewhere.[61, 76] The instrument has a response limit of approximately 10 ns. Luminescence decay curves for the wires and Δ65:wire complexes were fit in Igor Pro using a nonlinear least-squares algorithm according to the following expression (Equation 6):

$$I(t) = c_0 + \sum_n c_n e^{-k_n t} \tag{6}$$

where n = 1-3 for mono-, bi-, and triexponential decays respectively. Transient absorbance data was converted from intensity to optical density using Equation 7:

$$OD = -\log\left(\frac{I}{I_0}\right) \tag{7}$$

where I was the intensity of transmitted light after excitation and I_0 was taken as the average light intensity over the 200 ns prior to the laser shot. Decays of the Fe(II) signals observed upon photoreduction of the enzyme were fit using Equation 1. The yield of Fe(II) in each sample was calculated at t = 20 ns using the following expression (Equation 8):

$$[Fe(II)] = \frac{\Delta OD_{445}}{\Delta \varepsilon_{445}} \tag{8}$$

where $\Delta\varepsilon_{445}$ (6-coordinate Fe(III) – 6-coordinate Fe(II)) was estimated by subtracting the absorptivity measured for wire-bound ferric Δ65 iNOSoxy from the absorptivity reported for CO-bound ferrous iNOSoxy (105.4 mM^{-1} cm^{-1}).[40]

For picosecond transient absorption measurements, the samples were excited at 10 Hz with 70 ps, 355 nm pulses from a regeneratively amplified, mode-locked Nd:YAG laser. In order to eliminate interference from fluorescence either of free wire or protein, the sample was placed far from the detector and probed with 442-nm light from a continuous wave He:Cd laser. Stray light from the room was filtered with a 442-nm notch filter and light intensity with (I, 10,000 counts) and without (I_0, 10,000 counts) excitation of the sample was collected directly by a fiber optic (Fiberguide Industries) and detected with a Hamamatsu C5680 streak camera. The raw image files were converted to xy data using an in-house macro for Matlab. The raw data was then converted to optical density using Equation 7, and the rate of formation of ferrous heme was fit to one exponential using Equation 6.

This setup presented many challenges. Because the resting (ferric) heme already has appreciable absorbance at 442 nm, the initial probe light intensity, and, therefore, the overall signal strength was attenuated. Additionally, the protein would not tolerate more than about 20,000 pump/probe shots before it began to visibly deteriorate by precipitating from solution. A compromise between sample concentration, probe laser power, and total laser shots was therefore made in order to maximize signal to noise ratio.

Dissociation Constants

In the case of the Δ65:**3** complex, the equilibrium dissociation constant was calculated from the biexponential fit of the luminescence decay (Equation 6, n = 2) as described previously.[65] Briefly, k_{em1} and k_{em2} are the luminescence decay constants for the enzyme-bound and free wire complexes respectively, and K_d was calculated from the

ratio of c_1 to c_2. Due to the rapidity of the luminescence decay of bound wire **1**, the Δ65:**1** dissociation constant was calculated as described in earlier work from steady-state luminescence spectra.[67] Because of their low solubility and tendency to aggregate in water, dissociation constants for **2** and **4** with Δ65 could not be reproducibly determined. In approximate 1:1 wire:protein mixtures at 1-10μM concentrations, however, observation of significant Δ65 heme Soret shifts and visible luminescence quenching of the wires allowed for the estimation of micromolar dissociation constants for both wires.

Förster Energy Transfer

Förster energy transfer (FET) calculations were completed according to the following expression (Equation 9):

$$k_{en} = k_0 \left(\frac{R_0}{R} \right)^6 \qquad (9)$$

where k_0 is the intrinsic luminescence decay rate of the donor (the rhenium sensitizer), R is the distance between donor and acceptor (the iNOS heme group), and R_0, the Förster distance, is the distance at which half of the luminescence intensity of the donor is quenched by FET. R_0 was calculated (in cm) from Equation 10:

$$R_0^{\,6} = 8.8 \times 10^{-25} (\kappa^2 n^{-4} \phi_D J) \qquad (10)$$

where the overlap integral, $J = \int F_D(\lambda) \varepsilon_A(\lambda) \lambda^4 d\lambda$, κ^2 is a measure of the spatial orientation of the transition dipoles of the donor and acceptor with respect to each other ($\kappa^2 = 2/3$ in randomly oriented pairs), n is the refractive index of the solvent ($n = 1.34$ for water), and ϕ_D is the luminescence quantum yield of the donor.

Estimation of ET Rate Constants

The kinetics for luminescence quenching and electron transfer in this system were interpreted according to the model in Scheme 3. The observed rate constant (k_L) for the decay of Re(I*) in the presence of iNOSoxy is:

$$k_L = k_0 + k_{en} + k_Q \tag{11}$$

The rate of Fe(II) formation is dependent upon the concentration of "Re(0)," so the observed rate constant (k_f) is given by:

$$k_f = k_r + k_{ET} \tag{12}$$

Because k_r describes a non-productive reaction, k_{ET} can be extracted from k_f through the following expression:

$$\Phi_{ET} = \frac{k_{ET}}{k_{ET} + k_r} = \frac{k_{ET}}{k_f} \tag{13}$$

where Φ_{ET} is the yield of Fe(II) as a percentage of the total wire-bound sample.

Simulation of Quenching and ET Processes

The proposed electron hopping mechanism was simulated according to the expanded model shown in Figure **41**, leading to the following differential equations:

$$\frac{\partial A}{\partial t} = -(k_0 + k_1)A \tag{14}$$

$$\frac{\partial B}{\partial t} = k_1 A - (k_2 + k_3 + k_5)B + k_{-3}C \tag{15}$$

$$\frac{\partial C}{\partial t} = k_3 B - (k_{-3} + k_4)C \tag{16}$$

$$\frac{\partial D}{\partial t} = k_4 C + k_5 B \tag{17}$$

These equations were solved numerically in Matlab using the estimated distance and driving force parameters shown in Table **4** and $\lambda = 0.8$ V.

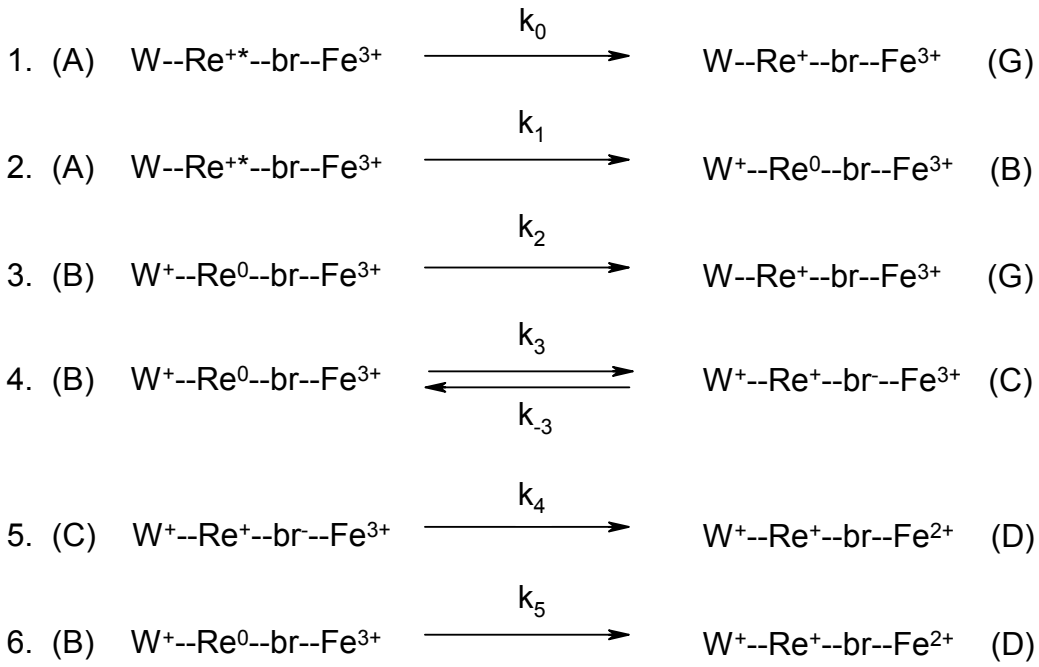

Figure 41. Expanded model for simulation of the hopping kinetics in photoexcited Re-Im-F_8bp-Im:Δ65. br ≡ perfluorobiphenyl bridge.

Table 4. Distance and driving force parameters for simulation of hopping kinetics.

*Reaction (Figure **41**)*	*estimated r (Å)*	*estimated -ΔG (V)*
1	NA	NA
2	3	0.35
3	3	2.4
4	6	-0.1-0.2
4 (reverse)	6	0.1-0.2
5	6	1.15-1.25
6	20	1.05

CHAPTER 4:

NANOSECOND PHOTOINDUCED REDUCTION OF INHIBITOR- AND SUBSTRATE-BOUND INDUCIBLE NITRIC OXIDE SYNTHASE BY A RU-DIIMINE ELECTRON TUNNELING WIRE[†]

 Belliston-Bittner, W., Dunn, A. R., Marletta, M. A., Winkler, J. R., and Gray, H. B., *J. Am. Chem. Soc.*, **submitted**.

Acknowledgement:

Many thanks to Alex Dunn for having synthesized the wire described in this paper and to Oliver Wenger for the gift of clean tmpd.

Chapter 4

NANOSECOND PHOTOINDUCED REDUCTION OF INHIBITOR- AND SUBSTRATE-BOUND INDUCIBLE NITRIC OXIDE SYNTHASE BY A RU-DIIMINE ELECTRON TUNNELING WIRE

Abstract

A Ru-diimine wire, $[(4, 4', 5, 5'\text{-tetramethylbipyridine})_2Ru(F_9bp)]^{2+}$ (tmRu-F_9bp), where F_9bp is 4-methyl, 4'-methylperfluorobiphenylbipyridine, binds tightly to the oxidase domain of inducible nitric oxide synthase (iNOSoxy). The binding of tmRu-F_9bp is independent of tetrahydrobiopterin, arginine, imidazole, and a wire, Re-F_8bp-im, that has been shown to occupy the active site channel of iNOSoxy, indicating that tmRu-F_9bp resides on the surface of the enzyme in a hydrophobic surface patch that has been postulated to be the docking site for the reductase module. Reductive flash-quench studies show that the bound wire is capable of reducing the imidazole- (inhibitor) bound active-site heme iron with a rate constant of $k_{ET} = 2.4(4) \times 10^7\ s^{-1}$, fully seven orders of magnitude faster than the comparable in vivo process. Preliminary results indicate that this wire/quencher system also rapidly reduces arginine- (substrate) bound iNOSoxy.

Introduction

Nitric oxide synthase is a heme-containing oxotransferase that catalyzes the conversion of L-arginine and O_2 to citrulline and nitric oxide (•NO). NOS completes this transformation in two turnover processes that require a total of five electrons supplied by NADPH from the NOS reductase module. Each turnover is expected to proceed through

a P450-type mechanism, central to which are two slow electron transfer steps. The first reduces the resting, substrate-bound heme to the ferrous state, which then binds oxygen to create the last observable (ferric-superoxo) intermediate. The second electron transfer produces one or more elusive, high-valent species. The hypothetical oxygen-transferring moiety is a ferryl-porphyrin$^{+\bullet}$ intermediate (compound I). The sluggishness of the second ET step combined with the short lifetime of compound I and other high-valent hemes, however, has so far prevented the characterization of the last intermediate(s) in this process.

In order to study these types of mechanisms, we have been developing methods for rapid electron transfer to and from the deeply buried active sites of redox-active enzymes. By using laser light to trigger rapid reduction of NOS, we hope to alter the rate-limiting step in the reaction and cause a build-up of the subsequent intermediates in order to characterize them spectroscopically. To this end, we have developed electron tunneling wires in which a photo- or electroactive moiety at the enzyme surface communicates with the active site through an electron tunneling bridge. Previously, functional electron tunneling wires have been developed for P450cam,[62, 65, 77] amine oxidase,[75] and nitric oxide synthase (Chapter 3).[68] While the wires described in these studies are effective at transferring electrons into and out of their respective proteins, they share a common drawback. They all block the active site channel. Previously, however, we reported a pair of Ru-diimine wires that bind tightly and specifically to the oxidase domain of inducible NOS distant from the active site (Chapter 2).[67] The work described herein reports the successful use of flash/quench methodology on the tmRu-

F_9bp:iNOSoxy system to reduce the inhibitor-bound heme in approximately 45 ns (k_{ET} = 2.4(4) × 10^7 s^{-1}).

Experimental

General

The tmRu-F_9bp complex was synthesized as described previously.[64, 65, 69] Tetramethylphenylenediamine (tmpd) was purchased from Aldrich and vacuum-sublimed before use. Excess tmpd was stored under argon away from light and at 4°C. Tetrahydrobiopterin was purchased from Aldrich and stored under argon at -20°C. All other chemicals were purchased from Sigma, JT Baker, Fischer, EM Sciences, or Malinckrodt and used as received. UV-visible absorption spectra were acquired on an Agilent 8453 UV spectrometer. Gel electrophoresis was run on a Phast System (Pharmacia) with 8-25 percent gradient precast agarose gels and SDS buffer strips. Samples were loaded in 2x or 4x SDS buffer and stained with Coomassie blue. Samples were run against Precision Plus All-Blue standards (BioRad).

NOS Expression and Purification

The heme domain of inducible nitric oxide synthase with a C-terminal 6 × His tag was overexpressed in *E. coli* and purified as described previously[40] with several exceptions. Briefly, expression cells were subjected to two rounds of chemical lysis by pelleting and resuspension in 40 mL of B-PER lysis buffer (Pierce). The lysis buffer included a cocktail of protease inhibitors (10 μg/mL benzamidine, 5 μg/mL leupeptin, 1 μg /mL each pepstatin, antipain, and chymotrypsin, and ~500 μM Pefabloc (Roche)) as

well as 100 μg /mL DNase, 100 μg/mL RNase, ~500 μg /mL lysozyme, and 20 mM imidazole per liter of cells. The suspensions were then shaken for 60 minutes at 4°C. The lysate was centrifuged and the supernatant was loaded directly onto a nickel column (5 mL HisTrap, Amersham). Once the protein was completely loaded onto the column, it was washed with 20 column volumes of 20 mM imidazole in 50 mM NaP_i/300 mM NaCl/pH 8. The protein was eluted with 150 mM imidazole and concentrated to ~3 mL in an Amicon Ultra centrifugation device (10,000 MWCO, Millipore). The concentrated sample was then further cleaned over a size-exclusion column as previously described.[40] The anion exchange column was omitted when ≥ 95 percent purity was confirmed by UV-visible spectroscopy and gel electrophoresis (Figure **42**). The purified protein was concentrated to ~200 μM, divided into 100 μL aliquots, and stored in 50 percent glycerol at -80°C.

Sample Preparation

Small aliquots of iNOSoxy were thawed and exchanged into phosphate buffer (50 mM KP_i, 50 mM KCl, pH 7.4) using a PD-10 desalting column (BioRad) immediately before use. The heme Soret maximum at 422 nm confirmed the presence of low-spin, water-bound heme. Monomeric, heme-containing protein concentration was determined using ε_{422} = 75 mM^{-1} cm^{-1}.[67] For inhibitor-bound samples, imidazole (400-500 μM) was added, and binding was confirmed by a Soret shift to 428 nm. For substrate-bound, pterin-free samples, 1 mM arginine was added to dilute (~2-20 μM) iNOSoxy and allowed to incubate at 4°C for approximately 30 min. In the absence of pterin, only partial conversion to high-spin heme (λ_{max} = 396 nm) was observed. For substrate- and

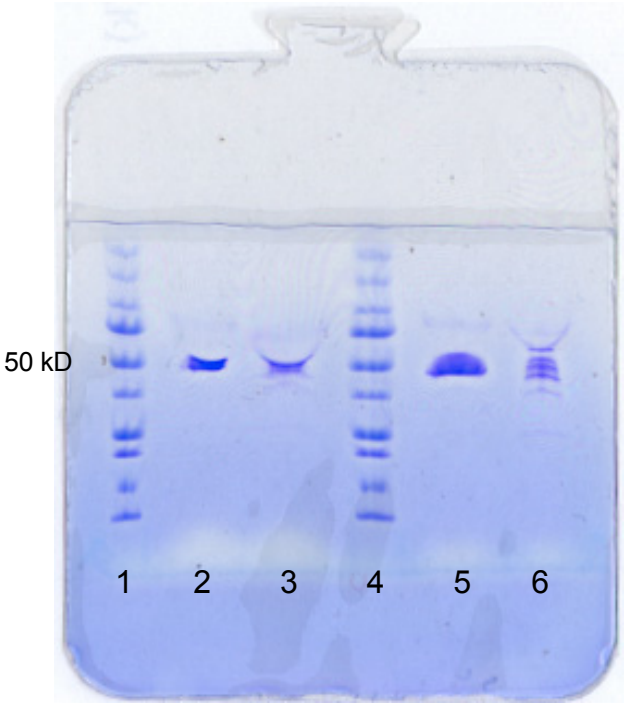

Figure 42. Gel of iNOSoxy after final purification. Lanes 2 and 3 were loaded in 4x SDS buffer and lanes 5 and 6 were loaded in 2x SDS buffer. The multiple bands are due to N-terminal truncations of the protein. Lanes 1 and 4 are Precision Plus All Blue standard (BioRad).

pterin-bound samples, fresh H_4B solutions were prepared daily. Phosphate buffer was thoroughly degassed by bubbling with argon for ≥ 10 min. H_4B was measured and added to the degassed buffer under a counterflow of argon. Dilute iNOSoxy (~2-20 μM) was degassed by at least thirty cycles of evacuation followed by backfilling with argon, taking care to avoid bubbling of the solution. Aliquots of concentrated, degassed pterin and arginine stocks were then added to the protein to final concentrations of 100 μM H_4B and 1 mM arginine, and the solution was incubated for 2 h at 4°C. Binding of H_4B and arginine was confirmed by a Soret shift to 396 nm.

For quenching experiments, 1 M stock solutions of ascorbate were prepared fresh daily by dissolving ascorbic acid in thoroughly degassed 1 M KOH. Ascorbate stock and solid tmpd were added to degassed protein solutions under a counterflow of argon.

Transient Spectroscopy

Luminescence lifetime and transient absorption measurements were made on an apparatus that has been described elsewhere.[61, 76, 149] The ~ 8 ns, 480 nm excitation pulses were produced by an optical parametric oscillator (OPO) pumped by a Nd:YAG laser. Data were gathered at 1 gigasample s^{-1} using a LeCroy digital oscilloscope. Transient absorbance data were converted from intensity to optical density using the following expression (Equation 18):

$$OD = -\log\left(\frac{I}{I_0}\right) \tag{18}$$

where I was the intensity of transmitted light after excitation and I_0 was the average light intensity over the 200 ns prior to the laser shot. Luminescence decay curves and transient

absorbance traces were fit to one, two, or three exponentials in Igor Pro using a nonlinear least-squares algorithm (Equation 19):

$$I(t) = c_0 + \sum_n c_n e^{-k_n t} \tag{19}$$

The yield of Fe(II) from the flash/quench experiments was calculated at t = 2 μs (Chapter 3) according to Equation 20:

$$[Fe(II)] = \frac{\Delta OD_{445}}{\Delta \varepsilon_{445}} \tag{20}$$

where $\Delta\varepsilon_{445}$ = 59.6 mM^{-1} cm^{-1}. The decay of the transient Fe(II) signal was fit to two exponentials using Equation 19. Each experiment was repeated at least three times unless otherwise indicated.

Calculation of ET Rate Constants

At a given time after excitation, the observed absorbance at a given wavelength between 400 and 450 nm is (Equation 21):

$$\Delta OD = \varepsilon_{Fe^{II}}\left[Fe^{II}\right] - \varepsilon_{Fe^{III}}\left[Fe^{III}\right] + \varepsilon_{Ru^{II}*}\left[Ru^{II}*\right] + \varepsilon_{Ru^{I}}\left[Ru^{I}\right] - \varepsilon_{Ru^{II}}\left[Ru^{II}\right] \tag{21}$$

Since the spectra of Asc and tmpd are blank in this window, these two species were neglected. At these wavelengths, the OD changes due to the Ru(II)*-Ru(II) bleach are large compared to those for Fe(II) formation. Additionally, in the systems described herein, the presence of free and NOS-bound wire as well as two separate quenchers, both of which are capable of reducing Ru(II)*, result in complex transient absorbance kinetics. Owing to these two findings, extraction of k_{ET} from raw transient absorbance traces was not possible.

The transient absorbance kinetics were corrected for the quenched Ru(II)* signal as follows. The low-spin, imidazole-bound Fe(III/II) isosbestic point occurs at 438 nm. In each experiment, therefore, transient absorbance of the Im-iNOS/wire/quencher system at 438 nm showed the Ru(II)* bleach and recovery, but no Fe-based signal. This trace was scaled for each wavelength of interest based on the observed Ru(II*/II) difference spectrum (Ru(II*/II) $\Delta\varepsilon_{452}/\Delta\varepsilon_{438} = 0.86$, $\Delta\varepsilon_{445}/\Delta\varepsilon_{438} = 1.12$, $\Delta\varepsilon_{425}/\Delta\varepsilon_{438} = 0.91$, and $\Delta\varepsilon_{418}/\Delta\varepsilon_{438} = 0.66$). The scaled 438-nm traces were then subtracted directly from the transient kinetics at each monitored wavelength. As the contribution of Ru(I) to the overall absorbance is < 10 percent of the Fe(II) signal, Ru(I) absorbance was neglected. The resulting corrected traces were then fit to a single exponential using Equation 19.

Results and Discussion

Binding of tmRu-F$_9$bp to iNOSoxy

Previous work has shown that tmRu-F$_9$bp (Figure **43**) binds to iNOSoxy independently of substrate and tetrahydrobiopterin with a dissociation constant of ~1μM as determined by transient luminescence decay (Chapter 2, Figure **15**).[67] This wire binds at a site distant from the active site channel, as evidenced by the fact that the channel-binding wire Re-Im-F$_8$bp-Im does not displace tmRu-F$_9$bp from the enzyme (Chapter 2, Figure **16**). While the exact binding site has not been definitively established, a low-resolution crystal structure[150] indicates that it may bind in the hydrophobic pocket that is thought to be the docking site for the reductase module of NOS (see Chapter 2, Figure

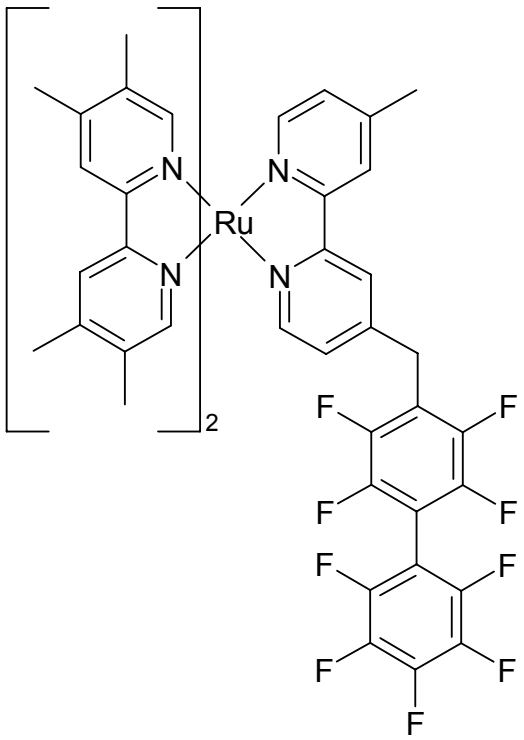

Figure 43. tmRu-F_9bp.

17b). In this model, hydrophobic contacts between the concave surface of the enzyme and the convex surface of the $Ru(bpy)_3^{2+}$ moiety provide the localization and binding energy for the wire. Recent tests with $Ru(bpy)_3^{2+}$, however, have shown that the sensitizer in the absence of the wire does not bind to the enzyme (Figure **44**). These data suggest that the unique perfluorobiphenyl unit contributes to the binding of the wire if not to the specificity of the binding site.

Quenching of the bound Ru-wire

In previous work, Dunn *et al.* reported Ru-diimine wires that reduced the heme of P450 directly upon photoexcitation.[65] In that experiment, the wires ligated the heme iron, giving the reducing electron a through-bond highway to the heme. This allowed electron transfer to compete effectively with energy transfer for depletion of the sensitizer excited state, even though the driving force was relatively low. The Ru wire described herein, however, binds away from the heme, leaving no through-bond pathway from Ru to Fe, and direct photoreduction does not occur. We therefore turned to a reductive flash/quench method in order to produce Fe(II) in this system.[71] In the reversible flash/quench experiment, an exogenous molecule reductively quenches the photoexcited sensitizer to create a strongly reducing Ru(I) species (Figure **45**). If the quenching reaction is diffusion-controlled, the yield of Ru(I) is dependent on sensitizer excited state lifetime and quencher concentration. In the absence of other electron-accepting species, the lifetime of the Ru(I) species is then dependent on the rate of recombination with the oxidized quencher (k_r in Figure **45**). Because of the low concentration of Q^+ with respect

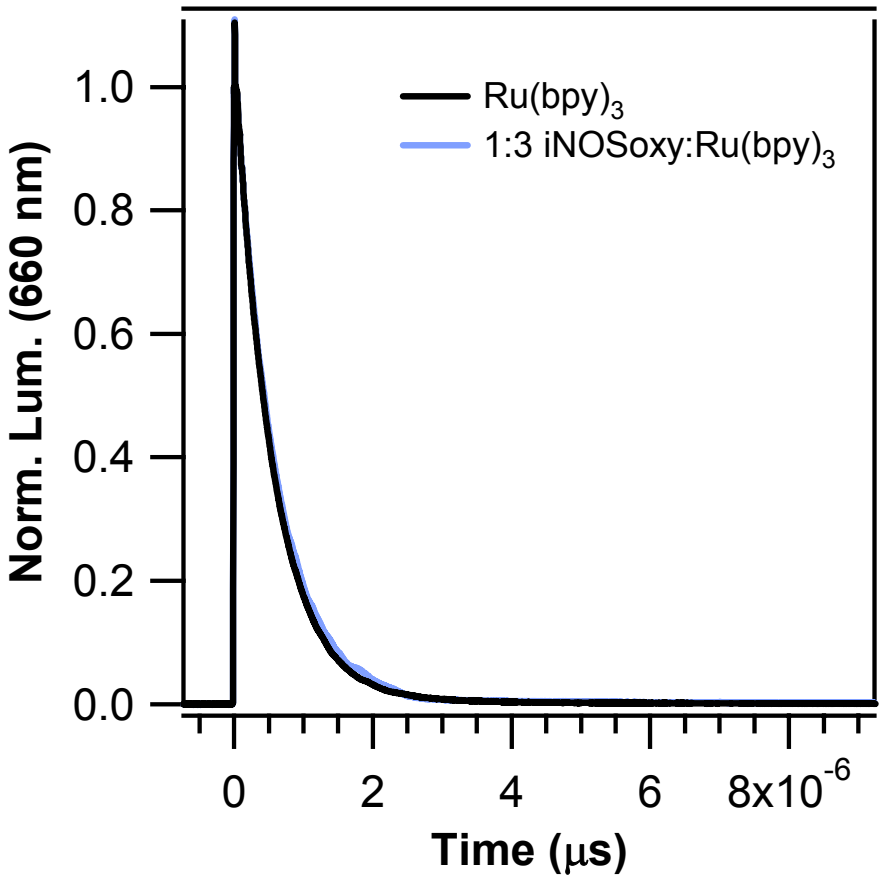

Figure 44. Transient luminescence of $Ru(bpy)_3^{2+}$ in the presence and absence of iNOSoxy. These data demonstrate that $Ru(bpy)_3^{2+}$ itself does not bind to iNOSoxy, even when present in three-fold excess. λ_{ex} = 480 nm.

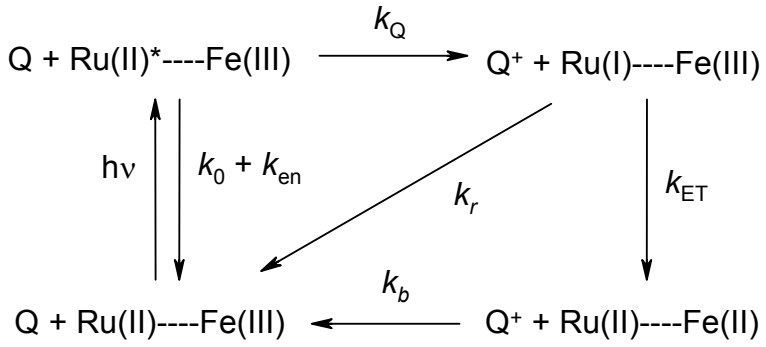

Figure 45. Representation of the reversible flash/quench experiment employed in this work. For simplicity, tmpd and ascorbate are represented together as Q. In a successful flash/quench experiment, quenching must compete with intrinsic relaxation (k_0) and energy transfer (k_{en}) for depletion of the Ru excited state ($k_Q \geq k_0 + k_{en}$) and the recombination of the oxidized quencher and reduced sensitizer must be slow with respect to electron transfer ($k_r < k_{ET}$).

to Q, recombination is usually slow. Thus, there is time for the resultant Ru(I) reductant to reduce the heme, even if a through-space jump is required.

Due to its high solubility in water and lack of spectral interference with heme Soret changes (Figure **46**, blue trace), ascorbate (Asc) is an attractive choice as a quencher for this system. Even at high concentrations, however ([Asc] up to 100 mM was tried), the quenching rate is barely comparable to the rate of Förster energy transfer from bound tmRu-F_9bp to the heme (Figure **47**), resulting in an extremely low yield of Fe(II) (Figure **48**) and poorly reproducible experiments. Tetramethylphenylenediamine (tmpd, Figure **49**) is a much more effective quencher than ascorbate. Unfortunately, in its neutral, reduced form, tmpd is only somewhat soluble in water,[151, 152] necessitating addition of excess solid quencher in order to maintain saturation conditions. A second drawback is that tmpd autoxidizes in water to create a highly soluble, bright blue cation radical.[151-153] At low concentrations, the spectrum of this radical does not interfere with the observation of changes in the heme Soret (Figure **46**, light green trace). Under saturation conditions, however, the radical rapidly turns the entire solution dark blue (Figure **46**, dark green dotted trace), overpowering small transient changes in the heme spectrum and robbing excitation light.

These problems were overcome by employing both quenchers. [154, 155] In a sample containing 10 mM Asc + saturated tmpd, the fast quenching capability of the tmpd can be exploited (Figure **47**, red dotted trace) while relying on the ascorbate to keep the tmpd from autoxidation. With ascorbate present, as shown in Figure **46**, no evidence of the blue, oxidized tmpd is apparent, even after 60 min of photoexcitation in the presence of tmRu-F_9bp.

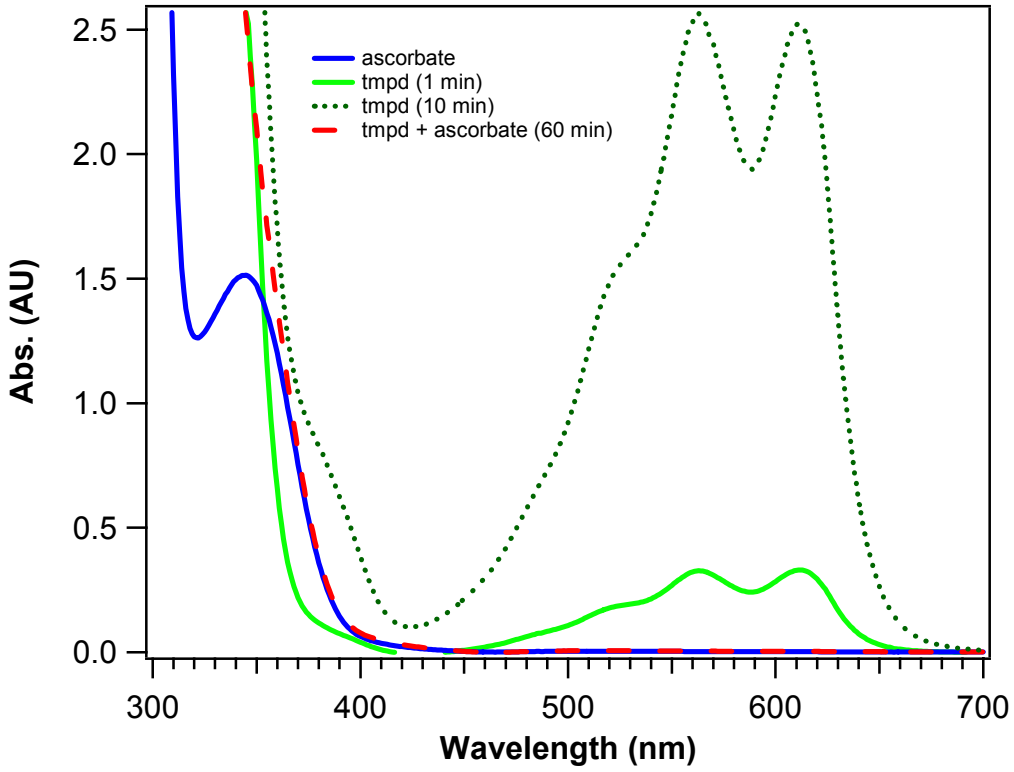

Figure 46. UV/visible absorption spectra of ascorbate and tmpd. Spectra were taken in the presence of tmRu-F_9bp (14 μM) before (blue and light green traces) and after (red dashed and green dotted traces) photolysis at 480 nm and then corrected for absorbance due to tmRu-F_9bp. For the tmpd radical cation, ε_{565} = 12.5 mM^{-1} cm^{-1} [152, 153] and ε_{612} = 12.0 mM^{-1} cm^{-1}.[151]

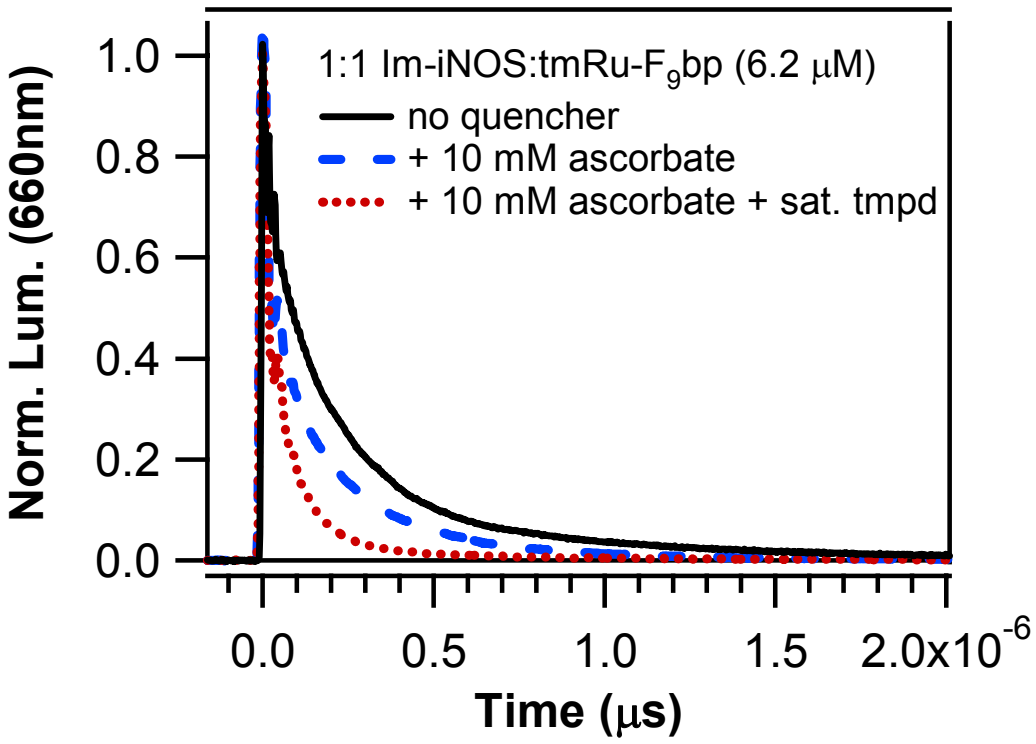

Figure 47. Luminescence decay of tmRu-F_9bp bound to Im-iNOSoxy in the absence of quenchers (black) and in the presence of 10 mM ascorbate (blue dashes) or 10 mM ascorbate and saturated tmpd (red dots). λ_{ex} = 480 nm and λ_{obs} = 660 nm.

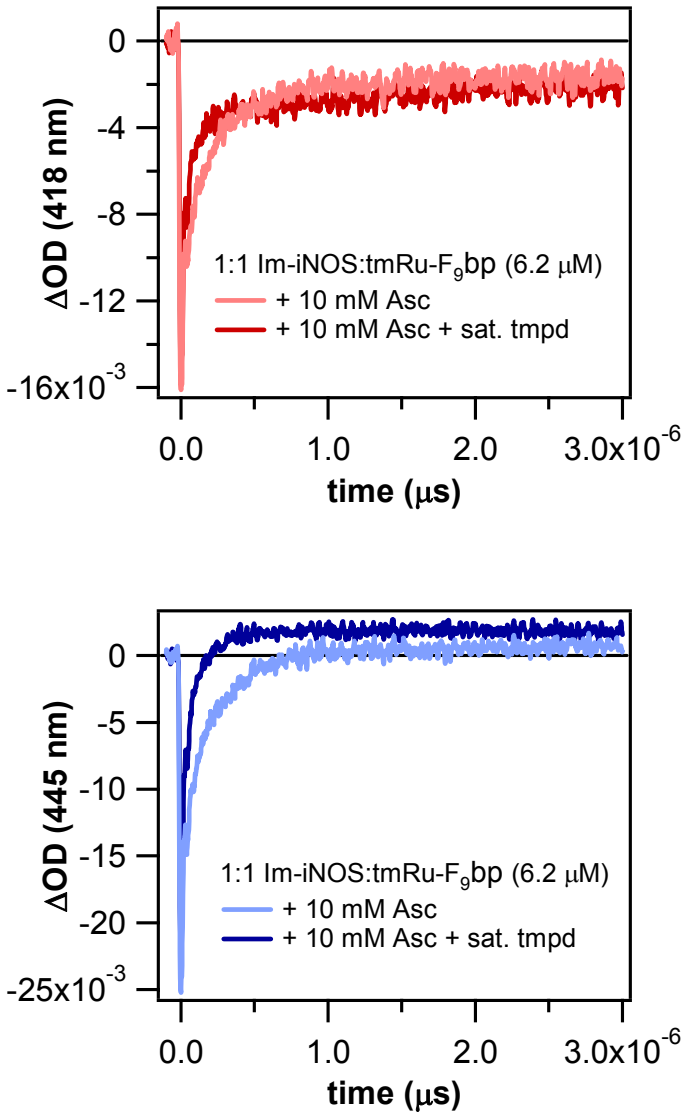

Figure 48. Transient absorbance of 1:1 mixtures of tmRu-F_9bp and Im-iNOSoxy in the presence of 10 mM ascorbate with (darker traces) and without (lighter traces) saturated tmpd. λ_{ex} = 480 nm. λ_{obs} = at 418 nm (top) and 445 nm (bottom). While ascorbate is capable of quenching the bound wire and producing Fe(II), the addition of tmpd increases the yield of reduced heme from ~0.2 percent to ~1 percent.

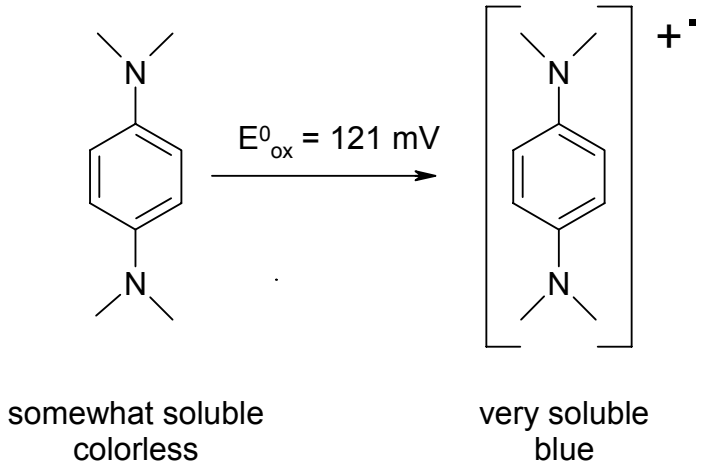

Figure 49. Tetramethylphenylenediamine (tmpd) in its reduced and oxidized forms.[151]

Rapid Production of Im-Fe(II)

Single wavelength transient absorbance of imidazole-bound iNOSoxy (Im-iNOSoxy) in the presence of one equivalent of tmRu-F_9bp, 10 mM Asc, and saturated tmpd produces Fe(II) within 50 ns of excitation at 480 nm (Figure **50**). This is confirmed by a point-by-point difference spectrum constructed from the single-wavelength data at 2 μs (Figure **51**) showing the bleach of the Im-Fe(III) Soret at 428 nm and the development of the Im-Fe(II) Soret at 445 nm. Control experiments with $Ru(bpy)_3^{2+}$ indicate that the perfluorobiphenyl moiety of tmRu-F_9bp is required for heme reduction. In the presence of $Ru(bpy)_3^{2+}$ and quenchers, transient absorbance traces show only the production of Ru(I) (Figure **52**). Once produced, the Fe(II) signal decays by at least two pathways with $k_{b1} = 1.29(4) \times 10^5$ s^{-1} and $k_{b2} = 1.7(1) \times 10^4$ s^{-1} (Figure **53**). This is not surprising given the presence in the sample of two reversible quenchers with multiple accessible redox states.

The yield of Fe(II) in each experiment (as calculated according to Equation 20 based on total heme content and $\Delta\varepsilon_{445} = 59.6$ mM^{-1} cm^{-1}) is 0.5-1 percent. Despite the fact that this is a low overall yield, its reproducibility and the lack of an Fe(II) signal from the iNOSoxy/$Ru(bpy)_3^{2+}$ mixture confirm that the signal is not an artifact.

Initial attempts to determine the rate of electron transfer to the heme (k_{ET}) were made by fitting the raw transient absorbance traces to multiple exponentials. Numerous complications were associated with this method. Due to the low yield of Fe(II), the Ru(II)* bleach and quenching kinetics dominate the observed signals (Figure **50**). Additionally, owing to the presence of both bound and free wire in solution, the

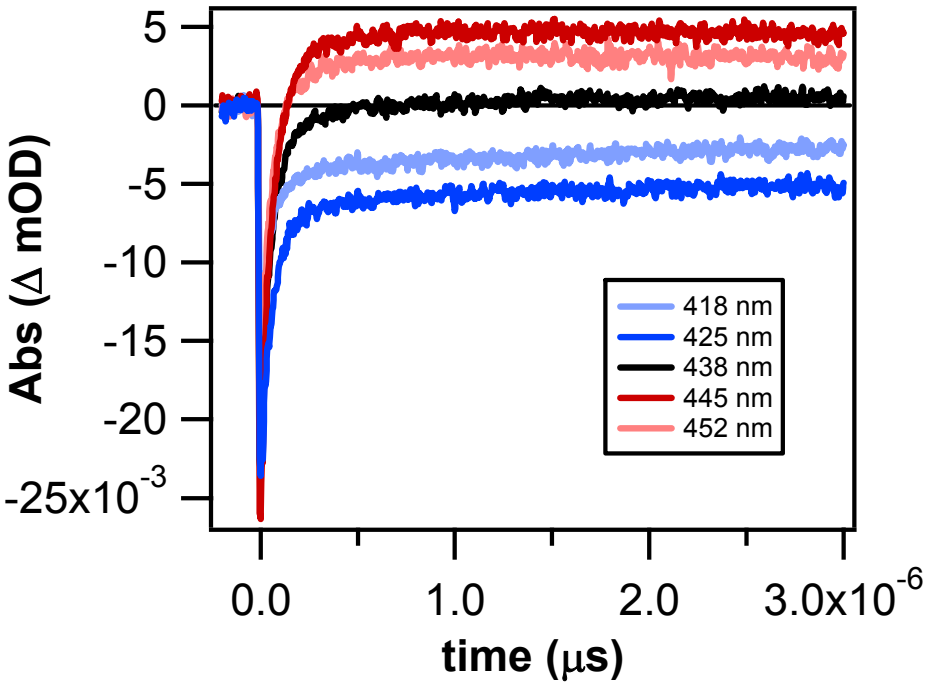

Figure 50. Transient absorbance of quenched Im-iNOSoxy bound to 1 equivalent of tmRu-F_9bp (11 μM with 10 mM ascorbate and saturated tmpd). λ_{ex} = 480 nm.

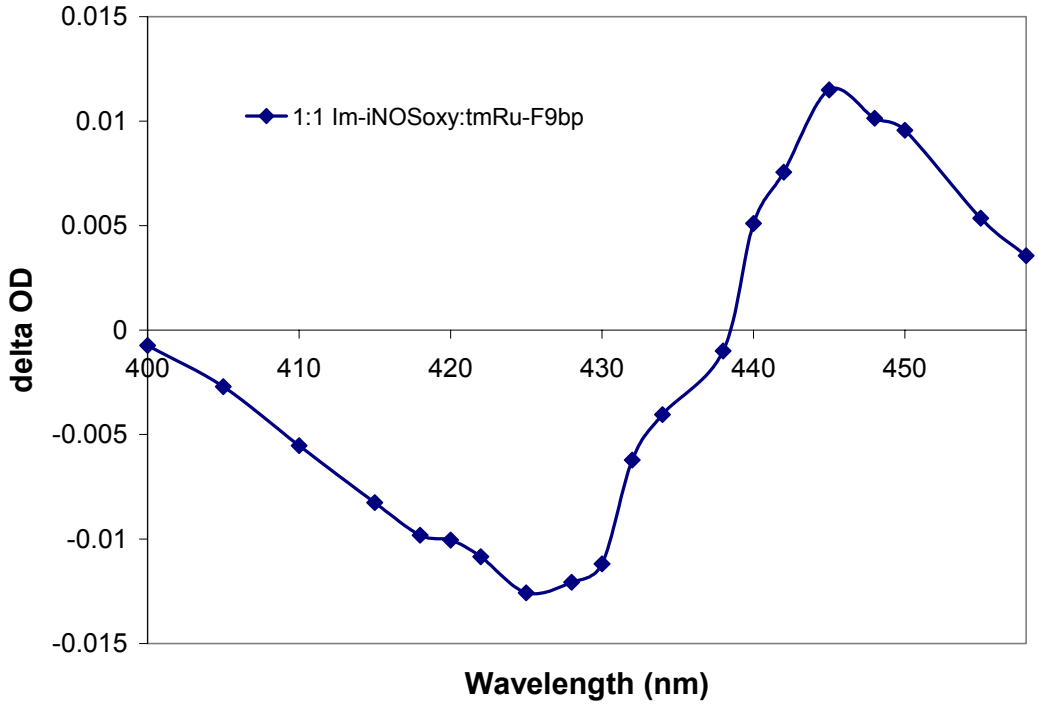

Figure 51. Transient absorbance of a 1:1 mixture of Im-iNOSoxy and tmRu-F_9bp (22 μM with 10 mM ascorbate and saturated tmpd) showing a characteristic Fe(III/II) difference spectrum. Individual points were taken from single wavelength transient absorbance traces, 2 μs after excitation at 480 nm.

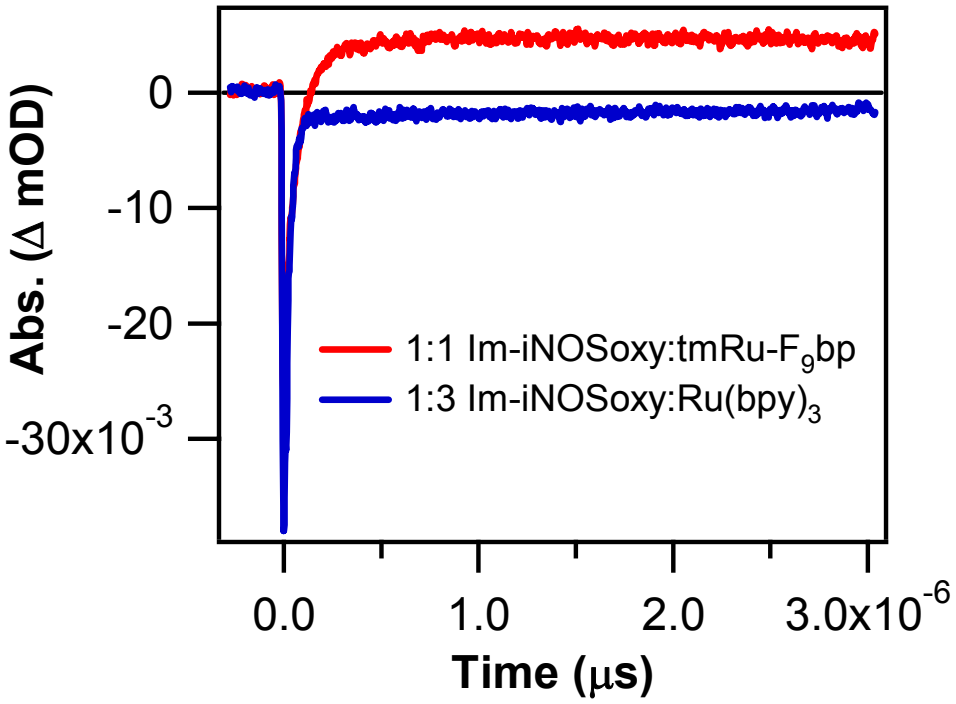

Figure 52. Transient absorbance of imidazole-bound iNOSoxy in the presence of tmRu-F_9bp or $Ru(bpy)_3^{2+}$ and quenchers (10 mM ascorbate + sat. tmpd). λ_{ex} = 480 nm, λ_{obs} = 445 nm. In the absence of the perfluorobiphenyl wire, quenched $Ru(bpy)_3^{2+}$ does not produce Fe(II). The long-lived bleach is due to Ru(I).

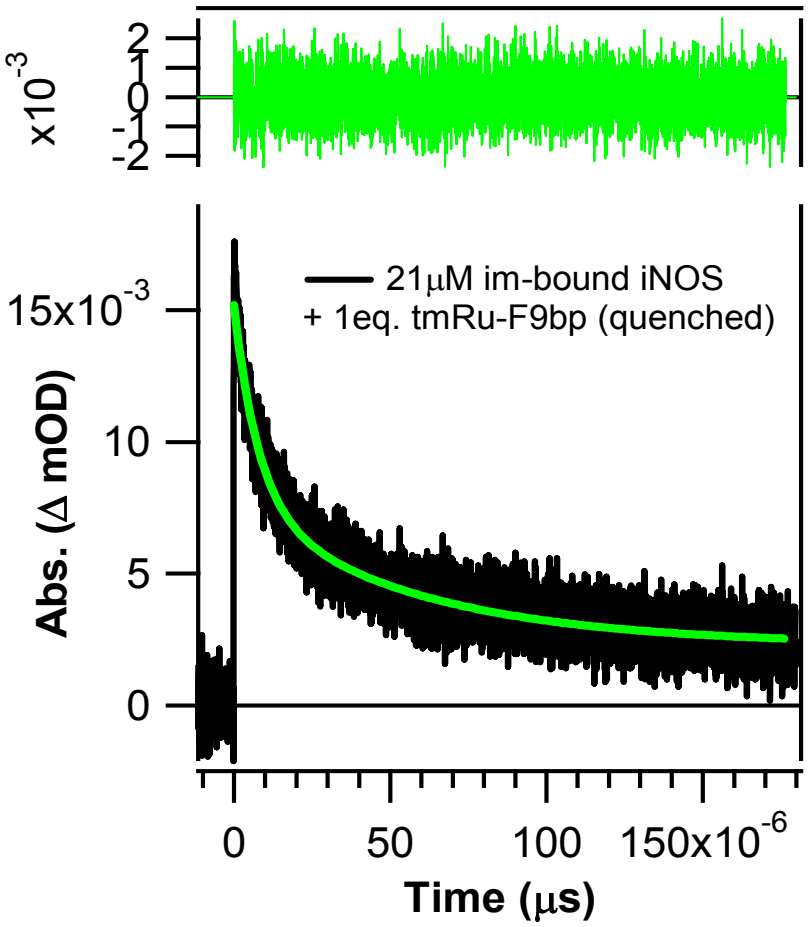

Figure 53. Transient absorbance of a 1:1 mixture of Im-iNOSoxy and tmRu-F_9bp in the presence of 10 mM ascorbate and saturated tmpd showing the multiexponential decay of Fe(II) (k_{b1} = 1.29(4) × 10^5 s^{-1}, k_{b2} = 1.7(1) × 10^4 s^{-1}).

quenching kinetics themselves are multiexponential (k_{Qbound} = 7.7(7) × 10^7 s^{-1} and k_{Qfree} = 1.0(4) × 10^7 s^{-1}). Finally, it was later discovered that $k_{ET} \approx k_{Qfree}$. Owing to one or more of these difficulties, the fitting program was unable to reproducibly extract k_{ET} from the raw transient absorbance data by this method.

Transient absorbance data were, therefore, corrected for the Ru(II)* signal as described in the Experimental section. While this method neglects any absorbance contributions from transiently produced Ru(I), reductive flash/quench experiments with μM solutions of tmRu-F_9bp in the absence of protein show ≤ 10 percent of the absorbance of the Fe(II) signals in the 400-450 nm window (Figure **54**). The assumption was made, therefore, that the contribution of the transient Ru(I) in the protein-bound system would be negligible. Removal of Ru(II)* from the picture clearly reveals the development of the Fe(II) signal (representative single-wavelength traces are shown in Figure **55**). The corrected traces (a minimum of four wavelengths from each of four different experiments completed on different days) were fit to one exponential using Equation 19 to obtain k_{ET} = 2.4(4) × 10^7 s^{-1}.

This is a remarkably fast reduction rate given the calculated Ru-heme distance of 20.2 Å[67] (Chapter 2) and the absence of a through-bond pathway to the heme. The mechanism by which this rapid electron transfer occurs is not known. Given its slim profile, extreme hydrophobicity, and potential to pi-stack with aromatic residues, the perfluorobiphenyl moiety of tmRu-F_9bp may intercalate into the protein interior, leaving open the possibility of a through-wire hopping mechanism such as that described in

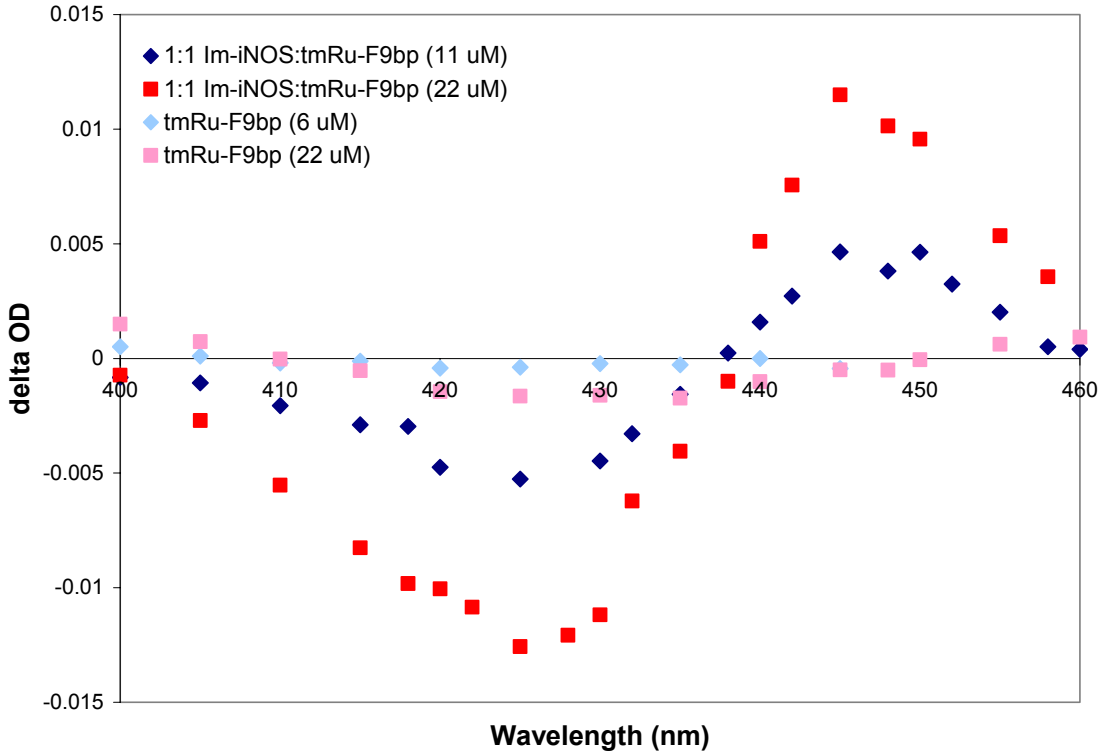

Figure 54. Transient absorbance at 2 μs of quenched tmRu-F_9bp in the presence and absence of one equivalent of Im-iNOSoxy demonstrating the negligible contribution of Ru(I) absorbance to the overall kinetics. Samples contain 10 mM ascorbate and saturated tmpd. λ_{ex} = 480 nm.

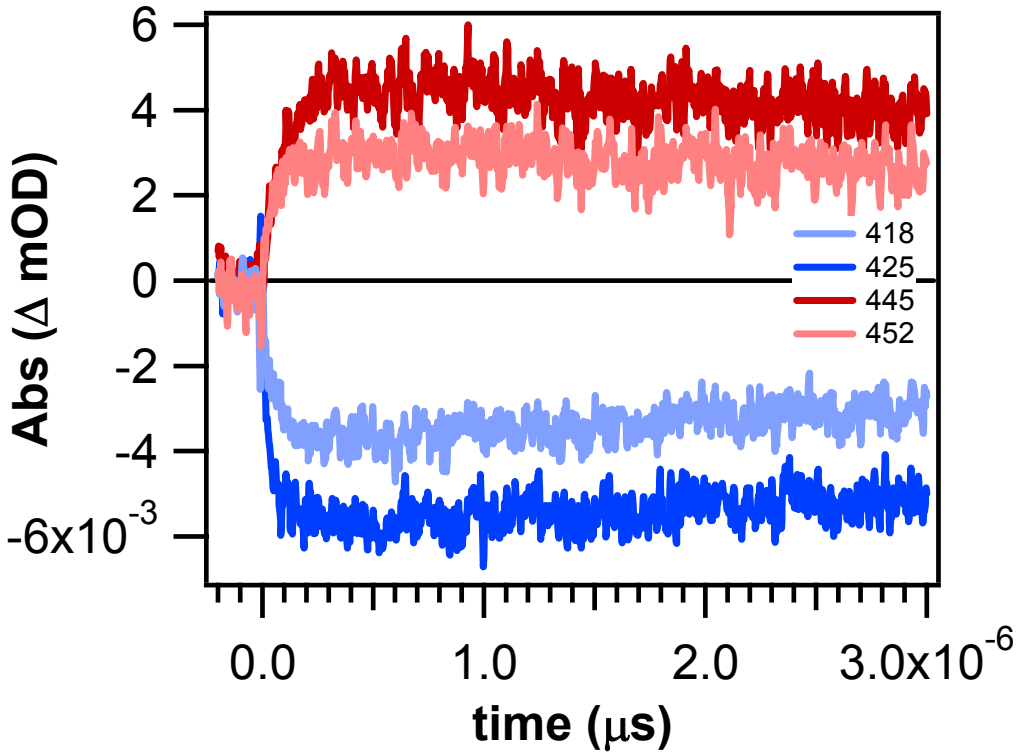

Figure 55. Transient absorbance of Im-iNOSoxy bound to 1 equivalent of tmRu-F_9bp (11 μM with 10 mM ascorbate and saturated tmpd) corrected for absorbance due to Ru(II)* to reveal $k_{ET} = 2.4(4) \times 10^7\ s^{-1}$. $\lambda_{ex} = 480$ nm.

Chapter 3 of this thesis. Other possibilities include a through-protein hopping mechanism or simply a fortuitous, highly-favorable tunneling pathway.

Heme Reduction in Substrate-Bound iNOSoxy

Irradiation at 480 nm of a solution of tmRu-F_9bp:iNOSoxy in the presence of 1 mM arginine (+ 10 mM Asc, + satd. tmpd) produces very small (~1 mOD) but reproducible (in 2 experiments) transient absorbance signals (Figure **56**). A difference spectrum constructed from single-wavelength measurements 2 μs after the laser pulse is shown in Figure **57** (red trace). While the tiny signal-to-noise ratio makes unambiguous interpretation of these data difficult, a few key points are worth noting. A point-by-point difference spectrum of quenched tmRu-F_9bp in the absence of protein (Figure **57**, green trace) confirms that the long-lived transient signals from the Arg-iNOSoxy:tmRu-F_9bp sample are not due to Ru(I). The most likely source of this difference spectrum is, therefore, Fe(II).

Operating under that assumption, identification of the Fe(II) species becomes the target. For 5-coordinate, high-spin Fe(II), the reported absorbance λ_{max} = 414 nm.[40, 156] While these authors reported the development of a pronounced shoulder at 445 nm upon high-spin heme reduction (in agreement with our results), the isosbestic point in each case was at 410 nm, well blue of the ~435 nm isosbestic point observed here. A possible explanation for this difference could lie in the incomplete conversion of the heme to high spin in the absence of H_4B. The affinity of pterin-free iNOSoxy for arginine is fairly poor. As observed previously,[40] addition of 1 mM arginine to a 9 μM sample of iNOSoxy in the absence of tetrahydrobiopterin produces only a partial shift to high spin

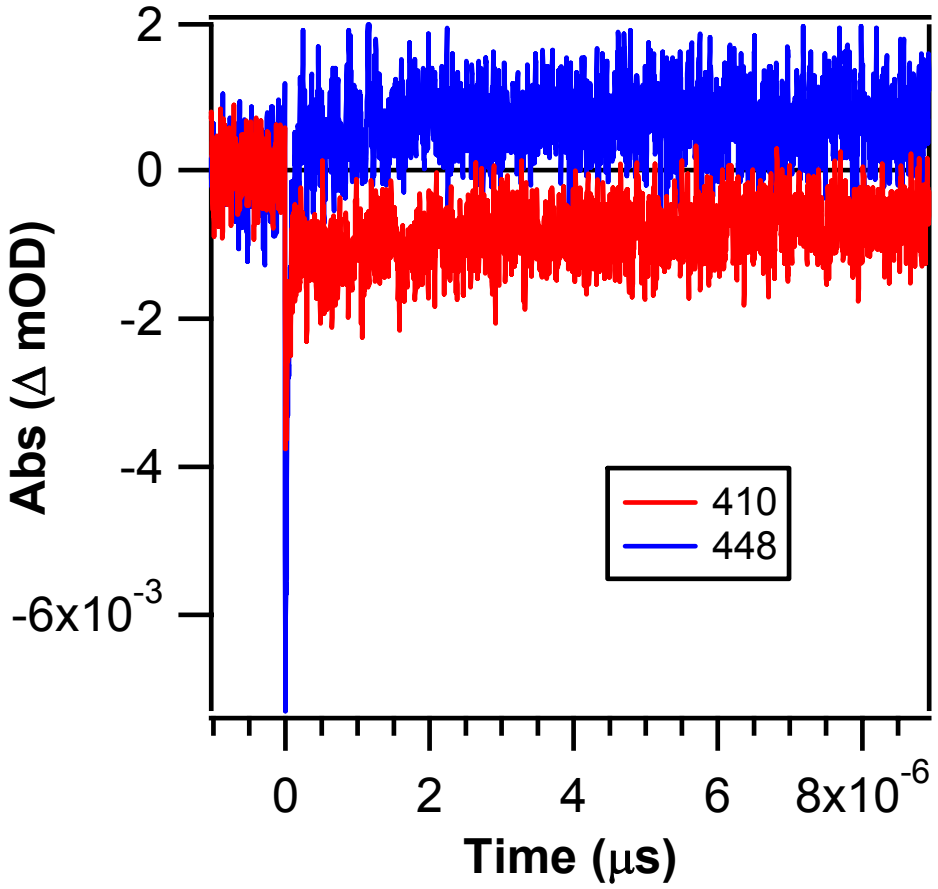

Figure 56. Transient absorbance of quenched Arg-iNOSoxy bound to 1 equivalent of tmRu-F$_9$bp (9 μM with 10 mM ascorbate and saturated tmpd). λ_{ex} = 480 nm, λ_{obs} = 410 nm (red), and λ_{obs} = 448 nm (blue).

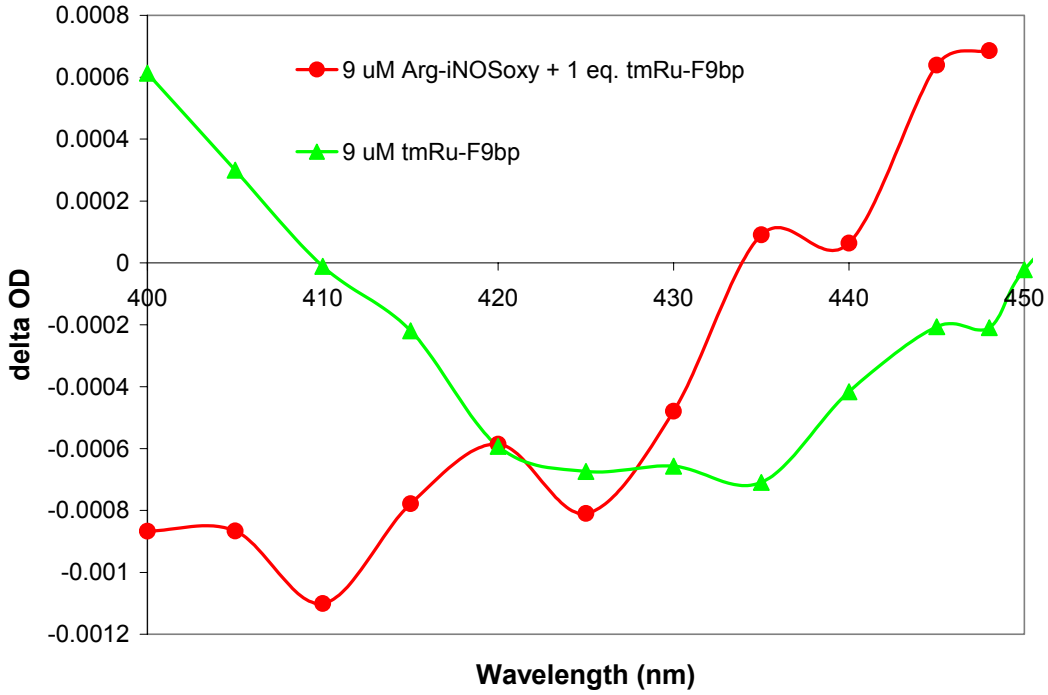

Figure 57. Transient absorbance of a 1:1 mixture of Arg-iNOSoxy and tmRu-F_9bp (9 μM, red) and tmRu-F_9bp only (9 μM, green), each with 10 mM ascorbate and saturated tmpd. Individual points were taken from single wavelength transient absorbance traces, 2 μs after excitation at 480 nm.

(Figure **58**, red trace). Concomitant reduction of both 5-coordinate and 6-coordinate (water-bound) heme could explain the shifted difference spectrum. In an effort to eliminate this ambiguity, Arg-iNOSoxy samples were incubated with 100 μM H_4B prior to addition of wire and quenchers in order to complete the conversion to the high-spin form (Figure **58**, green trace). Unfortunately, addition of H_4B to the sample completely inhibited Fe(II) production, whether the active site was imidazole- or arginine-bound. While care was taken to prepare the H_4B-bound samples in an oxygen-free environment, an absorbance shoulder at ~310 nm indicated the presence of oxidized pterin in the sample. It is, therefore, worth repeating this experiment. While (fully reduced) tetrahydrobiopterin is a poor electron acceptor,[157] fully- or partially-oxidized pterin contaminants could easily interfere with quenching and electron transfer.[§158, 159]

Redox titrations[48] and electrochemical measurements[160] (see Chapter 5) suggest that high-spin, arginine-bound iNOSoxy should be easier to reduce than its low-spin counterpart by ~115-130 mV. At first glance, therefore, one would expect electron transfer to even a partially high-spin heme to be more efficient than ET to Im-iNOSoxy. As such, the fact that we see less rather than more Fe(II) produced in the Arg-iNOSoxy samples is a mystery. As spin-state changes induce significant changes in heme conformation, however, it is possible that this result is due to a less favorable tunneling pathway to the arginine-bound heme.

[§] Inclusion of the ascorbate quencher at the beginning of the pterin incubation could be helpful in preventing pterin oxidation.

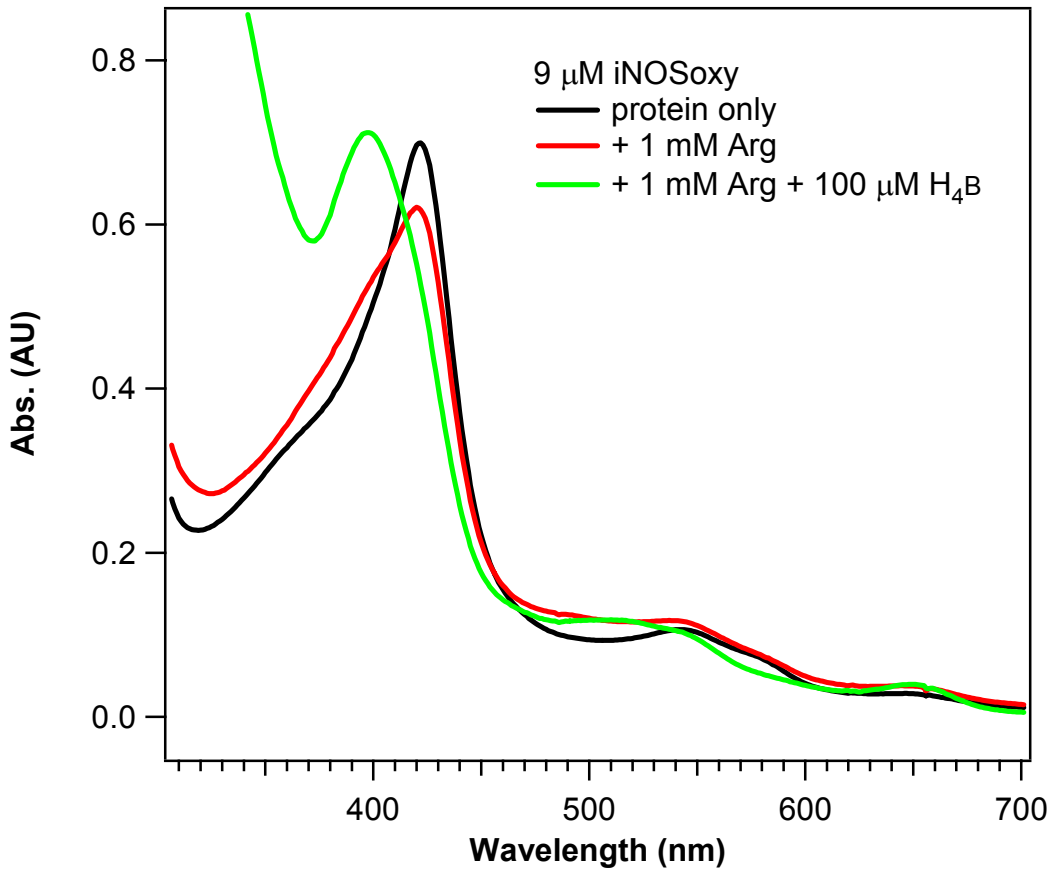

Figure 58. 9 μM iNOSoxy alone (black) and in the presence of 1 mM arginine (red) or 1 mM arginine + 100 μM H_4B (green).

Concluding Remarks

Herein we have described a system in which the heme of inducible nitric oxide synthase can be photoreduced rapidly without interfering with substrate/cofactor binding. Employing flash-quench experiments with a surface-binding Ru-diimine wire in combination with reductive quenchers, we observed reduction of the imidazole-bound heme of iNOSoxy in under 50 ns, fully seven orders of magnitude faster than the natural reduction. This finding represents an important step forward in our attempts to use wires to characterize the highly reactive intermediates of deeply-buried hemes in oxotransferase enzymes.

Preliminary results also indicate that the substrate-bound heme can be rapidly reduced using this system. Future work will focus on further development of these results through better quenchers and sensitizers as well as the study of the involvement of pterin in the NOS mechanism.

CHAPTER 5:

REDOX COUPLES OF INDUCIBLE NITRIC OXIDE SYNTHASE[†]

 Udit, A. K., Belliston-Bittner, W., Glazer, E. C., Nguyen, Y. H. L., Marletta, M. A., Goodin, D. B., and Gray, H. B., *J. Am. Chem. Soc.*, **submitted**.

Acknowledgement:

This work was completed in close collaboration with Andrew Udit, without whom the e-chem experiments would not have been completed. Many thanks are also owed to Phoebe Glazer and Yen Nguyen for their assistance in protein preparation and for their support in the e-chem lab on a Friday night. This one worked out for all of us!

Chapter 5

REDOX COUPLES OF INDUCIBLE NITRIC OXIDE SYNTHASE

Abstract

We report direct electrochemistry of the iNOS heme domain in a DDAB film on the surface of a basal plane graphite electrode. Cyclic voltammetry reveals Fe(III/II) and Fe(II/I) couples at -191 and -1049 mV (vs. Ag/AgCl). Added ligands imidazole and carbon monoxide shift the Fe(III/II) potential by +20 and +62 mV, while the addition of dioxygen results in large catalytic waves at the onset of Fe(III) reduction. Voltammetry at higher scan rates reveals that the Fe(III/II) cathodic peak can be resolved into two components, which are attributable to Fe(III/II) couples of 5- and 6-coordinate hemes. Scan rate analyses of the 5-coordinate iNOS heme indicate an ET rate constant (k^o) of $370 \pm 20\ s^{-1}$.

Introduction

The critical role of nitric oxide (•NO) in cellular signaling is now firmly established.[1] In higher animals, •NO is synthesized by nitric oxide synthase (NOS), which converts L-arginine to citrulline and •NO with NADPH and O_2 as co-substrates.[20] The enzyme consists of a reductase domain where reducing equivalents from NADPH are shuttled through bound flavins FAD and FMN, a calmodulin-binding region that controls electron transfer (ET) to the heme, and an oxidase domain that contains a cysteine-ligated heme and tetrahydrobiopterin (H_4B). Investigations reported here utilize the heme

domain of inducible NOS (iNOS), an immune system isoform implicated in a number of diseases in humans.[9]

The complexity of NOS and its impact on human health have thrust work on the NOS mechanism into the spotlight. It is well established that the catalytic cycle involves two turnovers of the enzyme. The first turnover converts L-arginine to N-hydroxyarginine: although envisioned as a P450-like hydroxylation, the reaction is dependent on one-electron oxidation of H_4B.[161] The second turnover is thought to involve a ferric peroxide nucleophile, but H_4B is also required for this cycle in a still undetermined role. Although many details of the NOS mechanism remain to be elucidated, it is certain that ET reactions are key, rate-limiting steps in the catalytic cycle. Recent structural studies of the neuronal NOS reductase module have led to the development of a model in which this slow electron transfer is due to a large scale movement of the FMN domain.[30] Demonstration of a well-coupled ET pathway between the oxidase domain surface and the heme would lend support to this model.

The study of protein electrochemistry has traditionally been difficult. Poor electronic coupling between a protein surface and its active site often lead to tiny signals that cannot be easily extracted from the background, and proteins tend to denature on bare surfaces.[162] Over the past several years, however, a number of different techniques for successful protein electrochemistry have been developed.[75, 84, 162, 163] One of the most broadly applicable is the use of thin surfactant films on an electrode surface (Figure **59**).[162, 164]

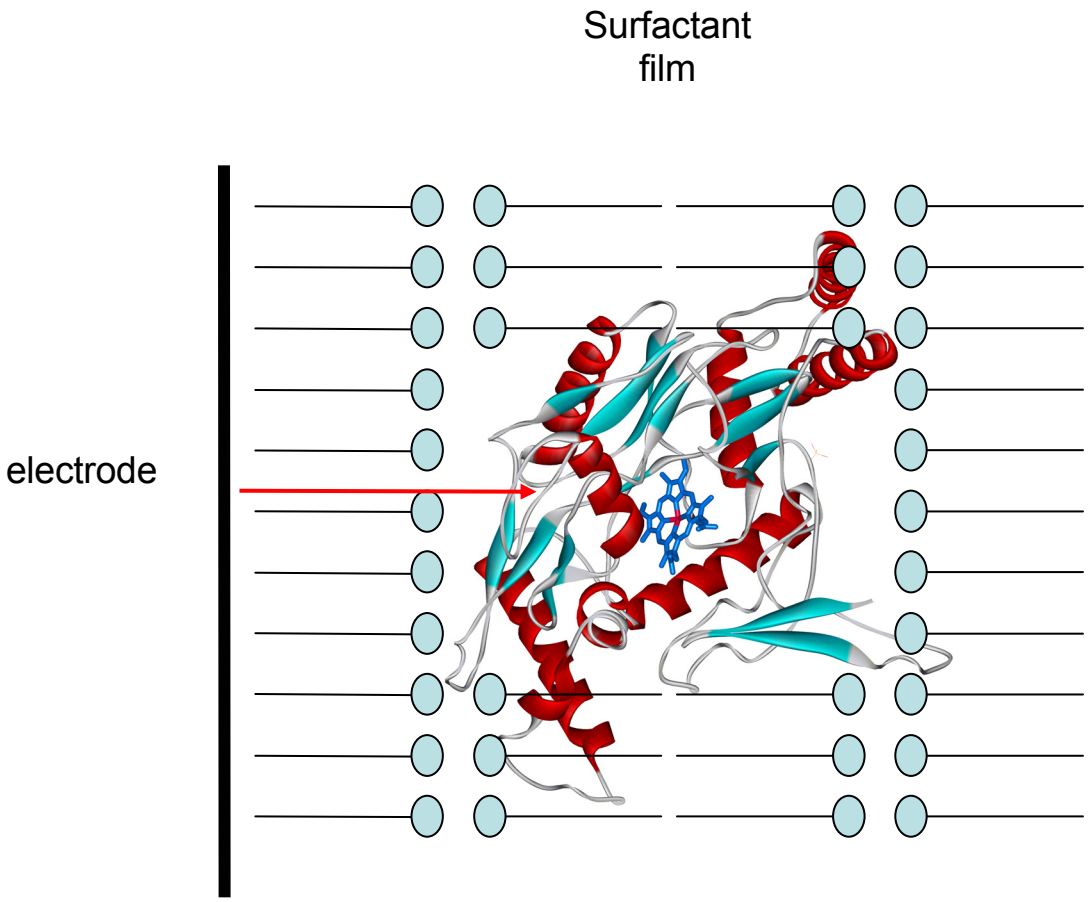

Figure 59. Graphical representation of iNOS electrochemistry at a DDAB-coated electrode.

Direct electrochemistry of the iNOS heme domain can be achieved by confining the protein in didodecyldimethylammonium bromide (DDAB) (Figure **60**) films on the surface of basal plane graphite electrodes (BPG) (Figure **61**).[§162, 165] Herein, we report reduction potentials for Fe(III/II) and Fe(II/I) couples, Fe(III/II) ET kinetics, catalytic reduction of dioxygen, and evidence for water-free and water-bound forms of the iNOS heme based on scan rate and pH dependence data.

Experimental

Protein Expression and Purification

iNOS heme domain was expressed and purified as previously described[40] with the following exceptions. Cells expressing protein were subjected to two rounds of chemical lysis. Cell pellets were resuspended in 40 mL of B-PER lysis buffer (Pierce) with 10 μg/mL benzamidine, 5 μg/mL leupeptin, 1 μg/mL each pepstatin, antipain, and chymotrypsin, ~500 μM Pefabloc (Roche), 100 μg/mL DNase, 100 μg/mL RNase, ~500 μg/mL lysozyme, and 20 mM imidazole per liter of cells and shaken for one hour at 4°C. The lysate was then spun down and the supernatant was loaded directly onto a nickel column (5 mL HisTrap, Amersham). The loaded column was washed with 20 column volumes of 20 mM imidazole in 50 mM NaP_i/300 mM NaCl/pH 8. The protein was eluted with 150 mM imidazole, concentrated to ~3 mL over an Amicon Ultra filtration device (10,000 MWCO, Millipore) and loaded onto a gel filtration column as previously

§ Direct electrochemistry of the neuronal nitric oxide heme domain utilizing surfactant film methodology has been reported. Square wave voltammetry confirms that the Fe(III/II) potential shifts in the presence of H_4B. A proton-coupled ET mechanism accounts for the observed pH dependence of the potential.

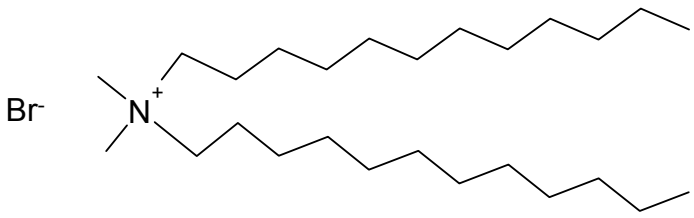

Figure 60. DDAB

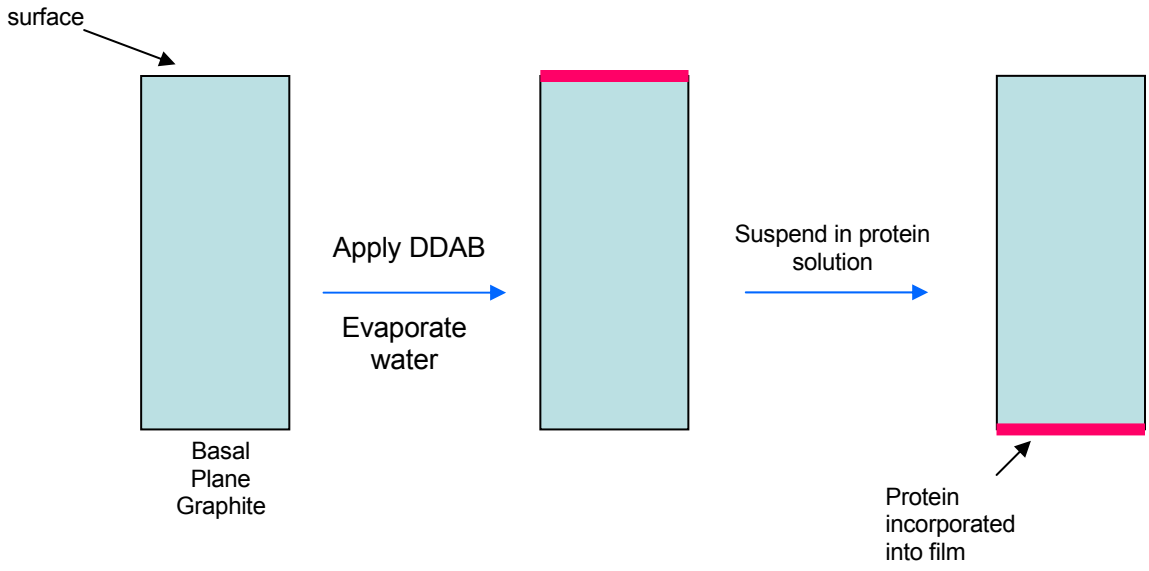

Figure 61. Protocol for preparing a DDAB film/protein-coated graphite electrode. Figure kindly provided by Andrew Udit.

described.[40] The anion exchange column was omitted when ≥ 95 percent purity was confirmed by UV-visible spectroscopy and gel electrophoresis.

Electrode Preparation and Voltammetry

Electrodes for voltammetry (0.07 cm^2) were made using the basal plane of pyrolytic graphite. The surfaces were prepared by sanding briefly with 600-grid sandpaper, followed by polishing with 0.3 and 0.05 μm alumina slurries. The electrodes were then sonicated and dried in air. DDAB films were formed by placing 5 μL of 10 mM DDAB in water on the surface of the electrodes, followed by slow drying in air overnight (Figure **61**). iNOS was incorporated into the film by soaking the DDAB-filmed electrode in a solution of enzyme (~ 20 μM in 50 mM KP_i, pH 7 buffer) for 30 minutes, followed by gentle rinsing with ddH_2O.

A CH Instruments Electrochemical Workstation system was used for the experiments. Voltammetry experiments were performed in a 3-compartment cell, using a platinum wire auxiliary and a Ag/AgCl reference electrode (BAS). All experiments were performed under argon in thoroughly degassed buffer (50 mM KP_i, 50 mM KCl, pH 7) unless otherwise stated.

Digital Simulations

Simulations were performed with software from the CH Instruments Electrochemical Workstation. The square scheme shown in Figure **62** was used for the model. k^o for the 5-coordinate heme ET reaction was experimentally determined to be 370 s^{-1}. For the 6-coordinate heme ET reaction, a k^o value of 10 s^{-1} (consistent with previous observations for NOSs)[42] resulted in the best simulated voltammograms.

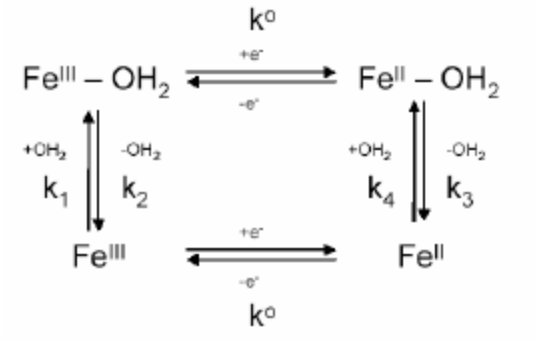

Figure 62. Square scheme model used for the digital simulation of cyclic voltammograms at various scan rates (Figure **69**).

A surface-confined system was modeled with the following parameters: capacitance = 4 μF, surface coverage = 5×10^{-11} mol/cm^2, electrode area = 0.07 cm^2, $E^o(Fe^{III/II})$ = -150 mV, $E^o(Fe^{III/II}–OH_2)$ = -250 mV. Values for k_1, k_2, and k_3 were entered into the simulation until a single set of rate constants was found that could adequately reproduce the experimentally derived voltammograms at 0.05, 1, and 8 V/s at pH 7 (Figure **64**a). For each simulation, k_4 was determined by the software. Notably, the simulation was insensitive for values of $k_3 > 100$ s^{-1}.

Results and Discussion

A voltammogram of iNOS in DDAB on BPG is shown in Figure **63**. We have assigned E_1 (-191 mV) and E_2 (-1049 mV) to heme Fe(III/II) and Fe(II/I) couples, consistent with other studies of heme proteins in DDAB films.[166, 167] Notably, a couple similar to E_2 was observed for neuronal nitric oxide synthase (nNOS), but was not assigned.[§,165] Our assignments of E_1 and E_2 are supported by voltammetry in the presence of carbon monoxide: E_1 shifts approximately +62 mV (consistent with other studies),[168, 169] while E_2 is not observed (presumably beyond the solvent window). For comparison, redox titrations of iNOS in its resting state (6-coordinate heme, low spin) conducted in solution yield a potential of -544 mV (vs. Ag/AgCl) for Fe(III/II).[48] As previously suggested, local electrostatic effects likely contribute to the altered potential on the electrode surface.[170]

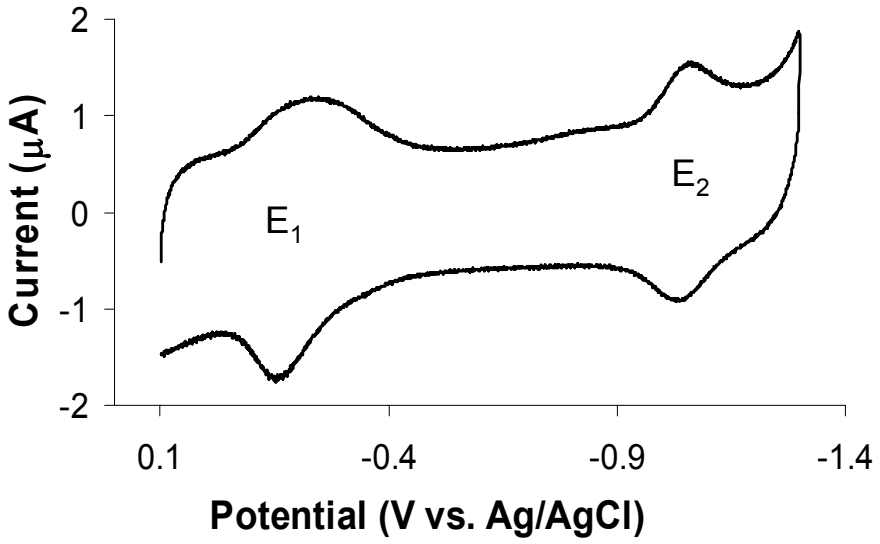

Figure 63. Cyclic voltammogram of iNOSoxy in DDAB on BPG (0.07 cm^2) at 200 mV/s in 50 mM KP_i/50 mM KCl, pH 7.

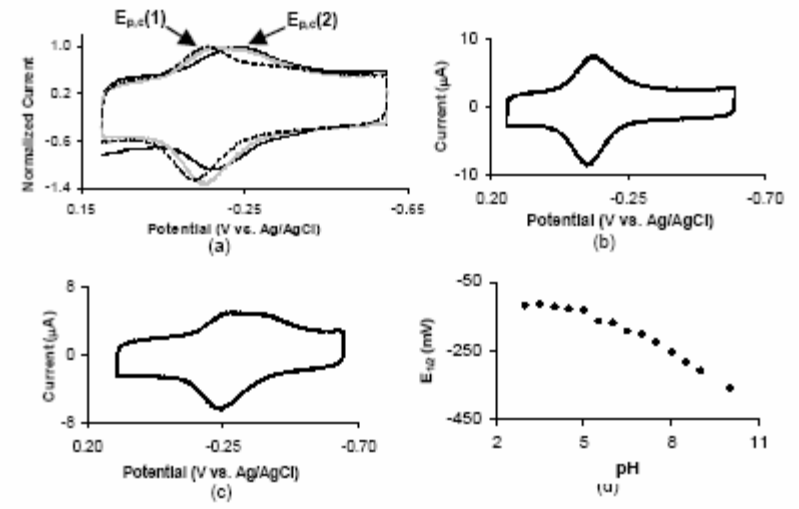

Figure 64. Cyclic voltammograms of iNOS in DDAB on BPG in 50 mM KP_i/50 mM KCl a) at 0.05 (black), 1 (gray), and 8 (dashed) V/s, pH 7; b) at 1 V/s, pH 5; c) at 1 V/s, pH 9. d) Variation of the average Fe(III/II) midpoint potential with pH at 200 mV/s.

Besides CO, other molecules in solution also bind the heme. In the presence of 500 μM imidazole, E_1 shifts +20 mV. When dioxygen is added, large catalytic reduction currents at the onset of E_1 are observed (Figure **65**). For E_1, the peak current is linear with scan rate (surface bound) up to 16.7 V/s, after which it is linear with the square root of the scan rate (diffusive) (Figure **66**).[171] This behavior is characteristic of thin film electrochemistry and indicates finite diffusion of the protein within the film.[172] Thus, up to 16.7 V/s, we treated the redox system as surface-confined.

Close inspection of Figure **63** reveals that the E_1 cathodic wave is slightly broader than the other waves. Voltammetry at variable scan rates allowed us to resolve this peak into two distinct cathodic processes, $E_{p,c}(1)$ and $E_{p,c}$ (2). Figure **64**a shows voltammograms recorded in pH 7 buffer at different scan rates. At high and low scan rates (8 vs. 0.05 V/s), only one cathodic peak ($E_{p,c}$ (1) vs. $E_{p,c}$ (2)) is present, while both cathodic processes are observed at intermediate (1 V/s) scan rates. In addition to being scan-rate dependent, these cathodic processes are also pH dependent. At pH 5 and 1 V/s (Figure **64**b), only one cathodic peak ($E_{p,c}$ (1)) is present. Conversely, at pH 9 (Figure **64**c) two distinct cathodic peaks are visible at 1 V/s; in fact, at higher pH, $E_{p,c}$ (2) is even more prominent. Notably, during the first cathodic sweep $E_{p,c}$ (2) predominates, while in subsequent cathodic sweeps both $E_{p,c}$ (1) and $E_{p,c}$ (2) are resolved.

This pH and scan-rate dependence led us to believe that the iNOS heme axial water ligand is involved in an equilibrium that gives rise to $E_{p,c}$ (1) and $E_{p,c}$ (2) (Figure **67**). At pH 7 and 1 V/s, the first cathodic sweep results in $E_{p,c}$ (2). This correlates with initial reduction of Fe(III) – OH_2. The lability of the Fe(II) – OH_2 bond results in rapid

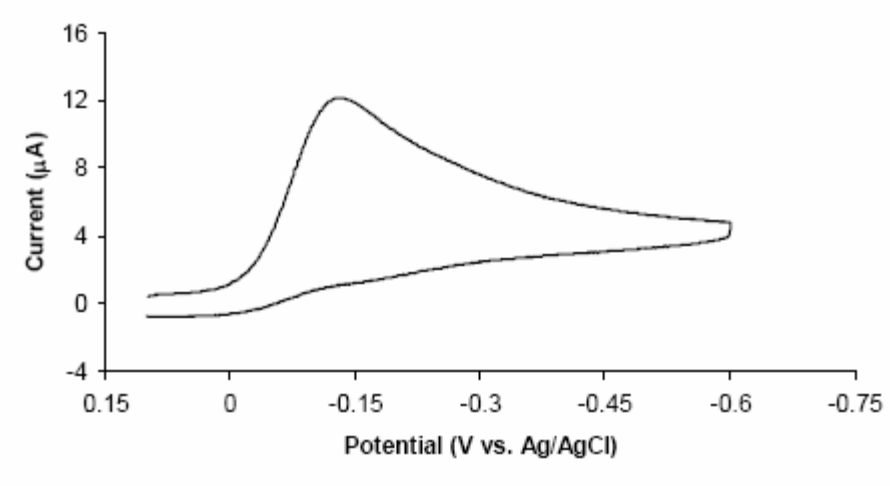

Figure 65. Cyclic voltammogram of iNOSoxy in DDAB on BPG (0.07 cm^2) at 200 mV/s in 50 mM KP_i/50 mM KCl, pH 7 and 94 μM O_2.

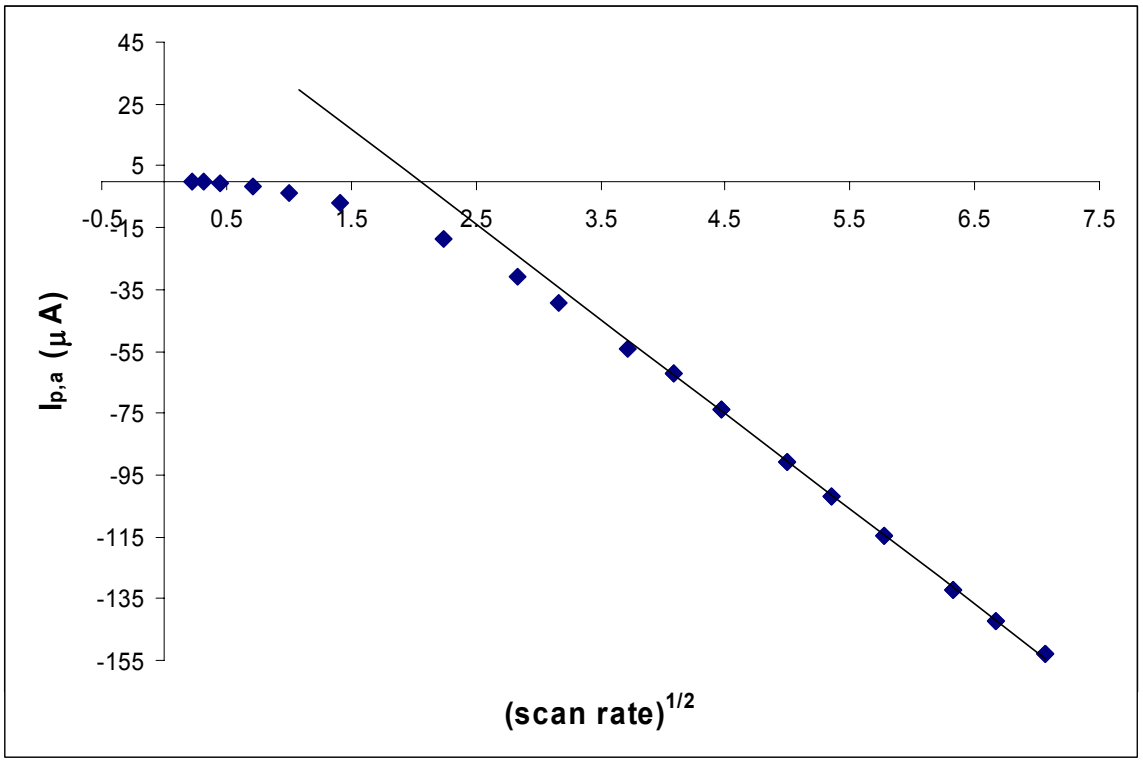

Figure 66. Plot of anodic peak current vs. the square root of the scan rate showing the surface-bound behavior of iNOS in the film up to 16.7 V/s, after which point the behavior becomes diffusive (linear with the square root of the scan rate).

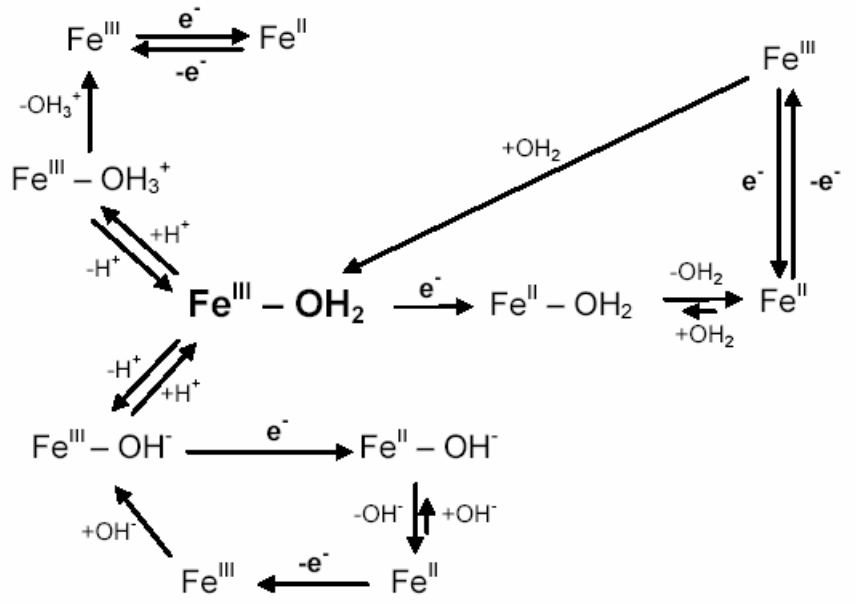

Figure 67. Proposed ET, proton transfer, and water-binding/dissociation processes occuring at a DDAB/NOS-coated BPG electrode.

conversion to a 5-coordinate heme.[62, 173] Oxidation of Fe(II) to Fe(III), followed by a second cathodic sweep at intermediate scan rates (1 V/s, Figure **64**a) gives rise to two reduction peaks, corresponding to reduction of water-free ($E_{p,c}$ (1)) and water-bound ($E_{p,c}$ (2)) Fe(III) hemes.

Our interpretation is supported by the following observations. First, $E_{p,c}$ (1) and $E_{p,c}$ (2) differ by approximately 133 ± 9 mV, a value consistent with the potential difference between 5- and 6-coordinate iNOS hemes.[48] Second, voltammetry at low pH results in a single cathodic peak attributable to $E_{p,c}$ (1). Under acidic conditions, disruption of hydrogen bonding in the heme pocket likely leads to dissociation of the axial water, resulting in a 5-coordinate heme. Third, voltammetry at high pH (Figure **64**c), where the axial water is partially deprotonated, shows that $E_{p,c}$ (2) is more prominent. It is expected that hydroxide will have greater affinity for the cationic metal center, thereby shifting the cathodic peak distribution further to $E_{p,c}$ (2). Fourth, voltammetry with imidazole present yields a single cathodic process, consistent with constant heme ligation as it cycles between oxidation states (Figure **68**).[174]

The dependence of the cathodic peak distribution on scan rate can be explained in terms of Figure **67**. At high scan rates, after oxidation of Fe(II), reduction of water-free Fe(III) occurs faster than water ligation to Fe(III), yielding only $E_{p,c}$ (1). Conversely, scanning slowly allows enough time for water ligation to Fe(III) before reduction occurs, shifting the cathodic peak distribution to $E_{p,c}$ (2). Thus, intermediate scan rates yield both $E_{p,c}$ (1) and $E_{p,c}$ (2).

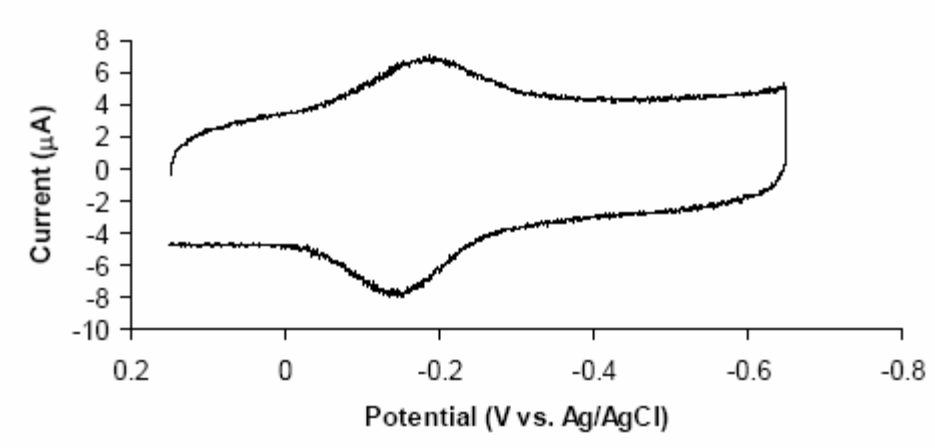

Figure 68. Cyclic voltammogram of iNOS in DDAB on BPG in 50 mM KP_i/50 mM KCl, pH 7 and 500 μM imidazole at 1 V/s. Note that only a single cathodic process is observed (cf. Figure **64**a).

Using $E_{p,c}$ (1), k^o (assuming $\Delta G^o = 0$) for ET to the 5-coordinate heme evaluated at 16.7 V/s and pH 7 is 370 ± 20 s^{-1}.[175] This rate indicates that a facile ET pathway from the enzyme surface to the active site exists and suggests that the slowness of the rate-limiting transfer of an electron from the FMN to the heme domain is not due to poor surface-heme coupling. Using this k^o value, we digitally simulated the experimental results in Figure **64**a (see Experimental section). ET kinetics were modeled according to the square scheme shown in Figure **62** in order to simulate the observed voltammograms. From the simulation, we estimated values for k_1, k_2, and k_3 of 1 s^{-1}, 0.5 s^{-1}, and 100 s^{-1}, respectively. Using this procedure, we were able to accurately model the voltammograms in Figure **64**a (see Figure **69**).

As expected,[62, 173] water dissociation from Fe(II) is rapid (k_3), while the kinetics of the Fe(III) equilibrium with water (k_1, k_2) appear to be slow. In the catalytic cycle of iNOS, the first ET event is proposed to be the rate-limiting step for substrate turnover, occurring at 1 s^{-1}.[43] Based on our simulation, we suggest that water dissociation from Fe(III) may function as a potential gating mechanism for the catalytic cycle. Although speculative for iNOS, water-gated ET is consistent with what is known for the similar cytochromes P450.

Proton-coupled ET was observed for nNOS in DDAB films as demonstrated by the variation of $E_{1/2}$ with pH.[165] For comparison, we performed voltammetry on iNOS at 200 mV/s and plotted the variation of $E_{1/2}$ with pH for E_1 (Figure **64**d).[†] The data reveal

[†] At 200 mV/s, the two cathodic peaks in E_1 collapse into a single peak, yielding a potential representative of the population distribution between $E_{p,c}$(1) and $E_{p,c}$(2) and permitting us to estimate a midpoint potential ($E_{1/2}$) for E_1.

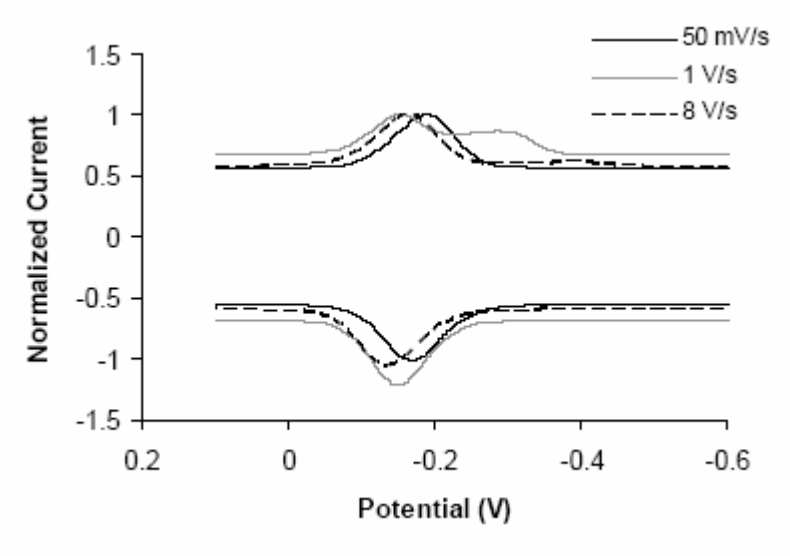

Figure 69. Digitally simulated voltammograms at 0.05 (black), 1 (gray), and 8 (dashed) V/s for iNOS in DDAB films. Simulation details are reported in the Experimental section.

no variation of $E_{1/2}$ for pH < 5, implying simple conversion of 5-coordinate Fe(III) to Fe(II). At pH > 7, $E_{1/2}$ varies linearly with pH according to -53 mV/pH unit, as is often found for heme proteins.[176, 177] The observation of proton-coupled ET in a pH range where the heme is water-ligated further underscores that the heme axial water ligand plays a significant role in iNOS ET.

CHAPTER 6:

CONCLUDING REMARKS AND FUTURE DIRECTIONS

Chapter 6

CONCLUDING REMARKS AND FUTURE DIRECTIONS

This thesis has described a body of work that was aimed at examining the catalytic mechanism of and electron transfer processes in inducible nitric oxide synthase. Through the development of a series of Ru- and Re-diimine wires that bind tightly to and rapidly reduce the iNOS oxidase domain, we have moved a few steps closer to our ultimate goal of characterizing highly reactive intermediates in electroactive heme enzymes.

The Re-diimine wires described in Chapter 3 reduce the iNOS heme extremely rapidly upon photoexcitation. The development of a system capable of rapid heme reduction in the absence of exogenous quenchers presents numerous advantages for the future. First and foremost is the possibility of observing ET processes in single crystals. Because the flash/quench method generally requires diffusive collision of the excited sensitizer and the quencher molecule, obtaining x-ray structural data before and after a flash/quench process would generally not be possible. As the "quencher" in this case appears to be a part of the enzyme, however, the diffusion issue is no longer a problem. Hurdles to overcome with respect to such an x-ray experiment include the development of quenched, channel-binding wires that will bind tightly to the tightly dimerized oxidase domain as well as manipulation of the system to produce a higher yield of Fe(II). Confirmation of the identity of the active amino-acid quencher and further studies to elucidate the mechanism by which the electron moves so rapidly from Re to Fe should

help to solve these issues and guide development of future generations of channel-binding wires for NOS.

A second advantage of the "quencherless" Re wires is the possibility of employing this system to effect the reduction of the ferric-superoxo intermediate without the hassle and potentially damaging effects of reductive quenchers and oxygen in the same solution. The Im-terminated wires, Re-Im-F_8bp-Im and Re-Im-C_3-F_8bp-Im, would prevent formation of the ferric-superoxo species because they ligate the heme. Re-Im-C_3-F_9bp, however, appears to be rapidly quenched without blocking the axial heme site. While it doesn't reduce 5-coordinate Fe(III) to Fe(II), this is likely due to the gap between the terminal fluorine and the heme iron. In an experiment designed to effect the *second* reduction in the NOS mechanism, however (Figure **70**), the presence of the superoxo moiety may bridge the gap and allow electron transfer to occur, leaving the opportunity for trapping and observation of one or more subsequent intermediates (blue species in Figure **70**).

The Ru-diimine wire described in Chapter 4 binds to the enzyme distant from the heme active site and independently of substrate and cofactors, yet is still capable of ns heme reduction under flash-quench conditions. This type of wire opens the door to future attempts to turn over the enzyme photochemically. Initial experiments in this direction will likely employ steady-state irradiation in the presence of pterin, arginine, and O_2 in order to look for measurable •NO and citrulline production. Further investigations can then be made using sequential excitation pulses and introduction of oxygen by a stopped-flow apparatus in order to observe the entire mechanistic cycle spectroscopically.

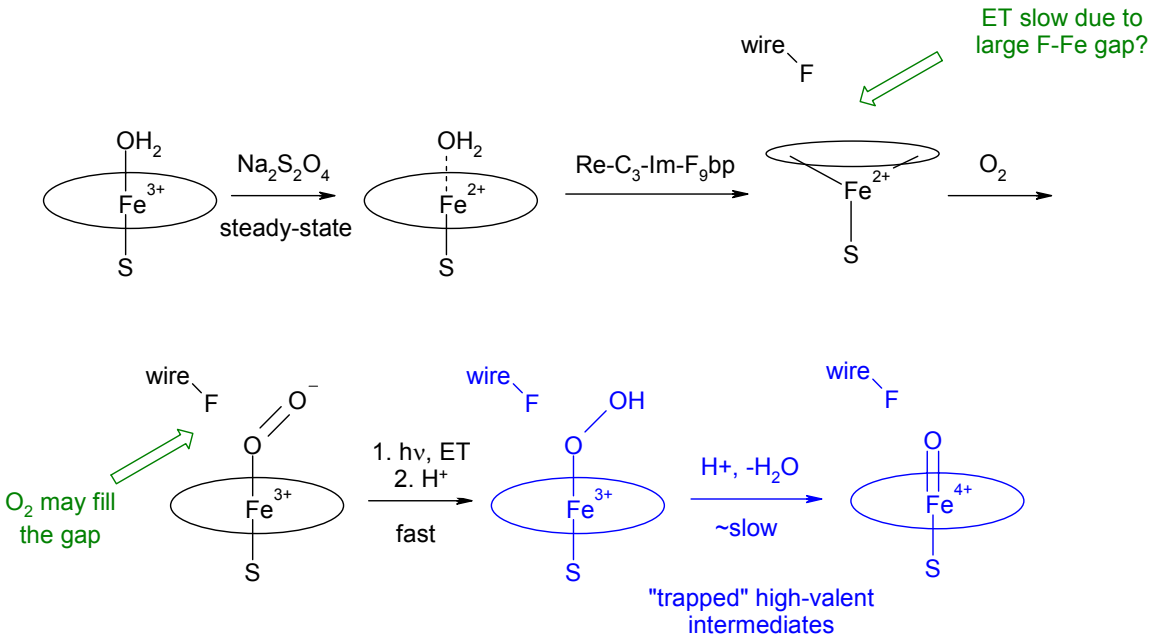

Figure 70. Possible experimental design for the observation of high-valent intermediates in NOS with the use of Re-Im-C_3-F_9bp.

Improvement of the yield of injected electrons could be accomplished in many ways. These include the improvement of sensitizer excited-state lifetime of the enzyme-bound wire, thereby increasing the probability of reductive quenching. This goal can be achieved by using a sensitizer with a more stable excited state, by employing a sensitizer with a red-shifted luminescence in order to minimize overlap with the heme absorbance (thereby minimizing Förster energy transfer quenching),[§] or even by constructing a wire that has *increased* luminescence upon binding at the hydrophobic site (such as the DNA "lightswitch," $[Ru(phen)_2(dppz)]^{2+}$).[178-180] Another consideration is the need to retain sensitizer bulk in order to prevent channel binding. Fortuitously, these objectives can be met simultaneously. Because binding to the NOS surface is expected to be controlled by the perfluorobiphenyl wire, alteration of the sensitizer should be as straightforward as adjusting the other diimine ligands on ruthenium or switching to any other large, metal-based sensitizer. By turning to Ru-diimines with extended π-systems[178-181] or to pseudo-octahedral iridium-cyclometalates (Figure **71**b),[182, 183] one or more of the three objectives (extended excited-state lifetime, red-shifted luminescence, and bulk) may be achieved simultaneously. Indeed, the first experiments in this direction have already been completed by Yen Nguyen, who has synthesized the wires shown in Figure **71**a.

[§] In so doing, care must be taken not to completely eliminate FET as this is likely to be the best (or only) spectroscopic handle for calculation of wire binding affinity.

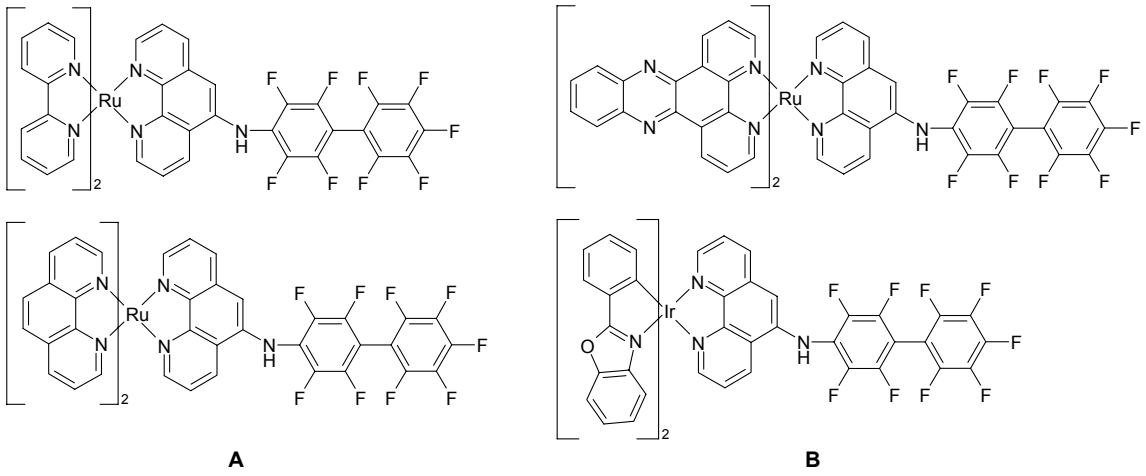

Figure 71. New generations of wires for binding to the surface of iNOSoxy. a) Wires that have been synthesized and are currently being tested by Yen Nguyen. b) Possible future wires for improvement of luminescence lifetime and bulk.

In addition to their rapid electron transfer capabilities, all of the wires described in this thesis present excellent opportunities for novel inhibition of NOS. Re-Im-F_8bp-Im binds to the active site of iNOSoxy (-H_4B) with a nM dissociation constant, within a factor of 10 of some of the tightest-binding NOS inhibitors reported.[184-188] This wire, which does not bind to tightly dimerized iNOSoxy, also resembles antifungal imidazoles that have been shown to block dimerization of iNOS.[189] This presents the intriguing possibility that Re-Im-F_8bp-Im may be not only a potent, but a selective inhibitor of iNOS as this is the only of the NOS isozymes to exhibit an *in vivo* monomer/dimer equilibrium. Future studies aimed at examining inhibition and isozyme selectivity are certainly warranted.

A recent structure of the dimerized nNOS reductase module has led to the development of a model for ET in NOS in which the entire FMN domain flips up to dock with the oxidase domain.[30] In this model, the sluggishness of the first electron transfer in the NOS cycle is accounted for by the necessity for this large-scale domain shift. The cyclic voltammetric studies of iNOS in DDAB films reported in Chapter 5 of this thesis lend support to this model. By showing heme reduction at a rate of ~400 s^{-1}, the CV studies confirm the existence of well-coupled ET pathways from the enzyme surface to the active site and suggest that ET itself is not rate-limiting.

Based on this proposed model for the interaction of the FMN and oxidase domains, inhibition studies with tmRu-F_9bp and full-length iNOS should be another excellent step forward in the wire project. tmRu-F_9bp is expected to bind to iNOSoxy at the site of FMN domain docking, and, as such, presents the possibility of inhibition through the disruption of protein:protein interactions. In 2004, Gestwicki and coworkers

made one of the year's breakthrough discoveries[190] by describing one of the first examples of disruption of large-scale protein interactions by a small molecule.[191] This type of inhibition is, therefore, a relatively unexplored field and could prove extremely valuable for the selective disruption of the NOS ET process. The same types of wire modifications that were discussed above for improvement of the Fe(II) yield in photoreduction (Figure **71**) may also prove beneficial in this kind of inhibition experiment. By increasing the size of the sensitizer on the bound wire, the chance for disruption of the key protein:protein interactions will be improved.

New NOS Wires

Aside from developing wires that bind distant from the active site, a way to avoid the problem of channel blockage in mechanistic ET studies is to attach the substrate directly to the wire. To that end, an entirely new generation of NOS-binding wires is being developed by Yen Nguyen. In the first round of substrate wires for NOS, arginine- and nitroarginine-based Re-diimine wires have been synthesized. The nitroarginine wire binds at the active site of iNOSoxy with a micromolar K_d, and preliminary studies indicate that it may reduce the heme upon 355-nm photoexcitation. Additionally, studies are underway to determine whether the enzyme is capable of turning over these wires.

Another outstanding question in the study of the NOS catalytic mechanism is the role that the tetrahydrobiopterin cofactor plays in electron transfer and heme reduction. In order to investigate these processes, Phoebe Glazer is developing pterin-based wires. Preliminary tests indicate that the wires bind to NOS, and flash/quench experiments to examine their heme-reducing capabilities will be underway soon.

As is the case with any complex and intriguing system, the experiments described in this thesis have raised at least as many questions as they have answered. With structural, mechanistic, and electron transfer studies on P450cam and amine oxidase already well underway, and now the description of a series of NOS binding wires, the wire project has entered its adolescence. Wires have been developed for binding into and away from the active sites of various enzymes, for flash/quench and photoinduced redox processes, and for structure, inhibition, and electrochemical studies. While many questions have been asked and answered, the ultimate goal of the characterization of high-valent heme intermediates still remains. Added to that are new goals for the structural characterization of NOS:wire conjugates, the better understanding of electron transfer pathways through the wires and through the enzyme, and the development of novel and selective inhibitors for the various NOS isozymes. Thus, this body of work closes leaving a bright outlook for the future of the wires project.

APPENDIX A: FURTHER CHARACTERIZATION OF RE-IM-F_9BP AND RE-IM-F_8BP-IM

Acknowledgement:

The crystal structure of Re-Im-F_9bp was completed by Larry Henling and Mike Day in the Beckman Institute x-ray crystallography laboratory.

Appendix A

FURTHER CHARACTERIZATION OF RE-IM-F_9BP AND RE-IM-F_8BP-IM

Introduction

^{1}H and ^{19}F NMR spectra were recorded in CD_2Cl_2 on a Varian Mercury 300 MHz spectrometer. The chemical shifts are reported relative to TMS for ^{1}H NMR. ^{19}F NMR spectra were taken without a standard and were used solely for verification of number of fluorine-containing species. Their quoted chemical shifts are, therefore, qualitative.

Tiny crystals of Re-Im-F_9bp$^+\cdot BF_4^-$ were isolated from saturated ethanol after 4-6 weeks at 4^{o}C. The crystal structure was obtained and solved by Larry Henling and Mike Day in the Beckman Institute x-ray crystallography laboratory. Crystallographic data have been deposited at the CCDC, 12 Union Road, Cambridge CB2 1EZ, UK and copies can be obtained on request, free of charge, by quoting the publication citation[68] and the deposition number 215559.

Special Crystal Structure Refinement Details

The fluorine atoms of the tetrafluoroborate counterion are disordered over two sites in an approximate 90:10 ratio (see Table **6**). The minor orientation was refined with isotropic displacement parameters and a weak restraint was applied to keep the B to F distances near 1.40Å (see Table **8**).

Refinement of F^2 against ALL reflections. The weighted R-factor (*w*R) and goodness of fit (S) are based on F^2, conventional R-factors (R) are based on F, with F set

to zero for negative F^2. The threshold expression of $F^2 > 2\sigma(F^2)$ is used only for calculating R-factors (gt) etc. and is not relevant to the choice of reflections for refinement. R-factors based on F^2 are statistically about twice as large as those based on F, and R-factors based on ALL data will be even larger.

All esds (except the esd in the dihedral angle between two l.s. planes) are estimated using the full covariance matrix. The cell esds are taken into account individually in the estimation of esds in distances, angles and torsion angles; correlations between esds in cell parameters are only used when they are defined by crystal symmetry. An approximate (isotropic) treatment of cell esds is used for estimating esds involving l.s. planes.

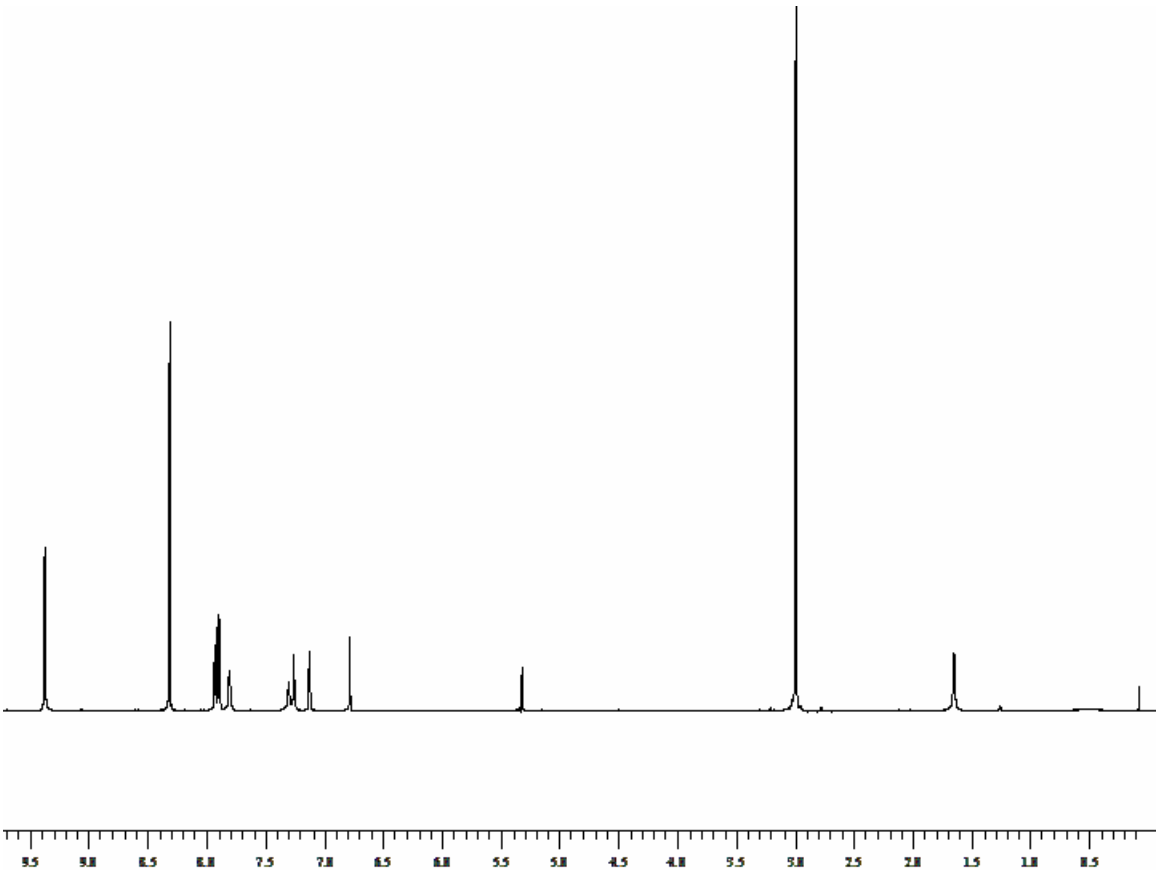

Figure 72. ^{1}H NMR (CD_2Cl_2) of Re-Im-F_8bp-Im.

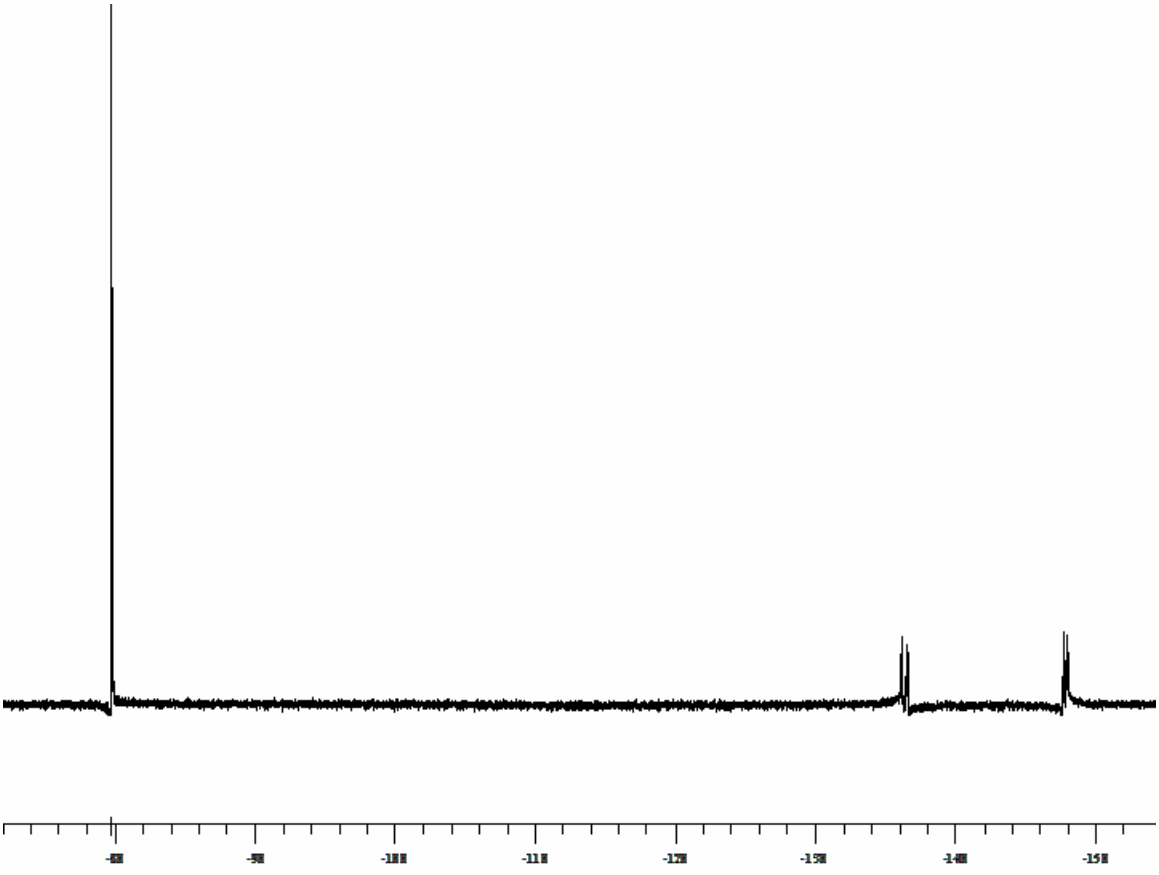

Figure 73. ^{19}F NMR (CD_2Cl_2) of Re-Im-F_8bp-$Im^+ \cdot OTf^-$.

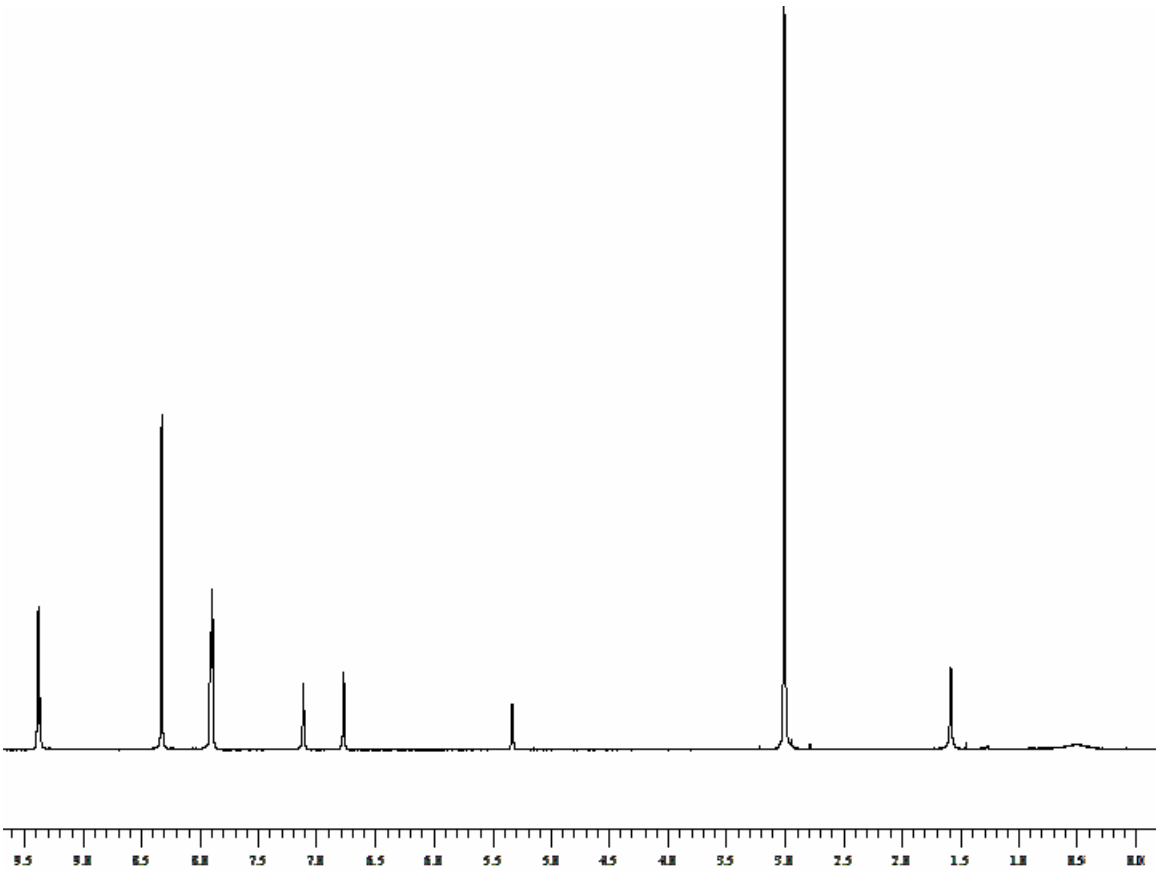

Figure 74. ^{1}H NMR (CD_2Cl_2) of Re-Im-F_9bp.

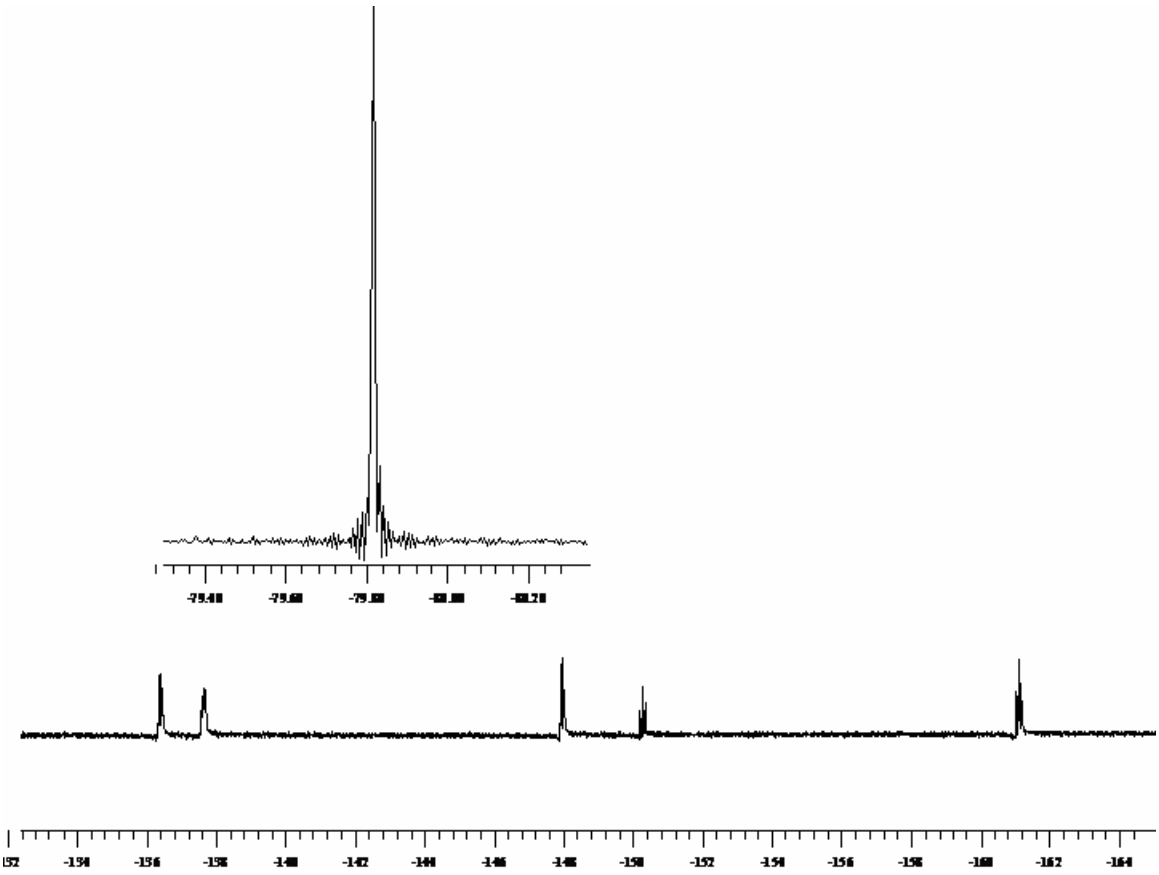

Figure 75. ^{19}F NMR (CD_2Cl_2) of Re-Im-F_9bp$^+$·OTf$^-$. The inset peak is due to the trifluoromethanesulfonate ion.

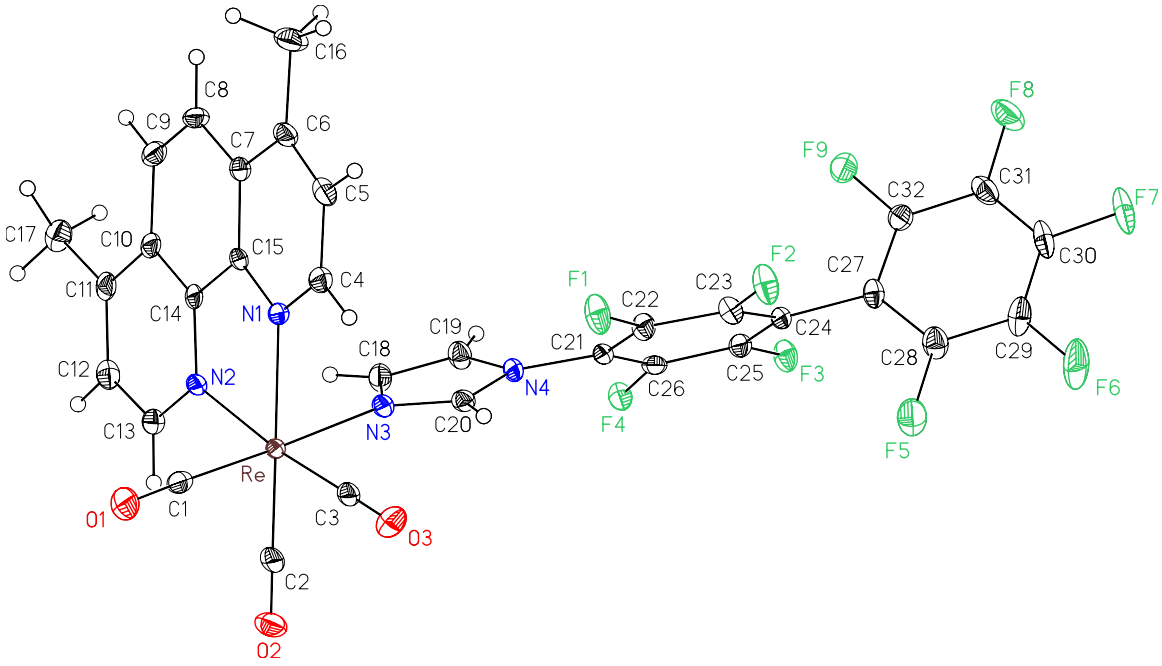

Figure 76. Crystal structure of Re-Im-F_9bp.

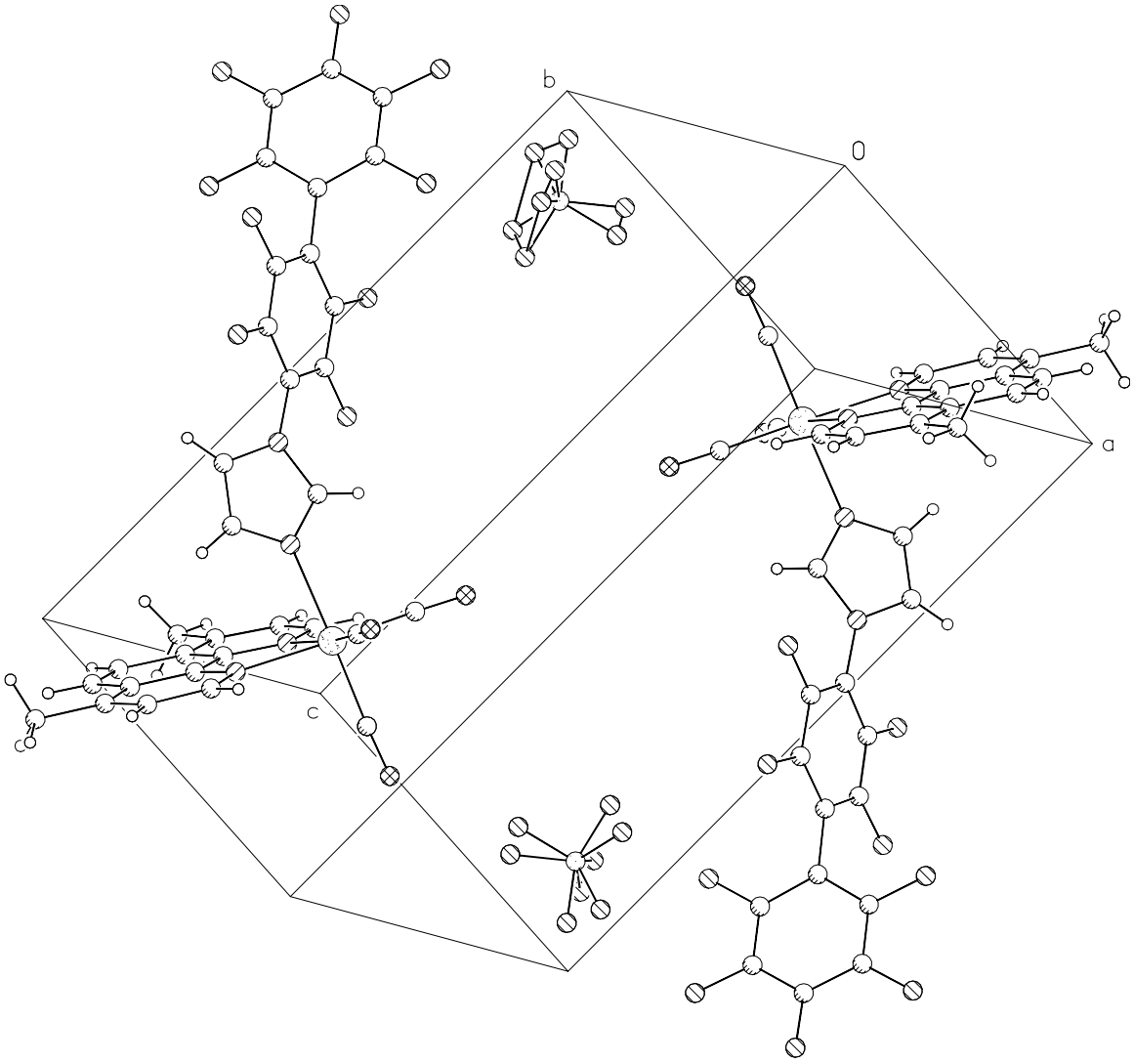

Figure 77. Crystal packing of Re-Im-F_9bp·BF_4.

Table 5. Crystal data and structure refinement for Re-Im-F9bp·BF_4 (CCDC 215559).

Empirical formula	$[C_{32}H_{15}F_9N_4O_3Re]^+[BF_4]^-$
Formula weight	947.49
Crystallization Solvent	Ethanol
Crystal Habit	Prism
Crystal size	0.43 x 0.11 x 0.08 mm^3
Crystal color	Pale yellow

Data Collection

Preliminary Photos	Rotation	
Type of diffractometer	Bruker SMART 1000	
Wavelength	0.71073 Å MoKα	
Data Collection Temperature	100(2) K	
θ range for 6602 reflections used in lattice determination	2.33 to 28.33°	
Unit cell dimensions	a = 8.5060(4) Å	α= 99.6870(10)°
	b = 10.6039(5) Å	β= 98.7180(10)°
	c = 17.9758(8) Å	γ = 95.9950(10)°
Volume	1565.66(13) $Å^3$	
Z	2	
Crystal system	Triclinic	
Space group	P-1	
Density (calculated)	2.010 Mg/m^3	
F(000)	912	
θ range for data collection	1.97 to 28.35°	
Completeness to θ = 28.35°	91.1 %	
Index ranges	$-11 \le h \le 11$, $-13 \le k \le 13$, $-23 \le l \le 23$	
Data collection scan type	ω scans at 7 ϕ settings	
Reflections collected	31670	
Independent reflections	7119 [R_{int}= 0.0699]	
Absorption coefficient	4.002 mm^{-1}	
Absorption correction	None	
Max. and min. transmission (predicted)	0.7402 and 0.2780	

Structure Solution and Refinement

Structure solution program	SHELXS-97 (Sheldrick, 1990)
Primary solution method	Patterson method
Secondary solution method	Difference Fourier map
Hydrogen placement	Geometric positions
Structure refinement program	SHELXL-97 (Sheldrick, 1997)
Refinement method	Full matrix least-squares on F^2
Data / restraints / parameters	7119 / 4 / 506
Treatment of hydrogen atoms	Constrained
Goodness-of-fit on F^2	1.385
Final R indices [$I>2\sigma(I)$, 6603 reflections]	R1 = 0.0219, wR2 = 0.0507
R indices (all data)	R1 = 0.0245, wR2 = 0.0512
Type of weighting scheme used	Sigma
Weighting scheme used	$w=1/\sigma^2(Fo^2)$
Max shift/error	0.002
Average shift/error	0.000
Largest diff. peak and hole	1.835 and -0.743 e.Å^{-3}

Table 6. Atomic coordinates (× 10^4) and equivalent isotropic displacement parameters (Å^2 × 10^3) for Re-Im-F9bp·BF_4 (CCDC 215559). U(eq) is defined as the trace of the orthogonalized U^{ij} tensor.

	x	y	z	U_{eq}	Occ
Re	4723(1)	1008(1)	2498(1)	12(1)	1
F(1)	10433(2)	3582(2)	4110(1)	25(1)	1
F(2)	12988(2)	4629(2)	5159(1)	25(1)	1
F(3)	13954(2)	501(2)	5596(1)	19(1)	1
F(4)	11297(2)	-546(1)	4623(1)	17(1)	1
F(5)	13660(2)	4064(2)	6893(1)	32(1)	1
F(6)	16394(2)	5297(2)	7795(1)	39(1)	1
F(7)	19244(2)	5142(2)	7309(1)	34(1)	1
F(8)	19366(2)	3595(2)	5943(1)	31(1)	1
F(9)	16629(2)	2389(2)	5041(1)	24(1)	1
O(1)	1454(2)	1590(2)	1741(1)	25(1)	1
O(2)	2997(2)	-801(2)	3370(1)	25(1)	1
O(3)	4594(2)	3322(2)	3757(1)	23(1)	1
N(1)	6196(2)	1979(2)	1819(1)	14(1)	1
N(2)	4966(2)	-495(2)	1566(1)	13(1)	1
N(3)	7089(2)	623(2)	3021(1)	14(1)	1
N(4)	9451(2)	896(2)	3756(1)	14(1)	1
C(1)	2672(3)	1351(3)	2009(2)	17(1)	1
C(2)	3619(3)	-108(3)	3048(2)	17(1)	1
C(3)	4661(3)	2441(3)	3288(2)	16(1)	1
C(4)	6804(3)	3221(3)	1961(2)	17(1)	1
C(5)	7846(3)	3736(3)	1528(2)	18(1)	1
C(6)	8323(3)	2962(3)	930(2)	18(1)	1
C(7)	7692(3)	1630(3)	764(2)	15(1)	1
C(8)	8069(3)	708(3)	159(2)	18(1)	1
C(9)	7439(3)	-545(3)	29(2)	18(1)	1
C(10)	6347(3)	-1028(3)	486(2)	15(1)	1
C(11)	5629(3)	-2334(3)	361(2)	16(1)	1
C(12)	4596(3)	-2647(3)	843(2)	18(1)	1
C(13)	4295(3)	-1730(3)	1433(2)	17(1)	1
C(14)	5972(3)	-150(3)	1084(2)	13(1)	1
C(15)	6638(3)	1188(3)	1228(2)	13(1)	1
C(16)	9472(3)	3499(3)	471(2)	25(1)	1
C(17)	5978(3)	-3342(3)	-267(2)	22(1)	1
C(18)	7847(3)	-446(3)	2828(2)	17(1)	1
C(19)	9302(3)	-291(3)	3275(2)	17(1)	1

C(20)	8071(3)	1420(3)	3579(2)	14(1)	1
C(21)	10809(3)	1479(3)	4318(2)	14(1)	1
C(22)	11269(3)	2804(3)	4487(2)	16(1)	1
C(23)	12607(3)	3348(3)	5026(2)	17(1)	1
C(24)	13568(3)	2601(3)	5407(2)	14(1)	1
C(25)	13092(3)	1283(3)	5237(2)	15(1)	1
C(26)	11735(3)	734(3)	4723(2)	14(1)	1
C(27)	15077(3)	3197(3)	5943(2)	15(1)	1
C(28)	15071(3)	3924(3)	6658(2)	21(1)	1
C(29)	16463(3)	4553(3)	7125(2)	24(1)	1
C(30)	17906(3)	4458(3)	6882(2)	23(1)	1
C(31)	17964(3)	3710(3)	6188(2)	21(1)	1
C(32)	16553(3)	3086(3)	5723(2)	17(1)	1
B	9914(3)	2762(3)	8353(2)	12(1)	1
F(10)	9394(3)	1502(2)	8428(2)	39(1)	0.901(5)
F(11)	10253(3)	2764(2)	7622(1)	36(1)	0.901(5)
F(12)	8675(3)	3520(2)	8459(2)	26(1)	0.901(5)
F(13)	11257(2)	3275(2)	8885(2)	38(1)	0.901(5)
F(10B)	9910(30)	1764(19)	8788(14)	37(7)	0.099(5)
F(11B)	9130(20)	2209(19)	7620(7)	38(6)	0.099(5)
F(12B)	9130(30)	3650(20)	8760(14)	36(7)	0.099(5)
F(13B)	11557(12)	3141(19)	8453(14)	31(5)	0.099(5)

Table 7. Selected bond lengths [Å] and angles [°] for Re-Im-F9bp·BF_4 (CCDC 215559).

Bond lengths:

Re-C(3)	1.908(3)
Re-C(2)	1.923(3)
Re-C(1)	1.930(3)
Re-N(2)	2.160(2)
Re-N(1)	2.178(2)
Re-N(3)	2.197(2)

Bond Angles:

C(3)-Re-C(2)	89.44(12)
C(3)-Re-C(1)	87.19(11)
C(2)-Re-C(1)	89.12(11)
C(3)-Re-N(2)	174.40(9)
C(2)-Re-N(2)	95.98(10)
C(1)-Re-N(2)	94.30(10)
C(3)-Re-N(1)	98.91(10)
C(2)-Re-N(1)	169.76(10)
C(1)-Re-N(1)	97.16(9)
N(2)-Re-N(1)	75.56(8)
C(3)-Re-N(3)	93.86(9)
C(2)-Re-N(3)	92.47(9)
C(1)-Re-N(3)	178.10(9)
N(2)-Re-N(3)	84.50(8)
N(1)-Re-N(3)	81.12(8)

Table 8. All bond lengths [Å] and angles [°] for Re-Im-F9bp·BF_4 (CCDC 215559).

Bond Lengths:

Re-C(3)	1.908(3)	C(11)-C(17)	1.505(4)
Re-C(2)	1.923(3)	C(12)-C(13)	1.387(4)
Re-C(1)	1.930(3)	C(12)-H(12)	0.9500
Re-N(2)	2.160(2)	C(13)-H(13)	0.9500
Re-N(1)	2.178(2)	C(14)-C(15)	1.436(4)
Re-N(3)	2.197(2)	C(16)-H(16A)	0.9800
F(1)-C(22)	1.346(3)	C(16)-H(16B)	0.9800
F(2)-C(23)	1.334(3)	C(16)-H(16C)	0.9800
F(3)-C(25)	1.343(3)	C(17)-H(17A)	0.9800
F(4)-C(26)	1.343(3)	C(17)-H(17B)	0.9800
F(5)-C(28)	1.347(3)	C(17)-H(17C)	0.9800
F(6)-C(29)	1.337(4)	C(18)-C(19)	1.347(4)
F(7)-C(30)	1.336(3)	C(18)-H(18)	0.9500
F(8)-C(31)	1.343(3)	C(19)-H(19)	0.9500
F(9)-C(32)	1.334(3)	C(20)-H(20)	0.9500
O(1)-C(1)	1.146(3)	C(21)-C(22)	1.388(4)
O(2)-C(2)	1.145(3)	C(21)-C(26)	1.387(4)
O(3)-C(3)	1.161(4)	C(22)-C(23)	1.381(4)
N(1)-C(4)	1.331(4)	C(23)-C(24)	1.383(4)
N(1)-C(15)	1.363(3)	C(24)-C(25)	1.383(4)
N(2)-C(13)	1.340(3)	C(24)-C(27)	1.492(3)
N(2)-C(14)	1.372(3)	C(25)-C(26)	1.372(4)
N(3)-C(20)	1.315(3)	C(27)-C(32)	1.383(4)
N(3)-C(18)	1.382(3)	C(27)-C(28)	1.383(4)
N(4)-C(20)	1.367(3)	C(28)-C(29)	1.377(4)
N(4)-C(19)	1.385(4)	C(29)-C(30)	1.372(4)
N(4)-C(21)	1.422(3)	C(30)-C(31)	1.371(5)
C(4)-C(5)	1.394(4)	C(31)-C(32)	1.387(4)
C(4)-H(4)	0.9500	B-F(11B)	1.383(9)
C(5)-C(6)	1.377(4)	B-F(12B)	1.383(10)
C(5)-H(5)	0.9500	B-F(13B)	1.389(9)
C(6)-C(7)	1.423(4)	B-F(13)	1.371(3)
C(6)-C(16)	1.499(4)	B-F(11)	1.387(4)
C(7)-C(15)	1.410(3)	B-F(10)	1.398(3)
C(7)-C(8)	1.433(4)	B-F(12)	1.407(3)
C(8)-C(9)	1.348(4)	B-F(10B)	1.418(10)
C(8)-H(8)	0.9500		
C(9)-C(10)	1.440(4)		
C(9)-H(9)	0.9500		
C(10)-C(14)	1.398(4)		
C(10)-C(11)	1.420(4)		
C(11)-C(12)	1.378(4)		

Bond Angles:

C(3)-Re-C(2)	89.44(12)	C(9)-C(8)-H(8)	119.2
C(3)-Re-C(1)	87.19(11)	C(7)-C(8)-H(8)	119.2
C(2)-Re-C(1)	89.12(11)	C(8)-C(9)-C(10)	121.9(3)
C(3)-Re-N(2)	174.40(9)	C(8)-C(9)-H(9)	119.0
C(2)-Re-N(2)	95.98(10)	C(10)-C(9)-H(9)	119.0
C(1)-Re-N(2)	94.30(10)	C(14)-C(10)-C(11)	118.6(2)
C(3)-Re-N(1)	98.91(10)	C(14)-C(10)-C(9)	117.5(2)
C(2)-Re-N(1)	169.76(10)	C(11)-C(10)-C(9)	123.9(3)
C(1)-Re-N(1)	97.16(9)	C(12)-C(11)-C(10)	117.1(3)
N(2)-Re-N(1)	75.56(8)	C(12)-C(11)-C(17)	121.0(3)
C(3)-Re-N(3)	93.86(9)	C(10)-C(11)-C(17)	121.9(2)
C(2)-Re-N(3)	92.47(9)	C(13)-C(12)-C(11)	121.3(3)
C(1)-Re-N(3)	178.10(9)	C(13)-C(12)-H(12)	119.3
N(2)-Re-N(3)	84.50(8)	C(11)-C(12)-H(12)	119.3
N(1)-Re-N(3)	81.12(8)	N(2)-C(13)-C(12)	122.6(2)
C(4)-N(1)-C(15)	117.9(2)	N(2)-C(13)-H(13)	118.7
C(4)-N(1)-Re	126.82(19)	C(12)-C(13)-H(13)	118.7
C(15)-N(1)-Re	115.03(17)	N(2)-C(14)-C(10)	123.1(2)
C(13)-N(2)-C(14)	117.2(2)	N(2)-C(14)-C(15)	116.0(2)
C(13)-N(2)-Re	126.75(18)	C(10)-C(14)-C(15)	121.0(2)
C(14)-N(2)-Re	115.94(17)	N(1)-C(15)-C(7)	123.0(2)
C(20)-N(3)-C(18)	107.2(2)	N(1)-C(15)-C(14)	117.1(2)
C(20)-N(3)-Re	124.74(18)	C(7)-C(15)-C(14)	120.0(2)
C(18)-N(3)-Re	128.02(18)	C(6)-C(16)-H(16A)	109.5
C(20)-N(4)-C(19)	107.4(2)	C(6)-C(16)-H(16B)	109.5
C(20)-N(4)-C(21)	126.4(2)	H(16A)-C(16)-H(16B)	109.5
C(19)-N(4)-C(21)	126.2(2)	C(6)-C(16)-H(16C)	109.5
O(1)-C(1)-Re	177.4(3)	H(16A)-C(16)-H(16C)	109.5
O(2)-C(2)-Re	177.7(2)	H(16B)-C(16)-H(16C)	109.5
O(3)-C(3)-Re	178.4(2)	C(11)-C(17)-H(17A)	109.5
N(1)-C(4)-C(5)	122.7(3)	C(11)-C(17)-H(17B)	109.5
N(1)-C(4)-H(4)	118.6	H(17A)-C(17)-H(17B)	109.5
C(5)-C(4)-H(4)	118.6	C(11)-C(17)-H(17C)	109.5
C(6)-C(5)-C(4)	120.9(3)	H(17A)-C(17)-H(17C)	109.5
C(6)-C(5)-H(5)	119.6	H(17B)-C(17)-H(17C)	109.5
C(4)-C(5)-H(5)	119.6	C(19)-C(18)-N(3)	109.4(2)
C(5)-C(6)-C(7)	117.7(2)	C(19)-C(18)-H(18)	125.3
C(5)-C(6)-C(16)	121.4(3)	N(3)-C(18)-H(18)	125.3
C(7)-C(6)-C(16)	121.0(3)	C(18)-C(19)-N(4)	106.3(2)
C(15)-C(7)-C(8)	118.0(2)	C(18)-C(19)-H(19)	126.9
C(15)-C(7)-C(6)	117.9(3)	N(4)-C(19)-H(19)	126.9
C(8)-C(7)-C(6)	124.1(2)	N(3)-C(20)-N(4)	109.7(2)
C(9)-C(8)-C(7)	121.6(2)	N(3)-C(20)-H(20)	125.1

N(4)-C(20)-H(20)	125.1	F(13)-B-F(11)	109.6(2)
C(22)-C(21)-C(26)	117.0(2)	F(11B)-B-F(10)	77.4(9)
C(22)-C(21)-N(4)	122.1(2)	F(12B)-B-F(10)	111.4(11)
C(26)-C(21)-N(4)	120.9(2)	F(13B)-B-F(10)	117.7(8)
F(1)-C(22)-C(21)	120.1(2)	F(13)-B-F(10)	110.6(3)
F(1)-C(22)-C(23)	118.7(2)	F(11)-B-F(10)	109.8(3)
C(21)-C(22)-C(23)	121.2(2)	F(11B)-B-F(12)	90.8(8)
F(2)-C(23)-C(24)	120.0(2)	F(12B)-B-F(12)	24.9(11)
F(2)-C(23)-C(22)	118.2(2)	F(13B)-B-F(12)	129.3(9)
C(24)-C(23)-C(22)	121.8(2)	F(13)-B-F(12)	109.6(3)
C(25)-C(24)-C(23)	116.5(2)	F(11)-B-F(12)	108.5(2)
C(25)-C(24)-C(27)	122.4(2)	F(10)-B-F(12)	108.7(2)
C(23)-C(24)-C(27)	121.0(2)	F(11B)-B-F(10B)	106.6(14)
F(3)-C(25)-C(26)	118.0(2)	F(12B)-B-F(10B)	101.9(15)
F(3)-C(25)-C(24)	119.7(2)	F(13B)-B-F(10B)	99.4(13)
C(26)-C(25)-C(24)	122.2(2)	F(13)-B-F(10B)	82.4(11)
F(4)-C(26)-C(25)	118.8(2)	F(11)-B-F(10B)	130.2(11)
F(4)-C(26)-C(21)	120.0(2)	F(10)-B-F(10B)	29.6(10)
C(25)-C(26)-C(21)	121.2(2)	F(12)-B-F(10B)	112.3(10)
C(32)-C(27)-C(28)	117.2(2)		
C(32)-C(27)-C(24)	120.3(3)		
C(28)-C(27)-C(24)	122.4(2)		
F(5)-C(28)-C(27)	119.2(2)		
F(5)-C(28)-C(29)	118.8(3)		
C(27)-C(28)-C(29)	122.0(3)		
F(6)-C(29)-C(30)	120.4(3)		
F(6)-C(29)-C(28)	119.9(3)		
C(30)-C(29)-C(28)	119.5(3)		
F(7)-C(30)-C(31)	120.2(3)		
F(7)-C(30)-C(29)	119.6(3)		
C(31)-C(30)-C(29)	120.1(3)		
F(8)-C(31)-C(30)	121.0(3)		
F(8)-C(31)-C(32)	119.2(3)		
C(30)-C(31)-C(32)	119.7(3)		
F(9)-C(32)-C(27)	119.7(2)		
F(9)-C(32)-C(31)	118.9(2)		
C(27)-C(32)-C(31)	121.4(3)		
F(11B)-B-F(12B)	115.7(14)		
F(11B)-B-F(13B)	117.4(13)		
F(12B)-B-F(13B)	112.8(14)		
F(11B)-B-F(13)	153.1(9)		
F(12B)-B-F(13)	86.1(11)		
F(13B)-B-F(13)	35.7(10)		
F(11B)-B-F(11)	45.2(9)		
F(12B)-B-F(11)	126.4(11)		
F(13B)-B-F(11)	74.6(10)		

Table 9. Anisotropic displacement parameters ($Å^2 \times 10^4$) for Re-Im-F9bp·BF_4 (CCDC 215559). The anisotropic displacement factor exponent takes the form: $-2\pi^2 [h^2 a^{*2} U^{11} + ... + 2 h k a^* b^* U^{12}]$.

	U^{11}	U^{22}	U^{33}	U^{23}	U^{13}	U^{12}
Re	78(1)	177(1)	100(1)	32(1)	14(1)	22(1)
F(1)	212(8)	193(8)	312(10)	88(8)	-97(7)	27(6)
F(2)	224(8)	159(8)	318(11)	31(8)	-82(7)	6(6)
F(3)	163(7)	181(8)	211(9)	75(7)	-41(6)	25(6)
F(4)	154(7)	154(8)	179(9)	40(7)	-6(6)	2(6)
F(5)	207(8)	445(11)	256(10)	-96(9)	27(7)	109(8)
F(6)	357(10)	388(12)	300(12)	-179(9)	-107(9)	120(8)
F(7)	237(8)	293(10)	379(12)	37(9)	-178(8)	-61(7)
F(8)	125(8)	429(11)	378(12)	117(9)	33(7)	13(7)
F(9)	194(8)	340(10)	178(9)	19(8)	25(7)	54(7)
O(1)	158(9)	371(12)	236(12)	78(10)	-5(9)	105(9)
O(2)	137(9)	378(13)	268(12)	173(10)	53(8)	39(8)
O(3)	279(10)	252(11)	172(11)	23(9)	48(9)	68(9)
N(1)	99(10)	198(12)	113(11)	42(9)	9(8)	19(8)
N(2)	85(9)	178(11)	123(12)	48(9)	6(8)	7(8)
N(3)	96(10)	178(11)	135(12)	41(9)	14(8)	27(8)
N(4)	90(9)	191(12)	121(12)	22(9)	3(8)	24(8)
C(1)	157(12)	243(15)	138(14)	56(12)	45(11)	32(10)
C(2)	84(11)	247(15)	187(15)	75(12)	5(10)	54(10)
C(3)	102(11)	233(15)	156(14)	76(12)	3(10)	21(10)
C(4)	141(12)	215(14)	152(14)	29(12)	13(10)	30(10)
C(5)	132(12)	171(14)	217(16)	63(12)	-14(11)	-10(10)
C(6)	100(12)	270(15)	187(15)	99(12)	6(11)	12(10)
C(7)	100(11)	223(14)	135(14)	63(11)	-4(10)	28(10)
C(8)	126(12)	303(16)	146(14)	75(12)	54(11)	42(11)
C(9)	157(12)	261(15)	127(14)	33(12)	32(10)	66(11)
C(10)	112(11)	228(14)	109(14)	39(11)	-9(10)	51(10)
C(11)	126(12)	222(14)	133(14)	23(11)	-27(10)	56(10)
C(12)	173(13)	171(14)	179(15)	39(11)	-18(11)	3(10)
C(13)	138(12)	210(14)	146(14)	49(11)	3(10)	13(10)
C(14)	91(11)	189(13)	107(13)	37(11)	-24(10)	32(9)
C(15)	63(11)	196(13)	120(13)	46(11)	-7(9)	29(9)
C(16)	199(14)	286(17)	293(18)	113(14)	97(13)	-28(12)
C(17)	235(14)	223(15)	180(15)	7(12)	12(12)	53(11)
C(18)	150(12)	193(14)	156(15)	-7(11)	4(11)	25(10)

C(19)	127(12)	182(14)	182(15)	3(11)	6(11)	41(10)
C(20)	111(11)	164(13)	143(14)	46(11)	29(10)	34(9)
C(21)	91(11)	207(14)	115(13)	41(11)	12(10)	7(10)
C(22)	136(12)	188(14)	157(14)	52(11)	-3(10)	57(10)
C(23)	136(12)	157(13)	199(15)	27(11)	7(11)	7(10)
C(24)	94(11)	216(14)	117(13)	29(11)	11(10)	18(10)
C(25)	121(11)	197(14)	131(14)	46(11)	15(10)	37(10)
C(26)	135(12)	157(13)	136(14)	30(11)	59(10)	0(10)
C(27)	145(12)	142(13)	159(14)	28(11)	-29(10)	22(10)
C(28)	169(13)	225(15)	220(16)	5(12)	-5(11)	56(11)
C(29)	267(15)	209(15)	193(16)	-35(12)	-61(12)	66(12)
C(30)	172(13)	202(15)	268(17)	43(13)	-107(12)	-21(11)
C(31)	120(12)	235(15)	268(17)	99(13)	-4(11)	9(10)
C(32)	165(12)	185(14)	154(14)	59(11)	13(11)	25(10)
B	92(12)	129(14)	142(15)	8(12)	37(11)	13(10)
F(10)	355(13)	205(11)	660(20)	141(12)	185(14)	17(9)
F(11)	575(16)	294(12)	243(12)	25(9)	158(10)	154(11)
F(12)	187(10)	238(11)	354(15)	41(10)	69(11)	35(8)
F(13)	244(11)	458(14)	365(16)	26(11)	-74(10)	50(9)

Table 10. Hydrogen coordinates (× 10^4) and isotropic displacement parameters (Å^2 × 10^3) for Re-Im-F9bp·BF_4 (CCDC 215559).

	x	y	z	U_{iso}
H(4)	6514	3780	2374	20
H(5)	8233	4633	1646	21
H(8)	8781	987	-158	22
H(9)	7723	-1127	-376	21
H(12)	4079	-3508	769	22
H(13)	3584	-1988	1756	20
H(16A)	9751	4431	657	38
H(16B)	8970	3336	-70	38
H(16C)	10447	3081	526	38
H(17A)	7022	-3616	-106	33
H(17B)	6000	-2979	-732	33
H(17C)	5140	-4088	-371	33
H(18)	7409	-1177	2442	21
H(19)	10072	-879	3261	20
H(20)	7855	2235	3821	16

APPENDIX B: BINDING OF RE-IM-F_9BP AND RE-IM-F_8BP-IM TO P450CAM

Acknowledgement:

These experiments were conducted in collaboration with Alex Dunn.

Appendix B

BINDING OF RE-IM-F_9BP AND RE-IM-F_8BP-IM TO P450cam

Due to their resemblance to previously published wires,[65, 66] Re-Im-F_9bp and Re-Im-F_8bp-Im were tested for binding to cytochrome P450cam. A heme Soret shift from 416 nm to 420 nm upon the addition of one equivalent of Re-Im-F_8bp-Im wire to an equimolar solution of P450cam indicates that the wire binds at the active site with the distal imidazole ligating the iron (Figure **78**, inset).[192] Further confirmation of binding at a single site was achieved through examination of the transient luminescence traces of Re-bis wire and P450cam in solution. As seen in Figure **78**, upon 355 nm excitation, P450cam is not luminescent at 620 nm, and wire alone shows a mono-exponential decay corresponding to the previously reported lifetime of 1 μs. When one equivalent of wire is added to a protein solution, however, the observed luminescence decay can be fit nicely to two exponentials. The slower part of the decay ($k_1 = 1 \times 10^6$ s^{-1}) corresponds to free wire in solution, and the faster part of the decay ($k_2 = 8 \times 10^6$ s^{-1}) corresponds to protein-bound wire. The fact that the bound wire decays at a single rate suggests that it's binding in one place only, and the heme Soret shift confirms that this is the active site. If the wire was binding non-specifically at other sites on the protein, we would expect to see a complex, multi-exponential decay. From the biexponential fit, an equilibrium dissociation constant of 0.6 ± 0.5 μM was calculated,

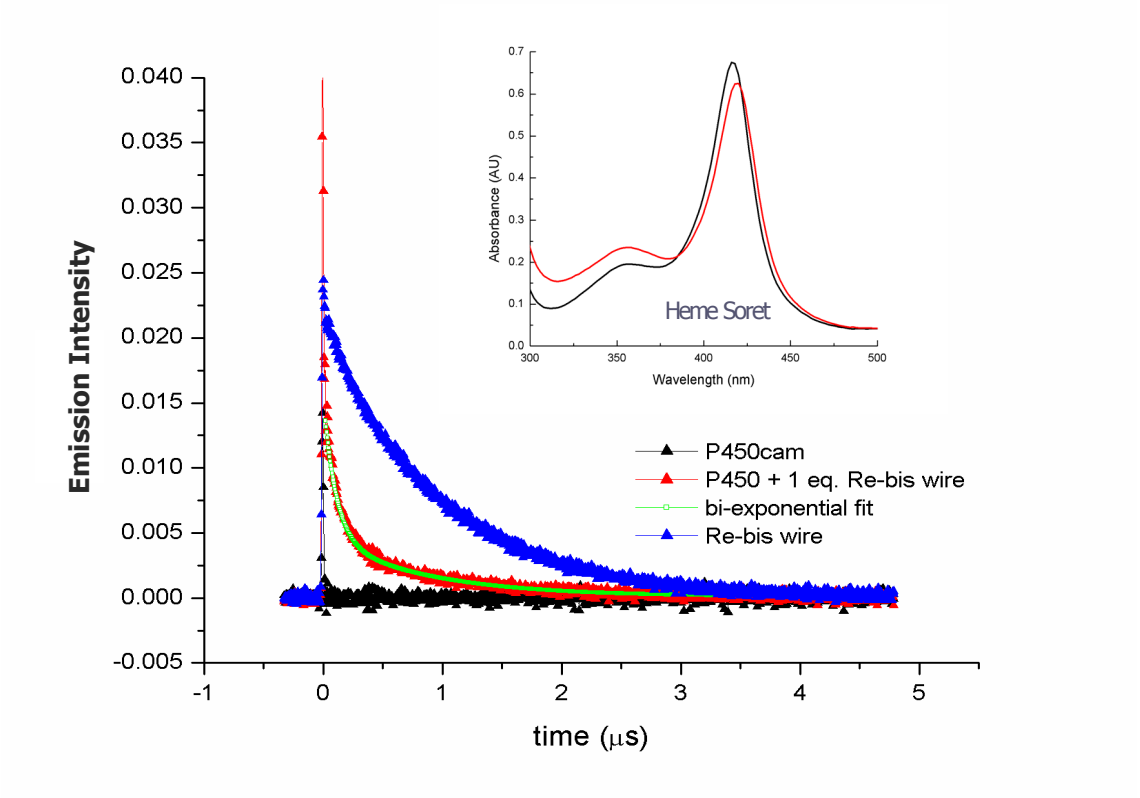

Figure 78. Luminescence decay of Re-bis wire at 620 nm (λ_{ex}=355 nm), free (blue) and bound to one equivalent of P450cam (red). The biexponential fit of the wire:P450 complex is in green ($k_1 = 1 \times 10^6$ s^{-1} and $k_2 = 8 \times 10^6$ s^{-1}). Inset: UV/visible absorption spectrum of P450cam alone (black) and the P450cam:Re-Im-F_8bp-Im complex (red) showing a shift in the heme Soret band of P450cam upon binding of Re-Im-F_8bp-Im. This shift from 416 nm to 420 nm is indicative of low-spin ferric heme ligated by N-phenyl imidazole.[192]

indicating that Re-bis wire binds more than twice as tightly to P450cam than the natural substrate.[193]

Re-Im-F_9bp was not expected to bind at the active site of P450cam due to the fact that it contains no heme-targeted group (such as imidazole). Addition of one equivalent of Re-Im-F_9bp to an equivalent amount of P450cam, however, produced a small spectral change indicative of a slight conversion toward high-spin Fe(III) (Figure **79**).[66, 194] Further, analysis of the luminescence decay of the wire in the presence and absence of P450cam showed a biexponential decay ($k_1 = 1 \times 10^6\ s^{-1}$ and $k_2 = 8 \times 10^6\ s^{-1}$), suggesting once again that the wire had a single binding site with a calculated dissociation constant of 22 ± 8 μM. A model of Re-Im-F_9bp docked in the active site channel of P450cam is shown in Figure **80**.

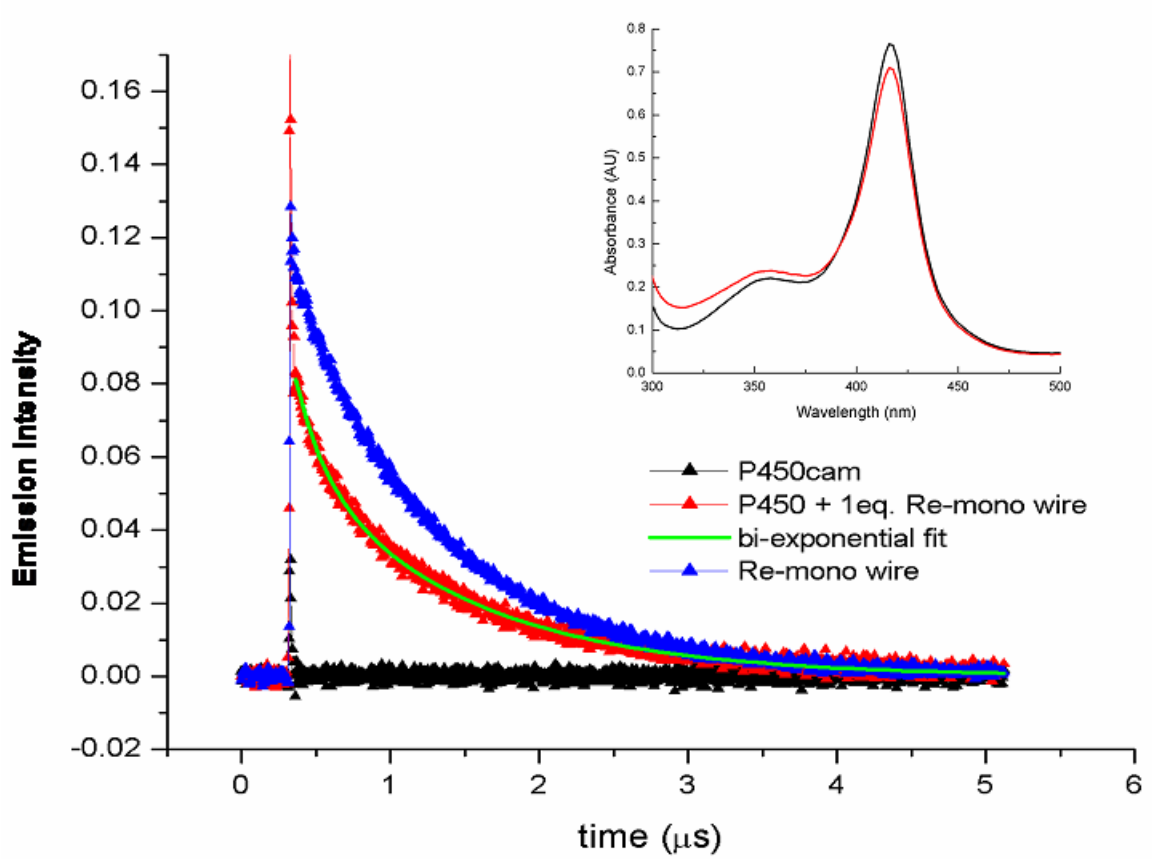

Figure 79. Luminescence decay of Re-Im-F_9bp at 575 nm (λ_{ex}=355 nm), free (blue) and bound to one equivalent of P450cam (red). The biexponential fit of the wire:P450 complex is in green ($k_1 = 1 \times 10^6$ s^{-1} and $k_2 = 8 \times 10^6$ s^{-1}). Inset: UV/visible absorption spectrum of P450cam alone (black) and the P450cam:Re-Im-F_9bp complex (red) showing a small shift in heme Soret band of P450cam upon binding of Re-Im-F_9bp. This shift is indicative of a partial conversion to high-spin heme.

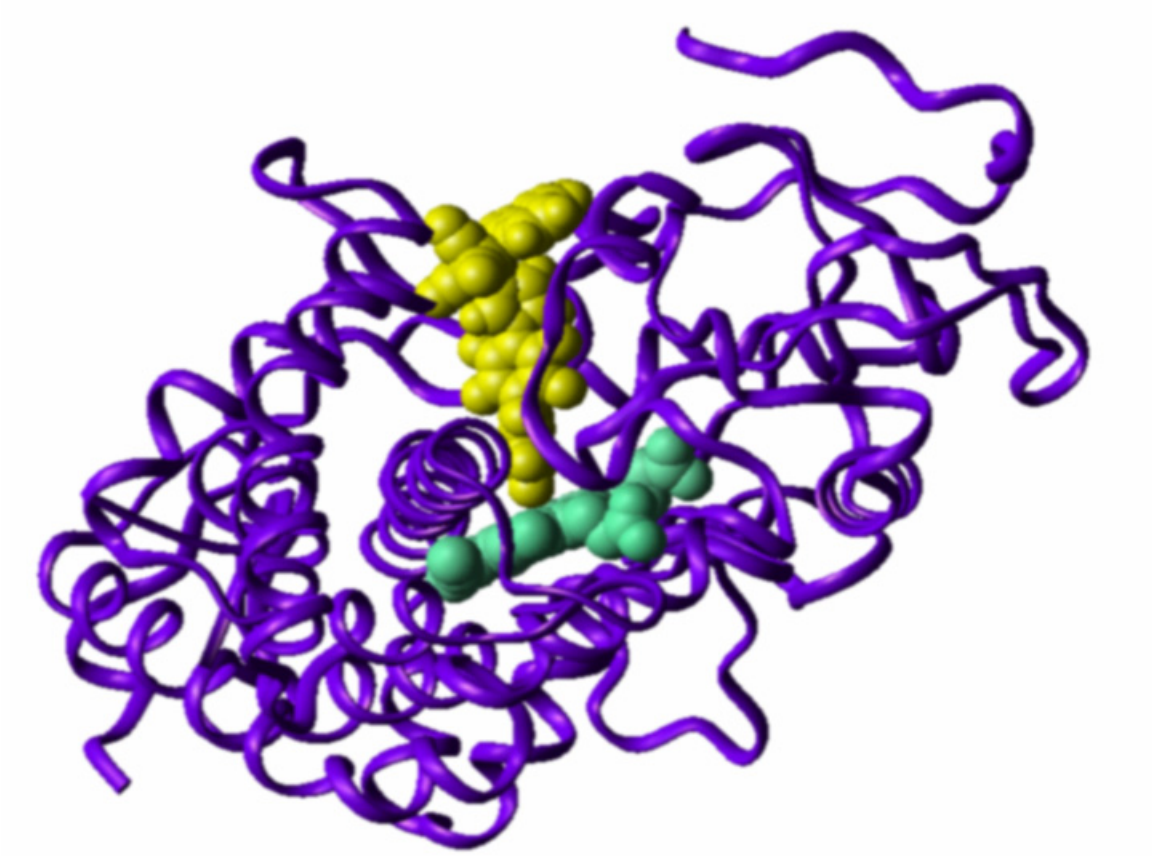

Figure 80. Model of Re-Im-F_9bp bound to P450cam. The model was created using InsightII from P450cam structure PDB code 1qmq.[66]

REFERENCES

REFERENCES

1.Culotta, E.; Koshland, D. E., No News Is Good-News. *Science* **1992,** 258, (5090), 1862-1865.

2.Raman, C. S.; Li, H. Y.; Martasek, P.; Kral, V.; Masters, B. S. S.; Poulos, T. L., Crystal structure of constitutive endothelial nitric oxide synthase: A paradigm for pterin function involving a novel metal center. *Cell* **1998,** 95, (7), 939-950.

3.Mayer, B.; Hemmens, B., Biosynthesis and action of nitric oxide in mammalian cells. *Trends in Biochemical Sciences* **1997,** 22, (12), 477-481.

4.Werner, E. R.; Gorren, A. C. F.; Heller, R.; Werner-Felmayer, G.; Mayer, B., Tetrahydrobiopterin and nitric oxide: Mechanistic and pharmacological aspects. *Experimental Biology and Medicine* **2003,** 228, (11), 1291-1302.

5.Moncada, S.; Higgs, E. A., Endogenous Nitric-Oxide - Physiology, Pathology And Clinical Relevance. *European Journal of Clinical Investigation* **1991,** 21, (4), 361-374.

6.Mayer, B., *Nitric Oxide*. ed.; Springer: Berlin, 2000.

7.Ignarro, L. J., *Nitric Oxide, Biology and Pathology*. Academic Press: San Diego, 2000.

8.Ignarro, L. J., Heme-Dependent Activation Of Cytosolic Guanylate-Cyclase By Nitric-Oxide - A Widespread Signal Transduction Mechanism. *Biochemical Society Transactions* **1992,** 20, (2), 465-469.

9.Aktan, F., iNOS-mediated nitric oxide production and its regulation. *Life Sciences* **2004,** 75, (6), 639-653.

10.DiabetesInControl.com.

11.Nathan, C., Inducible nitric oxide synthase: What difference does it make? *Journal of Clinical Investigation* **1997,** 100, (10), 2417-2423.

12.Christopherson, K. S.; Bredt, D. S., Nitric oxide in excitable tissues: Physiological roles and disease. *Journal of Clinical Investigation* **1997,** 100, (10), 2424-2429.

13.Santilli, F.; Cipollone, F.; Mezzetti, A.; Chiarelli, F., The role of nitric oxide in the development of diabetic angiopathy. *Hormone and Metabolic Research* **2004,** 36, (5), 319-335.

14.Park, K. C.; Chung, K. C.; Kim, Y. S.; Lee, J.; Joh, T. H.; Kim, S. Y., Transglutaminase 2 induces nitric oxide synthesis in BV-2 microglia. *Biochemical and Biophysical Research Communications* **2004,** 323, (3), 1055-1062.

15.Luoma, J. S.; Stralin, P.; Marklund, S. L.; Hiltunen, T. P.; Sarkioja, T.; Yla-Herttuala, S., Expression of extracellular SOD and iNOS in macrophages and smooth muscle cells in human and rabbit atherosclerotic lesions - Colocalization with epitopes characteristic of oxidized LDL and peroxynitrite-modified proteins. *Arteriosclerosis Thrombosis and Vascular Biology* **1998,** 18, (2), 157-167.

16.Hubbard, A. K.; Giardina, C., Regulation of ICAM-1 expression in mouse macrophages. *Inflammation* **2000,** 24, (2), 115-125.

17.Dorheim, M. A.; Tracey, W. R.; Pollock, J. S.; Grammas, P., Nitric-Oxide Synthase Activity Is Elevated In Brain Microvessels In Alzheimers-Disease. *Biochemical and Biophysical Research Communications* **1994,** 205, (1), 659-665.

18.Buttery, L. D. K.; Evans, T. J.; Springall, D. R.; Carpenter, A.; Cohen, J.; Polak, J. M., Immunochemical Localization Of Inducible Nitric-Oxide Synthase In Endotoxin-Treated Rats. *Laboratory Investigation* **1994,** 71, (5), 755-764.

19.Luth, H. J.; Holzer, M.; Gertz, H. J.; Arendt, T., Aberrant expression of nNOS in pyramidal neurons in Alzheimer's disease is highly co-localized with p21(ras) and p16(INK4a). *Brain Research* **2000,** 852, (1), 45-55.

20.Alderton, W. K.; Cooper, C. E.; Knowles, R. G., Nitric oxide synthases: structure, function and inhibition. *Biochemical Journal* **2001,** 357, 593-615.

21.Wang, M.; Roberts, D. L.; Paschke, R.; Shea, T. M.; Masters, B. S. S.; Kim, J. J. P., Three-dimensional structure of NADPH-cytochrome P450 reductase: Prototype for

FMN- and FAD-containing enzymes. *Proceedings of The National Academy of Sciences of the U. S. A.* **1997,** 94, (16), 8411-8416.

22.Paine, M. J. I.; Garner, A. P.; Powell, D.; Sibbald, J.; Sales, M.; Pratt, N.; Smith, T.; Tew, D. G.; Wolf, C. R., Cloning and characterization of a novel human dual flavin reductase. *Journal of Biological Chemistry* **2000,** 275, (2), 1471-1478.

23.Gruez, A.; Pignol, D.; Zeghouf, M.; Coves, J.; Fontecave, M.; Ferrer, J. L.; Fontecilla-Camps, J. C., Four crystal structures of the 60 kDa flavoprotein monomer of the sulfite reductase indicate a disordered flavodoxin-like module. *Journal of Molecular Biology* **2000,** 299, (1), 199-212.

24.Roman, L. J.; Martasek, P.; Masters, B. S. S., Intrinsic and extrinsic modulation of nitric oxide synthase activity. *Chemical Reviews* **2002,** 102, (4), 1179-1189.

25.Cho, H. J.; Xie, Q. W.; Calaycay, J.; Mumford, R. A.; Swiderek, K. M.; Lee, T. D.; Nathan, C., Calmodulin Is A Subunit Of Nitric-Oxide Synthase From Macrophages. *Journal of Experimental Medicine* **1992,** 176, (2), 599-604.

26.Chen, P. F.; Wu, K. K., Structural elements contribute to the calcium/calmodulin dependence on enzyme activation in human endothelial nitric-oxide synthase. *Journal of Biological Chemistry* **2003,** 278, (52), 52392-52400.

27.Bredt, D. S.; Snyder, S. H., Isolation Of Nitric-Oxide Synthetase, A Calmodulin-Requiring Enzyme. *Proceedings of the National Academy of Sciences of the U. S. A.* **1990,** 87, (2), 682-685.

28.Crane, B. R.; Rosenfeld, R. J.; Arvai, A. S.; Ghosh, D. K.; Ghosh, S.; Tainer, J. A.; Stuehr, D. J.; Getzoff, E. D., N-terminal domain swapping and metal ion binding in nitric oxide synthase dimerization. *Embo Journal* **1999,** 18, (22), 6271-6281.

29.Crane, B. R.; Arvai, A. S.; Ghosh, S.; Getzoff, E. D.; Stuehr, D. J.; Tainer, J. A., Structures of the N-omega-hydroxy-L-arginine complex of inducible nitric oxide synthase oxygenase dimer with active and inactive pterins. *Biochemistry* **2000,** 39, (16), 4608-4621.

30.Garcin, E. D.; Bruns, C. M.; Lloyd, S. J.; Hosfield, D. J.; Tiso, M.; Gachhui, R.; Stuehr, D. J.; Tainer, J. A.; Getzoff, E. D., Structural basis for isozyme-specific

regulation of electron transfer in nitric-oxide synthase. *Journal of Biological Chemistry* **2004,** 279, (36), 37918-37927.

31.Ratovitski, E. A.; Bao, C.; Quick, R. A.; McMillan, A.; Kozlovsky, C.; Lowenstein, C. J., An inducible nitric-oxide synthase (NOS)-associated protein inhibits NOS dimerization and activity. *Journal of Biological Chemistry* **1999,** 274, (42), 30250-30257.

32.McMillan, K.; Adler, M.; Auld, D. S.; Baldwin, J. J.; Blasko, E.; Browne, L. J.; Chelsky, D.; Davey, D.; Dolle, R. E.; Eagen, K. A.; Erickson, S.; Feldman, R. I.; Glaser, C. B.; Mallari, C.; Morrissey, M. M.; Ohlmeyer, M. H. J.; Pan, C. H.; Parkinson, J. F.; Phillips, G. B.; Polokoff, M. A.; Sigal, N. H.; Vergona, R.; Whitlow, M.; Young, T. A.; Devlin, J. J., Allosteric inhibitors of inducible nitric oxide synthase dimerization discovered via combinatorial chemistry. *Proceedings of the National Academy of Sciences of The U. S. A.* **2000,** 97, (4), 1506-1511.

33.Blasko, E.; Glaser, C. B.; Devlin, J. J.; Xia, W.; Feldman, R. I.; Polokoff, M. A.; Phillips, G. B.; Whitlow, M.; Auld, D. S.; McMillan, K.; Ghosh, S.; Stuehr, D. J.; Parkinson, J. F., Mechanistic studies with potent and selective inducible nitric-oxide synthase dimerization inhibitors. *Journal of Biological Chemistry* **2002,** 277, (1), 295-302.

34.Crane, B. R., et al., Structure of Nitric Oxide Synthase Oxygenase Dimer with Pterin and Substrate. *Science* **1998,** 279, 2121-2126.

35.Ghosh, D. K.; Wu, C. Q.; Pitters, E.; Moloney, M.; Werner, E. R.; Mayer, B.; Stuehr, D. J., Characterization of the inducible nitric oxide synthase oxygenase domain identifies a 49 amino acid segment required for subunit dimerization and tetrahydrobiopterin interaction. *Biochemistry* **1997,** 36, (35), 10609-10619.

36.Crane, B. R.; Arvai, A. S.; Gachhui, R.; Wu, C. Q.; Ghosh, D. K.; Getzoff, E. D.; Stuehr, D. J.; Tainer, J. A., The structure of nitric oxide synthase oxygenase domain and inhibitor complexes. *Science* **1997,** 278, (5337), 425-431.

37.Sorlie, M.; Gorren, A. C. F.; Marchal, S.; Shimizu, T.; Lange, R.; Andersson, K. K.; Mayer, B., Single-turnover of nitric-oxide synthase in the presence of 4-amino-tetrahydrobiopterin - Proposed role for tetrahydrobiopterin as a proton donor. *Journal of Biological Chemistry* **2003,** 278, (49), 48602-48610.

38.Sagami, I.; Sato, Y.; Noguchi, T.; Miyajima, M.; Rozhkova, E.; Daff, S.; Shimizu, T., Electron transfer in nitric-oxide synthase. *Coordination Chemistry Reviews* **2002,** 226, (1-2), 179-186.

39.Ghosh, D. K.; Abusoud, H. M.; Stuehr, D. J., Reconstitution Of The 2nd Step In No Synthesis Using The Isolated Oxygenase And Reductase Domains Of Macrophage No Synthase. *Biochemistry* **1995,** 34, (36), 11316-11320.

40.Hurshman, A. R.; Marletta, M. A., Reactions catalyzed by the heme domain of inducible nitric oxide synthase: Evidence for the involvement of tetrahydrobiopterin in electron transfer. *Biochemistry* **2002,** 41, (10), 3439-3456.

41.Adak, S.; Ghosh, S.; Abu-Soud, H. M.; Stuehr, D. J., Role of reductase domain cluster 1 acidic residues in neuronal nitric-oxide synthase - characterization of the FMN-free enzyme. *Journal of Biological Chemistry* **1999,** 274, (32), 22313-22320.

42.Stuehr, D. J.; Santolini, J.; Wang, Z. Q.; Wei, C. C.; Adak, S., Update on mechanism and catalytic regulation in the NO synthases. *Journal of Biological Chemistry* **2004,** 279, (35), 36167-36170.

43.Presta, A.; Siddhanta, U.; Wu, C. Q.; Sennequier, N.; Huang, L. X.; Abu-Soud, H. M.; Erzurum, S.; Stuehr, D. J., Comparative functioning of dihydro- and tetrahydropterins in supporting electron transfer, catalysis, and subunit dimerization in inducible nitric oxide synthase. *Biochemistry* **1998,** 37, (1), 298-310.

44.Groves, J. T.; Wang, C. C. Y., Nitric oxide synthase: models and mechanisms. *Current Opinions in Chemical Biology* **2000,** 4, (6), 687-695.

45.Davydov, R.; Ledbetter-Rogers, A.; Martasek, P.; Larukhin, M.; Sono, M.; Dawson, J. H.; Masters, B. S. S.; Hoffman, B. M., EPR and ENDOR characterization of intermediates in the cryoreduced oxy-nitric oxide synthase heme domain with bound L-arginine or N-G-hydroxyarginine. *Biochemistry* **2002,** 41, (33), 10375-10381.

46.Sono, M.; Roach, M. P.; Coulter, E. D.; Dawson, J. H., Heme-containing oxygenases. *Chemical Reviews* **1996,** 96, (7), 2841-2887.

47.Groves, J. T.; Han, Y., In *Cytochrome P450*, Ortiz de Montellano, P. R., Ed. Plenum Press: New York, 1995; pp 3-48.

48.Presta, A.; Weber-Main, A. M.; Stankovich, M. T.; Stuehr, D. J., Comparative Effects of Substrates and Pterin Cofactor on the Heme Midpoint Potential in Inducible and Neuronal Nitric Oxide Synthases. *Journal of the American Chemical Society* **1998,** 120, (37), 9460-9465.

49.Boggs, S.; Huang, L. X.; Stuehr, D. J., Formation and reactions of the heme-dioxygen intermediate in the first and second steps of nitric oxide synthesis as studied by stopped-flow spectroscopy under single-turnover conditions. *Biochemistry* **2000,** 39, (9), 2332-2339.

50.Wei, C. C.; Wang, Z. Q.; Hemann, C.; Hille, R.; Stuehr, D. J., A tetrahydrobiopterin radical forms and then becomes reduced during N-omega-hydroxyarginine oxidation by nitric-oxide synthase. *Journal of Biological Chemistry* **2003,** 278, (47), 46668-46673.

51.Wei, C. C.; Crane, B. R.; Stuehr, D. J., Tetrahydrobiopterin radical enzymology. *Chemical Reviews* **2003,** 103, (6), 2365-2383.

52.Ost, T. W. B.; Daff, S., Thermodynamic and kinetic analysis of the nitrosyl, carbonyl, and dioxy heme complexes of neuronal nitric-oxide synthase - The roles of substrate and tetrahydrobiopterin in oxygen activation. *Journal of Biological Chemistry* **2005,** 280, (2), 965-973.

53.Hurshman, A. R.; Krebs, C.; Edmondson, D. E.; Huynh, B. H.; Marletta, M. A., Formation of a pterin radical in the reaction of the heme domain of inducible nitric oxide synthase with oxygen. *Biochemistry* **1999,** 38, (48), 15689-15696.

54.Bec, N.; Gorren, A. F. C.; Mayer, B.; Schmidt, P. P.; Andersson, K. K.; Lange, R., The role of tetrahydrobiopterin in the activation of oxygen by nitric-oxide synthase. *Journal of Inorganic Biochemistry* **2000,** 81, (3), 207-211.

55.Schlichting, I.; Berendzen, J.; Chu, K.; Stock, A. M.; Maves, S. A.; Benson, D. E.; Sweet, B. M.; Ringe, D.; Petsko, G. A.; Sligar, S. G., The catalytic pathway of cytochrome P450cam at atomic resolution. *Science* **2000,** 287, (5458), 1615-1622.

56.Davydov, R.; Makris, T. M.; Kofman, V.; Werst, D. E.; Sligar, S. G.; Hoffman, B. M., Hydroxylation of camphor by-reduced oxy-cytochrome P450cam: Mechanistic implications of EPR and ENDOR studies of catalytic intermediates in native and mutant enzymes. *Journal of the American Chemical Society* **2001,** 123, (7), 1403-1415.

57.Bec, N.; Gorren, A. C. F.; Voelker, C.; Mayer, B.; Lange, R., Reaction of neuronal nitric-oxide synthase with oxygen at low temperature - Evidence for reductive activation of the oxy-ferrous complex by tetrahydrobiopterin. *Journal of Biological Chemistry* **1998,** 273, (22), 13502-13508.

58.Rosen, G. M.; Tsai, P.; Pou, S., Mechanism of free-radical generation by nitric oxide synthase. *Chemical Reviews* **2002,** 102, (4), 1191-1199.

59.Li, H. Y.; Shimizu, H.; Flinspach, M.; Jamal, J.; Yang, W. P.; Xian, M.; Cai, T. W.; Wen, E. Z.; Jia, Q. A.; Wang, P. G.; Poulos, T. L., The novel binding mode of N-Alkyl-N '-hydroxyguanidine to neuronal nitric oxide synthase provides mechanistic insights into NO biosynthesis. *Biochemistry* **2002,** 41, (47), 13868-13875.

60.Berglund, J.; Pascher, T.; Winkler, J. R.; Gray, H. B., Photoinduced oxidation of horseradish peroxidase. *Journal of the American Chemical Society* **1997,** 119, (10), 2464-2469.

61.Low, D. W.; Winkler, J. R.; Gray, H. B., Photoinduced oxidation of microperoxidase-8: Generation of ferryl and cation-radical porphyrins. *Journal of the American Chemical Society* **1996,** 118, (1), 117-120.

62.Wilker, J. J.; Dmochowski, I. J.; Dawson, J. H.; Winkler, J. R.; Gray, H. B., Substrates for Rapid Delivery of Electrons and Holes to Buried Active Sites in Proteins. *Angewandte Chemie International Edition* **1999,** 38, (1/2), 89-92.

63.Dmochowski, I. J.; Crane, B. R.; Wilker, J. J.; Winkler, J. R.; Gray, H. B., Optical Detection of cytochrome P450 by Sensitizer-Linked Substrates. *Proceedings of the National Academy of Sciences of the U. S. A.* **1999,** 96, (23), 12987-90.

64.Dmochowski, I. J., Probing Cytochrome P450 with Sensitizer-Linked Substrates. California Institute of Technology, Pasadena, CA, 2000.

65.Dunn, A. R.; Dmochowski, I. J.; Winkler, J. R.; Gray, H. B., Nanosecond Photoreduction of Cytochrome P450cam by Channel-Specific Ru-diimine Electron Tunneling Wires. *Journal of the American Chemical Society* **2003,** 125, (41), 12450-12456.

66.Dunn, A. R.; Dmochowski, I. J.; Bilwes, A. M.; Gray, H. B.; Crane, B. R., Probing the Open State of Cytochrome P450cam with Ruthenium-linker Substrates. *Proceedings of the National Academy of Sciences of the U. S. A.* **2001,** 98, (22), 12420-25.

67.Dunn, A. R., Belliston-Bittner, W., Winkler, J. R., Getzoff, E. D., Stuehr, D. J., and Gray, H. B., Luminescent Ruthenium(II)- and Rhenium(I)-Diimine Wires Bind Nitric Oxide Synthase. *Journal of the American Chemical Society* **2005,** 127, (14), 5169-5173.

68.Belliston-Bittner, W.; Dunn, A. R.; Nguyen, Y. H. L.; Stuehr, D. J.; Winkler, J. R.; Gray, H. B., Picosecond Photo-induced Reduction of Inducible Nitric Oxide Synthase by Re-diimine Wires. *Journal of the American Chemical Society* **2005,** submitted.

69.Dunn, A. R., Sensitizer-Linked Substrates as Probes of Heme Enzyme Structure and Catalysis. California Institute of Technology, Pasadena, CA, 2003.

70.Scott, J. R.; Willie, A.; McLean, M.; Stayton, P. S.; Sligar, S. G.; Durham, B.; Millett, F., Intramolecular Electron-Transfer In Cytochrome-B(5) Labeled With Ruthenium(Ii) Polypyridine Complexes - Rate Measurements In The Marcus Inverted Region. *Journal of the American Chemical Society* **1993,** 115, (15), 6820-6824.

71.Mines, G. A.; Bjerrum, M. J.; Hill, M. G.; Casimiro, D. R.; Chang, I. J.; Winkler, J. R.; Gray, H. B., Rates of heme oxidation and reduction in Ru(His33)cytochrome c at very high driving forces. *Journal of the American Chemical Society* **1996,** 118, (8), 1961-1965.

72.Gray, H. B.; Winkler, J. R., Electron tunneling through proteins. *Quarterly Reviews of Biophysics* **2003,** 36, (3), 341-372.

73.Crane, B. R.; Di Bilio, A. J.; Winkler, J. R.; Gray, H. B., Electron Tunneling in Single Crystals of Pseudomonas aeruginosa Azurins. *Journal of the American Chemical Society* **2001,** 123, (47), 11623-31.

74.Babini, E.; Bertini, I.; Borsari, M.; Capozzi, F.; Luchinat, C.; Zhang, X. Y.; Moura, G. L. C.; Kurnikov, I. V.; Beratan, D. N.; Ponce, A.; Di Bilio, A. J.; Winkler, J. R.; Gray, H. B., Bond-mediated electron tunneling in ruthenium-modified high-potential iron-sulfur protein. *Journal of the American Chemical Society* **2000,** 122, (18), 4532-4533.

75.Hess, C. R.; Juda, G. A.; Dooley, D. M.; Amii, R. N.; Hill, M. G.; Winkler, J. R.; Gray, H. B., Gold electrodes wired for coupling with the deeply buried active site of Arthrobacter globiformis amine oxidase. *Journal of the American Chemical Society* **2003,** 125, (24), 7156-7157.

76.Dmochowski, I. J.; Winkler, J. R.; Gray, H. B., Enantiomeric discrimination of Ru-substrates by cytochrome P450(cam). *Journal of Inorganic Biochemistry* **2000,** 81, (3), 221-228.

77.Dmochowski, I. J.; Dunn, A. R.; Wilker, J. J.; Crane, B. R.; Green, M. T.; Dawson, J. H.; Sligar, S. G.; Winkler, J. R.; Gray, H. B., Sensitizer-linked substrates and ligands: Ruthenium probes of cytochrome P450 structure and mechanism. In *Cytochrome P450, Pt C*, 2002; 357, pp 120-133.

78.Hays, A. M. A.; Dunn, A. R.; Chiu, R.; Gray, H. B.; Stout, C. D.; Goodin, D. B., Conformational states of cytochrome P450cam revealed by trapping of synthetic molecular wires. *Journal of Molecular Biology* **2004,** 344, (2), 455-469.

79.Dunn, A. R.; Hays, A.-M. A.; Goodin, D. B.; Stout, C. D.; Chiu, R.; Winkler, J. R.; Gray, H. B., Fluorescent Probes for Cytochrome P450 Structural Characterization and Inhibitor Screening. *Journal of the American Chemical Society* **2002,** 124, (35), 10254-55.

80.Contakes, S., *personal communication*.

81.Contakes, S. M.; Dunn, A. R.; Morales, N.; Winkler, J. R.; Gray, H. B., Substrate-tethered probes for investigating the active site of myeloperoxidase. *Journal of Inorganic Biochemistry* **2003,** 96, (1), 120-120.

82.Hays, A. M. A.; Gray, H. B.; Goodin, D. B., Trapping of peptide-based surrogates in an artificially created channel of cytochrome c peroxidase. *Protein Science* **2003,** 12, (2), 278-287.

83.Immoos, C.; Di Bilio, A. J.; Cohen, M. S.; Van der Veer, W.; Gray, H. B.; Farmer, P. J., Electron Transfer Chemistry of Ru-Linker-(Heme)-Modified Myoglobin: Rapid Intraprotein Reduction of a Photogenerated Porphyrin Cation Radical. *Inorganic Chemistry* **2004**.

84.Udit, A. K.; Hill, M. G.; Bittner, V. G.; Arnold, F. H.; Gray, H. B., Reduction of dioxygen catalyzed by pyrene-wired heme domain cytochrome P450BM3 electrodes. *Journal of the American Chemical Society* **2004,** 126, (33), 10218-10219.

85.Franzen, S.; Goldstein, R. F.; Boxer, S. G., Distance Dependence Of Electron-Transfer Reactions In Organized Systems - The Role Of Superexchange And Non-Condon Effects In Photosynthetic Reaction Centers. *Journal of Physical Chemistry* **1993,** 97, (12), 3040-3053.

86.Kirmaier, C.; Holten, D., Primary Photochemistry Of Reaction Centers From The Photosynthetic Purple Bacteria. *Photosynthesis Research* **1987,** 13, (3), 225-260.

87.Park, H. W.; Kim, S. T.; Sancar, A.; Deisenhofer, J., Crystal-Structure Of Dna Photolyase From Escherichia-Coli. *Science* **1995,** 268, (5219), 1866-1872.

88.Aubert, C.; Vos, M. H.; Mathis, P.; Eker, A. P. M.; Brettel, K., Intraprotein radical transfer during photoactivation of DNA photolyase. *Nature* **2000,** 405, (6786), 586-590.

89.Stubbe, J.; Nocera, D. G.; Yee, C. S.; Chang, M. C. Y., Radical initiation in the class I ribonucleotide reductase: Long-range proton-coupled electron transfer? *Chemical Reviews* **2003,** 103, (6), 2167-2201.

90.Marcus, R. A.; Sutin, N., Electron Transfers in Chemistry and Biology. *Biochimica et Biophysica Acta* **1985,** 811, 265-322.

91.Winkler, J. R.; Di Bilio, A. J.; Farrow, N. A.; Richards, J. H.; Gray, H. B., Electron Tunneling in Biological Molecules. *Pure and Applied Chemistry* **1999,** 71, (9), 1753-1764.

92.Winkler, J. R.; WittungStafshede, P.; Leckner, J.; Malmstrom, B. G.; Gray, H. B., Effects of folding on metalloprotein active sites. *Proceedings of the National Academy of Sciences of the U. S. A.* **1997,** 94, (9), 4246-4249.

93.Gray, H. B.; Malmstrom, B. G.; Williams, R. J. P., Copper coordination in blue proteins. *Journal of Biological Inorganic Chemistry* **2000,** 5, (5), 551-559.

94.Wiedenfeld, D.; Bachrach, M.; McCleskey, T. M.; Hill, M. G.; Gray, H. B.; Winkler, J. R., Temperature and isotope effects on the rates of photoinduced iridium(I)-pyridinium electron-transfer reactions. *Journal of Physical Chemistry B* **1997,** 101, (44), 8823-8826.

95.Wasielewski, M. R.; Niemczyk, M. P.; Svec, W. A.; Pewitt, E. B., Dependence Of Rate Constants For Photoinduced Charge Separation And Dark Charge Recombination On The Free-Energy Of Reaction In Restricted-Distance Porphyrin Quinone Molecules. *Journal of the American Chemical Society* **1985,** 107, (4), 1080-1082.

96.Closs, G. L.; Miller, J. R., Intramolecular Long-Distance Electron-Transfer In Organic-Molecules. *Science* **1988,** 240, (4851), 440-447.

97.Closs, G. L.; Calcaterra, L. T.; Green, N. J.; Penfield, K. W.; Miller, J. R., Distance, Stereoelectronic Effects, And The Marcus Inverted Region In Intramolecular Electron-Transfer In Organic Radical-Anions. *Journal of Physical Chemistry* **1986,** 90, (16), 3673-3683.

98.Fox, L. S.; Kozik, M.; Winkler, J. R.; Gray, H. B., Gaussian Free-Energy Dependence Of Electron-Transfer Rates In Iridium Complexes. *Science* **1990,** 247, (4946), 1069-1071.

99.Chen, P. Y.; Duesing, R.; Graff, D. K.; Meyer, T. J., Intramolecular Electron-Transfer In The Inverted Region. *Journal of Physical Chemistry* **1991,** 95, (15), 5850-5858.

100.McLendon, G.; Miller, J. R., The Dependence Of Biological Electron-Transfer Rates On Exothermicity - The Cytochrome-C Cytochrome-B5 Couple. *Journal of the American Chemical Society* **1985,** 107, (26), 7811-7816.

101.McCleskey, T. M.; Winkler, J. R.; Gray, H. B., Driving-Force Effects On The Rates Of Bimolecular Electron-Transfer Reactions. *Journal of the American Chemical Society* **1992,** 114, (17), 6935-6937.

102.Brunschwig, B. S.; Sutin, N., *Comments on Inorganic Chemistry* **1987,** 6, 209-235.

103.Gray, H. B.; Winkler, J. R., Long-range electron transfer. *Proceedings of the National Academy of Sciences of the U. S. A.* **2005,** 102, (10), 3534-3539.

104.Wenger, O. S.; Leigh, B. S.; Villahermosa, R. M.; Gray, H. B.; Winkler, J. R., Electron tunneling through organic molecules in frozen glasses. *Science* **2005,** 307, (5706), 99-102.

105.McConnell, H., Intramolecular Charge Transfer In Aromatic Free Radicals. *Journal of Chemical Physics* **1961,** 35, (2), 508-&.

106.Winkler, J. R.; Nocera, D. G.; Yocom, K. M.; Bordignon, E.; Gray, H. B., Electron-Transfer Kinetics Of Pentaammineruthenium(Iii)(Histidine-33)-Ferricytochrome-C - Measurement Of The Rate Of Intramolecular Electron-Transfer Between Redox Centers Separated By 15-A In A Protein. *Journal of the American Chemical Society* **1982,** 104, (21), 5798-5800.

107.Winkler, J. R.; Gray, H. B., Electron-Transfer In Ruthenium-Modified Proteins. *Chemical Reviews* **1992,** 92, (3), 369-379.

108.Villahermosa, R., Electron Tunneling through Phenylene Bridges. California Institute of Technology, 2002.

109.Smalley, J. F.; Finklea, H. O.; Chidsey, C. E. D.; Linford, M. R.; Creager, S. E.; Ferraris, J. P.; Chalfant, K.; Zawodzinsk, T.; Feldberg, S. W.; Newton, M. D., Heterogeneous electron-transfer kinetics for ruthenium and ferrocene redox moieties through alkanethiol monolayers on gold. *Journal of the American Chemical Society* **2003,** 125, (7), 2004-2013.

110.Regan, J. J.; Dibilio, A. J.; Langen, R.; Skov, L. K.; Winkler, J. R.; Gray, H. B.; Onuchic, J. N., Electron-Tunneling In Azurin - The Coupling Across A Beta-Sheet. *Chemistry & Biology* **1995,** 2, (7), 489-496.

111.Langen, R.; Chang, I. J.; Germanas, J. P.; Richards, J. H.; Winkler, J. R.; Gray, H. B., Electron-Tunneling In Proteins - Coupling Through A Beta-Strand. *Science* **1995,** 268, (5218), 1733-1735.

112.Gray, H. B.; Winkler, J. R., Electron transfer in proteins. *Annual Review of Biochemistry* **1996,** 65, 537-561.

113.Farver, O.; Pecht, I., Copper proteins as model systems for investigating intramolecular electron transfer processes. In *Electron Transfer-From Isolated Molecules To Biomolecules, Pt 2*, 1999; Vol. 107, pp 555-589.

114.Mize, R. R.; Dawson, T. M.; Dawson, V. L.; Friedlander, M. J., *Nitric Oxide in Brain Development, Plasticity and Disease*. Elsevier: Amsterdam, 1998.

115.Lancaster, J., *Nitric Oxide: Principles and Actions*. Academic Press: San Diego, CA, 1996.

116.Ko, G. Y.; Kelly, P. T., Nitric oxide acts as a postsynaptic signaling molecule in calcium/calmodulin-induced synaptic potentiation in hippocampal CA1 pyramidal neurons. *Journal of Neuroscience* **1999,** 19, (16), 6784-6794.

117.Kendrick, K. M.; GuevaraGuzman, R.; Zorrilla, J.; Hinton, M. R.; Broad, K. D.; Mimmack, M.; Ohkura, S., Formation of olfactory memories mediated by nitric oxide. *Nature* **1997,** 388, (6643), 670-674.

118.Huang, P. L.; Huang, Z. H.; Mashimo, H.; Bloch, K. D.; Moskowitz, M. A.; Bevan, J. A.; Fishman, M. C., Hypertension In Mice Lacking The Gene For Endothelial Nitric-Oxide Synthase. *Nature* **1995,** 377, (6546), 239-242.

119.Hingorani, A. D.; Liang, C. F.; Fatibene, J.; Lyon, A.; Monteith, S.; Parsons, A.; Haydock, S.; Hopper, R. V.; Stephens, N. G.; O'Shaughnessy, K. M.; Brown, M. J., A common variant of the endothelial nitric oxide synthase (Glu(298)-> Asp) is a major risk factor for coronary artery disease in the UK. *Circulation* **1999,** 100, (14), 1515-1520.

120.Hobbs, A. J.; Higgs, A.; Moncada, S., Inhibition of nitric oxide synthase as a potential therapeutic target. *Annual Review of Pharmacology and Toxicology* **1999,** 39, 191-220.

121.Heales, S. J. R.; Bolanos, J. P.; Stewart, V. C.; Brookes, P. S.; Land, J. M.; Clark, J. B., Nitric oxide, mitochondria and neurological disease. *Biochimica et Biophysica Acta-Bioenergetics* **1999,** 1410, (2), 215-228.

122.Stuehr, D. J., Mammalian nitric oxide synthases. *Biochimica et Biophysica Acta-Bioenergetics* **1999,** 1411, (2-3), 217-230.

123.Bredt, D. S.; Hwang, P. M.; Glatt, C. E.; Lowenstein, C.; Reed, R. R.; Snyder, S. H., Cloned And Expressed Nitric-Oxide Synthase Structurally Resembles Cytochrome-P-450 Reductase. *Nature* **1991,** 351, (6329), 714-718.

124.Siddhanta, U.; Wu, C. Q.; AbuSoud, H. M.; Zhang, J. L.; Ghosh, D. K.; Stuehr, D. J., Heme iron reduction and catalysis by a nitric oxide synthase heterodimer containing one reductase and two oxygenase domains. *Journal of Biological Chemistry* **1996,** 271, (13), 7309-7312.

125.Siddhanta, U.; Presta, A.; Fan, B. C.; Wolan, D.; Rousseau, D. L.; Stuehr, D. J., Domain swapping in inducible nitric-oxide synthase - Electron transfer occurs between flavin and heme groups located on adjacent subunits in the dimer. *Journal of Biological Chemistry* **1998,** 273, (30), 18950-18958.

126.Panda, K.; Ghosh, S.; Stuehr, D. J., Calmodulin activates intersubunit electron transfer in the neuronal nitric-oxide synthase dimer. *Journal of Biological Chemistry* **2001,** 276, (26), 23349-23356.

127.Kobayashi, K.; Tagawa, S.; Daff, S.; Sagami, I.; Shimizu, T., Rapid calmodulin-dependent interdomain electron transfer in neuronal nitric-oxide synthase measured by pulse radiolysis. *Journal of Biological Chemistry* **2001,** 276, (43), 39864-39871.

128.Abu-Soud, H. M.; Yoho, L. L.; Stuehr, D. J., Calmodulin Controls Neuronal Nitric-Oxide Synthase By A Dual Mechanism - Activation Of Intradomain And Interdomain Electron-Transfer. *Journal of Biological Chemistry* **1994,** 269, (51), 32047-32050.

129.Poulos, T. L.; Li, H. Y.; Raman, C. S.; Schuller, D. J., Structures of gas-generating heme enzymes: Nitric oxide synthase and heme oxygenase. In *Advances In Inorganic Chemistry.* 2001; Vol. 51, pp 243-293.

130.Ortiz de Montellano, P. R., *Cytochrome P450*. Plenum Press: New York, 1995.

131.Sligar, S. G.; Gunsalus, I. C., Thermodynamic Model Of Regulation - Modulation of Redox Equilibria In Camphor Monoxygenase. *Proceedings of the National Academy of Sciences of the U. S. A.* **1976,** 73, (4), 1078-1082.

132.Zaslavsky, D.; Sadoski, R. C.; Wang, K. F.; Durham, B.; Gennis, R. B.; Millett, F., Single electron reduction of cytochrome c oxidase compound F: Resolution of partial steps by transient spectroscopy. *Biochemistry* **1998,** 37, (42), 14910-14916.

133.Zaslavsky, D.; Kaulen, A. D.; Smirnova, I. A.; Vygodina, T.; Konstantinov, A. A., Flash-Induced Membrane-Potential Generation By Cytochrome-C-Oxidase. *Febs Letters* **1993,** 336, (3), 389-393.

134.Connick, W. B.; DiBilio, A. J.; Hill, M. G.; Winkler, J. R.; Gray, H. B., Tricarbonyl(1,1O-phenanthroline)(imidazole)rhenium(I): A powerful photooxidant for investigations of electron tunneling in proteins. *Inorganica Chimica Acta* **1995,** 240, (1-2), 169-173.

135.Sacksteder, L.; Zipp, A. P.; Brown, E. A.; Streich, J.; Demas, J. N.; Degraff, B. A., Luminescence Studies Of Pyridine Alpha-Diimine Rhenium(I) Tricarbonyl Complexes. *Inorganic Chemistry* **1990,** 29, (21), 4335-4340.

136.Gerstein, M., A Resolution-Sensitive Procedure For Comparing Protein Surfaces And Its Application To The Comparison Of Antigen-Combining Sites. *Acta Crystallographica Section A* **1992,** 48, 271-276.

137.Vallance, P.; Leiper, J., Blocking NO synthesis: How, where and why? *Nature Reviews Drug Discovery* **2002,** 1, (12), 939-950.

138.Salerno, L.; Sorrenti, V.; Di Giacomo, C.; Romeo, G.; Siracusa, M. A., Progress in the development of selective nitric oxide synthase (NOS) inhibitors. *Current Pharmaceutical Design* **2002,** 8, (3), 177-200.

139.Aktan, F., iNOS-mediated nitric oxide production and its regulation. *Life Sciences* **2003,** 75, 639-653.

140.Luth, H. J.; Holzer, M.; Gartner, U.; Staufenbiel, M.; Arendt, T., Expression of endothelial and inducible NOS-isoforms is increased in Alzheimer's disease, in APP23 transgenic mice and after experimental brain lesion in rat: evidence for an induction by amyloid pathology. *Brain Research* **2001,** 913, (1), 57-67.

141.Hingorani, A. D.; Cross, J.; Kharbanda, R. K.; Mullen, M. J.; Bhagat, K.; Taylor, M.; Donald, A. E.; Palacios, M.; Griffin, G. E.; Deanfield, J. E.; MacAllister, R. J.; Vallance,

P., Acute systemic inflammation impairs endothelium-dependent dilatation in humans. *Circulation* **2000,** 102, (9), 994-999.

142.Wei, C. C.; Wang, Z. Q.; Arvai, A. S.; Hemann, C.; Hille, R.; Getzoff, E. D.; Stuehr, D. J., Structure of tetrahydrobiopterin tunes its electron transfer to the heme-dioxy intermediate in nitric oxide synthase. *Biochemistry* **2003,** 42, (7), 1969-1977.

143.Dunn, A. R., Belliston-Bittner, W., Winkler, J. R., Getzoff, E. D., Stuehr, D. J., and Gray, H. B., Luminescent Ruthenium(II)- and Rhenium(I)-Diimine Wires Bind Nitric Oxide Synthase. *Journal of the American Chemical Society* **2004,** submitted.

144.Harriman, A., Further Comments On The Redox Potentials Of Tryptophan And Tyrosine. *Journal of Physical Chemistry* **1987,** 91, (24), 6102-6104.

145.Elliott, C. M.; Freitag, R. A.; Blaney, D. D., Electrochemistry, Spectroelectrochemistry, And Photochemistry Of A Series Of New Covalently Linked Tris(2,2'-Bipyridine)Ruthenium(Ii) Diquat Complexes. *Journal of the American Chemical Society* **1985,** 107, (16), 4647-4655.

146.Gunsalus, I. C.; Meeks, J. R.; Lipscomb, J. D., Cytochrome P-450cam Substrate And Effector Interactions. *Annals of the New York Academy of Sciences* **1973,** 212, (JUN22), 107-121.

147.Miller, J. E.; Grodinaru, C.; Di Bilio, A. J.; Wehbi, W. A.; Crane, B. R.; Winkler, J. R.; Gray, H. B., Spectroscopy and Reactivity of a Photogenerated Tryptophan Radical in a Structurally Defined Protein Environment. *Journal of the American Chemical Society* **2003,** 125, (47), 14220-14221.

148.van Houten; Watts, *Journal of the American Chemical Society* **1976,** 98, (16), 4853-4858.

149.Kuciauskas, D.; Freund, M. S.; Gray, H. B.; Winkler, J. R.; Lewis, N. S., Electron transfer dynamics in nanocrystalline titanium dioxide solar cells sensitized with ruthenium or osmium polypyridyl complexes. *Journal of Physical Chemistry B* **2001,** 105, (2), 392-403.

150.Garcin, E. D.; Getzoff, E. D., *personal communication*.

151.Rao, P. S.; Hayon, E., Oxidation Of Aromatic-Amines And Diamines By Oh Radicals - Formation And Ionization-Constants Of Amine Cation Radicals In Water. *Journal of Physical Chemistry* **1975,** 79, (11), 1063-1066.

152.Fujita, S.; Ststeenken, Pattern Of Oh Radical-Addition To Uracil And Methyl-Substituted And Carboxyl-Substituted Uracils - Electron-Transfer Of Oh Adducts With N,N,N',N'-Tetramethyl-Para-Phenylenediamine And Tetranitromethane. *Journal of the American Chemical Society* **1981,** 103, (10), 2540-2545.

153.Hobel, B.; von Sonntag, C., OH-radical induced degradation of ethylenediaminetetraacetic acid (EDTA) in aqueous solution: a pulse radiolysis study. *Journal of the Chemical Society-Perkin Transactions 2* **1998**, (3), 509-513.

154.Schweizer, M.; Richter, C., Nitric-Oxide Potently And Reversibly Deenergizes Mitochondria At Low-Oxygen Tension. *Biochemical and Biophysical Research Communications* **1994,** 204, (1), 169-175.

155.Devoe, I. W.; Gilchrist, J. E., Localization Of "Tetramethylphenylenediamine-Oxidase In Outer Cell-Wall Layer Of Neisseria-Meningitidis. *Journal of Bacteriology* **1976,** 128, (1), 144-148.

156.Wei, C. C.; Wang, Z. Q.; Wang, Q.; Meade, A. L.; Hemann, C.; Hille, R.; Stuehr, D. J., Rapid kinetic studies link tetrahydrobiopterin radical formation to heme-dioxy reduction and arginine hydroxylation in inducible nitric-oxide synthase. *Journal of Biological Chemistry* **2001,** 276, (1), 315-319.

157.Gorren, A. C. F.; Kungl, A. J.; Schmidt, K.; Werner, E. R.; Mayer, B., Electrochemistry of pterin cofactors and inhibitors of nitric oxide synthase. *Nitric Oxide-Biology and Chemistry* **2001,** 5, (2), 176-186.

158.Kuzkaya, N.; Weissmann, N.; Harrison, D. G.; Dikalov, S., Interactions of Peroxynitrite, Tetrahydrobiopterin, Ascorbic Acid, and Thiols. *Journal of Biological Inorganic Chemistry* **2003,** 278, (25), 22546-22554.

159.Heller, R.; Unbehaun, A.; Schellenberg, B.; Mayer, B.; Werner-Felmayer, G.; Werner, E. R., L-ascorbic acid potentiates endothelial nitric oxide synthesis via a chemical stabilization of tetrahydrobiopterin. *Journal of Biological Chemistry* **2001,** 276, (1), 40-47.

160.Udit, A. K.; Belliston-Bittner, W.; Glazer, E. C.; Nguyen, Y. H. L.; Hill, M. G.; Marletta, M. A.; Goodin, D. B.; Gray, H. B., Redox Couples of Inducible Nitric Oxide Synthase. *Journal of the American Chemical Society* **2005,** submitted.

161.Hurshman, A. R.; Krebs, C.; Edmondson, D. E.; Marletta, M. A., Ability of tetrahydrobiopterin analogues to support catalysis by inducible nitric oxide synthase: Formation of a pterin radical is required for enzyme activity. *Biochemistry* **2003,** 42, (45), 13287-13303.

162.Rusling, J. F., Enzyme bioelectrochemistry in cast biomembrane-like films. *Accounts of Chemical Research* **1998,** 31, (6), 363-369.

163.Fujita, K.; Nakamura, N.; Ohno, H.; Leigh, B. S.; Niki, K.; Gray, H. B.; Richards, J. H., Mimicking protein-protein electron transfer: Voltammetry of Pseudomonas aeruginosa azurin and the Thermus thermophilus Cu-A domain at omega-derivatized self-assembled-monolayer gold electrodes. *Journal of the American Chemical Society* **2004,** 126, (43), 13954-13961.

164.Rusling, J. F.; Nassar, A. E. F., Enhanced Electron-Transfer For Myoglobin In Surfactant Films On Electrodes. *Journal of the American Chemical Society* **1993,** 115, (25), 11891-11897.

165.Bayachou, M.; Boutros, J. A., Direct electron transfer to the oxygenase domain of neuronal nitric oxide synthase (NOS): Exploring unique redox properties of NOS enzymes. *Journal of the American Chemical Society* **2004,** 126, (40), 12722-12723.

166.Ma, H. Y.; Hu, N. F., Electrochemistry and electrocatalysis with myoglobin in 2C(12)N(+)PSS(-) multibilayer composite films. *Analytical Letters* **2001,** 34, (3), 339-361.

167.Immoos, C. E.; Chou, J.; Bayachou, M.; Blair, E.; Greaves, J.; Farmer, P. J., Electrocatalytic reductions of nitrite, nitric oxide, and nitrous oxide by thermophilic cytochrome P450CYP119 in film-modified electrodes and an analytical comparison of its catalytic activities with myoglobin. *Journal of the American Chemical Society* **2004,** 126, (15), 4934-4942.

168.Zhang, Z.; Nassar, A. E. F.; Lu, Z. Q.; Schenkman, J. B.; Rusling, J. F., Direct electron injection from electrodes to cytochrome P450(cam) in biomembrane-like films. *Journal of the Chemical Society-Faraday Transactions* **1997,** 93, (9), 1769-1774.

169.Fleming, B. D.; Tian, Y.; Bell, S. G.; Wong, L. L.; Urlacher, V.; Hill, H. A. O., Redox properties of cytochrome P450(BM3) measured by direct methods. *European Journal of Biochemistry* **2003,** 270, (20), 4082-4088.

170.Lvov, Y. M.; Lu, Z. Q.; Schenkman, J. B.; Zu, X. L.; Rusling, J. F., Direct electrochemistry of myoglobin and cytochrome p450(cam) in alternate layer-by-layer films with DNA and other polyions. *Journal of the American Chemical Society* **1998,** 120, (17), 4073-4080.

171.Bard, A. J.; Faulkner, L. R., *Electrochemical Methods*. Second ed.; John Wiley & Sons, Inc.: New York, 2001.

172.Lin, R.; Immoos, C. E.; Farmer, P. J., Unusual voltammetry of manganese-substituted myoglobin in surfactant film: evidence for two redox pathways. *Journal of Biological Inorganic Chemistry* **2000,** 5, (6), 738-747.

173.Crutchley, R. J.; Ellis, W. R.; Gray, H. B., Long-Distance Electron-Transfer In Pentaammineruthenium (Histidine-48)-Myoglobin - Reorganizational Energetics Of A High-Spin Heme. *Journal of the American Chemical Society* **1985,** 107, (17), 5002-5004.

174.Dawson, J. H.; Andersson, L. A.; Sono, M., The Diverse Spectroscopic Properties Of Ferrous Cytochrome-P-450-Cam Ligand Complexes. *Journal of Biological Chemistry* **1983,** 258, (22), 3637-3645.

175.Laviron, E., General Expression Of The Linear Potential Sweep Voltammogram In The Case Of Diffusionless Electrochemical Systems. *Journal of Electroanalytical Chemistry* **1979,** 101, (1), 19-28.

176.Munge, B.; Estavillo, C.; Schenkman, J. B.; Rusling, J. F., Optimization of electrochemical and peroxide-driven oxidation of styrene with ultrathin polyion films containing cytochrome p450(cam) and myoglobin. *Chembiochem* **2003,** 4, (1), 82-89.

177.Aguey-Zinsou, K. F.; Bernhardt, P. V.; De Voss, J. J.; Slessor, K. E., Electrochemistry of P450(cin): new insights into P450 electron transfer. *Chemical Communications* **2003**, (3), 418-419.

178.Ruba, E.; Hart, J. R.; Barton, J. K., [Ru(bpy)(2)(L)]Cl-2: Luminescent metal complexes that bind DNA base mismatches. *Inorganic Chemistry* **2004,** 43, (15), 4570-4578.

179.Olofsson, J.; Onfelt, B.; Lincoln, P., Three-state light switch of [Ru(phen)(2)dppz](2+): Distinct excited-state species with two, one, or no hydrogen bonds from solvent. *Journal of Physical Chemistry A* **2004,** 108, (20), 4391-4398.

180.Ortmans, I.; Elias, B.; Kelly, J. M.; Moucheron, C.; Kirsch-DeMesmaker, A., [Ru(TAP)(2)(dppz)](2+): a DNA intercalating complex, which luminesces strongly in water and undergoes photo-induced proton-coupled electron transfer with guanosine-5 '-monophosphate. *Dalton Transactions* **2004**, (4), 668-676.

181.Moon, S. J.; Kim, J. M.; Choi, J. Y.; Kim, S. K.; Lee, J. S.; Jang, H. G., [Ru(phen)2DPPZ]2+ is in Contact with DNA Bases When It Forms a Luminescent Complex with Single-Stranded Oligonucleotides. *Journal of Inorganic Biochemistry* **2005,** 99, (5), 994-1000.

182.Brooks, J.; Babayan, Y.; Lamansky, S.; Djurovich, P. I.; Tsyba, I.; Bau, R.; Thompson, M. E., Synthesis and characterization of phosphorescent cyclometalated platinum complexes. *Inorganic Chemistry* **2002,** 41, (12), 3055-3066.

183.Lamansky, S.; Djurovich, P.; Murphy, D.; Abdel-Razzaq, F.; Kwong, R.; Tsyba, I.; Bortz, M.; Mui, B.; Bau, R.; Thompson, M. E., Synthesis and characterization of phosphorescent cyclometalated iridium complexes. *Inorganic Chemistry* **2001,** 40, (7), 1704-1711.

184.Shearer, B. G.; Lee, S.; Oplinger, J. A.; Frick, L. W.; Garvey, E. P.; Furfine, E. S., Substituted N-Phenylisothioureas: Potent Inhibitors of Human Nitric Oxide Synthase with Neuronal Isoform Selectivity. *Journal of Medicinal Chemistry* **1997,** 40, (12), 1901-1905.

185.Garvey, E. P.; Oplinger, J. A.; Tanoury, G. J.; Sherman, P. A.; Fowler, M.; Marshall, S.; Harmon, M. F.; Paith, J. E.; Furfine, E. S., Potent and Selective Inhibition of Human Nitric Oxide Synthases. *Journal of Biological Chemistry* **1994,** 269, (43), 26669-26676.

186.Garvey, E. P.; Oplinger, J. A.; Furfine, E. S.; Kiff, R. J.; Laszlo, F.; Whittle, B. J. R.; Knowles, R. G., 1400W is a Slow, Tight Binding, and Highly Selective Inhibitor of

Inducible Nitric-oxide Synthase in Vitro and in Vivo. *Journal of Biological Chemistry* **1997,** 272, (8), 4959-4963.

187.Furfine, E. S.; Harmon, M. F.; Paith, J. E.; Knowles, R. G.; Salter, M.; Kiff, R. J.; Duffy, C.; Hazelwood, R.; Oplinger, J. A.; Garvey, E. P., Potent and Selective Inhibition of Human Nitric Oxide Synthases. *Journal of Biological Chemistry* **1994,** 269, (43), 26677-26683.

188.Kawanaka, Y.; Kobayashi, K.; Kusuda, S.; Tatsumi, T.; Murota, M.; Nishiyama, T.; Hisaichi, K.; Fujii, A.; Hirai, K.; Nishizaki, M.; Naka, M.; Komeno, M.; Nakai, H.; Toda, M., Design and Synthesis of Orally Bioavailable Inhibitors of Inducible Nitric Oxide Synthase. Synthesis and Biological Evaluation of Dihydropyridin-2(1H)-imines and 1,5,6,7-Tetrahydro-2H-azepin-2-imines. *Bioorganic and Medicinal Chemistry* **2002,** 11, 689-702.

189.Sennequier, N.; Wolan, D.; Stuehr, D. J., Antifungal Imidazoles Block Assembly of Inducible NO Synthase into an Active Dimer. *Journal of Biological Chemistry* **1999,** 274, (2), 930-938.

190.Borman, S., Chemistry Highlights 2004. *Chemical & Engineering News* **2004,** 82, (51), 53-61.

191.Gestwicki, J. E.; Crabtree, G. R.; Graef, I. A., Harnessing chaperones to generate small-molecule inhibitors of amyloid beta aggregation. *Science* **2004,** 306, (5697), 865-869.

192.Dawson, J. H.; Andersson, L. A.; Sono, M., Spectroscopic Investigations of Ferric Cytochrome P-450-CAM Ligand Complexes. *The Journal of Biological Chemistry* **1982,** 257, (7), 3606-3617.

193.Atkins, W. M.; Sligar, S. G., The Roles Of Active-Site Hydrogen-Bonding In Cytochrome P-450cam As Revealed By Site-Directed Mutagenesis. *Journal of Biological Chemistry* **1988,** 263, (35), 18842-18849.

194.Roach, M. P.; Pond, A. E.; Thomas, M. R.; Boxer, S. G.; Dawson, J. H., The Role of the Distal and Proximal Protein Environments in Controlling the Ferric Spin State and in Stabilizing Thiolate Ligation in Heme Systems: Thiolate Adducts of the Myoglobin H93G Cavity Mutant. *Journal of the American Chemical Society* **1999,** 121, (51), 12088-12093.